

August 2016

# Addressing Instability Issues in Microgrids Caused By Constant Power Loads Using Energy Storage Systems

Eklas Hossain

*University of Wisconsin-Milwaukee*

Follow this and additional works at: <https://dc.uwm.edu/etd>



Part of the [Engineering Commons](#), and the [Oil, Gas, and Energy Commons](#)

---

## Recommended Citation

Hossain, Eklas, "Addressing Instability Issues in Microgrids Caused By Constant Power Loads Using Energy Storage Systems" (2016).  
*Theses and Dissertations*. 1275.  
<https://dc.uwm.edu/etd/1275>

This Dissertation is brought to you for free and open access by UWM Digital Commons. It has been accepted for inclusion in Theses and Dissertations by an authorized administrator of UWM Digital Commons. For more information, please contact [open-access@uwm.edu](mailto:open-access@uwm.edu).

ADDRESSING INSTABILITY ISSUES IN MICROGRIDS CAUSED BY  
CONSTANT POWER LOADS USING ENERGY STORAGE SYSTEMS

by

Eklas Hossain

A Dissertation Submitted in  
Partial Fulfillment of the  
Requirements for the Degree of

Doctor of Philosophy  
in Engineering

at

The University of Wisconsin-Milwaukee

August 2016

# ABSTRACT

## ADDRESSING INSTABILITY ISSUES IN MICROGRIDS CAUSED BY CONSTANT POWER LOADS USING ENERGY STORAGE SYSTEMS

by

Eklas Hossain

The University of Wisconsin-Milwaukee, 2016  
Under the Supervision of Professor Ron Perez and Professor Adel Nasiri

Renewable energy sources, the most reasonable fuel-shift taken over the naturally limited conventional fuels, necessarily deal with the self-functional microgrid system rather than the traditional grid distribution system. The study shows that the microgrid system, a comparatively low-powered system, experiences the challenge of instability due to the constant power load (CPL) from many electronic devices such as inverter-based systems. In this dissertation, as a methodical approach to mitigate the instability complication, AC microgrid stability is thoroughly investigated for each and every considerable parameter of the system. Furthermore, a specific loading limit is depicted by evaluating the stability margin from the small signal analysis of the microgrid scheme. After demonstrating all cases regarding the instability problem, the storage-based virtual impedance power compensation method is introduced to restore the system stability and literally extend the loading limit of the microgrid system. Here, a PID controller is implemented to maintain the constant terminal voltage of CPL via current injection method from storage. Since the system is highly nonlinear by nature, advanced nonlinear control techniques, such as Sliding Mode Control and Lyapunov Redesign Control technique, are implemented to control the entire nonlinear system. Robustness, noise rejection, and frequency variation are scrutinized rigorously in a

virtual platform such as Matlab/Simulink with appreciable aftermaths. After that, a comparative analysis is presented between SMC and LRC controller robustness by varying CPL power. From this analysis, it is evident that Lyapunov redesign controller performs better than the previous one in retaining microgrid stability for dense CPL-loaded conditions. Finally, to ensure a robust storage system, Hybrid Energy Storage System is introduced and its advantages are discussed as extended research work.

© Copyright by Eklas Hossain, 2016  
All Rights Reserved

*Dedicated to all those philanthropic souls without whose support it would be impossible for  
me to thrive on this long expedition*

# TABLE OF CONTENTS

TABLE OF CONTENTS.....	vi
LIST OF FIGURES .....	ix
LIST OF TABLES.....	xv
LIST OF ABBREVIATIONS.....	xvi
LIST OF NOMENCLATURE.....	xviii
ACKNOWLEDGMENTS .....	xxi
Chapter 1 : Introduction .....	1
1.1 Introduction.....	1
1.2 State of Art.....	3
1.2.1 Stability Issues in DC Microgrids.....	4
1.2.2 Stability Issues in AC Microgrids.....	7
1.3 Problem Statement.....	9
Chapter 2 : Available Compensation Techniques for CPLs and Prior Art.....	11
2.1 Introduction.....	11
2.2 Feeder Side Compensation .....	12
2.3 Compensation by Adding Intermediate Circuitry or Element .....	13
2.4 Compensation by Load Side Converter .....	14
2.5 Constant Power Loads in Microgrids .....	15
2.6 Contributions.....	16
Chapter 3 : Nonlinear Modeling of Microgrid with CPL and CVL Loads.....	18
3.1 Introduction.....	18
3.2 Modeling of Loads.....	20
3.2.1 Resistive Loads .....	20
3.2.2 Constant Power Loads (CPLs).....	21
3.3 Modeling of Hybrid Microgrid .....	23
3.4 Modeling the Proposed Real Power Compensation Method .....	30
3.5 Modeling the Proposed Reactive Power Compensation Method .....	33
3.6 CPL with both Real and Reactive Power Component.....	35
Chapter 4 : Stability Margin Analysis .....	38
4.1 Introduction.....	38
4.2 Stability Margin of Proposed Model.....	38
4.2.1 Stability of the Conventional Model.....	38
4.2.2 Stability of Proposed Active Power Compensation.....	44

4.2.3 Stability of Proposed Reactive Power Compensation .....	50
4.3 Lyapunov Stability Criteria.....	58
Chapter 5 : Simulation Results and Discussion .....	61
5.1 Introduction.....	61
5.2 Simulation Results for PID Control Technique .....	61
5.3 Simulation Results from Sliding Mode Control .....	70
5.3.1 Sliding Mode Control .....	70
5.4 Robustness Analysis of Sliding Mode Controller.....	84
5.4.1 Sliding Mode Controller, Robustness against Parametric Uncertainties .....	84
5.4.2 Sliding Mode Controller Robustness against Parametric Uncertainties Including Uncertainties in Power of CPL .....	88
5.4.3 Sliding Mode Controller Robustness against Parametric Uncertainties and Frequency Variations .....	92
5.4.4 Sliding Mode Controller Robustness against Parametric Uncertainties, Frequency Variations and Additive White Gaussian Noise (AWGN) .....	95
5.5 Performance Analysis of Lyapunov Redesign Control Technique.....	109
5.5.1 Lyapunov Redesign, Robustness against Parametric Uncertainties .....	118
5.5.2 Lyapunov Redesign Controller Robustness against Parametric Uncertainties Including Uncertainties in Power of CPL .....	122
5.5.3 Lyapunov Redesign, Robustness against Parametric Uncertainties and Frequency Variations .....	126
5.5.4 Lyapunov Redesign Control Technique for Robustness against Parametric Uncertainties, Frequency Variations and Additive White Gaussian Noise (AWGN) ...	130
5.6 Conclusion .....	148
Chapter 6 : Extended Research .....	150
6.1 Introduction.....	150
6.2 Ultracapacitor as Energy Compensation Element .....	150
6.2.1 What is Ultracapacitor?.....	150
6.2.2 Ultracapacitor vs Battery Performance .....	151
6.3 Conventional Energy Storage System for Microgrid Applications .....	152
6.3.1 Battery-Only Compensator .....	154
6.3.2 Ultracapacitor-Only Compensator .....	157
6.4 Proposed Hybrid Energy Storage for Microgrid.....	159
6.5 Performance Evaluation and Findings .....	165
Chapter 7 : Summary .....	167
7.1 Salient Accomplishments.....	167
7.2 Discussion and Conclusion .....	168
7.3 Future Work .....	169
7.3.1 Selection of Storage System Based on Microgrid Capacity and Operating Specification .....	169
7.3.1.1 Applications Summary.....	170

7.3.2 Load-ability Calculation of “Microgrid with CPL” Using Droop control strategy .....	171
7.3.2.1 Droop Control .....	172
7.3.2.2 Stability Analysis Using Popov’s Stability Criterion .....	172
7.3.3 Reviewing the Feeder Side and by Adding Intermediate Circuitry Methodologies for CPL Compensation on Microgrid .....	172
Bibliography .....	174
Appendix: A.....	185
Appendix: B.....	191
Appendix: C.....	192
Curriculum Vitae .....	195

# LIST OF FIGURES

Figure 1:1: Voltage-current characteristic of CPL load, representing the negative incremental resistance [7,108].	2
Figure 2:1: Compensation methods [7].	11
Figure 2:2: Classification of different methods of compensating CPLs [7].	12
Figure 3:1: v-i characteristics of typical voltage source and loads. [11,111].	18
Figure 3:2: Negative impedance characteristic of CPL [1].	19
Figure 3:3: (a) Resistor circuit, (b) modeling of CPL circuit [9].	20
Figure 3:4: Resistive load (a) load current vs. input voltage (b) load power vs. input voltage.	21
Figure 3:5: Resistor circuit with regulated power converter. [84,112].	22
Figure 3:6: Constant power loads (a) load current vs input voltage (b) load power vs input voltage.	22
Figure 3:7: Schematic diagram of microgrid with CPL [9].	23
Figure 3:8: Block diagram of a microgrid system loaded by a CPL.	25
Figure 3:9: Line current and output voltage of the model of a microgrid system, which has been made unstable by a CPL.	26
Figure 3:10: d-axis model of microgrid.	27
Figure 3:11: q-axis model of microgrid.	27
Figure 3:12: d-axis bus voltage instability due to CPL.	29
Figure 3:13: q-axis bus voltage instability due to CPL.	29
Figure 3:14: Schematic diagram of microgrid with CPL and storage (with active power compensation).	30
Figure 3:15: d-axis model of proposed real power compensation method.	31
Figure 3:16: q-axis model of proposed real power compensation method.	31
Figure 3:17: Schematic diagram of microgrid with CPL and storage (with reactive power compensation).	33
Figure 3:18: d-axis model of proposed reactive power compensation method.	34
Figure 3:19: q-axis model of proposed reactive power compensation method.	34
Figure 4:1: Typical model of microgrid.	38
Figure 4:2: Equivalent circuit of AC microgrid with CPL and CVL [9].	39
Figure 4:3: Movement of system poles with (a) equivalent resistance $R_{eq}$ , (b) equivalent capacitance $C_{eq}$ , (c) equivalent inductance $L_{eq}$ . (d) CVL resistance $R_{CVL}$ (e) CVL inductance $L_{CVL}$ [9].	42
Figure 4:4: Stability status of conventional model.	43
Figure 4:5: Modified model with proposed stability enhancement method (with real power compensation).	44
Figure 4:6: Movement of system poles with (a) equivalent resistance $R_{eq}$ , (b) equivalent capacitance $C_{eq}$ , (c) equivalent inductance $L_{eq}$ . (d) CVL resistance $R_{CVL}$ . (e) CVL inductance $L_{CVL}$ . (f) virtual resistance $R_B$ .	46
Figure 4:7: Stability status of proposed model with active power compensation.	47
Figure 4:8: Stable and unstable region for the conventional(blue) and proposed(red) system from table 1 and equation (4.16) and equation (4.17) where $R_{CVL}$ is varied from 0 : 0.05 : 0.25 ohms.	48

Figure 4:9: Impact of $R_{eq}$ on system stability for both conventional(blue) and proposed(red) system where $R_{eq}$ is varied from 0 : 0.05 : 0.25 Ohms (stability improves with the increases of $R_{eq}$ ).	48
Figure 4:10: Impact of $L_{eq}$ on system stability for both conventional(blue) and proposed(red) system where $L_{eq}$ is varied from 0 : 0.1e-3 : 0.5e-3 H (stability decreases with the increases of $L_{eq}$ ).	49
Figure 4:11: Impact of $C_{eq}$ on system stability for both conventional(blue) and proposed(red) system where $C_{eq}$ is varied from 0 : 2e-4 : 10e-4 F (stability improves with the increases of $C_{eq}$ ).	49
Figure 4:12: Impact of $L_{CVL}$ on system stability for both conventional(blue) and proposed(red) system where $L_{CVL}$ is varied from 0 : 1e-3 : 5e-3 H (stability decreases with the increases of $L_{CVL}$ ).	50
Figure 4:13: Impact of $R_B$ on system stability for both conventional(blue) and proposed(red) system where $R_B$ is varied from 0 : 2 : 10 H (stability increases with the increases of $R_B$ ).	50
Figure 4:14: Modified model with proposed stability enhancement method (with reactive power compensation).	51
Figure 4:15: Movement of system poles with (a) equivalent resistance $R_{eq}$ , (b) equivalent capacitance $C_{eq}$ , (c) equivalent inductance $L_{eq}$ , (d) CVL inductance $L_{CVL}$ , (d) CVL resistance $R_{CVL}$ (f) virtual capacitance $C_B$ (g) virtual inductance $LB$ .	53
Figure 4:16: Stability status of proposed microgrid system with reactive power compensation.	54
Figure 4:17: Stable and unstable region for the conventional(blue), with active power compensation(red) and with reactive power compensation(green) system from table 1 and equation (4.19), equation (4.20) and equation (4.21) where $R_{CVL}$ is varied from 0 : 0.1 : 0.25 ohms.	55
Figure 4:18: Impact of $R_{eq}$ on system stability for both conventional(blue), with active power compensation(red) and with reactive power compensation(green) system where $R_{eq}$ is varied from 0 : 0.05 : 0.25 ohms (stability improves with the increases of $R_{eq}$ ).	56
Figure 4:19: Impact of $L_{eq}$ on system stability for both conventional(blue), with active power compensation(red) and with reactive power compensation(green) system where $L_{eq}$ is varied from 0 : 0.1e-3 : 0.4e-3 H (stability decreases with the increases of $L_{eq}$ ).	56
Figure 4:20: Impact of $C_{eq}$ on system stability for both conventional(blue), with active power compensation(red) and with reactive power compensation(green) system where $C_{eq}$ is varied from 0 : 2e-6 : 10e-6 F (stability improves with the increases of $C_{eq}$ ).	56
Figure 4:21: Impact of $L_{CVL}$ on system stability for both conventional(blue), with active power compensation(red) and with reactive power compensation(green) system where $L_{CVL}$ is varied from 0 : 1e-3 : 5e-3 H (stability decreases with the increases of $L_{CVL}$ ).	57
Figure 4:22: Impact of $R_B$ on system stability for both conventional(blue), with active power compensation(red) and with reactive power compensation(green) system where $R_B$ is varied from 0 : 2 : 10 Ohm (stability increases with the increases of $R_B$ ).	57

Figure 4:23: Impact of $C_B$ on system stability for both conventional(blue), with active power compensation(red) and with reactive power compensation(green) system where $C_B$ is varied from 0 : 0.2e-6 : 1e-6 F (stability increases with the increases of $C_B$ ). .....	58
Figure 4:24: Impact of $LB$ on system stability for both conventional(blue), with active power compensation(red) and with reactive power compensation(green) system where $LB$ is varied from 0 : 0.2e-3 : 1e-3 H (stability decreases with the increase of $LB$ ). .....	58
Figure 5:1: Modified controller model of microgrid system to implement the proposed storage base virtual resistor stabilization technique. ....	61
Figure 5:2: Simulation platform of proposed controller using PID control technique .....	62
Figure 5:3: Comparison between the Input and Output Parameters (voltage and current) after adopting proposed compensation technique. ....	63
Figure 5:4: Contribution of the battery compensator in case of voltage, current, SOC, and power. ....	63
Figure 5:5: Comparison between input and output (voltage and current) of the microgrid system before adopting compensation technique. ....	64
Figure 5:6: Comparison of input and output power (both real and reactive) after adopting the proposed compensation technique. ....	65
Figure 5:7: Representation of CPL-loaded system with controlled current source. ....	65
Figure 5:8: Representation of CPL load performance parameters (terminal voltage, current and power) .....	66
Figure 5:9: Representation of CVL load performance parameters (terminal voltage, current and power) .....	67
Figure 5:10: Reference voltage, microgrid output voltage, error signal, and the control signal regarding the proposed PID controller. ....	67
Figure 5:11: (a) Block diagram of the proposed controller using PID control technique, (b) gate signal of the MOSFET/ diode universal bridge. ....	68
Figure 5:12: Schematic representation of sliding mode control scheme [69]. ....	70
Figure 5:13: Chattering as a result of imperfect control switching [43]. ....	71
Figure 5:14: Matlab/Simulink schematic model of sliding mode control of microgrid. ....	75
Figure 5:15: The schematic diagram of a microgrid system, which has been made unstable by a CPL while control inputs are absent. ....	79
Figure 5:16: The terminal voltage (active) of CPL while using SMC control technique. ....	80
Figure 5:17: The terminal voltage (active) of CPL while using SMC control technique chattering free. ....	80
Figure 5:18: The terminal voltage (reactive) of CPL while using SMC control technique. ....	81
Figure 5:19: Line current $i_L$ (active) of system while using SMC control technique. ....	81
Figure 5:20: Line current $i_L$ (reactive) of system while using SMC control technique. ....	82
Figure 5:21: CVL current $i_{CVL}$ (active) of system while using SMC control technique. ....	82
Figure 5:22: CVL current $i_{CVL}$ (reactive) of system while using SMC control technique. ....	83
Figure 5:23: Storage current $i_b$ (active/ d axis current) of system while using SMC control technique. ....	83
Figure 5:24: Storage current $i_b$ (reactive/ q axis current) of system while using SMC control technique. ....	84

Figure 5:25: Performance comparison between PID (blue) and SMC (red) in the case of (a) real axis output voltage ( $V_d$ ), (b) reactive axis output voltage ( $V_q$ ) for nonlinear system applications. ....	100
Figure 5:26: Performance comparison between PID (blue) and SMC (red) in the case of (a) real axis output voltage ( $V_d$ ), (b) reactive axis output voltage ( $V_q$ ) considering parametric uncertainties. ....	101
Figure 5:27: Performance comparison between PID (blue) and SMC (red) in the case of (a) real axis output voltage ( $V_d$ ), (b) reactive axis output voltage ( $V_q$ ) considering noise rejection. ....	102
Figure 5:28: d-axis current comparison between robustness analysis against parametric variation and robustness analysis against parametric uncertainties, frequency variation, and additive gaussian noise using SMC control technique based on boundary conditions. ....	103
Figure 5:29: q-axis current comparison between robustness analysis against parametric variation and robustness analysis against parametric uncertainties, frequency variation, and additive gaussian noise using SMC control technique based on boundary conditions. ....	104
Figure 5:30: d-axis bus voltage comparison between robustness analysis against parametric variation and robustness analysis against parametric uncertainties, frequency variation, and additive gaussian noise using SMC control technique based on boundary conditions. ....	104
Figure 5:31: q-axis bus voltage comparison between robustness analysis against parametric variation and robustness analysis against parametric uncertainties, frequency variation, and additive gaussian noise using SMC control technique based on boundary conditions. ....	105
Figure 5:32: d-axis current (CVL load) comparison between robustness analysis against parametric variation and robustness analysis against parametric uncertainties, frequency variation, and additive gaussian noise using SMC control technique based on boundary conditions. ....	105
Figure 5:33: q-axis current (CVL load) comparison between robustness analysis against parametric variation and robustness analysis against parametric uncertainties, frequency variation, and additive gaussian noise using SMC control technique based on boundary conditions. ....	106
Figure 5:34: d-axis current compensation (d-axis control signal) comparison between robustness analysis against parametric variation and robustness analysis against parametric uncertainties, frequency variation, and additive gaussian noise using SMC control technique based on boundary conditions. ....	106
Figure 5:35: q-axis current compensation (q-axis control signal) comparison between robustness analysis against parametric variation and robustness analysis against parametric uncertainties, frequency variation, and additive gaussian noise using SMC control technique based on boundary conditions. ....	107
Figure 5:36: Matlab/Simulink schematic model of Lyapunov redesign control of microgrid. ....	112
Figure 5:37: Control signal of system while using Lyapunov redesign control technique. ..	115
Figure 5:38: d axis current of $i_L$ while using Lyapunov redesign control technique. ....	115
Figure 5:39: q axis current of $i_L$ while using Lyapunov redesign control technique. ....	116

Figure 5:40: The d axis terminal voltage of CPL while using Lyapunov redesign control technique.....	116
Figure 5:41: The q axis terminal voltage of CPL while using Lyapunov redesign control technique.....	117
Figure 5:42: d axis current of CVL while using Lyapunov redesign control technique.....	117
Figure 5:43: q axis current of CVL while using Lyapunov redesign control technique.....	118
Figure 5:44: Performance comparison between the PID (blue) and LRC (red) in the case of (a) real axis output voltage (Vd), (b) reactive axis output voltage (Vq) for nonlinear system applications.....	137
Figure 5:45: Performance comparison between the PID (blue) and LRC (red) in the case of (a) real axis output voltage (Vd), (b) reactive axis output voltage (Vq) considering parametric uncertainties. ....	138
Figure 5:46: Performance comparison between the PID (blue) and LRC (red) in the case of (a) real axis output voltage (Vd), (b) reactive axis output voltage (Vq) considering noise rejection. ....	139
Figure 5:47: d-axis current comparisons between robustness analysis against parametric variation and robustness analysis against parametric uncertainties, frequency variation, and additive gaussian noise using Lyapunov redesign control technique based on boundary conditions. ....	140
Figure 5:48: q-axis current comparisons between robustness analysis against parametric variation and robustness analysis against parametric uncertainties, frequency variation, and additive gaussian noise using Lyapunov redesign control technique based on boundary conditions. ....	141
Figure 5:49: d-axis bus voltage comparisons between robustness analysis against parametric variation and robustness analysis against parametric uncertainties, frequency variation, and additive gaussian noise using Lyapunov redesign control technique based on boundary conditions. ....	141
Figure 5:50: q-axis bus voltage comparisons between robustness analysis against parametric variation and robustness analysis against parametric uncertainties, frequency variation, and additive gaussian noise using Lyapunov redesign control technique based on boundary conditions. ....	142
Figure 5:51: d-axis current (CVL load) comparisons between robustness analysis against parametric variation and robustness analysis against parametric uncertainties, frequency variation, and additive gaussian noise using Lyapunov redesign control technique based on boundary conditions.....	142
Figure 5:52: q-axis current (CVL load) comparisons between robustness analysis against parametric variation and robustness analysis against parametric uncertainties, frequency variation, and additive gaussian noise using Lyapunov redesign control technique based on boundary conditions.....	143
Figure 5:53: d-axis current compensation (d-axis control signal) comparisons between robustness analysis against parametric variation and robustness analysis against parametric uncertainties, frequency variation, and additive gaussian noise using Lyapunov redesign control technique based on boundary conditions.....	143
Figure 5:54: q-axis current compensation (q-axis control signal) comparisons between robustness analysis against parametric variation and robustness analysis against	

parametric uncertainties, frequency variation, and additive gaussian noise using Lyapunov redesign control technique based on boundary conditions.....	144
Figure 5:55: Performance comparison between the SMC (blue) and LRC (red) in the case of (a) d- axis output voltage, (b) q- axis output voltage considering CPL power variation and parametric uncertainties.....	147
Figure 5:56: Performance comparison between the SMC (blue) and LRC (red) in the case of (a) d-axis control input current (U1), (b) q-axis control input current (U2) considering CPL power variation and parametric uncertainties.....	148
Figure 6:1: Comparisons of various electrochemical storage devices in energy density, power density and charging time [106]. .....	151
Figure 6:2: Microgrid bus voltage without any compensation (in the presence of CPL).....	152
Figure 6:3: Simulation platform for entire microgrid system using compensator unit in Matlab/Simulink. ....	153
Figure 6:4: The characteristics of the battery terminal voltage, current, SOC, and power (in the presence of CPL) when battery-only is used as compensator. ....	154
Figure 6:5: The simulation platform for performance comparisons between battery-only compensator and ultracapacitor-only compensator. ....	155
Figure 6:6: (a) Representation of the battery power support and the power demand, (b) representation of the transient power demand and respective battery support... ..	156
Figure 6:7: Load profile of CPL-loaded microgrid system. ....	156
Figure 6:8: (a) Representation of the ultracapacitor power support and power demand, (b) representation of the transient power demand and respective ultracapacitor support. ....	158
Figure 6:9: Characteristics of the ultracapacitor terminal voltage, current, SOC, and power (in the presence of CPL) when ultracapacitor-only is used as compensator.....	159
Figure 6:10: Hybrid energy storage system for microgrid [73].....	160
Figure 6:11: Basic structure of hybrid energy storage system.....	161
Figure 6:12: Energy management algorithm form hybrid energy storage system (in the presence of CPL). ....	161
Figure 6:13: Microgrid bus voltage (in the presence of hybrid energy CPL) when storage system is used as compensator. ....	162
Figure 6:14: Microgrid current (in the presence of CPL) when hybrid energy storage system is used as compensator.....	162
Figure 6:15: Microgrid frequency (in the presence of CPL) when hybrid energy storage system is used as compensator. ....	163
Figure 6:16: Microgrid power (in the presence of CPL) when hybrid energy storage system is used as compensator. ....	163
Figure 6:17: Characteristics of the HESS terminal voltage, current, SOC, and power (in the presence of CPL) when hybrid energy storage system is used as compensator. ....	164
Figure 6:18: Performance comparisons of microgrid bus voltage (in the presence of CPL) among battery-only compensator, ultracapacitor-only compensator, HESS compensator.....	164
Figure 7:1: Grid energy storage technology and applications [82].....	170

# LIST OF TABLES

Table 4-1: Table of Parameters.....	54
Table 5-1: Boundary Conditions.....	108
Table 6-1: Battery vs Ultracapacitor Parameters [82]. .....	153
Table 7-1: Detailed Classification of Microgrid [18]. .....	169
Table 7-2: Reactive Power Compensator in Microgrid Technology [81]. .....	171

# LIST OF ABBREVIATIONS

<b>Abbreviation</b>	<b>Elaboration</b>
CPL	Constant Power Load
CVL	Constant Voltage Load
PID	Proportional Integral Derivative
SMC	Sliding Mode Control
LRC	Lyapunov Redesign Control
POL	Point of Load
CIL	Constant Impedance Load
DC	Direct Current
AC	Alternative Current
PWM	Pulse Width Modulation
CCL	Constant Current Load
DPS	Distributed Power System
VAR	Volt-Ampere Reactive
STATCOM	Static Synchronous Compensator
CCM	Continuous Conduction Mode
DCM	Discontinuous Conduction Mode

RMS	Root Mean Square
LHP	Left Half Plane, Left Hand Side of s-Plane
RHP	Right Half Plane, Right Hand Side of s-Plane
HESS	Hybrid Energy Storage System
LC	Inductive Capacitive Filter Component
KVL	Kirchhoff's Voltage Law
KCL	Kirchhoff's Current Law
DQ axis	Direct Quadrature Axis
AWGN	Additive White Gaussian Noise
EDLC	Electrochemical Double Layer Capacitors
SOC	State Of Charge
FACT	Flexible Alternating Current Transmission
UPS	Uninterruptible Power Supply

## LIST OF NOMENCLATURE

<b>Symbol</b>	<b>Unit</b>	<b>Elaboration</b>
$P_{CPL}$	Watt	Value of the constant power load
$d$	Dimensionless	Duty Cycle
$T$	Second	Switching Period
$V_{REF}$	Volt	Reference Voltage
$V_{output}$	Volt	Microgrid Output Voltage
$f_{SW}$	Hz	Switching Frequency of the Converter
$V_{in}$	Volt	System Input Voltage
$R_{eq}$	Ohm	Equivalent Resistance of Microgrid
$L_{eq}$	Henry	Equivalent Inductance of Microgrid
$C_{eq}$	Farad	Equivalent Capacitance of Microgrid
$\omega$	Rad/s	Speed Term
$V_S$	Volt	Supply Voltage of Microgrid
$V$	Volt	Voltage
$I$	Ampere	Current
$F$	Hz	Frequency
$X_{1(abc)}$	Ampere	Line Current of the System

$X_{2(abc)}$	Volt	Equivalent Capacitor Voltage
$X_{3(abc)}$	Ampere	Load Current of CVLs
$X_{1(dq)}$	Ampere	Active Line Current of the System
$X_{2(dq)}$	Ampere	Reactive Line Current of the System
$X_{3(dq)}$	Voltage	Active Terminal Voltage of CPL
$X_{4(dq)}$	Voltage	Reactive Terminal Voltage of CPL
$X_{5(dq)}$	Ampere	Active CVL Current of the System
$X_{6(dq)}$	Ampere	Reactive CVL Current of the System
$s$	Dimensionless	Sliding Surface
$e$	Dimensionless	Error Function
$v$	Dimensionless	Lyapunov Function
$R_B$	Ohm	Equivalent Resistance of the Battery
$C_B$	Farad	Equivalent Capacitance of the Battery
$L_B$	Henry	Equivalent Inductance of the Battery
$\beta$	Dimensionless	Switching Gain Function
$\kappa$	Dimensionless	Controller Gain
$\delta$	Dimensionless	Boundary Limit
$u$	Ampere	Control Input of the System
$\eta$	Dimensionless	Efficiency

$A$	Dimensionless	Eigen Value Matrix
$P$	Dimensionless	Polynomial Matrix
$L$	Henry	Inductor Value of the Convertor's LC Filter
$C$	Farad	Capacitor Value of the convertor's LC Filter
$P$	Watt	Power
$I_L$	Ampere	Load Current
$P_L$	Watt	Power Dissipated
$R_{CVL}$	Ohm	Equivalent Linear Resistance of CVL
$R_{CPL}$	Ohm	Equivalent -ve Incremental Resistance, CPL
$L_{CVL}$	Henry	Equivalent Inductance of CVL

# ACKNOWLEDGMENTS

To begin with, I am grateful to the almighty creator, to whom we belong and to whom we will return, for uncountable blessings. Next, I would like to express my sincere gratitude to my advisor Professor Ron Perez and Professor Adel Nasiri for their continuous support, motivation, and patience throughout my PhD study and research. Their continuous guidance and wise advice always helped me to do innovative research. Without the torch of their extensive knowledge in my research field, it would have not been possible for me to make a strong contribution in the field of renewable energy, microgrid, and advanced control systems. I would like to thank Prof. Anoop Dhingra, Prof. Brian Armstrong, and Prof. Yaoyu Li from the bottom of my heart for recognizing my potential and for their tremendous help during the initial phase of my PhD. I would also like to thank my committee members and Prof. Ramazan Bayindir for their valuable suggestions and discussions that enriched my research dissertation.

I would like to thank all my colleagues and friends for sharing their ideas and research experiences with me. I would like to express my special gratitude to Luke Weber, Abedalsalam, and Ahmad Hamidi.

Finally I would like to thank my wife, parents, and siblings for their unconditional love and care. Their selfless support and motivation inspired me during this long journey.

# **Chapter 1 : Introduction**

## **1.1 Introduction**

Today the power industry faces many problems including rising cost of energy, power quality and stability, aging infrastructure, mass electrification, climate change, and so on [19]. Moreover, fossil fuel availability and cost, quality of power, stability issues and many more problems are arising today in the power system industry. To reduce carbon emissions and make environment-friendly power generation systems, there will be no choice but to adopt renewable energy. Hence, distributed power systems are becoming popular nowadays and researchers have focused on this emerging technology. Microgrid is a compact organization of interconnected loads as well as distributed energy resources within specified electrical boundaries, functioning as a single controllable individual with respect to the grid. In this way, it can connect to and disconnect from the conventional grid to enable it to operate in both grid-connected and islanded modes [18].

However, managing distributed resources (renewables, conventional, storage) and loads within a microgrid in case of islanded and grid-tied modes and the transition between several phases is a challenge [107]. It requires both short-term and long-term stability analysis of microgrid systems for reliable operation. Furthermore, there are several key control concerns for microgrid such as maintaining stability, regulating voltage and frequency, sharing active and reactive load, and handling various types of loads, for example inductive motor load and constant power load. The constant power load has a negative impedance effect towards the system which causes huge stability concerns for inverter-based power systems. However, microgrids, multi-converter cascaded systems, is strictly regulated point-of-load (POLs) converters those exhibits negative incremental impedance and, in practice, act as CPLs. This

behavior causes a serious stability concern for microgrid systems since the overall system is poorly damped [6]. The constant power load characteristics curve is shown in Figure 1.1.

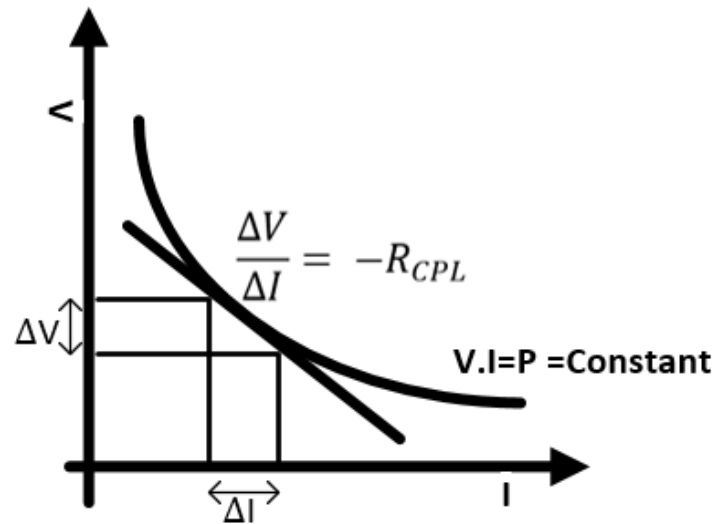


Figure 1.1: Voltage-current characteristic of CPL load, representing the negative incremental resistance [7,108].

Based on load function, electrical loads can be classified into two main types: constant impedance loads (CIL) and constant power loads (CPL). Traditional loads are of the former category, e.g. incandescent lighting, induction motors, resistive heating, etc. These typically present constant impedance to the electrical network and are modelled by a resistor or resistor- inductor combination. Since the early days of electrical energy, these have been the only loads which grid operators have faced. However, with the arrival of modern micro/power electronics, non-traditional loads have been appeared which do not behave in a similar way in power systems. Non-traditional loads such as switch-mode supplies with regulation, back-to-back converters, electric motor drives, and power electronic circuits fall into this second category called constant power loads.

Today's devices require strict control and regulation of operating parameters to function. Strictly regulated point-of-load converters mean that the power output of these devices remains constant, even though the input voltage changes. The use of active rectifiers is

becoming a wide-spread choice as the preferred interface for loads in distribution systems with the increasing concern on power quality issues [8]. As electronic loads increase, the proportion of CPLs in the overall load will rise. This change in proportion brings about problems in system stability due to CPL characteristics. While these problems were known before, the fraction of CPL was too small to demand much concern. With changes occurring worldwide in both ways, electrical energy distribution and consumption, these problems now require further investigation. Within the last decade, a number of research works have been done to overcome the CPLs instability issue. But, none of them are able to provide the comprehensive solution of this phenomenon with sensitivity analysis of the entire system and appropriate compensation technique for microgrid application. Therefore, more research work is still required in this field.

In this dissertation, the recent developments in compensation techniques to solve this problem will be presented. Besides that, a novel technique will be proposed to handle this problem; robustness analysis will be included. To support the system performance, necessary mathematical analysis, and simulation results performed in Matlab/Simulink will be presented as a tool of verification.

## **1.2 State of Art**

A general microgrid with two distributed generators supplying a CPL is studied in [2]. It shows the dependence of stability on the proportion of CPL and CIL. It also outlines simple methods of improving stability by changing R/L value of distribution feeders, increasing C by adding capacitors, or by raising the bus voltage level. However, modifying the distribution feeders is often not a feasible option and adding capacitance to stabilize a system is comparatively expensive. Similarly, increasing the bus voltage may not be an option since

most protection devices only work at certain voltages and that cannot be changed. Thus, alternative methods are being investigated to provide stability for microgrids. The research work on CPLs in microgrid applications is categorized into two sections: DC microgrid applications and AC microgrid applications. The majority of the work on control techniques for microgrid stabilization has been done in the former category.

### 1.2.1 Stability Issues in DC Microgrids

In [3], Kwasinski and Onwuchekwa outlined the typical strategies for mitigating the problems of CPL in DC microgrids. In this discussion, the effect of adding filters and capacitors was studied. But, this is an expensive system with the additional problem of capacitor failure which increases with rated voltage. Load shedding of CPLs can restore stability, but this is of little practical value since it only temporarily restores the system without increasing long-term capacity. Linear and non-linear controllers can also be used but the former cannot guarantee global stability of the desired equilibrium point and the latter is very challenging in its design and changing with each system's parameters. Stabilizing power can be generated and sent to the load power reference for slightly modifying the CPL behavior of the load. Using such a constrained optimization technique, a method to design the stabilizing system is proposed in [4]. Coupling two systems together can allow the oscillating characteristics of the two systems to dampen each other out [5]. The systems may have slightly different characteristics, usually different inductances, or they may be identical, but coupled with a small delay factor. Mathematical analysis for two systems has been done to find the region of stability. However, with large systems, the stability characteristics become more difficult to establish. To use the original, non-linear models of the system, sliding mode control has been implemented in DC microgrids [6] by finding a sliding surface and using a discontinuous sliding-mode controller to improve voltage stability. The mechanism of

instability and oscillation along with some passive methods for compensating CPLs are explained and a novel method of compensating CPLs based on the feedback linearization technique of nonlinear system have been proposed by Amir M. Rahimi, which is a comprehensive overview of the stabilizing control methods for power electronic converters [7]. In [12], Jesse Leonard has proposed the Volterra Series to model nonlinear responses of constant power loads through Volterra kernel measurement by using a switch-mode power converter to synthesize large-signal perturbations to measure frequency domain Volterra kernels. Alireza Khaligh at [13,109] has proposed a fixed frequency pulse adjustment digital control technique to mitigate the constant power load instability. Xiaonan Lu at [14] proposed a virtual resistance based method to improve the stability status of DC microgrid by impedance matching approach. Fei Zhao and Ningning Li at [15] showed eigenvalue analysis of highly nonlinear loads. Santiago Sanchez at [16] introduced a comprehensive analysis with the nonlinear tools for stability in operating systems influenced by the interconnection of power electronics and delivered by the discrete generation. Here, systems like renewable as well as non-renewable energy sources can easily supply power to the microgrid, and their loads function as CPL. Hence, the inspection of Hopf bifurcation points is applied to prevent oscillations and instabilities in the operating system. Awang bin Jusoh at [1] has presented an analysis of constant power load instability of DC microgrid by using small signal analysis and passive damping method.

A multi-converter with a centralized stabilizer for a DC microgrid was designed by Mehdi Karbalaye Zadeh and Bijan Zahedi et al at [90]. After that, in [40], Vinicius Stramosk and Daniel J. Pagano proposed a novel Sliding Mode Controller to control the DC bus voltage precisely. In like manner, a non-linear sliding surface was proposed by the two researchers from the Indian Institute of Technology Jodhpur, Suresh Singh and Deepak Fulwani at [91, 99] to mitigate CPL instability. Their proposed non-linear surface confirmed that the constant

power was maintained, in practice, by the converter. Thus, the proposed controller was necessarily able to mitigate the CPL's oscillating effect of tightly regulated POLs and assured the stable operation of DC micro-grid under a number of disturbances. In [42, 51], a precise geometric control using circular switching surfaces was proposed for CPL based electric vehicle's power system by Matias Anun et al.

On another occasion, in [92], Santiago Sanchez and Marta Molina presented the approach to estimate the grid impedance by using two different techniques, such the Kalman filtration method and the recursive least squares method. Apart from that, for the automotive power systems, Mahesh Srinivasan and Alexis Kwasinski presented the autonomous control technique of a DC microgrid at [93]. In [94], Marco Cupelli et al investigated the application of adaptive back-stepping to deal with the voltage stability of the DC microgrids. On another occasion at [95], researchers Ahmed-Bilal Awan et al, in their paper, addressed the global stability analysis of the regarding electrical system consisted of the DC power supply, an actuator, and an LC Filter. In this case, they used Circle Criterion to study the global stability of the system. Besides that scenario, at [96], M. Ashourloo et al, in their paper, addressed stability problems of the CPLs and proposed a simple active damping strategy to efficiently dampen the oscillations caused by CPLs. Marco Cupelli et al adopted the particle swarm optimization algorithm to find the best values of the parameters at [97]. After that, Sheng Liu et al at [98,110] worked on modeling and small-signal stability analysis of an islanded DC microgrid with dynamic loads.

Apart from that, researchers Aditya R. Gautam et al presented, at [99], a robust sliding mode control technique is introduced to investigate CPL instability. On another occasion at [109], Suresh Singh and Deepak Fulwani researched on voltage regulation and stabilization of DC/DC buck converter under constant power loading. Here, it dealt with the stabilization and voltage control of DC/DC buck converter feeding a combination of the CVL and CPL in DC

microgrid applications. Besides that, in [101], Shirazul Islam and Sandeep Anand from IIT Kanpur focused on the stability analysis of the microgrid treating the converter interfaced loads as constant power loads. Virtual impedance based compensation technique is analyzed for DC microgrid by Xiaonan Lu et al at [102]. On another occasion, at [103], M. Su et al analyzed the factors which engendered major instability of a DC microgrid with the multiple DC-DC converters. In this course, they presented two stabilization methods for two operation modes: one was constant voltage source mode and another was droop mode. At [104], by M. Srinivasan and A. Kwasinski, in their paper, the stability analysis of the microgrid was presented using the droop loop control technique. At [105], Gustavo Cezar et al researched in a paper on stability of interconnected DC converters. In particular, this paper addressed the stability issues of DC networks with CPLs.

### 1.2.2 Stability Issues in AC Microgrids

For AC systems, an investigation of stability has been carried out in [2, 8]. Injection of reactive VAR to support voltage stability of AC grid by using a distributed static synchronous compensator (STATCOM) has been demonstrated. Feedback from output taken to modify reference levels and introduce virtual resistance for increased damping has also been shown to be an efficient method of improving AC microgrid stability [9]. The proposed controller modifies the system transfer function by adding a virtual resistor. The proportion of power between CPL and CVL for stability is changed to insure the desired stability condition. In this way, virtual damping is used to improve stability without the cost of wasted energy. Though this improves the loading limit, the enhancement is not substantial and the upper limit of the amelioration remains quite unchanged. An observer-based nonlinear controller can also be used by adopting the input-output feedback linearization [10]. It offers the advantage of robustness analysis against the parametric uncertainties. The usual methods that

can be applied to stabilize CPLs, especially in automotive systems, have been summarized in [11] with broad categorizations of converter-level analysis and control, large-signal phase plane analysis, and system-level analysis. Vilathgamuwa, D.M. et al obtained the state space model from physical microgrid system. And from that, they accomplished the linearized plant stability analysis with constant power load by using PID control technique [2]. Zeng Liu and Jinjun Liu at [22] proposed the technique to investigate the stability condition for AC system by using Nyquist Stability Criterion.

In [83], four-wire-grid architecture has been achieved by Santiago Sanchez Acevedo and Marta Molinas for islanded microgrid operation. Dq frame analysis is shown for three-phase AC system to investigate small signal stability at [62]. Besides that, the stability criterion for Distributed Power System (DPS) analysis is presented using infinite norms input-output impedance matrix by Zeng Liu et al at [57]. In 2013, Nadeem Jelani et al at [41] investigate how the voltage stability is affected with the rising proportion of the CPL loads to the system and proposed the static synchronous compensator to solve the CPL instability problem. After that, in [27], Dena Karimipour and Farzad R. Salmasi, based on Popov's Absolute Stability Criterion, introduced stability analysis of the AC microgrid system. At [23] of Yanjun Dong et al, developed a simulation model for constant power loads in AC system by using Pulse Width Modulation rectifier. In the sequence of these developments, in [22], Zeng Liu et al, by using infinite-norm of the impedance (admittance) matrixes, investigated stability of the power system by adopting boost rectifier as a constant power load.

After that, in [17], researcher Nadeem Jelani et al have shown a phase margin analysis of a AC distribution system by using vector control techniques where voltage source converter used as a constant power load. On another occasion, Ali Emadi at [84], in his paper, using the generalized state-space averaging method, they modeled negatively incremental CPL loads

and presented a comprehensive assessment in case of AC distribution systems. Besides that, in [85], Mohd Fakhizan Romlie et al, using simulation in PSCAD, investigated the stability as a function of system parameter in application of constant power loads (CPL) in DPS. P.J.M. Heskes, J.M.A. Myrzik, and W.L. Kling discussed the effect of negative differential impedance loads on voltage stability in local power grid at [86]. Apart from that, in [87], Nadeem Jelani et al, in their article, used shunt filter as a CPL load compensator by using vector control techniques and discrete Fourier transformation. After that, Immersion and Invariance control technique, at [88], and single phase matrix control (SPMC) technique, at [89], were introduced for analyzing CPL instability.

### **1.3 Problem Statement**

Power System loads can be classified into two basic categories. One is constant voltage load, which maintains a constant voltage drop and the equivalent resistance of this kind of load remains constant, and the other kind is the constant power loads, like modern power electronics based devices such as Converter and Inverter which have internal voltage control strategy that can regulate the output voltage. It exhibits negative impedance characteristics, i.e. when the output current is decreasing, the output voltage is increasing, or vice versa to maintain the constant power throughout the device, thus acting like constant power loads. This type of constant power load has a negative impact on microgrid stability and can cause a blackout or brownout situation. To overcome this severe problem, specialized concentration in this field is required. Negative impedance of constant power loads causes a destabilizing effect on microgrids leading to voltage level oscillations. As the proportion of constant power loads to constant impedance loads increases, this problem is aggravated. So, a control technique should be developed which will be robust, cost effective, and viable in both islanded and grid-tied mode operations to assure the desired stability of the microgrid system.

As has been seen from the literature review, most of the research works have been done on DC distribution systems. Researchers endeavored to linearize the nonlinear CPL Loads around an operating point and used linear control techniques to maintain system stability. However, the majority of the CPL characteristics have been reduced by linearizing the highly nonlinear CPL loads; this simplification hampers the proper stability functioning. Moreover, with the advancement of technology, the power electronic interfaced renewable resources and loads are increasing dramatically in power system/microgrid applications. So, the necessity to stabilize continually increasing CPL based system is intensified day by day. Hence, more research is required to be conducted in the area of AC distributed system and the investigation of nonlinear control techniques is to be demonstrated in detail. Since the proportion of the constant power load is increasing in advanced power system applications, it is necessary to take care or handle the real and reactive power compensation independently. Apart from that, in case of compensation technology, the conventional storage system is only comprised of the energy density unit which does not experience a sound functionality in microgrid arrangement. In course of highly variable distributed energy systems like renewable energy sources, the scenario is intensified. In this particular case, the storage is to provide high power density with quick charging and discharging time to maintain transient and steady state instability introduced by CPL loads; hence the point load compensation has to be adopted. Finally, a detail parameter sensitivity analysis will help the researchers in this area to select appropriate compensation techniques needed to be addressed.

## Chapter 2 : Available Compensation Techniques for CPLs and Prior Art

### 2.1 Introduction

During the literature review for our research studies, we have noticed that all available techniques for CPLs compensation can be classified into several groups of common criteria based on the location of providing compensation. This classification is mentioned below.

- Compensation done in feeder side to make the system robust against CPL instability.
- Compensation done by adding intermediate circuitry or elements between the feeder side and load to enhance system stability.
- Compensation done in load side so that the system doesn't experience the effect of constant power loads.



Figure 2:1: Compensation methods [7].

A hierarchical diagram for various methods of CPLs compensation has been represented in figure 2.1 and the proposed new methods for CPLs compensation from the load side will be discussed in detail in the next chapters.

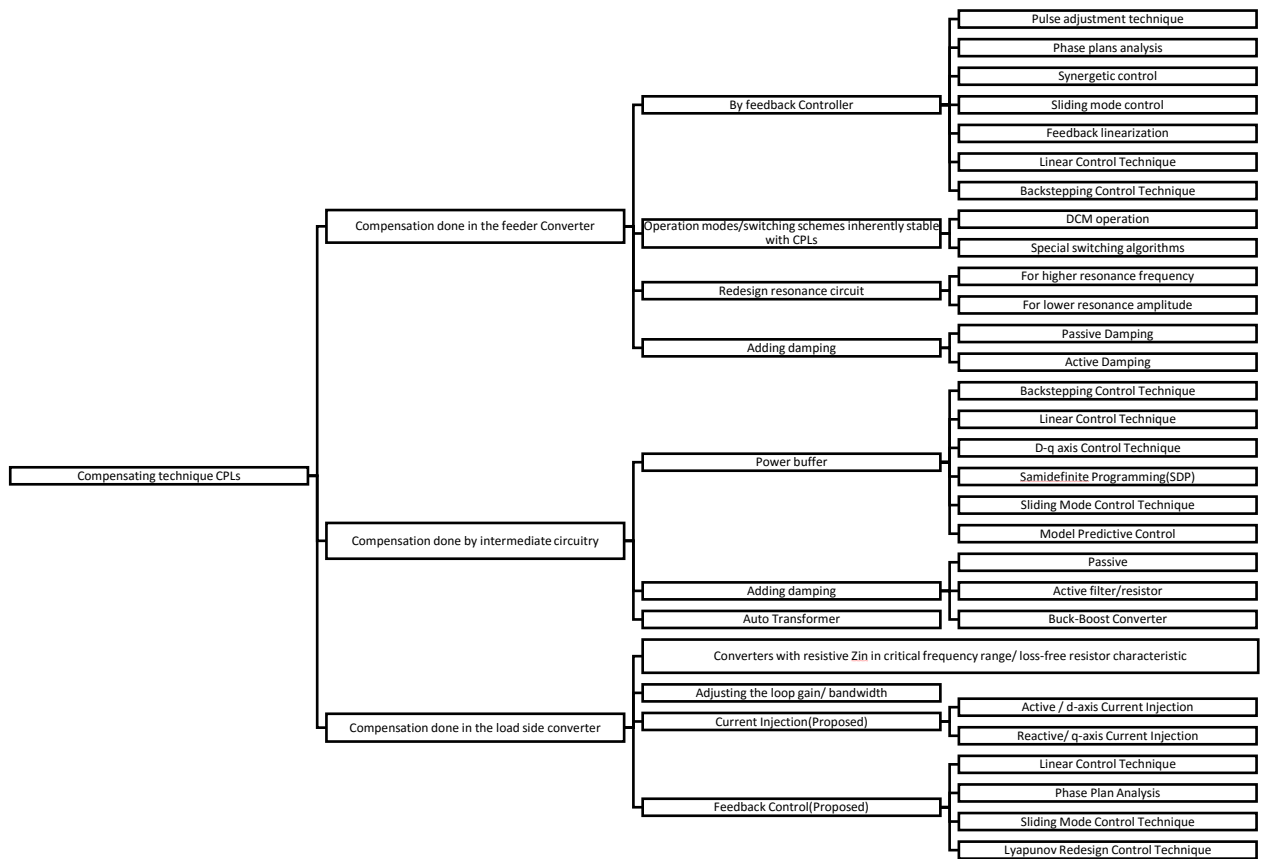


Figure 2:2: Classification of different methods of compensating CPLs [7].

## 2.2 Feeder Side Compensation

In this category, researchers try to modify the feeder side parameters such as voltage and current controller gain of the feeder side. The available methods in this category are listed below.

- By Using Feedback Controller
  - Pulse adjustment technique [26]
  - Phase plane analysis [21,25,16,35,44,64,66]
  - Synergetic control [67,68,69]
  - Sliding mode control [6,33,40,43,45,47]

- Feedback linearization [20,10,24,59]
- Linear control technique [56,62]
- Back stepping control technique [31]
- By Controlling Switching Modes
  - DCM operation [22,23,54]
  - Special switching algorithms [17,3,61]
- By Redesigning Resonance Circuit
  - For higher resonance frequency [2]
  - For lower resonance amplitude [5]
- By Adding Damping
  - Passive damping
  - Active damping [9]

### **2.3 Compensation by Adding Intermediate Circuitry or Element**

In this method, some intermediate circuitry or element is implemented whether in series or in parallel which prevents the feeder side to experience the load as constant power loads besides providing necessary compensation. Some of the techniques in this category are listed below.

- By Inserting Power Buffer [41,42,51]
  - Backstepping control technique [30]
  - Linear control technique [14,15,29,46]
  - D-q axis control technique [27,28,50]
  - Semi-definite Programming (SDP) [32]
  - Sliding mode control technique [34]
  - Model predictive control [60]

- By Adding Damping
  - Passive damping [8,37,39,52,53,63,65]
  - Active filter/resistor [4,36,38,55]
  - Buck-Boost Converter [48,49,57]
- By Using Auto-transformer [58]

## **2.4 Compensation by Load Side Converter**

In this method, researchers try to manipulate the load side by inserting supplementary arrangement such that the CPLs are not viewed by feeder side and providing necessary compensation to maintain system stability. Techniques fall in to this category are mentioned below.

- By Using Converter with Loss Less Resistor [70]
- By Regulating the Loop Gain/ Bandwidth
- By Injecting Current from the Load Side [Proposed]
  - Active current injection
  - Reactive current injection
- By feedback control [Proposed]
  - Sliding mode control
  - Lyapunov Redesign technique
  - Linear control technique
  - Phase plans analysis

## **2.5 Constant Power Loads in Microgrids**

With the advancement of technology, applications of power electronics devices is rising, thus increasing constant power loads (CPLs) in a tremendous rate which creates more effects on stability in power systems especially in distributed power system like microgrid systems. In most of the microgrid systems, loads are in the generation side. So, load side stability management is the key in microgrid system and that's why we select load side compensation. Moreover, load side compensation is point load compensation which means it can be accomplished in the certain point we desire. Microgrid loads can be categorized into several types such as controllable loads and critical loads. Controllable loads include Electric Vehicle charging stations, heat pumps etc, and data center, security system are fallen into the category of critical loads. Critical loads consisting of both constant power loads (CPLs) and constant voltage loads (CVLs) require proper attention for better performance. To ensure so, managing those sensitive loads from the load side is the best way of compensation to maintain system stability. In microgrid applications, it is good practice to use load side compensation of CPLs instability due to combination of CPLs and CVLs. Moreover, in this practice, we can combine all CPLs in one single branch to handle their voltage collapse phenomena. In that case, we are compensating where it is required only.

Furthermore, microgrid bus/feeder consists of several intermitting sources where there is always some voltage/generation mismatch. So, it is relatively tough and costly to provide compensation from feeder side or using intermediate circuitry. If we add up those compensating techniques in feeder side or intermediate circuitry, the proposed system also is needed to consider of those disturbances. Moreover, load side compensation arrangement can be made portable which is a great advantage over feeder side or intermediate circuitry type compensation method.

## 2.6 Contributions

Our studies and approaches for solving the instability issues created by CPLs in microgrid have been presented in brief. According to our investigation, various conventional methods to compensate CPLs have been presented. In addition, this dissertation gives a quick summary of all the possible techniques to the designers that helps them to decide the proper methods for their required specifications. We have re-derived a detailed mathematical model of microgrid with CPL and CVL load. Here, we have used microgrid bus voltage to feed the rest of the system where the fluctuation of input voltage has been considered as illustrated in [9]. Moreover, we have considered CVL as an R-L load which is much more practical and simplified our system using RMS value and unity power factor. Here, we have represented microgrid as an arrangement where the  $V_{\text{Output}}$  and stability margin vary with the change of  $R_{\text{eq}}$ ,  $L_{\text{eq}}$ , and  $C_{\text{eq}}$ .

- a) We have determined the stability margin/criteria for CPL load with the consideration of parameter variation by considering the Routh-Hurwitz stability criterion and Lyapunov stability criterion.
- b) We have performed system analysis by d-q axis modelling and determined the nonlinear state space model to implement the nonlinear control strategies, where the speed voltage term is to cover up the fluctuations in system frequency.
- c) We have implemented the linear control technique such as PID controller and Sliding Mode Control (SMC) and Lyapunov Redesign Control (LRC) for nonlinear control have been implemented.

- d) We have proposed a storage system to handle CPL instability. Load side compensation has been achieved by using a storage based virtual impedance method where compensation is provided through the d-axis and q-axis current.
- e) We have designed a Hybrid Energy Storage System which is a portable device consisting of both ultracapacitor and battery. As microgrid is a distributed power system, we can compensate in load side using that portable CPL compensator. Here, Ultracapacitor contributes also in transient power demand where battery handles the nominal power requirements. Performance comparison and analysis for various storage systems with designed hybrid storage system have been performed and relevant graphical analogies have been represented.
- f) Robustness and Disturbance analysis with the variation of frequency, CPL Power, CVL Power, Bus voltage, and Gaussian White Noise rejection have been performed both analytically and graphically by using Sliding Mode Control (SMC) and Lyapunov Redesign Control (LRC) technique. A comparative performance analysis has been presented for SMC and LRC technique with the variation of the CPL power.

# Chapter 3 : Nonlinear Modeling of Microgrid with CPL and CVL Loads

## 3.1 Introduction

Traditional loads display linear relationships of voltage and current as mentioned in Ohms law while constant power loads display a nonlinear relationship as shown in Figure 3.1.

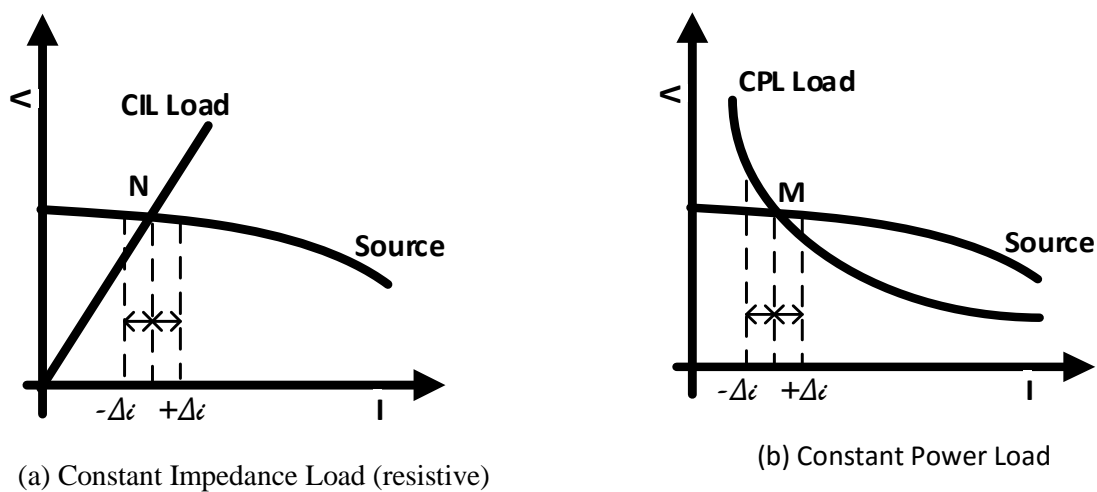


Figure 3.1: v-i characteristics of typical voltage source and loads. [11,111].

The two different graphs are indicative of the dissimilarity in the problems that these loads present in power systems. CILs require a narrow band of allowed voltages to function safely and effectively. They present constant, positive impedance to the source as its voltage varies. Transient surges due to changes in the source or load are quickly damped out. The CPL, on the other hand, adjusts to consume a constant amount of power. Although the instantaneous impedance of a CPL is positive, the incremental input impedance is negative as explained in the equation 3.1, 3.2, and 3.3 below [111].

$$P_{load} = vi = \text{constant} \quad (3.1)$$

$$v = P_{load}/i \quad (3.2)$$

$$\partial Z = \frac{dv}{di} = -P_{load}/i^2 \quad (3.3)$$

Traditionally, positive resistance leads to damping of oscillations in the LC filter of circuits and dissipation of energy. But, negative impedance leads to oscillations being increased rather than being damped out, leading to instability being introduced into the system [1], as shown in figure 3.2. As the CPL loads increase in a network, the effect of this instability is intensified.

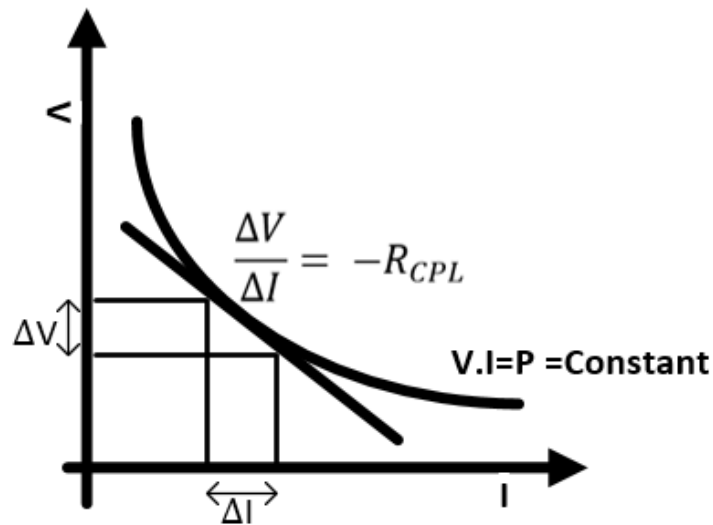


Figure 3:2: Negative impedance characteristic of CPL [1].

This is even more evident in a microgrid with distributed generation, energy storage and rectifier-inverter sets. Transient conditions like load-shedding of CILs or sudden increase of CPLs could destabilize the system [9]. Hence, the instability characteristics of CPLs must be studied and techniques should be devised to maximize the stability of the grid.

### 3.2 Modeling of Loads

#### 3.2.1 Resistive Loads

Electrical loads are generally considered as resistive loads those dissipate heat and converting electrical energy into thermal energy. Most of the practical loads are resistive in general consideration which shows linear I-V characteristics

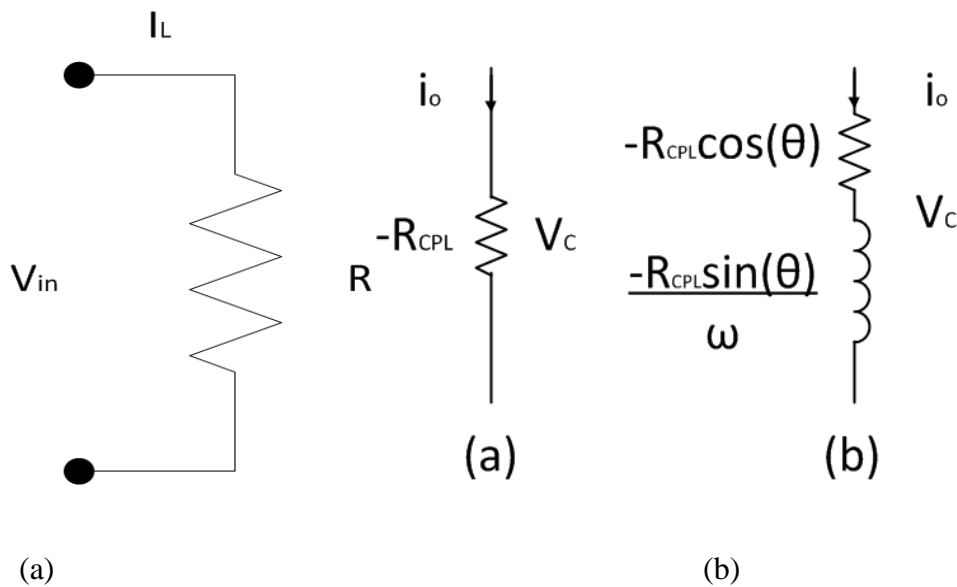


Figure 3.3: (a) Resistor circuit, (b) modeling of CPL circuit [9].

i.e. when terminal voltage decreases, the load current also decreases, and when terminal voltage increases, the load current also increases as shown in figure 3.4(a). The linear characteristics curve of resistive type load is governed by the Ohm's law which expressed in equation 3.4. A schematic representation of resistive load is shown in figure 3.3. Here,  $V_{in}$  is the independent variable and  $I_L$  is function of  $V_{in}$ .

$$I_L = \frac{V_{in}}{R} \quad (3.4)$$

$$P_L = I_L^2 R = \frac{V_{in}^2}{R} \quad (3.5)$$

Power dissipation is a function of the square of load current. Power dissipation in resistive type loads will increase if the load current increases, more and more electrical energy will be converted into thermal energy and vice versa. The relationship between load current and load power is represented in equation 3.5. From equation 3.5, power dissipation is also proportional to the square of the input voltage that is using non-regulating voltage sources or rapidly changing voltage level. Eventually, it could overheat the component and make damage to the circuit component. Here, the load power vs. input voltage and I-V characteristics of load represented in figure 3.4.

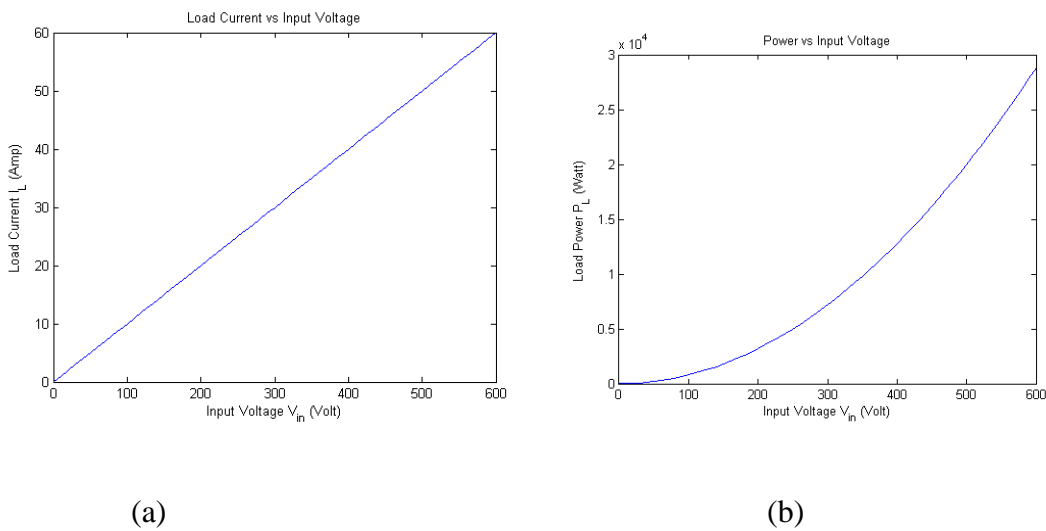


Figure 3.4: Resistive load (a) load current vs. input voltage (b) load power vs. input voltage.

### 3.2.2 Constant Power Loads (CPLs)

While load power remains constant from the power relation equation 3.2, we can see that the I-V characteristics of the load become nonlinear; that is, while input voltage is decreasing the input current keep increasing or vice versa to maintain a constant output power thus shows negative resistance characteristics. Modern power electronics based devices like power inverter/Converter etc. show this

type of behavior and termed as CPL. In case of CPL the characteristics behavior can be formulated by equation 3.3 where the load current is function of input voltage.

$$I_L = \frac{P_L}{V_{in}} \quad (3.6)$$

A schematic representation of constant power load is represented in figure 3.5. Here, a regulated power converter is used to keep the output power of the resistive load constant regardless of input voltage changes. The load current vs. input voltage characteristics and the load power as a function of input voltage curve is represented in figure 3.6 [112].

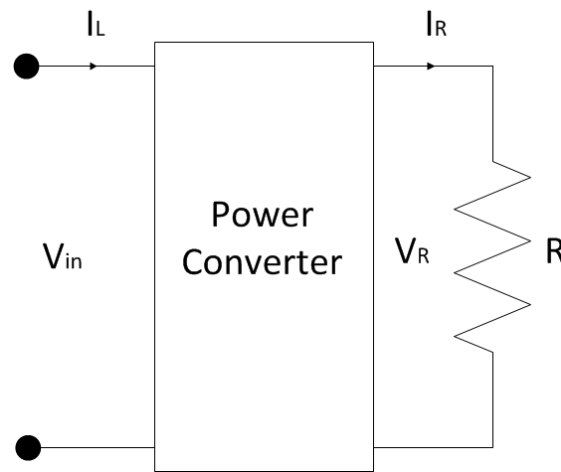


Figure 3:5: Resistor circuit with regulated power converter. [84,112].

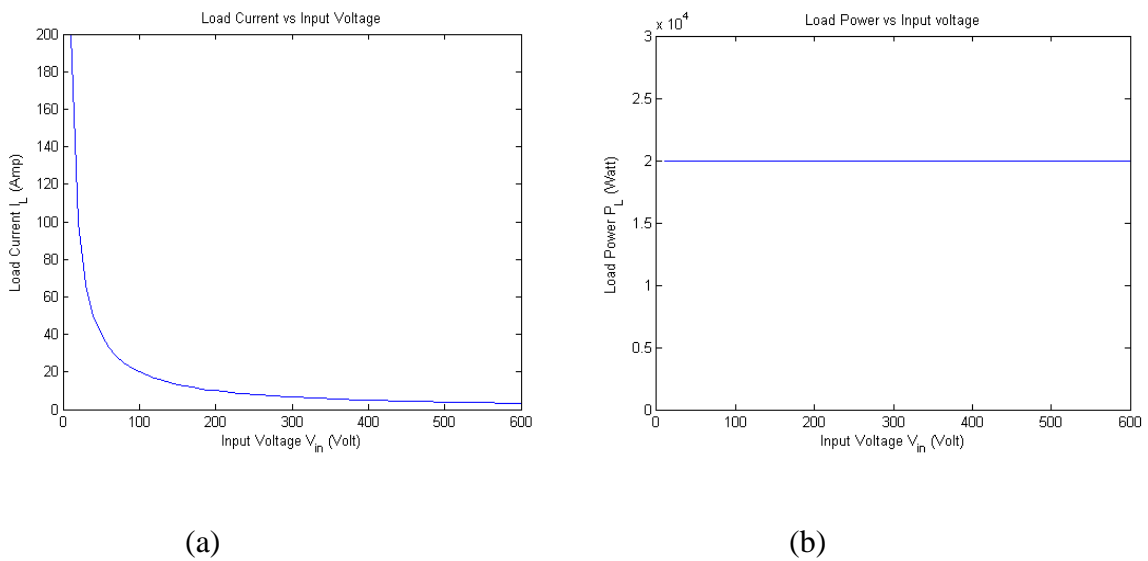


Figure 3:6: Constant power loads (a) load current vs input voltage (b) load power vs input voltage.

### 3.3 Modeling of Hybrid Microgrid

Nonlinear state space model of microgrid is shown in below.

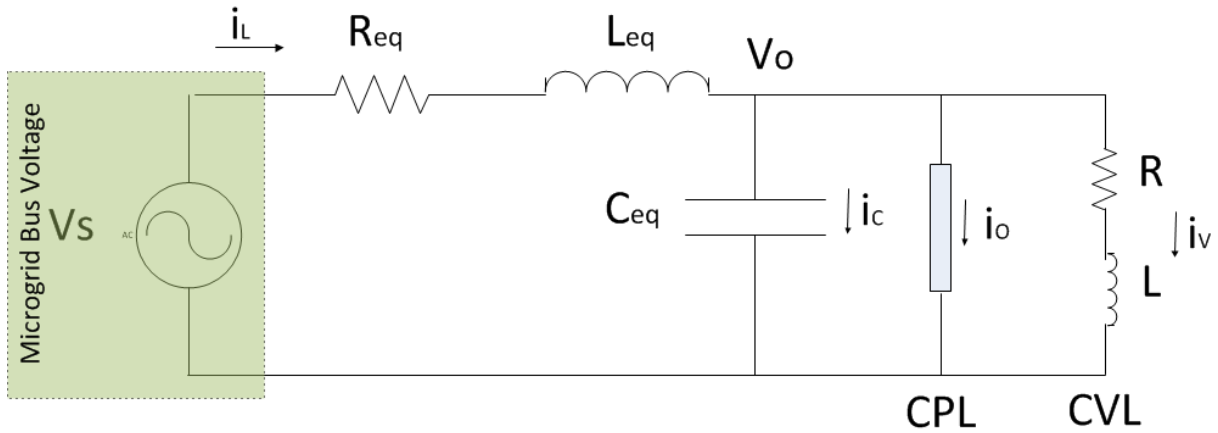


Figure 3:7: Schematic diagram of microgrid with CPL [9].

From the circuit

Let's take  $L_{eq} = L_1$ ,  $R_{eq} = R_1$ ,  $C_{eq} = C$  for simplicity

Applying KVL to the circuit we have

$$V_s - V_{R1} - V_{L1} - V_C = 0 \quad (3.7)$$

$$\rightarrow V_s - R_1 i_L - L_1 \frac{di_L}{dt} - V_C = 0 \quad (3.8)$$

$$\rightarrow \frac{di_L}{dt} = -\frac{R_1}{L_1} i_L - \frac{1}{L_1} V_C + \frac{V_s}{L_1} \quad (3.9)$$

Again, By applying KCL to the circuit we have

$$i_C + i_O + i_V = i_L \quad (3.10)$$

$$\rightarrow C \frac{dV_C}{dt} + \frac{P_O}{V_C} + i_V = i_L \quad (3.11)$$

By taking output current  $i_O$  as a function of capacitor voltage  $V_C$

$$i.e; i_O = \frac{P_O}{V_C}; [P_O \text{ is the Power of constant power load (CPL) and also a constant}] \quad (3.12)$$

$$\rightarrow \frac{dV_C}{dt} = \frac{1}{C} i_L - \frac{1}{C} \frac{P_O}{V_C} - \frac{1}{C} i_V \quad (3.13)$$

Again,

$$R i_V + L \frac{di_V}{dt} = V_C \quad (3.14)$$

$$\rightarrow \frac{di_V}{dt} = \frac{1}{L} V_C - \frac{R}{L} i_V \quad (3.15)$$

Defining the state variables as

$$x_1 = i_L; x_2 = V_C; \text{ and } x_3 = i_V;$$

And system input  $V_s$

Nonlinear state-space model will be from equation (3.7) to (3.15)

$$\begin{bmatrix} \dot{x}_1 \\ \dot{x}_2 \\ \dot{x}_3 \end{bmatrix} = \begin{bmatrix} -\frac{R_1}{L_1} x_1 - \frac{1}{L_1} x_2 + \frac{1}{L_1} V_S \\ \frac{1}{C} x_1 - \frac{1}{C} \frac{P_O}{x_2} - \frac{1}{C} x_3 \\ \frac{1}{L} x_2 - \frac{R}{L} x_3 \end{bmatrix} \quad (3.16)$$

In the following illustration at figure 3.8, the entire design of the microgrid arrangement loaded with CPLs is depicted. The figure exhibits the undamped oscillation due to the perturbation created by the CPL loads in case of microgrid line current and the bus voltage. This disturbance in the line current and the output voltage leads to the undesired power collapse in the microgrid system.

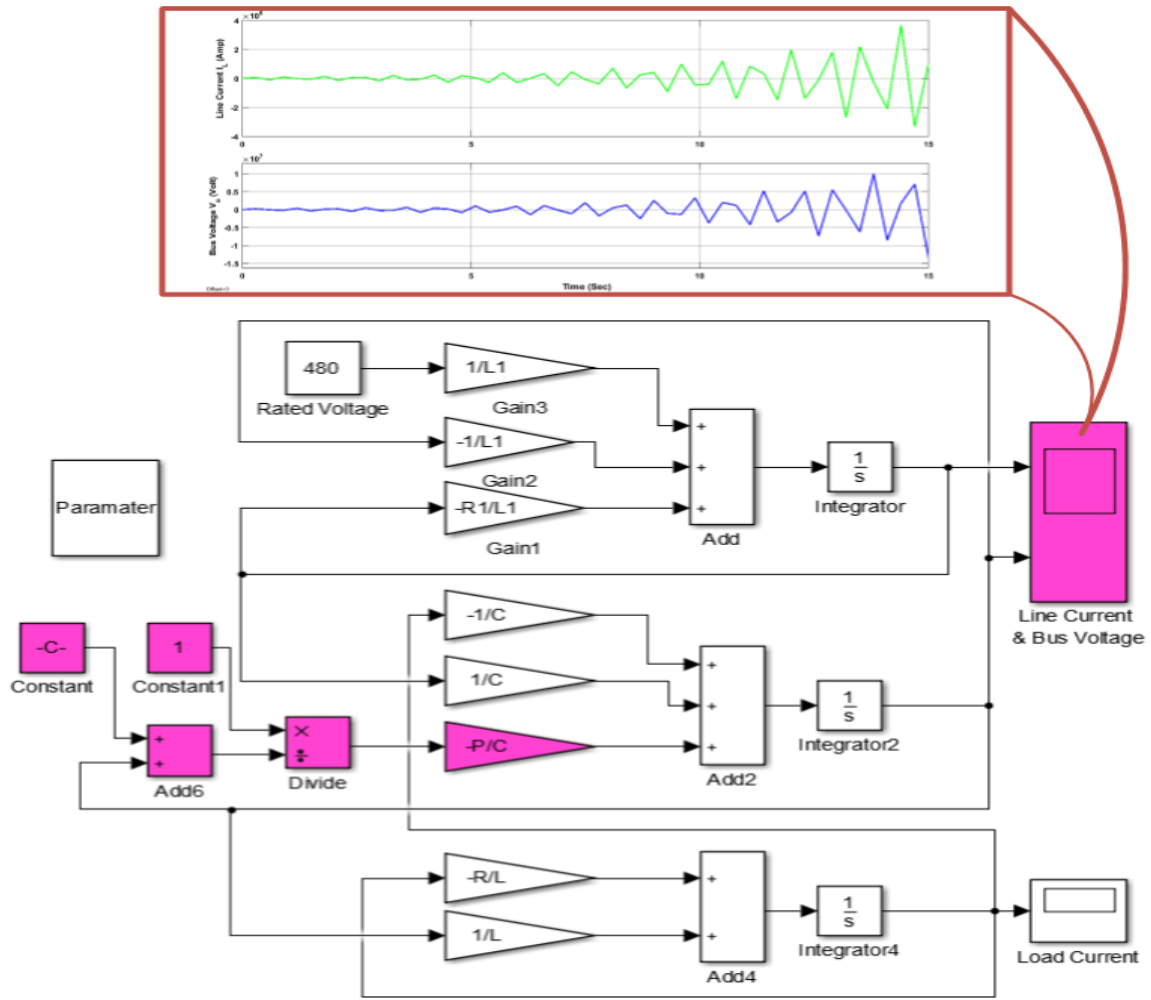


Figure 3:8: Block diagram of a microgrid system loaded by a CPL.

At figure 3.9, the line current and the output voltage of the unstable microgrid system particularly due to the CPL oscillations are presented in a closer view. In both cases, after a certain time, the output voltage and the line current are increased exponentially and oscillated randomly, hence the entire system will collapse. In this scenario, if the proper control technique would not be adopted, it would experience temporary brown out or, in severe cases, long-term black out.

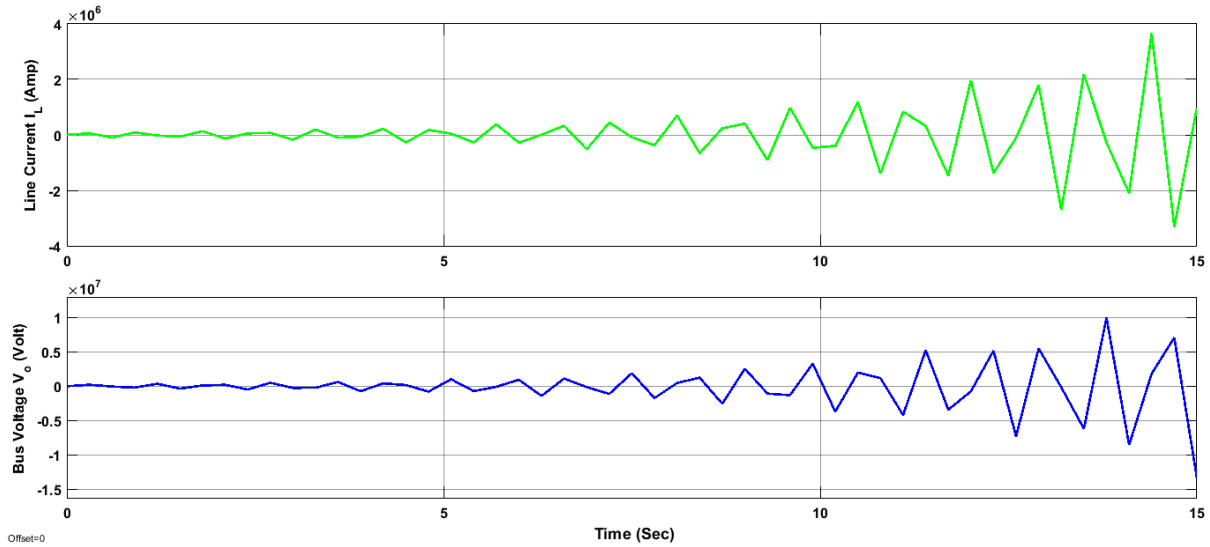


Figure 3:9: Line current and output voltage of the model of a microgrid system, which has been made unstable by a CPL.

### **d-q transformation:**

The dq model has some patent advantages over the conventional abc model. The particular feature of the dq frame is that if a space vector with constant magnitude rotates at the same speed of the frame, the d and q components will remain constant [113]. On the other hand, if it rotates at a different speed or it exhibits time variable magnitude, the constituent components will vary. One of the main advantages of dq frame is that it allows instantaneous compensation of reactive power, because it waives the need for averaging. Active and reactive power can be controlled independently by controlling the dq components [114]. For the ease of controlling uncompensated nonlinear systems and detailed analysis of state variable to implement the advanced nonlinear control algorithms, we have derived d-q axis modelling in our system. The equivalent d-q axis model circuit is represented in figure 3.10 and 3.11. When we consider line frequency is 60 Hz, then  $\omega$ (speed term) becomes static. However, in practical cases line frequency always fluctuates which depends on various characteristics of the system. So, in those cases,  $\omega$  (speed term) becomes dynamic and nonlinear.

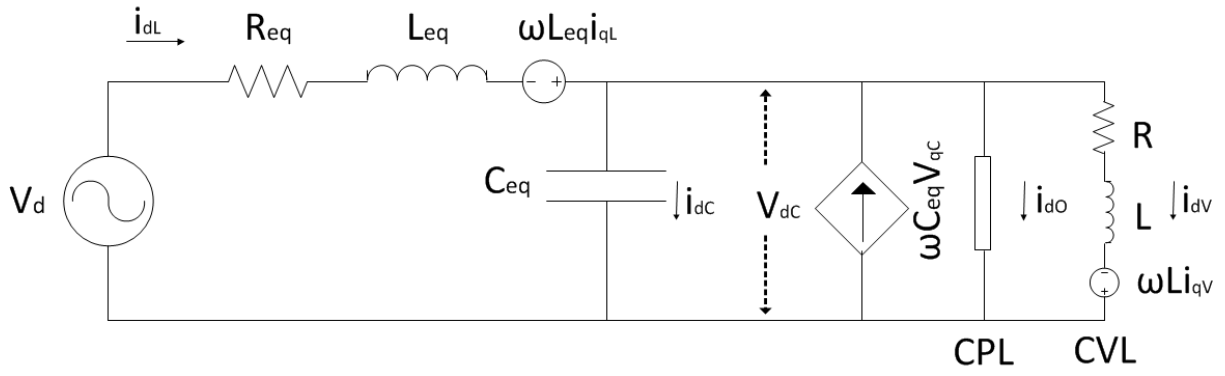


Figure 3:10: d-axis model of microgrid.

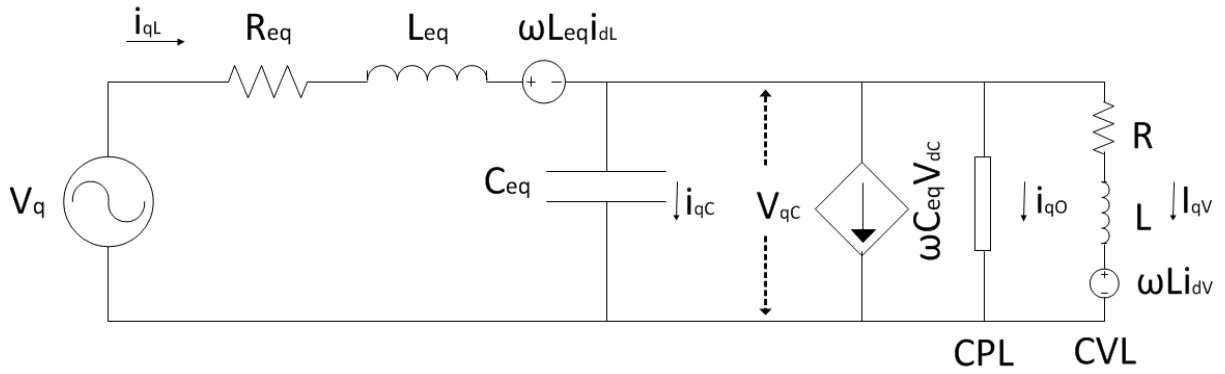


Figure 3:11: q-axis model of microgrid.

From KCL we know that  $i_a + i_b + i_c = 0$  and d-q transformation matrix

$$\begin{bmatrix} x_d \\ x_q \end{bmatrix} = \frac{2}{3} \begin{bmatrix} \cos \omega t & \cos(\omega t - 120) & \cos(\omega t + 120) \\ -\sin \omega t & -\sin(\omega t - 120) & -\sin(\omega t + 120) \end{bmatrix} \times \begin{bmatrix} x_a \\ x_b \\ x_c \end{bmatrix}$$

Using d-q transformation matrix

$$i_{dL} = \frac{2}{3} [i_{aL} \cos \omega t + i_{bL} \cos(\omega t - 120) + i_{cL} \cos(\omega t + 120)] \quad (3.17)$$

$$i_{qL} = -\frac{2}{3} [i_{aL} \sin \omega t + i_{bL} \sin(\omega t - 120) + i_{cL} \sin(\omega t + 120)] \quad (3.18)$$

Differentiating equation (3.17) with respect to t

$$\frac{di_{dL}}{dt} = \frac{2}{3} \left[ \frac{di_{aL}}{dt} \cos \omega t + \frac{di_{bL}}{dt} \cos(\omega t - 120) + \frac{di_{cL}}{dt} \cos(\omega t + 120) \right] - \frac{2}{3} \omega [i_{aL} \sin \omega t + i_{bL} \sin(\omega t - 120) + i_{cL} \sin(\omega t + 120)] \quad (3.19)$$

From equation (3.9) and (3.16) to (3.19) can be written as

$$\frac{di_{dL}}{dt} = \omega i_{qL} - \frac{R_1}{L_1} i_{dL} - \frac{V_{dc}}{L_1} + \frac{V_d}{L_1} \quad (3.20)$$

Similarly,

$$\frac{di_{qL}}{dt} = -\omega i_{dL} - \frac{R_1}{L_1} i_{qL} - \frac{V_{qc}}{L_1} + \frac{V_q}{L_1} \quad (3.21)$$

Again from equation (3.9), Using d-q transformation

$$\frac{dV_{dc}}{dt} = \omega V_{qc} + \frac{1}{c} i_{dL} - \frac{1}{c} \frac{P_O}{V_{dc}} - \frac{1}{c} i_{dV} \quad (3.22)$$

$$\frac{dV_{qc}}{dt} = -\omega V_{dc} + \frac{1}{c} i_{qL} - \frac{1}{c} \frac{P_O}{V_{qc}} - \frac{1}{c} i_{qV} \quad (3.23)$$

From equation state equation (3.15), Using d-q transformation

$$\frac{di_{dV}}{dt} = \omega i_{qV} + \frac{1}{L} V_{dc} - \frac{R}{L} i_{dV} \quad (3.24)$$

$$\frac{di_{qV}}{dt} = -\omega i_{dV} + \frac{1}{L} V_{qc} - \frac{R}{L} i_{qV} \quad (3.25)$$

d-q transformed state equations from equation (3.20) to (3.25)

$$\begin{bmatrix} \frac{di_{dL}}{dt} \\ \frac{di_{qL}}{dt} \\ \frac{dV_{dc}}{dt} \\ \frac{dV_{qc}}{dt} \\ \frac{di_{qV}}{dt} \\ \frac{di_{dV}}{dt} \end{bmatrix} = \begin{bmatrix} \omega i_{qL} - \frac{R_1}{L_1} i_{dL} - \frac{V_{dc}}{L_1} + \frac{V_d}{L_1} \\ -\omega i_{dL} - \frac{R_1}{L_1} i_{qL} - \frac{V_{qc}}{L_1} + \frac{V_q}{L_1} \\ \omega V_{qc} + \frac{1}{c} i_{dL} - \frac{1}{c} \frac{P_O}{V_{dc}} - \frac{1}{c} i_{dV} \\ -\omega V_{dc} + \frac{1}{c} i_{qL} - \frac{1}{c} \frac{P_O}{V_{qc}} - \frac{1}{c} i_{qV} \\ \omega i_{qV} + \frac{1}{L} V_{dc} - \frac{R}{L} i_{dV} \\ -\omega i_{dV} + \frac{1}{L} V_{qc} - \frac{R}{L} i_{qV} \end{bmatrix} \quad (3.26)$$

Using the equation 3.16, at figure 3.12, the bus voltage instability of d-axis due to the constant power loads is presented schematically. In this case, an abrupt and random change is observed in d-axis bus voltage.

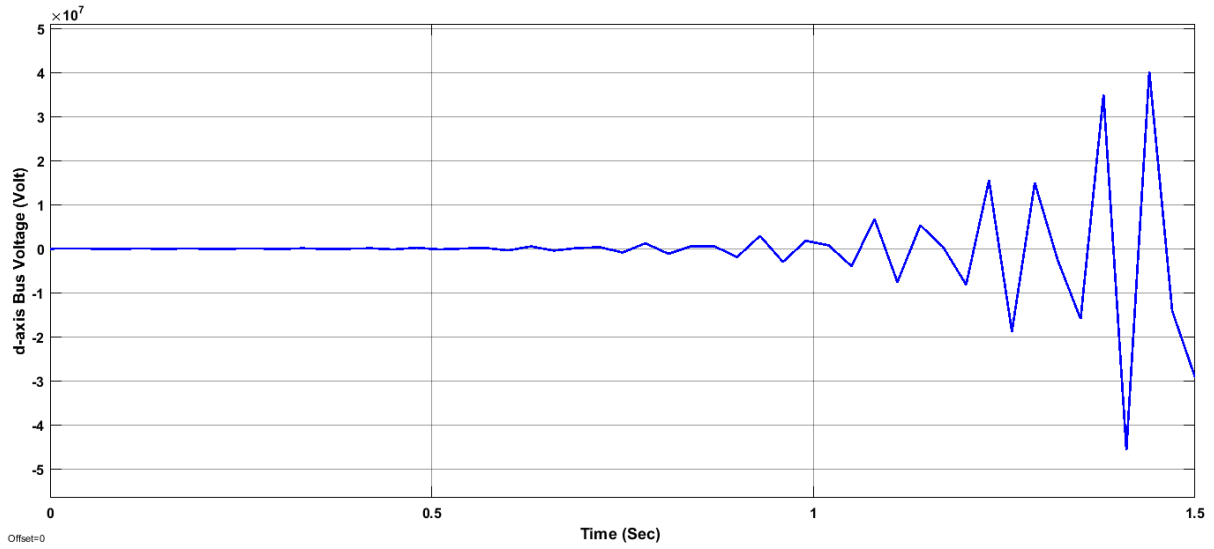


Figure 3:12: d-axis bus voltage instability due to CPL.

In this sequence, at figure 3.13, the bus voltage instability of q-axis due to the constant power loads is presented implementing the equation 3.16. Like the d-axis bus voltage, the exponentially increased signal and random oscillations are also demonstrated in the case of the q-axis bus voltage.

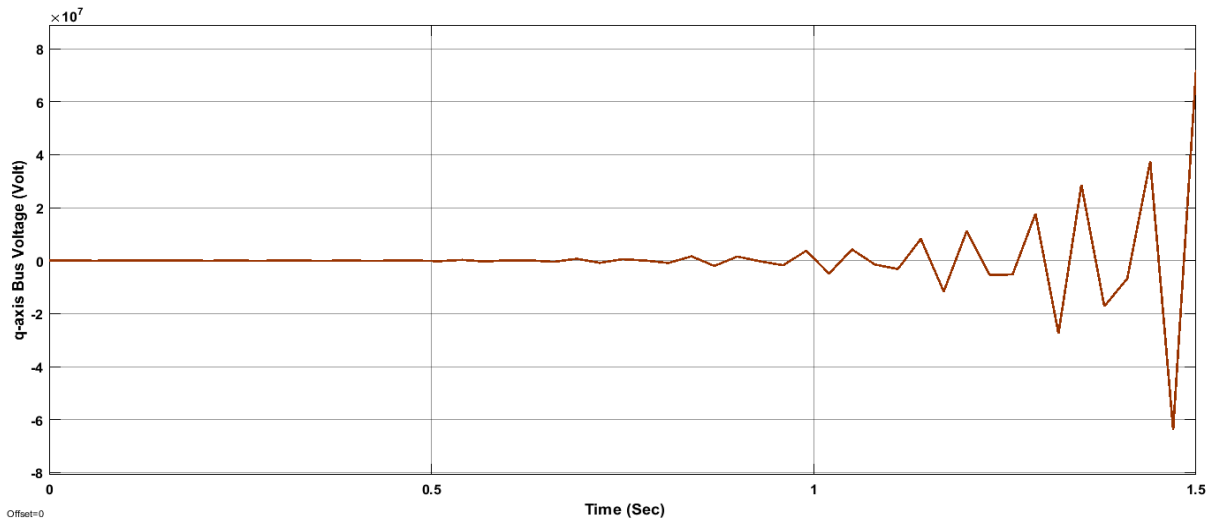


Figure 3:13: q-axis bus voltage instability due to CPL.

### 3.4 Modeling the Proposed Real Power Compensation Method

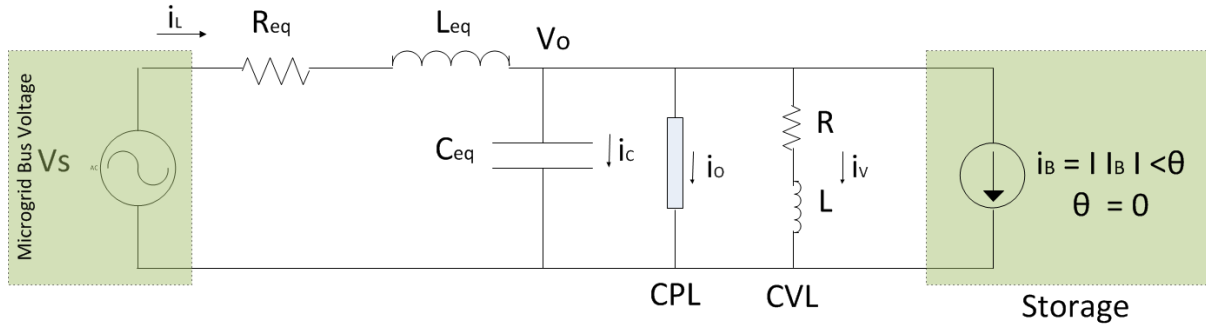


Figure 3:14: Schematic diagram of microgrid with CPL and storage (with active power compensation).

From the circuit,

Let's take  $L_{eq} = L_1$ ,  $R_{eq} = R_1$ ,  $C_{eq} = C$  for simplicity

Applying KVL to the circuit of figure 3.14, we have

$$V_s - V_{R1} - V_{L1} - V_C = 0 \quad (3.27)$$

$$\rightarrow V_s - R_1 i_L - L_1 \frac{di_L}{dt} - V_C = 0 \quad (3.28)$$

$$\rightarrow \frac{di_L}{dt} = -\frac{R_1}{L_1} i_L - \frac{1}{L_1} V_C + \frac{V_s}{L_1} \quad (3.29)$$

Again, By applying KCL to the circuit we have

$$i_C + i_O + i_V + i_B = i_L \quad (3.30)$$

$$\rightarrow C \frac{dV_C}{dt} + \frac{P_O}{V_C} + i_V + i_B = i_L \quad (3.31)$$

By taking output current  $i_O$  as a function of capacitor voltage  $V_C$

$$\text{I.e; } i_O = \frac{P_O}{V_C}; \text{ [} P_O \text{ is the power of constant power load (CPL) and also a constant]} \quad (3.32)$$

$$\rightarrow \frac{dV_C}{dt} = \frac{1}{C} i_L - \frac{1}{C} \frac{P_O}{V_C} - \frac{1}{C} i_V - \frac{1}{C} i_B \quad (3.33)$$

Again,

$$R i_V + L \frac{di_V}{dt} = V_C \quad (3.34)$$

$$\rightarrow \frac{di_V}{dt} = \frac{1}{L} V_C - \frac{R}{L} i_V \quad (3.35)$$

Defining the state variables as

$$x_1 = i_L; x_2 = V_C; \text{ and } x_3 = i_V;$$

And system input  $V_s$  and control input  $i_B$  and  $V_{CB}$ , control output  $V_{dC}$  and  $V_{qC}$

Nonlinear state-space model will be from equation (3.27) to (3.35)

$$\begin{bmatrix} \dot{x}_1 \\ \dot{x}_2 \\ \dot{x}_3 \end{bmatrix} = \begin{bmatrix} -\frac{R_1}{L_1}x_1 - \frac{1}{L_1}x_2 + \frac{1}{L_1}V_S \\ \frac{1}{C}x_1 - \frac{1}{C}x_2 - \frac{1}{C}x_3 - \frac{1}{C}i_B \\ \frac{1}{L}x_2 - \frac{R}{L}x_3 \end{bmatrix} \quad (3.36)$$

d-q axis transformation

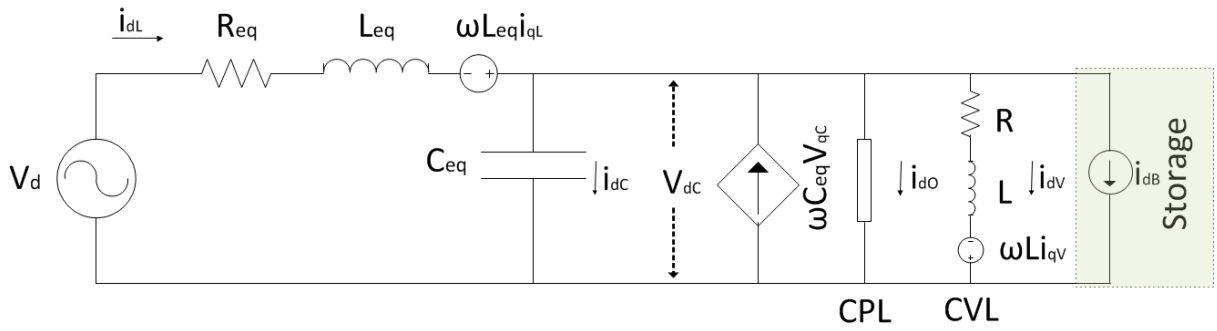


Figure 3:15: d-axis model of proposed real power compensation method.

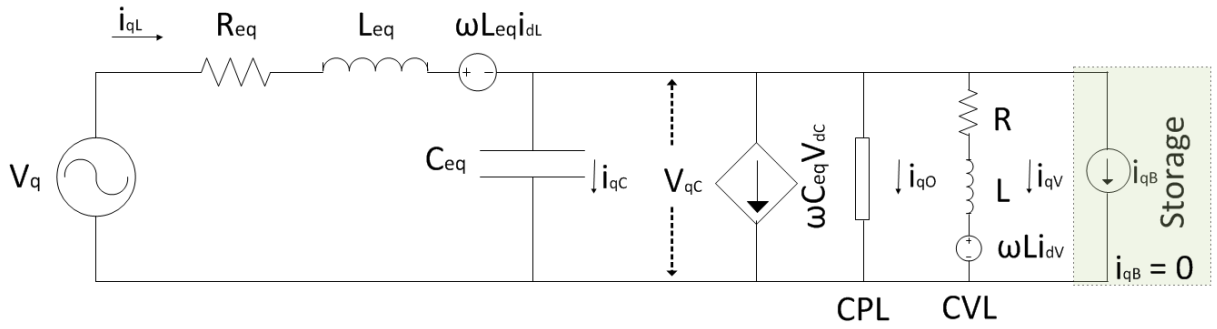


Figure 3:16: q-axis model of proposed real power compensation method.

from equation (3.29) using d-q transformation mentioned above we have

$$\frac{di_{dL}}{dt} = \omega i_{qL} - \frac{R_1}{L_1} i_{dL} - \frac{V_{dC}}{L_1} + \frac{V_d}{L_1} \quad (3.37)$$

Similarly,

$$\frac{di_{qL}}{dt} = -\omega i_{dL} - \frac{R_1}{L_1} i_{qL} - \frac{V_{qc}}{L_1} + \frac{V_q}{L_1} \quad (3.38)$$

From equation (3.33) using d-q transformation

$$\frac{dV_{dc}}{dt} = \omega V_{qc} + \frac{1}{C} i_{dL} - \frac{1}{C} \frac{P_O}{V_{dc}} - \frac{1}{C} i_{dV} - \frac{1}{C} i_{dB} \quad (3.39)$$

$$\frac{dV_{qc}}{dt} = -\omega V_{dc} + \frac{1}{C} i_{qL} - \frac{1}{C} \frac{P_O}{V_{qc}} - \frac{1}{C} i_{qV} - \frac{1}{C} i_{qB} \quad (3.40)$$

Again from equation (3.35) using d-q transformation

$$\frac{di_{qV}}{dt} = \omega i_{qV} + \frac{1}{L} V_{dc} - \frac{R}{L} i_{dV} \quad (3.41)$$

$$\frac{di_{dV}}{dt} = -\omega i_{dV} + \frac{1}{L} V_{qc} - \frac{R}{L} i_{qV} \quad (3.42)$$

d-q transformation state equation

$$\begin{bmatrix} \frac{di_{dL}}{dt} \\ \frac{di_{qL}}{dt} \\ \frac{dV_{dc}}{dt} \\ \frac{dV_{qc}}{dt} \\ \frac{di_{qV}}{dt} \\ \frac{di_{dV}}{dt} \end{bmatrix} = \begin{bmatrix} \omega i_{qL} - \frac{R_1}{L_1} i_{dL} - \frac{V_{dc}}{L_1} + \frac{V_d}{L_1} \\ -\omega i_{dL} - \frac{R_1}{L_1} i_{qL} - \frac{V_{qc}}{L_1} + \frac{V_q}{L_1} \\ \omega V_{qc} + \frac{1}{C} i_{dL} - \frac{1}{C} \frac{P_O}{V_{dc}} - \frac{1}{C} i_{dV} - \frac{1}{C} i_{dB} \\ -\omega V_{dc} + \frac{1}{C} i_{qL} - \frac{1}{C} \frac{Q_O}{V_{qc}} - \frac{1}{C} i_{qV} - \frac{1}{C} i_{qB} \\ \omega i_{qV} + \frac{1}{L} V_{dc} - \frac{R}{L} i_{dV} \\ -\omega i_{dV} + \frac{1}{L} V_{qc} - \frac{R}{L} i_{qV} \end{bmatrix} \quad (3.43)$$

Note: for real power compensation  $Q_0 = 0$ .

### 3.5 Modeling the Proposed Reactive Power Compensation Method

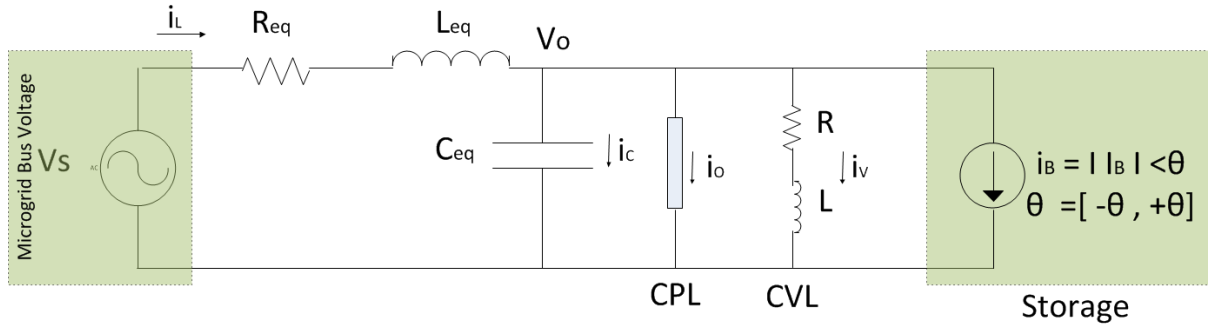


Figure 3:17: Schematic diagram of microgrid with CPL and storage (with reactive power compensation).

From the circuit

Let's take  $L_{eq} = L_1$ ,  $R_{eq} = R_1$ ,  $C_{eq} = C$  for simplicity

Applying KVL to the circuit we have

$$V_s - V_{R1} - V_{L1} - V_C = 0 \quad (3.44)$$

$$\rightarrow V_s - R_1 i_L - L_1 \frac{di_L}{dt} - V_C = 0 \quad (3.45)$$

$$\rightarrow \frac{di_L}{dt} = -\frac{R_1}{L_1} i_L - \frac{1}{L_1} V_C + \frac{V_s}{L_1} \quad (3.46)$$

Again, by applying KCL to the circuit we have

$$i_C + i_O + i_V + i_B = i_L \quad (3.47)$$

$$\rightarrow C \frac{dV_C}{dt} + \frac{P_O}{V_C} + i_V + i_B = i_L \quad (3.48)$$

By taking output current  $i_O$  as a function of capacitor voltage  $V_C$

I.e;  $i_O = \frac{P_O}{V_C}$ ; [ $P_O$  is the Power of constant power load (CPL) and also a constant]

$$\rightarrow \frac{dV_C}{dt} = \frac{1}{C} i_L - \frac{1}{C} \frac{P_O}{V_C} - \frac{1}{C} i_V - \frac{1}{C} i_B \quad (3.49)$$

Again,

$$R i_V + L \frac{di_V}{dt} = V_C \quad (3.50)$$

$$\rightarrow \frac{di_V}{dt} = \frac{1}{L} V_C - \frac{R}{L} i_V \quad (3.51)$$

Defining the state variables as

$x_1 = i_L$ ;  $x_2 = V_C$ ; and  $x_3 = i_V$

And system input  $V_s$  and control input  $i_B$  and  $V_{CB}$ , control output  $V_{dc}$  and  $V_{qc}$

Nonlinear state-space model will be from equation (3.44) to (3.51)

$$\begin{bmatrix} \dot{x}_1 \\ \dot{x}_2 \\ \dot{x}_3 \end{bmatrix} = \begin{bmatrix} -\frac{R_1}{L_1}x_1 - \frac{1}{L_1}x_2 + \frac{1}{L_1}V_s \\ \frac{1}{C}x_1 - \frac{1}{C}x_2 - \frac{1}{C}x_3 - \frac{1}{C}i_B \\ \frac{1}{L}x_2 - \frac{R}{L}x_3 \end{bmatrix} \quad (3.52)$$

d-q axis transformation

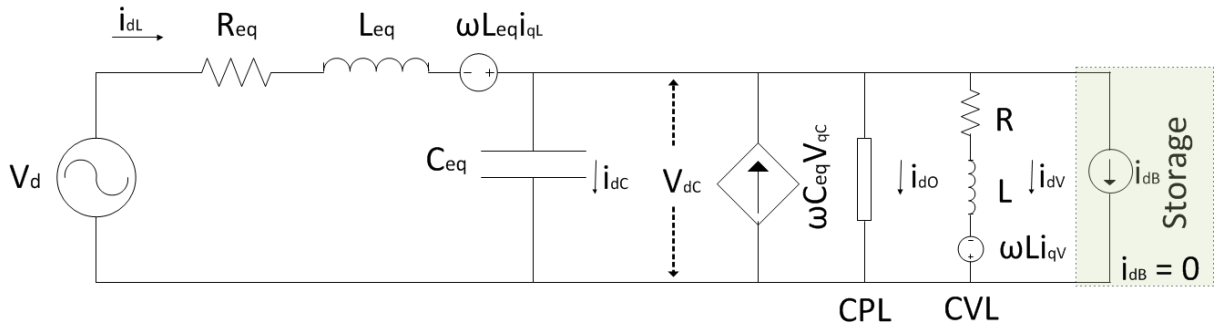


Figure 3:18: d-axis model of proposed reactive power compensation method.

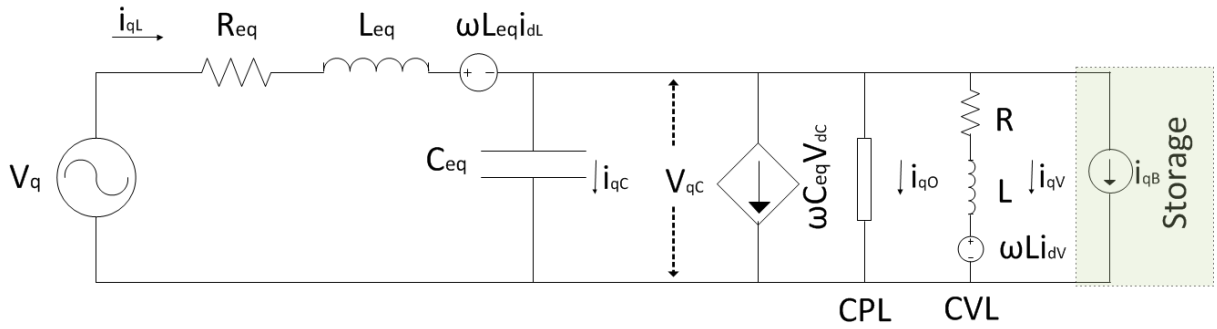


Figure 3:19: q-axis model of proposed reactive power compensation method.

from equation (3.46) using d-q transformation mentioned above we have

$$\frac{di_{dL}}{dt} = \omega i_{qL} - \frac{R_1}{L_1} i_{dL} - \frac{V_{dc}}{L_1} + \frac{V_d}{L_1} \quad (3.53)$$

$$\frac{di_{qL}}{dt} = -\omega i_{dL} - \frac{R_1}{L_1} i_{qL} - \frac{V_{qc}}{L_1} + \frac{V_q}{L_1} \quad (3.54)$$

From equation (3.48) using d-q transformation

$$\frac{dV_{dC}}{dt} = \omega V_{qC} + \frac{1}{C} i_{dL} - \frac{1}{C} \frac{P_O}{V_{dC}} - \frac{1}{C} i_{dV} - \frac{1}{C} i_{dB} \quad (3.55)$$

$$\frac{dV_{qC}}{dt} = -\omega V_{dC} + \frac{1}{C} i_{qL} - \frac{1}{C} \frac{P_O}{V_{qC}} - \frac{1}{C} i_{qV} - \frac{1}{C} i_{qB} \quad (3.56)$$

Again from equation (3.51) using d-q transformation

$$\frac{di_{qV}}{dt} = \omega i_{qV} + \frac{1}{L} V_{dC} - \frac{R}{L} i_{dV} \quad (3.57)$$

$$\frac{di_{dV}}{dt} = -\omega i_{dV} + \frac{1}{L} V_{qC} - \frac{R}{L} i_{qV} \quad (3.58)$$

d-q transformation State equation

$$\begin{bmatrix} \frac{di_{dL}}{dt} \\ \frac{di_{qL}}{dt} \\ \frac{dV_{dC}}{dt} \\ \frac{dV_{qC}}{dt} \\ \frac{di_{qV}}{dt} \\ \frac{di_{dV}}{dt} \end{bmatrix} = \begin{bmatrix} \omega i_{qL} - \frac{R_1}{L_1} i_{dL} - \frac{V_{dC}}{L_1} + \frac{V_d}{L_1} \\ -\omega i_{dL} - \frac{R_1}{L_1} i_{qL} - \frac{V_{qC}}{L_1} + \frac{V_q}{L_1} \\ \omega V_{qC} + \frac{1}{C} i_{dL} - \frac{1}{C} \frac{P_O}{V_{dC}} - \frac{1}{C} i_{dV} - \frac{1}{C} i_{dB} \\ -\omega V_{dC} + \frac{1}{C} i_{qL} - \frac{1}{C} \frac{Q_O}{V_{qC}} - \frac{1}{C} i_{qV} - \frac{1}{C} i_{qB} \\ \omega i_{qV} + \frac{1}{L} V_{dC} - \frac{R}{L} i_{dV} \\ -\omega i_{dV} + \frac{1}{L} V_{qC} - \frac{R}{L} i_{qV} \end{bmatrix} \quad (3.59)$$

Note: for reactive power compensation  $P_0 = 0$ .

### 3.6 CPL with both Real and Reactive Power Component

Finally, we have also considered some special cases for the system analysis which are absent in the current discussion. If CPL load consists of both real and reactive power component, then we can analysis system as below.

$$P_{d0} = P_O$$

$$P_{q0} = Q_O$$

d-q axis modeling of microgrid based on equation (3.59)

$$\frac{dV_{dC}}{dt} = \omega V_{qC} + \frac{1}{C} i_{dL} - \frac{1}{C} \frac{P_O}{V_{dC}} - \frac{1}{C} i_{dV} \quad (3.60)$$

$$\frac{dV_{qC}}{dt} = -\omega V_{dC} + \frac{1}{C} i_{qL} - \frac{1}{C} \frac{Q_O}{V_{qC}} - \frac{1}{C} i_{qV} \quad (3.61)$$

$$\begin{bmatrix} \frac{di_{dL}}{dt} \\ \frac{di_{qL}}{dt} \\ \frac{dV_{dC}}{dt} \\ \frac{dV_{qC}}{dt} \\ \frac{di_{qV}}{dt} \\ \frac{di_{dV}}{dt} \end{bmatrix} = \begin{bmatrix} \omega i_{qL} - \frac{R_1}{L_1} i_{dL} - \frac{V_{dC}}{L_1} + \frac{V_d}{L_1} \\ -\omega i_{dL} - \frac{R_1}{L_1} i_{qL} - \frac{V_{qC}}{L_1} + \frac{V_q}{L_1} \\ \omega V_{qC} + \frac{1}{C} i_{dL} - \frac{1}{C} \frac{P_O}{V_{dC}} - \frac{1}{C} i_{dV} \\ -\omega V_{dC} + \frac{1}{C} i_{qL} - \frac{1}{C} \frac{Q_O}{V_{qC}} - \frac{1}{C} i_{qV} \\ \omega i_{qV} + \frac{1}{L} V_{dC} - \frac{R}{L} i_{dV} \\ -\omega i_{dV} + \frac{1}{L} V_{qC} - \frac{R}{L} i_{qV} \end{bmatrix} \quad (3.62)$$

Real power compensation

$$\frac{dV_{dC}}{dt} = \omega V_{qC} + \frac{1}{C} i_{dL} - \frac{1}{C} \frac{P_O}{V_{dC}} - \frac{1}{C} i_{dV} - \frac{1}{C} i_{dB} \quad (3.63)$$

$$\frac{dV_{qC}}{dt} = -\omega V_{dC} + \frac{1}{C} i_{qL} - \frac{1}{C} \frac{Q_O}{V_{qC}} - \frac{1}{C} i_{qV} - \frac{1}{C} i_{qB} \quad (3.64)$$

$$\begin{bmatrix} \frac{di_{dL}}{dt} \\ \frac{di_{qL}}{dt} \\ \frac{dV_{dC}}{dt} \\ \frac{dV_{qC}}{dt} \\ \frac{di_{qV}}{dt} \\ \frac{di_{dV}}{dt} \end{bmatrix} = \begin{bmatrix} \omega i_{qL} - \frac{R_1}{L_1} i_{dL} - \frac{V_{dC}}{L_1} + \frac{V_d}{L_1} \\ -\omega i_{dL} - \frac{R_1}{L_1} i_{qL} - \frac{V_{qC}}{L_1} + \frac{V_q}{L_1} \\ \omega V_{qC} + \frac{1}{C} i_{dL} - \frac{1}{C} \frac{P_O}{V_{dC}} - \frac{1}{C} i_{dV} - \frac{1}{C} i_{dB} \\ -\omega V_{dC} + \frac{1}{C} i_{qL} - \frac{1}{C} \frac{Q_O}{V_{qC}} - \frac{1}{C} i_{qV} - \frac{1}{C} i_{qB} \\ \omega i_{qV} + \frac{1}{L} V_{dC} - \frac{R}{L} i_{dV} \\ -\omega i_{dV} + \frac{1}{L} V_{qC} - \frac{R}{L} i_{qV} \end{bmatrix} \quad (3.65)$$

Reactive power compensation

$$\frac{dV_{dC}}{dt} = \omega V_{qC} + \frac{1}{C} i_{dL} - \frac{1}{C} \frac{P_O}{V_{dC}} - \frac{1}{C} i_{dV} - \frac{1}{C} i_{dB} \quad (3.66)$$

$$\frac{dV_{qc}}{dt} = -\omega V_{dc} + \frac{1}{C} i_{qL} - \frac{1}{C} \frac{Q_0}{V_{qc}} - \frac{1}{C} i_{qV} - \frac{1}{C} i_{qB} \quad (3.67)$$

$$\begin{bmatrix} \frac{di_{dL}}{dt} \\ \frac{di_{qL}}{dt} \\ \frac{dV_{dc}}{dt} \\ \frac{dV_{qc}}{dt} \\ \frac{di_{qV}}{dt} \\ \frac{di_{dV}}{dt} \end{bmatrix} = \begin{bmatrix} \omega i_{qL} - \frac{R_1}{L_1} i_{dL} - \frac{V_{dc}}{L_1} + \frac{V_d}{L_1} \\ -\omega i_{dL} - \frac{R_1}{L_1} i_{qL} - \frac{V_{qc}}{L_1} + \frac{V_q}{L_1} \\ \omega V_{qc} + \frac{1}{C} i_{dL} - \frac{1}{C} \frac{P_0}{V_{dc}} - \frac{1}{C} i_{dV} - \frac{1}{C} i_{dB} \\ -\omega V_{dc} + \frac{1}{C} i_{qL} - \frac{1}{C} \frac{Q_0}{V_{qc}} - \frac{1}{C} i_{qV} - \frac{1}{C} i_{qB} \\ \omega i_{qV} + \frac{1}{L} V_{dc} - \frac{R}{L} i_{dV} \\ -\omega i_{dV} + \frac{1}{L} V_{qc} - \frac{R}{L} i_{qV} \end{bmatrix} \quad (3.68)$$

Note 1: When considering line frequency,  $\omega$  is 60 Hz, then this term becomes constant.

Note 2: In practical cases, line frequency always varies, hence  $\omega$  becomes dynamic and nonlinear.

## Chapter 4 : Stability Margin Analysis

### 4.1 Introduction

A classic AC-microgrid contains different types of power supply as well as loads as presented in figure 4.1. From the figure, power suppliers could be wide-ranged of its kind like a diesel generator, a photovoltaic system, a wind generator, etc. Likewise, the loads of the AC microgrid system may be either the CVL (constant voltage load), like heating or lighting, or the CPL (constant power load), like the motor drives or the modern power electronic interfaced loads [9]. In particular on such systems, in the case of small signal analysis, CVLs can be recognized as the constant impedance loads [1].

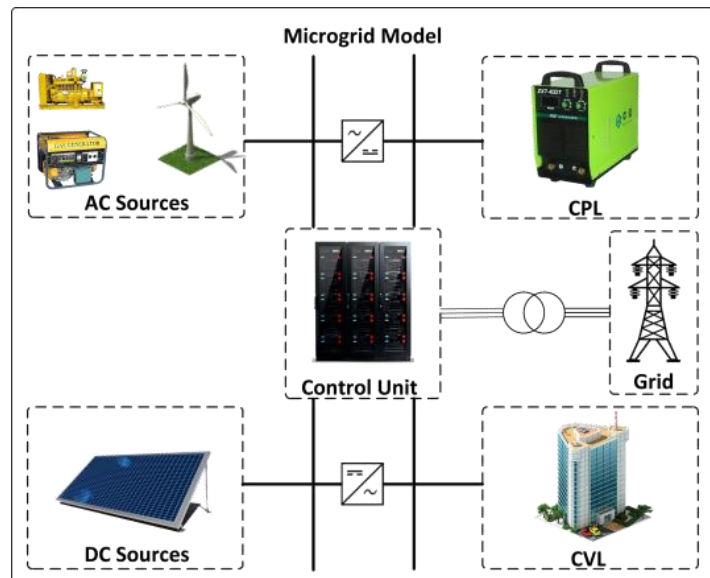


Figure 4:1: Typical model of microgrid.

### 4.2 Stability Margin of Proposed Model

#### 4.2.1 Stability of the Conventional Model

Based on the typical model as mentioned earlier, the small signal equivalent model of microgrid can be represented as figure 4.2 where combination of  $R_{eq}$  and  $L_{eq}$  is the line impedance or generator impedance and  $C_{eq}$  represents the filter capacitance.

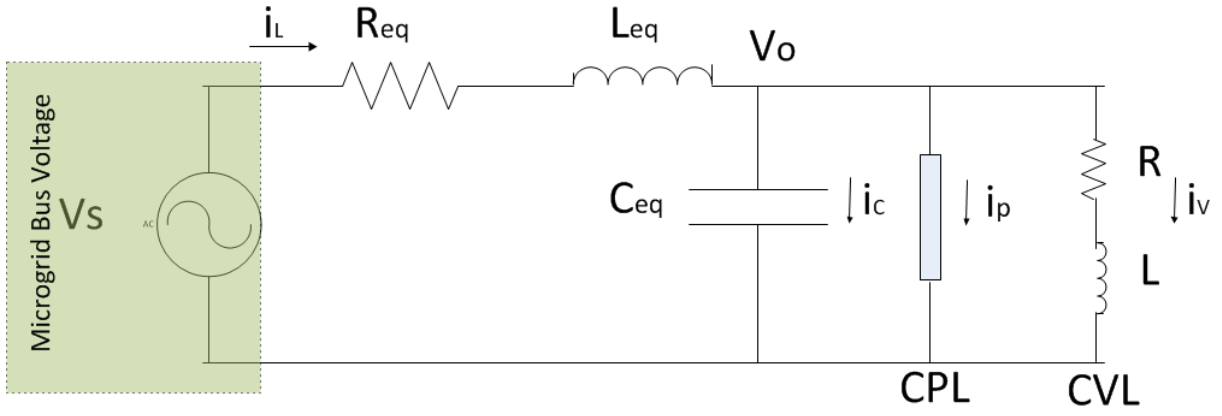


Figure 4:2: Equivalent circuit of AC microgrid with CPL and CVL [9].

By applying KVL to the equivalent model of microgrid as in figure 4.2, considering the Laplace equivalent model, we can derive the voltage and current equation of the circuit. For simplicity, we have considered  $R_{CVL} = R$  and  $L_{CVL} = L$  in equation (4.1).

$$V_s = (sL_{eq} + R_{eq})I_L + V \quad (4.1)$$

Where  $V_s$  is the input voltage and  $V_o$  is the output voltage of the system and  $I_L$  is the input circuit current. By applying KCL, we have the current equation of the circuit as shown in equation (4.2).

$$I_L = I_C + I_P + I_V \quad (4.2)$$

Here,  $I_C$  is the capacitive branch current,  $I_P$  is the constant power load current (CPL) and  $I_V$  represents the current of the constant voltage load (CVL). From the linear relation of current, those branch currents can be represented using circuit parameters. As shown in equation (4.3), the output voltage can be expressed as

$$V_o = \frac{1}{C_{eq}} \int I_C dt \quad (4.3)$$

$$I_C = sC_{eq}V_o \quad (4.4)$$

The CPL current is the function of the input voltage while load power remains constant as in equation 4.5.  $R_{CPL}$  is the dynamic resistance of CPL.

$$I_P = \frac{V_0}{R_{CPL}} \quad (4.5)$$

Constant voltage load follows the Ohms law, so the CVL current can be found from equation (4.6).

$$I_V = \frac{V_0}{sL+R} \quad (4.6)$$

From the equation (4.4), (4.5) and (4.6), equation (4.7) can be written as below.

$$I_L = sCeqVo + \frac{Vo}{R_{CPL}} + \frac{Vo}{sL+R} \quad (4.7)$$

Substituting equation (4.1) to equation (4.7), the transfer function of the system can be derived in equation (4.8).

$$Vs = (sLeq + Req) \left( sCeqVo + \frac{Vo}{R_{CPL}} + \frac{Vo}{sL+R} \right) + Vo$$

$$\Rightarrow \frac{V_0}{V_S} = \frac{1}{[(sLeq + Req) \left( sCeq + \frac{1}{R_{CPL}} + \frac{1}{sL+R} \right) + 1]} \quad (4.8)$$

For the ease of calculation, equation (4.8) can be rewritten in simplified form as equation (4.9).

$$\frac{V_0}{V_S} = \frac{R_{CPL}(Ls+R)}{m_3s^3 + m_2s^2 + m_1s + m_0} \quad (4.9)$$

Where

$$m_0 = R(R_{CPL} - Req) + R_{CPL}Req$$

$$m_1 = L(R_{CPL} - Req) + Leq(R_{CPL} - R) + CeqReqRR_{CPL}$$

$$m_2 = ReqCeqLR_{CPL} - LeqL + CeqLeqRR_{CPL}$$

$$m_3 = CeqLeqLR_{CPL}$$

The small signal stability of the system can be verified by applying Routh-Hurwitz Stability Criteria to the characteristics equation of the transfer function in equation (4.9) [9]. The necessary conditions to maintain the system pole at the LHP have been illustrated in equation (4.10), from which for simple

consideration two necessary conditions derived in equation (4.11). To be stable, the CPL power must be less than that of CVL and other system components combined.

$$\left\{ \begin{array}{l} a_0 = CeqLeqLR_{CPL} > 0 \\ a_1 = ReqCeqLR_{CPL} - LeqL + CeqLeqRR_{CPL} > 0 \\ a_2 = L(R_{CPL} - Req) + Leq(R_{CPL} - R) + CeqReqRR_{CPL} > 0 \\ a_3 = R(R_{CPL} - Req) + R_{CPL}Req \\ b_1 = \frac{a_2a_1 - a_0a_3}{a_1} > 0 \end{array} \right\} \quad (4.10)$$

$$\left\{ \begin{array}{l} R_{CPL} > \frac{RReq}{R+Req} \\ P_{CVL} + V_0^2 \frac{ReqCeq}{Leq} > P_{CPL} \end{array} \right\} \quad (4.11)$$

Here, we are trying to anticipate the stability of the system from the pole movement shown in figure 4.3 with respect to distinctions of key parameters like *Req*, *Ceq*, *Leq* and so on [9].

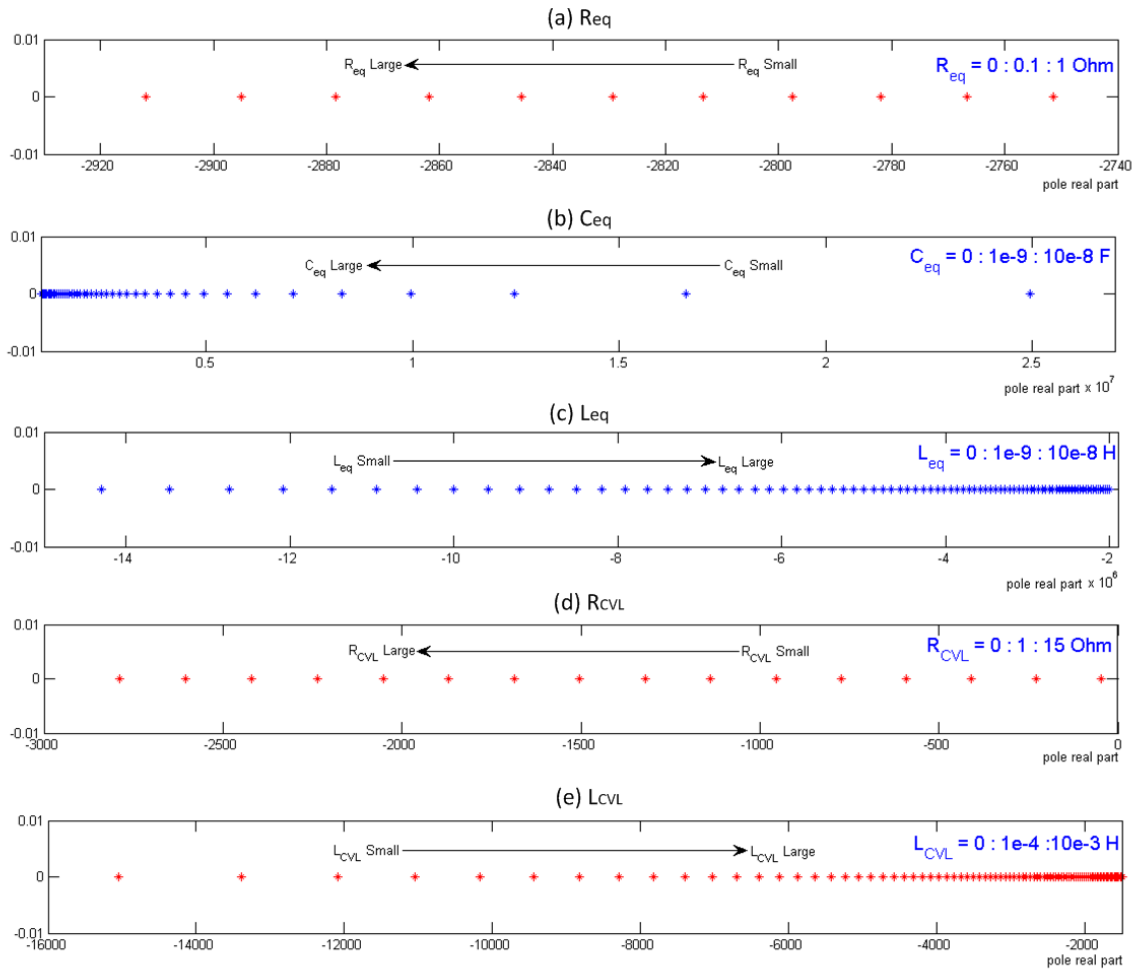


Figure 4.3: Movement of system poles with (a) equivalent resistance  $R_{eq}$ , (b) equivalent capacitance  $C_{eq}$ , (c) equivalent inductance  $L_{eq}$ . (d) CVL resistance  $R_{CVL}$  (e) CVL inductance  $L_{CVL}$  [9].

With the increase of  $R_{eq}$  and  $C_{eq}$ , the system becomes more stable, as the dominant pole moves to the left as depicted in figure 4.3(a) and 4.3(b) respectively. On the other hand, with the increase of  $L_{eq}$ , the system becomes unstable, as the dominant pole moves towards the right side as shown in Figure 4.3(c). Similar analysis can be performed for  $R_{CVL}$  in figure 4.3(d) and  $L_{CVL}$  in Figure 4.3(e). An increase in the  $L_{CVL}$  also hampers the system stability conditions. The parameter table is represented in Table 4.1. Figure 4.4 represents the stability status of the microgrid by using linear control technique such as pole-zero constellations.

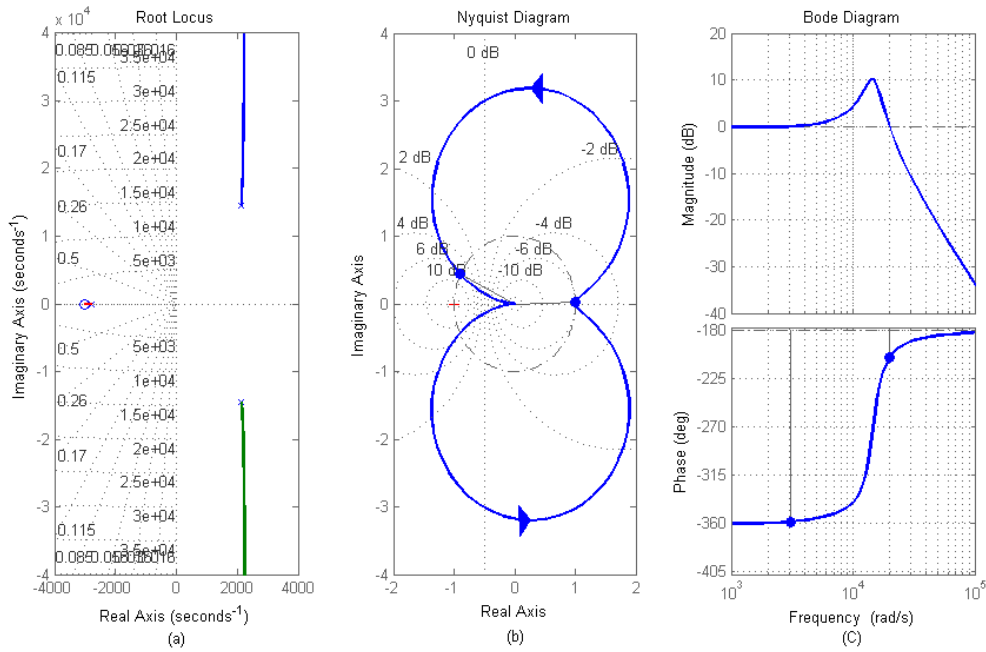


Figure 4.4: Stability status of conventional model.

From the figure 4.4(a), in root locus analysis, the nominal system have poles on the right half of the s-plane; and in figure 4.4(b), encirclement of  $(-1+j0)$  point is absent which indicates there are poles in the right half s-plane i.e;  $Z>0$ . Finally, from figure 4.4(c), the gain margin and phase margin of the system don't have a similar sign. All these three criteria indicate that the conventional microgrid model is an unstable system.

According to the above analysis as shown in figure 4.4, the movement of the system real part of the pole, it can be summarized that stability margin of the microgrid can be extended by increasing  $R_{eq}$ ,  $C_{eq}$  and  $R_{CVL}$  or by decreasing  $L_{eq}$  and  $L_{CVL}$  [9]. Generally, there are some practical restrictions in combination of the  $R_{eq}$ ,  $C_{eq}$  or  $R_{CVL}$  with the use of physical constituents. Likewise, it is not realistic to drop  $L_{eq}$  or  $L_{CVL}$ .

## 4.2.2 Stability of Proposed Active Power Compensation

Allowing to the above stability analysis of CPL, the limit of the stability in microgrid applications can be prolonged by increasing  $R_{eq}$  and  $C_{eq}$  or by diminishing  $L_{eq}$ . Nevertheless, there are several practical restrictions in multiplying  $R_{eq}$  and  $C_{eq}$  with the use of physical constituents which is explained in [9]. Likewise, it is hard to minimize  $L_{eq}$  from microgrid system. Therefore, a storage-based virtual impedance method is suggested in this dissertation to maintain microgrid stability with CPL by using load side compensation shown in figure 4.5. The transfer function of the proposed system is shown in equation (4.12).

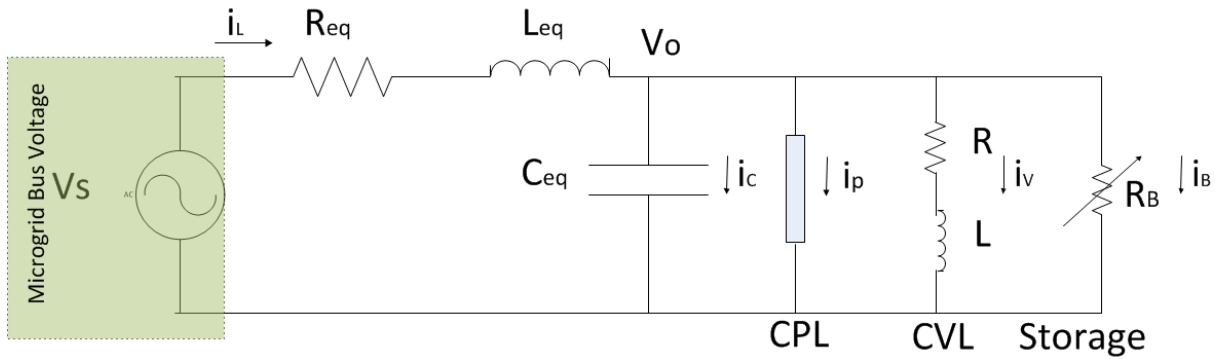


Figure 4:5: Modified model with proposed stability enhancement method (with real power compensation).

Transfer Function of the proposed system as shown in figure 4.5

$$\frac{V_O}{V_S} = \frac{sL+R}{C_1s^3+C_2s^2+C_3s+C_4} \quad (4.12)$$

Where

$$C_1 = LeqCeqL$$

$$C_2 = LeqCeqR - \frac{LeqL}{R_{CPL}} + \frac{LeqL}{R_B} + LeqL + LCeqReq$$

$$C_3 = Leq + LeqR - \frac{LeqR}{R_{CPL}} + \frac{LeqR}{R_B} + CeqRReq - \frac{LReq}{R_{CPL}} + \frac{LReq}{R_B} + LReq$$

$$C_4 = Req - \frac{RReq}{R_{CPL}} + \frac{RReq}{R_B} + RReq$$

Necessary conditions trivial signal stability of system in figure 4.5 can be derived by Routh-Hurwitz stability criterion from the transfer function of equation (4.12) and represented in equation (4.13)

$$\left\{ \begin{array}{l} a_0 = LeqCeql > 0 \\ a_1 = LeqCeqR - \frac{Leql}{R_{CPL}} + \frac{Leql}{R_B} + Leql + LCeqReq > 0 \\ a_2 = Leq + LeqR - \frac{LeqR}{R_{CPL}} + \frac{LeqR}{R_B} + CeqRReq - \frac{LReq}{R_{CPL}} + \frac{LReq}{R_B} + LReq > 0 \\ a_3 = Req - \frac{RReq}{R_{CPL}} + \frac{RReq}{R_B} + RReq \\ b_1 = \frac{a_3a_2 - a_1a_4}{a_2} > 0 \end{array} \right\} \quad (4.13)$$

Then the condition for system stability, equation (4.14)

$$\left\{ \begin{array}{l} R_{CPL} > \frac{RR_B}{R_B + RR_B + R} \\ P_{CVL} + V_0^2 \frac{ReqCeql}{Leq} + P_B > P_{CPL} \end{array} \right\} \quad (4.14)$$

Here, we have a number of approaches to stabilize the operating system built on equation (4.14).

- By keeping a greater R/L proportion for the feeder impedance connecting the distributed generators and loads. Typically, supply level feeders possess greater R/L rate associated with that of the transmission level feeders.
- By enhancing  $C_{eq}$  of the regarding couple of feeder lines. This can readily be accomplished by addition of the filter capacitor.
- By increasing the system supply voltage  $V_{S,rms}$  which is inappropriate; that is why keeping microgrid system stable is a huge challenge as the base voltage increase.

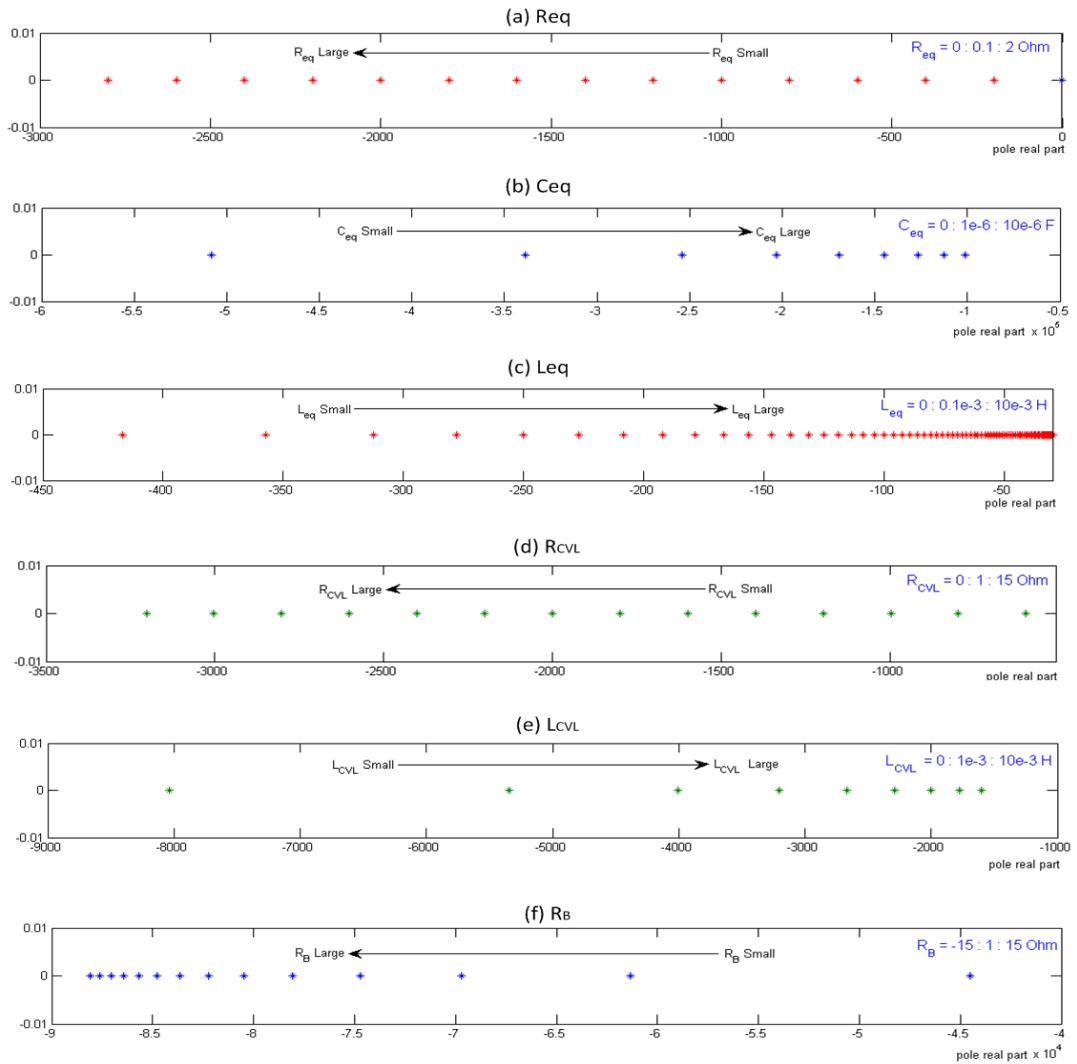


Figure 4:6: Movement of system poles with (a) equivalent resistance  $R_{eq}$ , (b) equivalent capacitance  $C_{eq}$ , (c) equivalent inductance  $L_{eq}$ . (d) CVL resistance  $R_{CVL}$ . (e) CVL inductance  $L_{CVL}$ . (f) virtual resistance  $R_B$ .

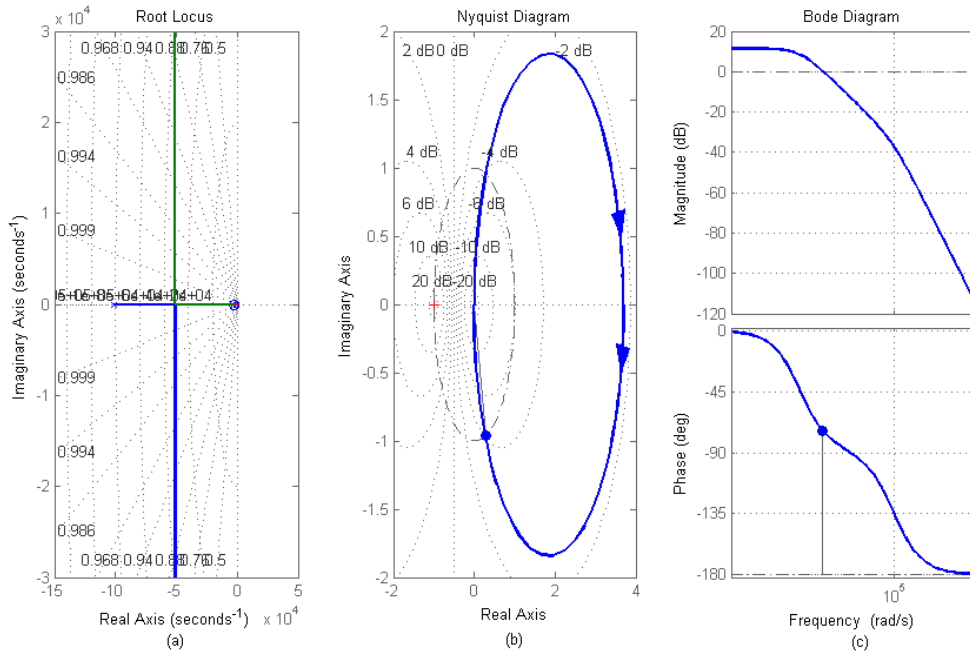


Figure 4.7: Stability status of proposed model with active power compensation.

The stability has been achieved by using active power compensation for the proposed microgrid system shown for the three different linear control techniques in figure 4.7 (a), 4.7 (b), and 4.7(c) respectively.

The impact of various parameters on system stability (sensitivity analysis) is presented below.

Power relation of conventional model in equation (4.15)

$$P_{CPL} < \frac{P_{CVL} \left( \frac{L}{L_{eq}} + 1 \right) V^2 + R_{eq} \frac{C_{eq}}{L_{eq}} V^4}{\frac{L}{L_{eq}} P_{CVL} + V^2} \quad (4.15)$$

Power relation of proposed model in equation (4.16)

$$P_{CPL} < V^2 \frac{L_{eq} R_B P_{CVL} + L_{eq} R_B V^2 + L_{eq} V^2 + C_{eq} R_{eq} R_B V^2 + L R_{eq} P_{CVL} + L R_{eq} R_B P_{CVL}}{R_B (L_{eq} V^2 + L R_{eq} P_{CVL})} \quad (4.16)$$

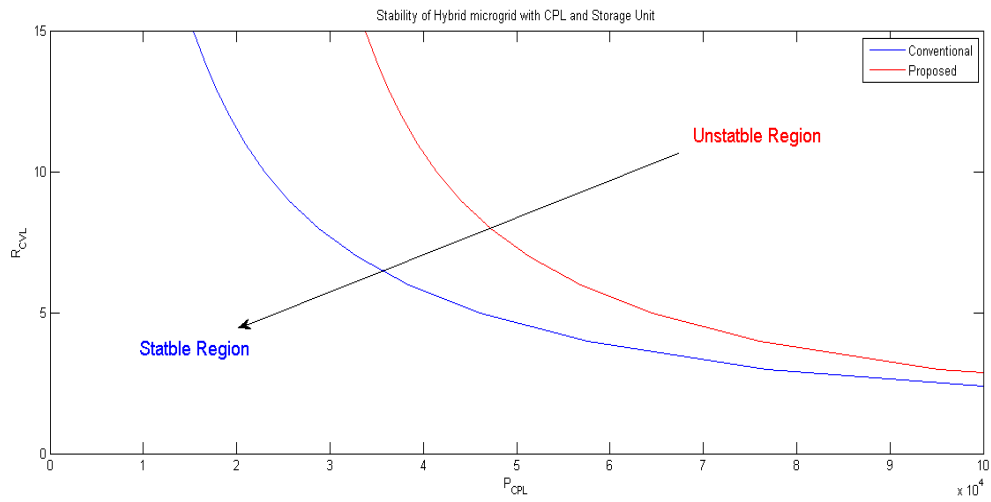


Figure 4:8: Stable and unstable region for the conventional(blue) and proposed(red) system from table 1 and equation (4.16) and equation (4.17) where  $R_{CvL}$  is varied from 0 : 0.05 : 0.25 ohms.

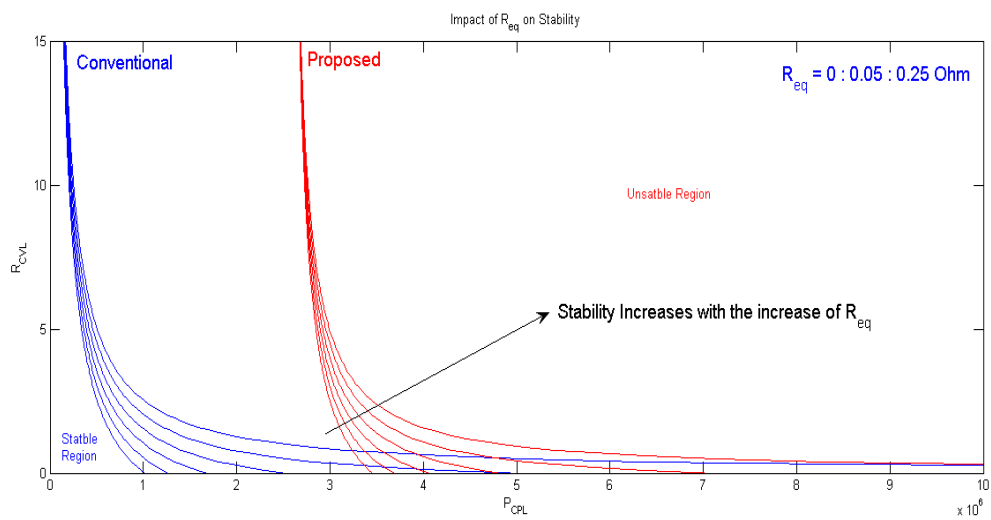


Figure 4:9: Impact of  $R_{eq}$  on system stability for both conventional(blue) and proposed(red) system where  $R_{eq}$  is varied from 0 : 0.05 : 0.25 Ohms (stability improves with the increases of  $R_{eq}$ ).

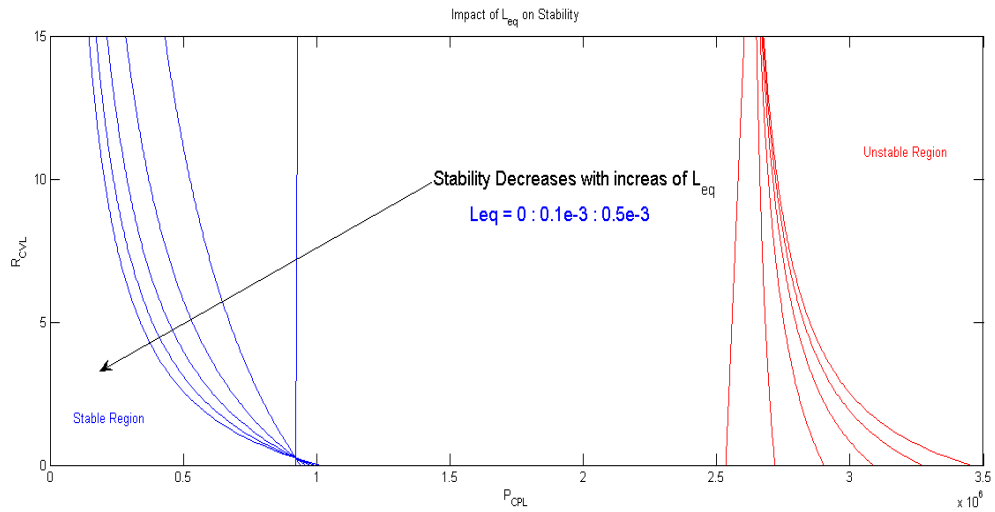


Figure 4:10: Impact of  $L_{eq}$  on system stability for both conventional(blue) and proposed(red) system where  $L_{eq}$  is varied from  $0 : 0.1e-3 : 0.5e-3$  H (stability decreases with the increases of  $L_{eq}$ ).

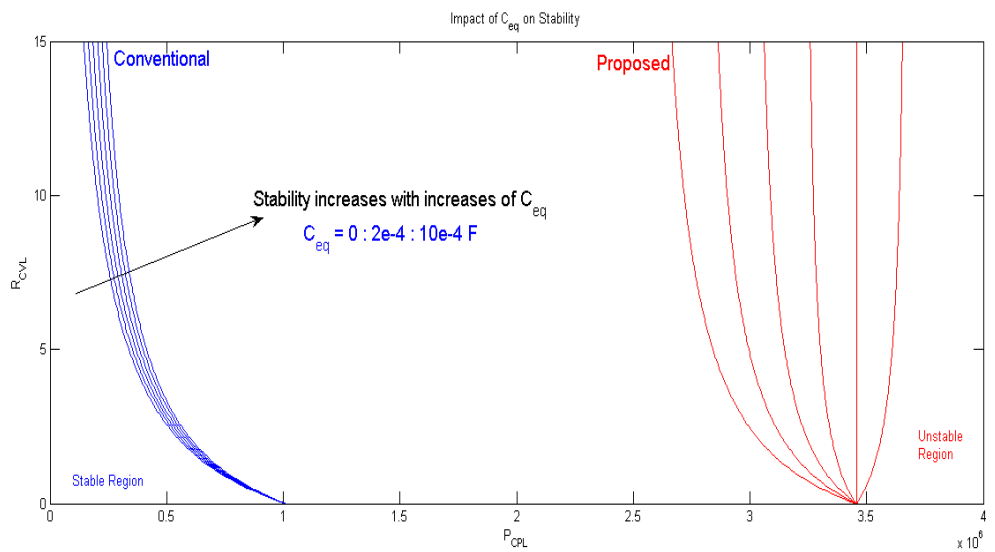


Figure 4:11: Impact of  $C_{eq}$  on system stability for both conventional(blue) and proposed(red) system where  $C_{eq}$  is varied from  $0 : 2e-4 : 10e-4$  F (stability improves with the increases of  $C_{eq}$ ).

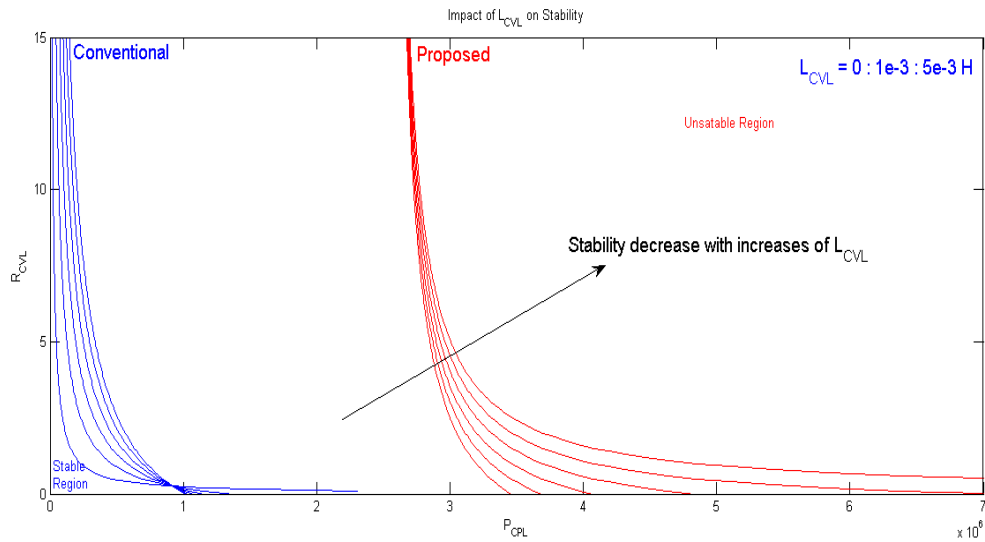


Figure 4:12: Impact of  $L_{CVL}$  on system stability for both conventional(blue) and proposed(red) system where  $L_{CVL}$  is varied from 0 : 1e-3 : 5e-3 H (stability decreases with the increases of  $L_{CVL}$ ).

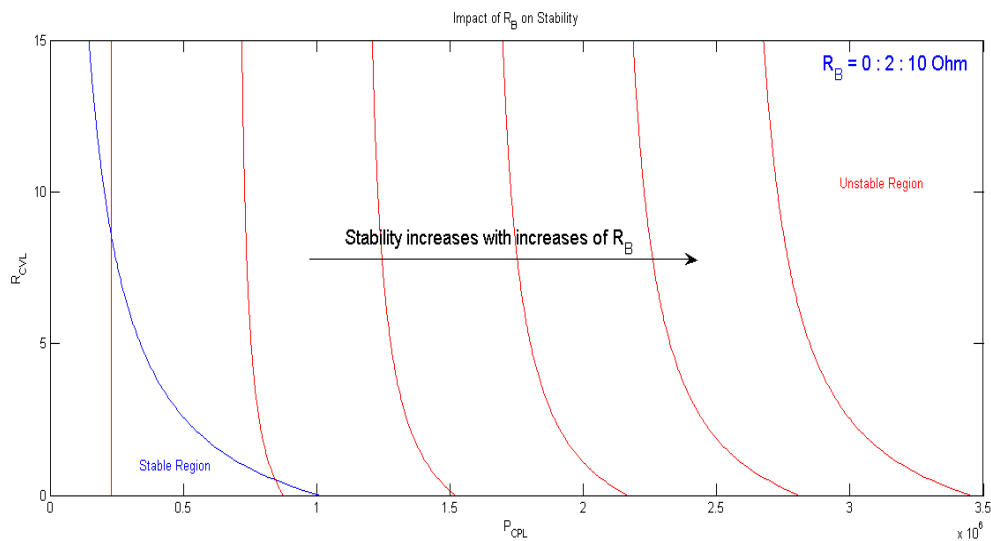


Figure 4:13: Impact of  $R_B$  on system stability for both conventional(blue) and proposed(red) system where  $R_B$  is varied from 0 : 2 : 10 H (stability increases with the increases of  $R_B$ ).

### 4.2.3 Stability of Proposed Reactive Power Compensation

For the reactive power compensation, we need to replace real component  $R_B$  with a combination of reactive element as represented in figure 4.14.

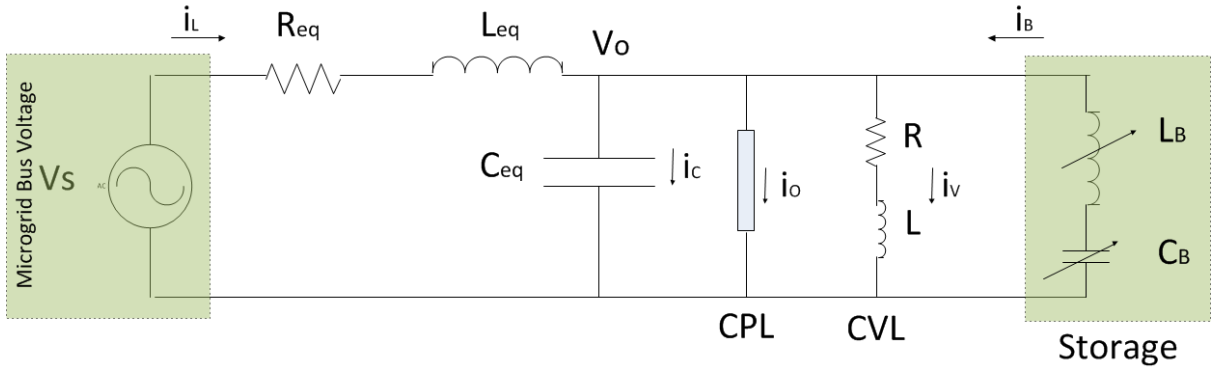


Figure 4:14: Modified model with proposed stability enhancement method (with reactive power compensation).

Transfer function is given in equation (4.17)

$$\frac{V_o}{V_s} = \frac{N_0}{D_1 s^5 + D_2 s^4 + D_3 s^3 + D_4 s^2 + D_5 s + D_6} \quad (4.17)$$

Where,

$$N_0 = ((C_b L L_b R_{cpl}) s^3 + (C_b L R_b R_{cpl} + C_b L_b R R_{cpl}) s^2 + (L R_{cpl} + C_b R R_b R_{cpl}) s + R R_{cpl})$$

$$D_1 = (C_b C_{eq} L L_b L_{eq} R_{cpl})$$

$$D_2 = (C_b L L_b L_{eq} R_{cpl} - C_b L L_b L_{eq} + C_b C_{eq} L L_b R_{eq} R_{cpl} + C_b C_{eq} L L_{eq} R_b R_{cpl} + C_b C_{eq} L_b L_{eq} R R_{cpl})$$

$$D_3 = (C_b L L_{eq} R_{cpl} - C_b L L_{eq} R_b - C_b L_b L_{eq} R - C_b L L_b R_{eq} + C_{eq} L L_{eq} R_{cpl} + C_b L_b L_{eq} R_{cpl} + C_b L L_b R_{eq} R_{cpl}$$

$$+ C_b L L_{eq} R_b R_{cpl} + C_b L_b L_{eq} R R_{cpl} + C_b C_{eq} L R_b R_{cpl} R_{eq}$$

$$+ C_b C_{eq} L_b R R_{cpl} R_{eq} + C_b C_{eq} L_{eq} R R_b R_{cpl})$$

$$D_4 = (L L_{eq} R_{cpl} - L L_{eq} - C_b L R_b R_{eq} - C_b L_b R R_{eq} - C_b L_{eq} R R_b + C_b L R_{cpl} R_{eq}$$

$$+ C_b L_{eq} R R_{cpl} + C_{eq} L R_{cpl} R_{eq} + C_{eq} L_{eq} R R_{cpl} + C_b L_b R_{cpl} R_{eq}$$

$$+ C_b L_{eq} R_b R_{cpl} + C_b L R_{eq} R_b R_{cpl} + C_b R R_{eq} L_b R_{cpl} + C_b R L_{eq} R_b R_{cpl} + C_b R C_{eq} R_b R_{cpl} R_{eq})$$

$$D_5 = (L_{eq} R_{cpl} - L_{eq} R - L R_{eq} \mp L R_{cpl} R_{eq} + R R_{cpl} L_{eq} - R R_b R_{eq} C_b + R R_{cpl} R_{eq} C_b + R R_{cpl} R_{eq} C_{eq}$$

$$+R_{cpl}R_{eq}C_bR_b + R_{cpl}RC_bR_bR_{eq})$$

$$D_6 = -RR_{eq} + R_{cpl}R_{eq} + RR_{cpl}R_{eq}$$

We used Routh-Hurwitz stability criterion to find the small signal stability of the system shown in equation 4.17. The stability has been achieved by using reactive power compensation for the proposed microgrid system shown for the three different linear control techniques in figure 4.16 (a), 4.16 (b), and 4.16(c) respectively.

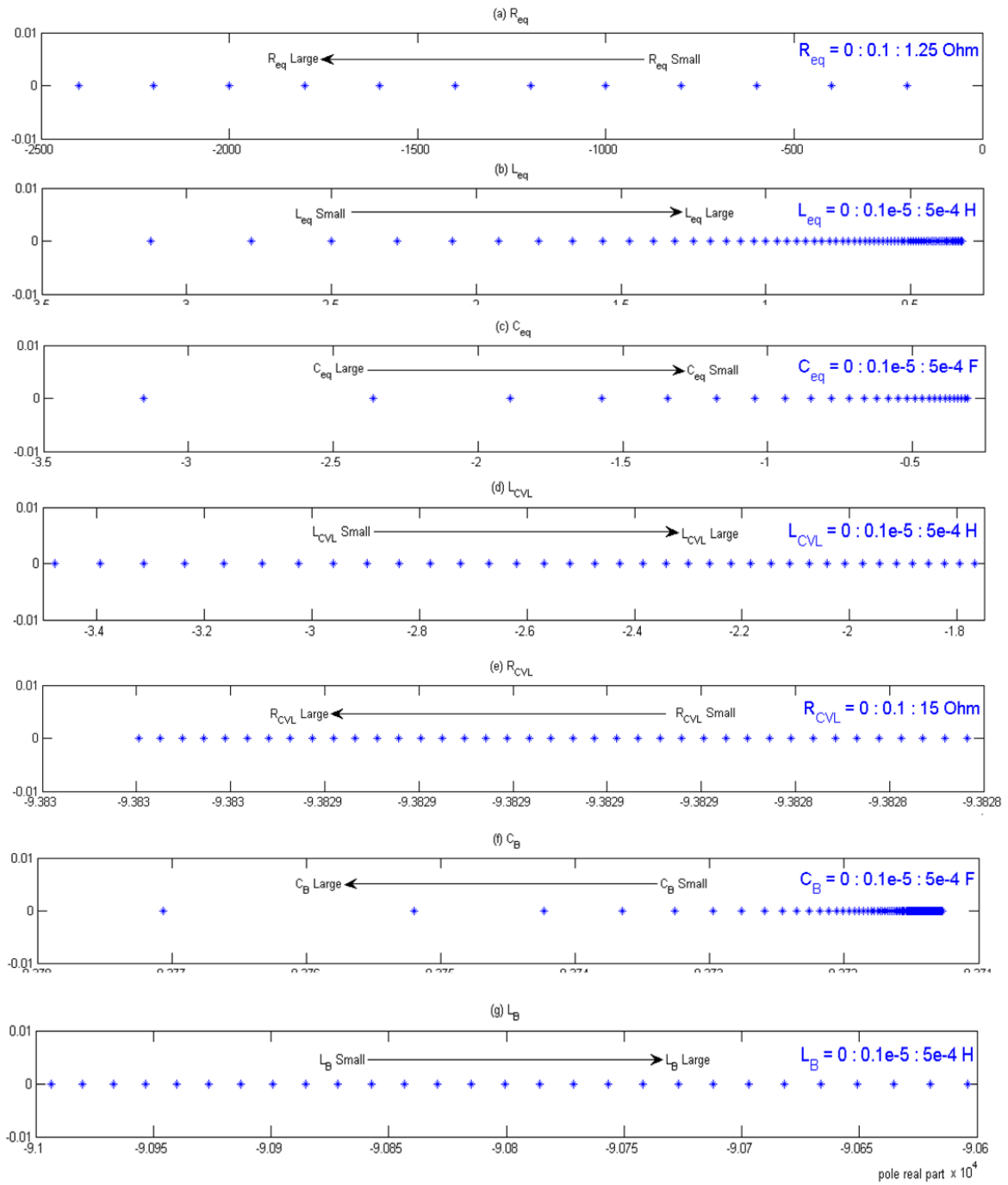


Figure 4:15: Movement of system poles with (a) equivalent resistance  $R_{eq}$ , (b) equivalent capacitance  $C_{eq}$ , (c) equivalent inductance  $L_{eq}$ . (d) CVL inductance  $L_{CVL}$ . (d) CVL resistance  $R_{CVL}$  (f) virtual capacitance  $C_B$  (g) virtual inductance  $L_B$ .

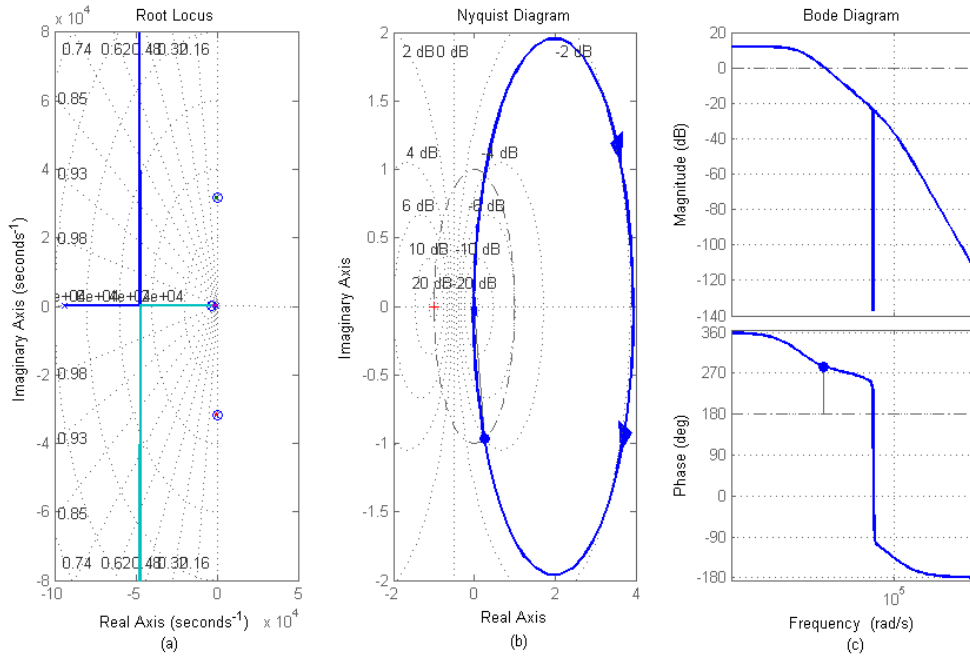


Figure 4:16: Stability status of proposed microgrid system with reactive power compensation.

Table 4-1: Table of Parameters.

Symbol	Standard Value	Range of Variation
$R_{eq}$	0.25 Ohm	0 : 0.05 : 0.25
$L_{eq}$	0.5e-3 H	0 : 0.1e-3 : 0.5e-3
$C_{eq}$	10e-6 F	0 : 2e-4 : 10e-4
$R_{CVL}$	15 Ohm	0 : 0.1 : 15
$L_{CVL}$	5e-3 H	0: 1e-3 : 5e-3
$R_B$	10 Ohm	0 : 2 : 10
$C_B$	1e-6 F	0 : 0.2e-6 : 1e-6
$L_B$	1e-3 H	0 : 0.2e-3 : 1e-3

Power relation of conventional model in equation (4.18)

$$P_{CPL} < \frac{P_{CVL} \left( \frac{L}{L_{eq}} + 1 \right) V^2 + R_{eq} \frac{C_{eq}}{L_{eq}} V^4}{\frac{L}{L_{eq}} P_{CVL} + V^2} \quad (4.18)$$

Power relation of proposed model in equation (4.19)

$$P_{CPL} < V^2 \frac{L_{eq}R_B P_{CVL} + L_{eq}R_B V^2 + L_{eq}V^2 + C_{eq}R_{eq}R_B V^2 + LR_{eq}P_{CVL} + LR_{eq}R_B P_{CVL}}{R_B(L_{eq}V^2 + LR_{eq}P_{CVL})} \quad (4.19)$$

Power relation ZB (with reactive power compensation) in equation (4.20)

$$P_{CPL} > V^2 \frac{C_B L L_{eq} + C_{eq} L L_{eq} + C_B L B L_{eq} + C_B L L B R_{eq} + C_B L B L_{eq} R + C_B C_{eq} L B R R_{eq}}{C_B L L B R_{eq} + C_B L B L_{eq} R} \quad (4.20)$$

Impact of various parameters on system stability (sensibility analysis)

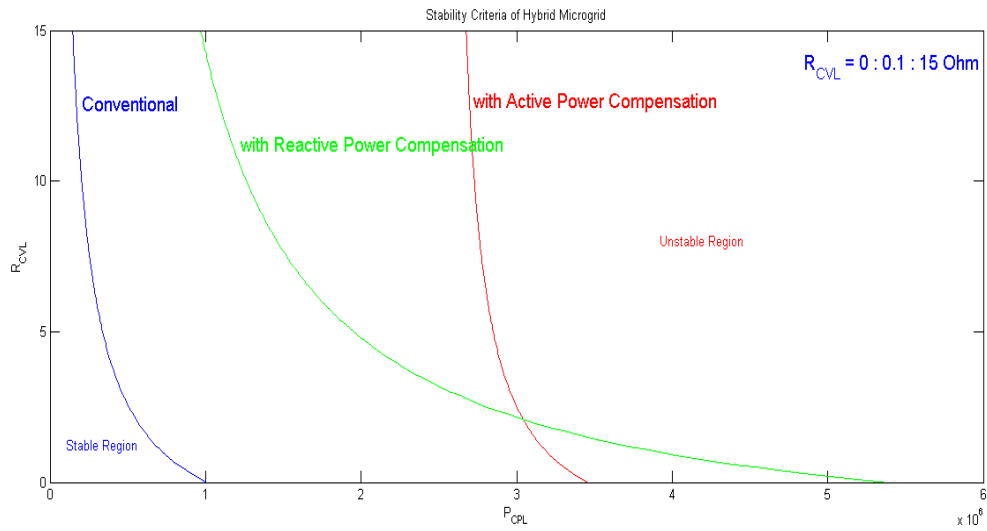


Figure 4:17: Stable and unstable region for the conventional(blue), with active power compensation(red) and with reactive power compensation(green) system from table 1 and equation (4.19), equation (4.20) and equation (4.21) where  $R_{CVL}$  is varied from 0 : 0.1 : 0.25 ohms.

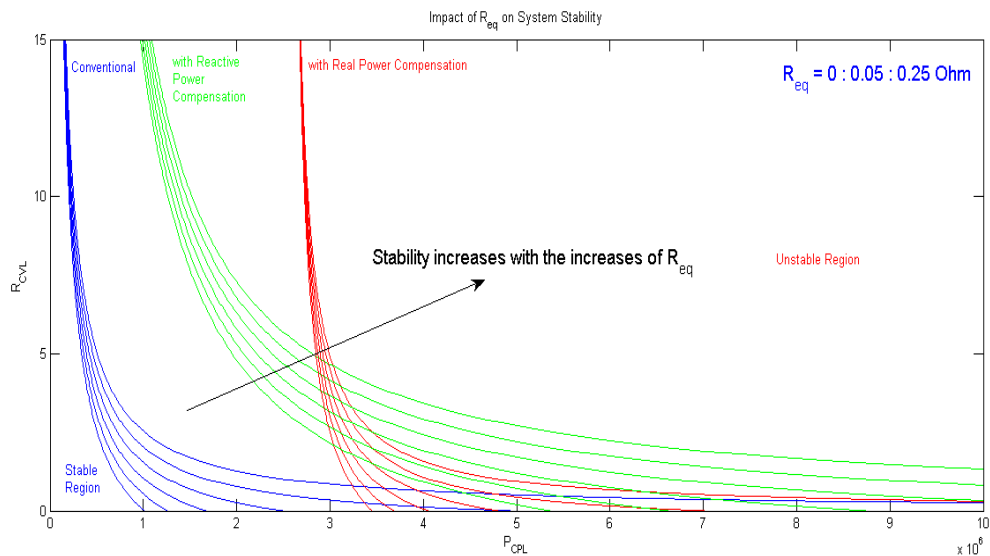


Figure 4:18: Impact of  $R_{eq}$  on system stability for both conventional(blue), with active power compensation(red) and with reactive power compensation(green) system where  $R_{eq}$  is varied from 0 : 0.05 : 0.25 ohms (stability improves with the increases of  $R_{eq}$ ).

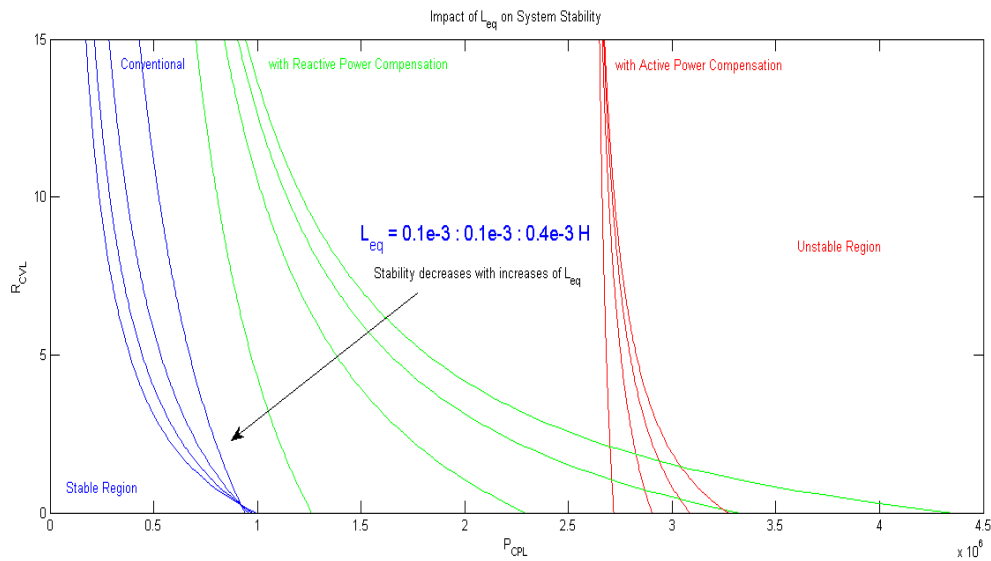


Figure 4:19: Impact of  $L_{eq}$  on system stability for both conventional(blue), with active power compensation(red) and with reactive power compensation(green) system where  $L_{eq}$  is varied from 0 : 0.1e-3 : 0.4e-3 H (stability decreases with the increases of  $L_{eq}$ ).

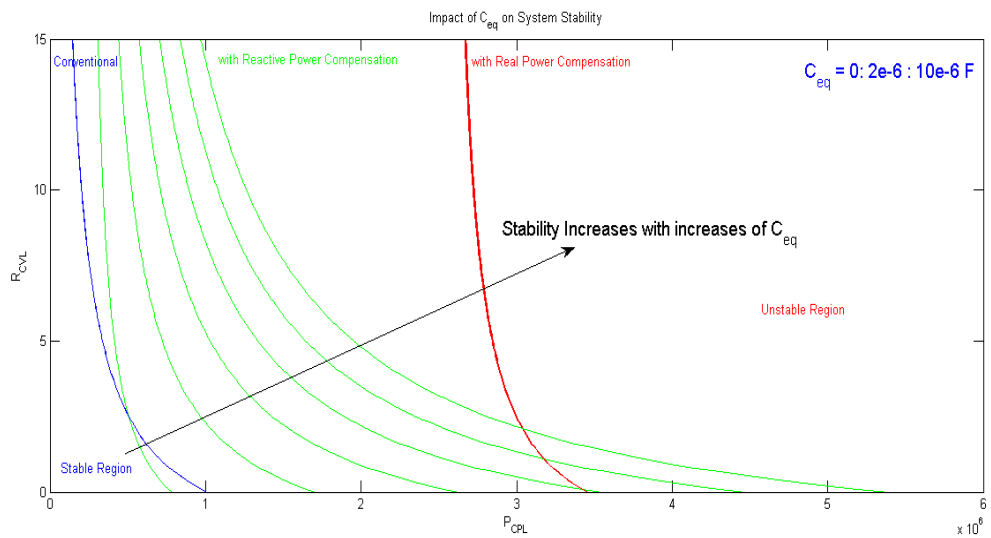


Figure 4:20: Impact of  $C_{eq}$  on system stability for both conventional(blue), with active power compensation(red) and with reactive power compensation(green) system where  $C_{eq}$  is varied from 0 : 2e-6 : 10e-6 F (stability improves with the increases of  $C_{eq}$ ).

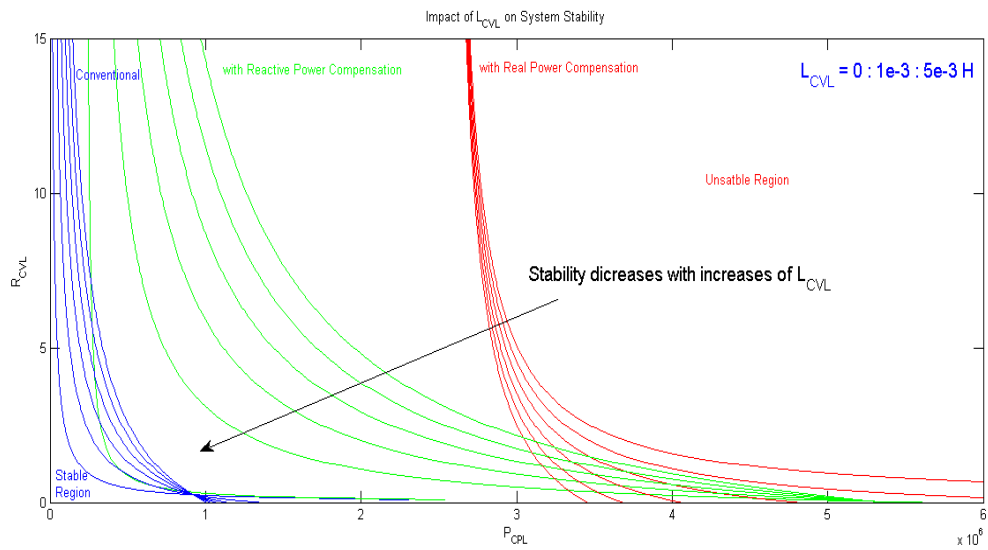


Figure 4:21: Impact of  $L_{CVL}$  on system stability for both conventional(blue), with active power compensation(red) and with reactive power compensation(green) system where  $L_{CVL}$  is varied from 0 : 1e-3 : 5e-3 H (stability decreases with the increases of  $L_{CVL}$ ).

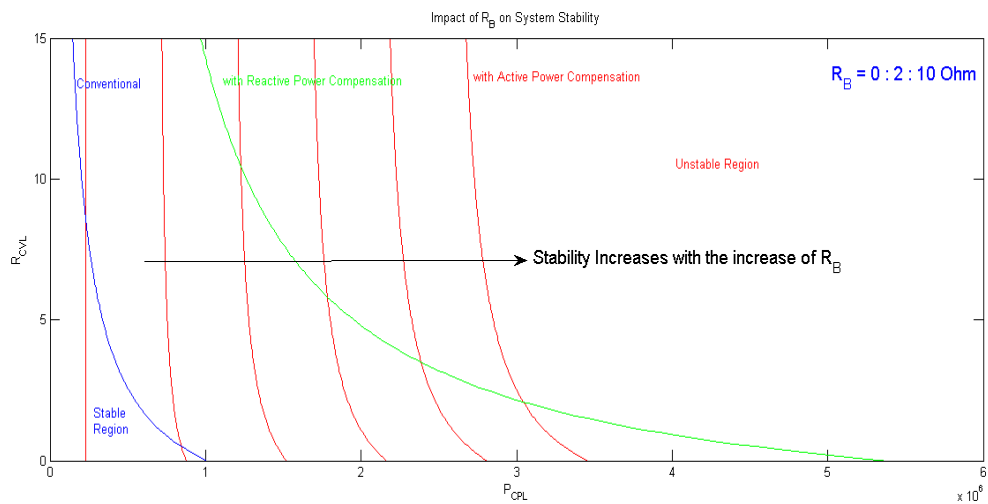


Figure 4:22: Impact of  $R_B$  on system stability for both conventional(blue), with active power compensation(red) and with reactive power compensation(green) system where  $R_B$  is varied from 0 : 2 : 10 Ohm (stability increases with the increases of  $R_B$ ).

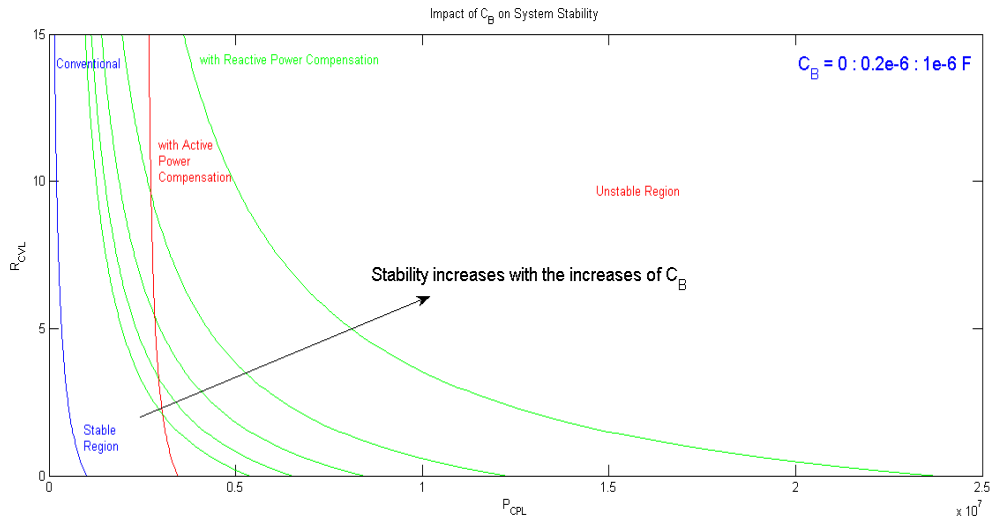


Figure 4:23: Impact of  $C_B$  on system stability for both conventional(blue), with active power compensation(red) and with reactive power compensation(green) system where  $C_B$  is varied from 0 : 0.2e-6 : 1e-6 F (stability increases with the increases of  $C_B$ ).

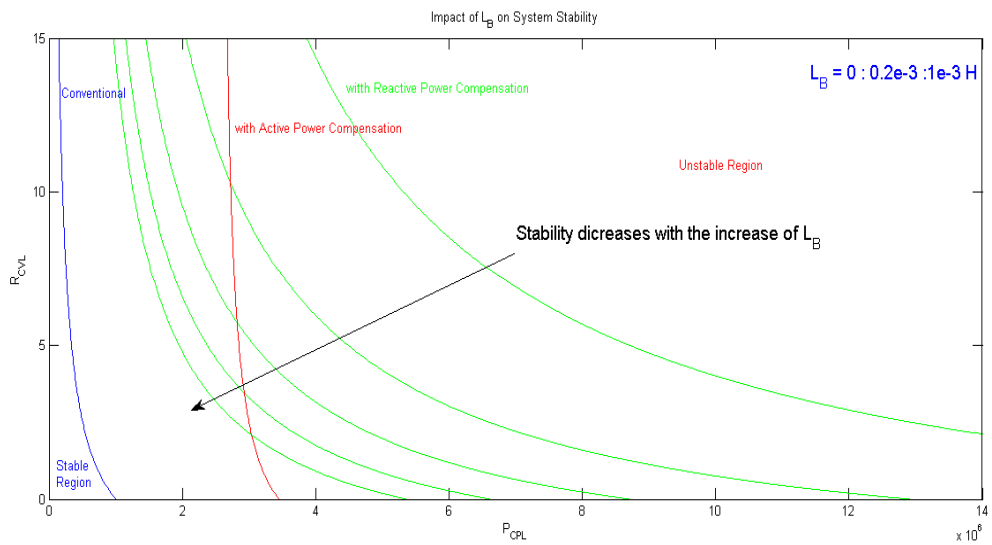


Figure 4:24: Impact of  $L_B$  on system stability for both conventional(blue), with active power compensation(red) and with reactive power compensation(green) system where  $L_B$  is varied from 0 : 0.2e-3 : 1e-3 H (stability decreases with the increase of  $L_B$ ).

### 4.3 Lyapunov Stability Criteria

Consider the state-space equation (4.21) to (4.23)

$$\dot{x}_1 = \frac{-R}{L}x_1 - \frac{1}{L}x_2 + \frac{1}{L}u \quad (4.21)$$

$$\dot{x}_2 = \frac{x_1}{C} + \frac{P_0}{C*x_2} - \frac{x_3}{C} - \frac{u}{C} \quad (4.22)$$

$$\dot{x}_3 = \frac{1}{L}x_2 - \frac{R}{L}x_3 \quad (4.23)$$

The control objective is for the state  $x_2$  to follow the set point  $V_S$  even the input  $V_S$  vary in equation (4.24).

$$x_2 \rightarrow V_S \quad (4.24)$$

Let the tracking problem error dynamics as in equation (4.25)

$$e = V_S - x_2 \quad (4.25)$$

According to the control objective, let the sliding surface be in equation (4.26) and (4.27)

$$s = e \quad (4.26)$$

$$\dot{s} = \dot{e} \quad (4.27)$$

The sliding mode controller design uses the Lyapunov stability criterion.

Let the Lyapunov function candidate be in equation (4.28) to (4.30)

$$V = \frac{s^2}{2} > 0 \quad (4.28)$$

$$\dot{V} = s\dot{s} < 0 \quad (4.29)$$

$$\dot{V} = s \left( \dot{V}_S - \frac{x_1}{C} - \frac{P_0}{C*x_2} + \frac{x_3}{C} + \frac{u}{C} \right) < 0 \quad (4.30)$$

$$\text{Let, } u = u_0 + u_1 \quad (4.31)$$

$$\text{Let } u_0 = -C \left[ \dot{V}_S - \frac{x_1}{C} - \frac{P_0}{C*x_2} + \frac{x_3}{C} \right] = x_1 + \frac{P_0}{x_2} - x_3 - C\dot{V}_S \quad (4.32)$$

$$\text{Let, } u_1 = C[-s - k\text{sign}(s)] \quad (4.33)$$

If there are uncertainties and perturbations with unknown magnitude but bounded, the input  $u$  with the discontinuous control,  $u_1$  as,  $C*[-s-k*\text{sign}(s)]$  keeps the  $\dot{V}$  to be negative or less than zero, thus ensuring the stability of the system according to Lyapunov stability criterion.

# Chapter 5 : Simulation Results and Discussion

## 5.1 Introduction

In this chapter, we are going to present our simulation results with different control techniques. If the graphical illustrations satisfy the control objectives, they will validate the system stability.

## 5.2 Simulation Results for PID Control Technique

To verify the proposed stabilization method a simulation of proposed technique in MATLAB/SIMULINK platform has been performed. A representation of schematic diagram Simulink modified control scheme of microgrid is shown in figure 5.1.

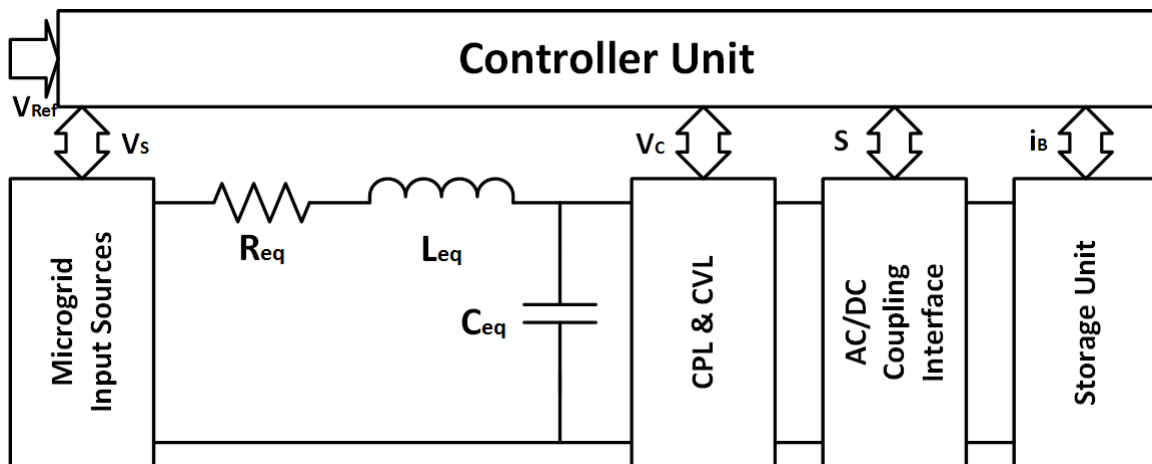


Figure 5:1: Modified controller model of microgrid system to implement the proposed storage base virtual resistor stabilization technique.

The active power compensation has been achieved by using active component of energy storage system, RB fed by the load side. Likely, the reactive power compensation has been achieved by using reactive component of energy storage system, a combination of LB and CB. In both cases, current of the energy storage system has been injected to the system via that virtual impedance. The required compensation has been obtained by the virtual impedance. The bus voltage of the CPL loads can be maintained within the stability limit by injecting current from energy storage system; hence the



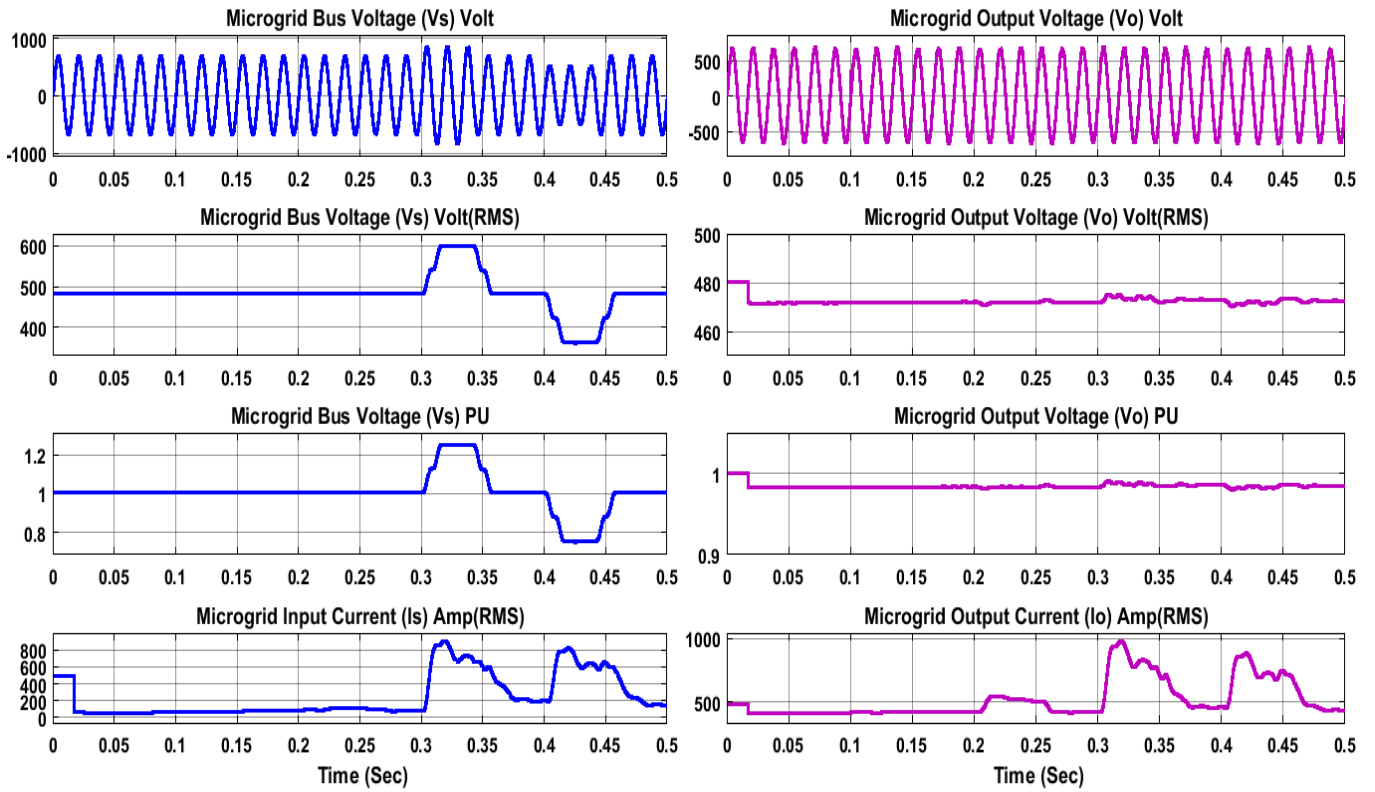


Figure 5:3: Comparison between the Input and Output Parameters (voltage and current) after adopting proposed compensation technique.

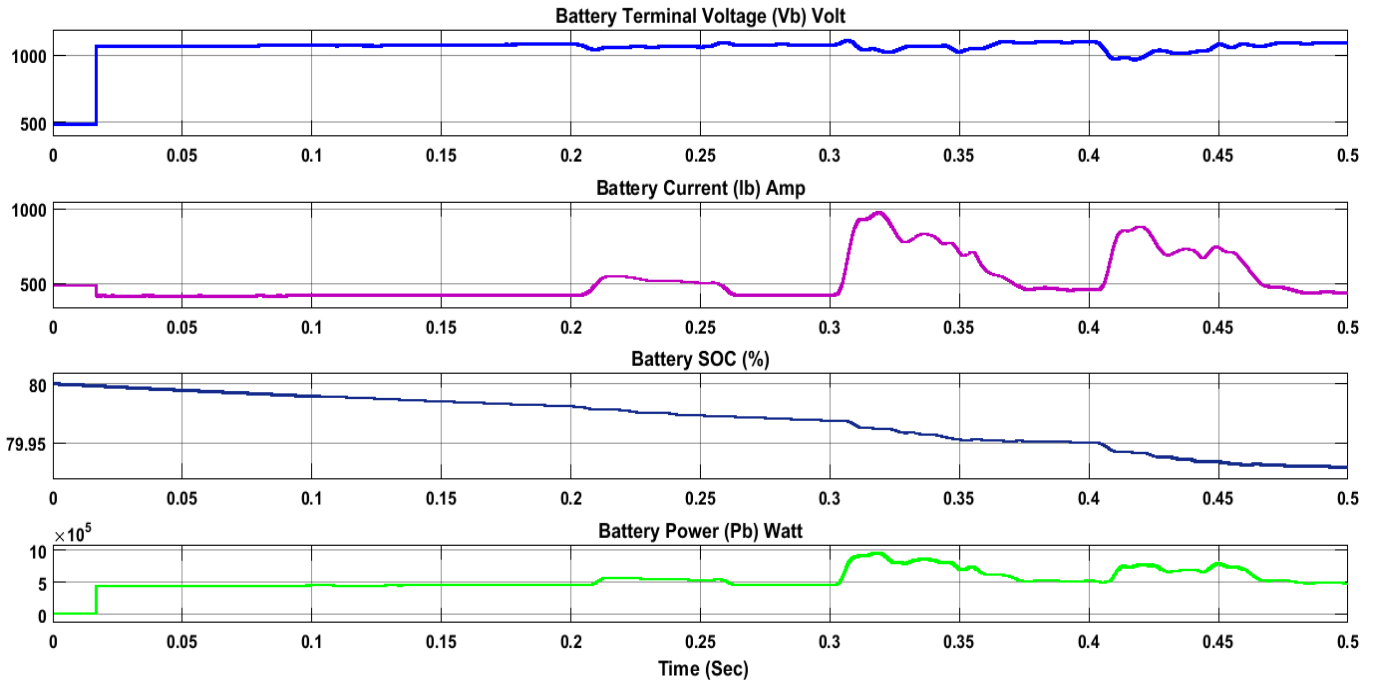


Figure 5:4: Contribution of the battery compensator in case of voltage, current, SOC, and power.

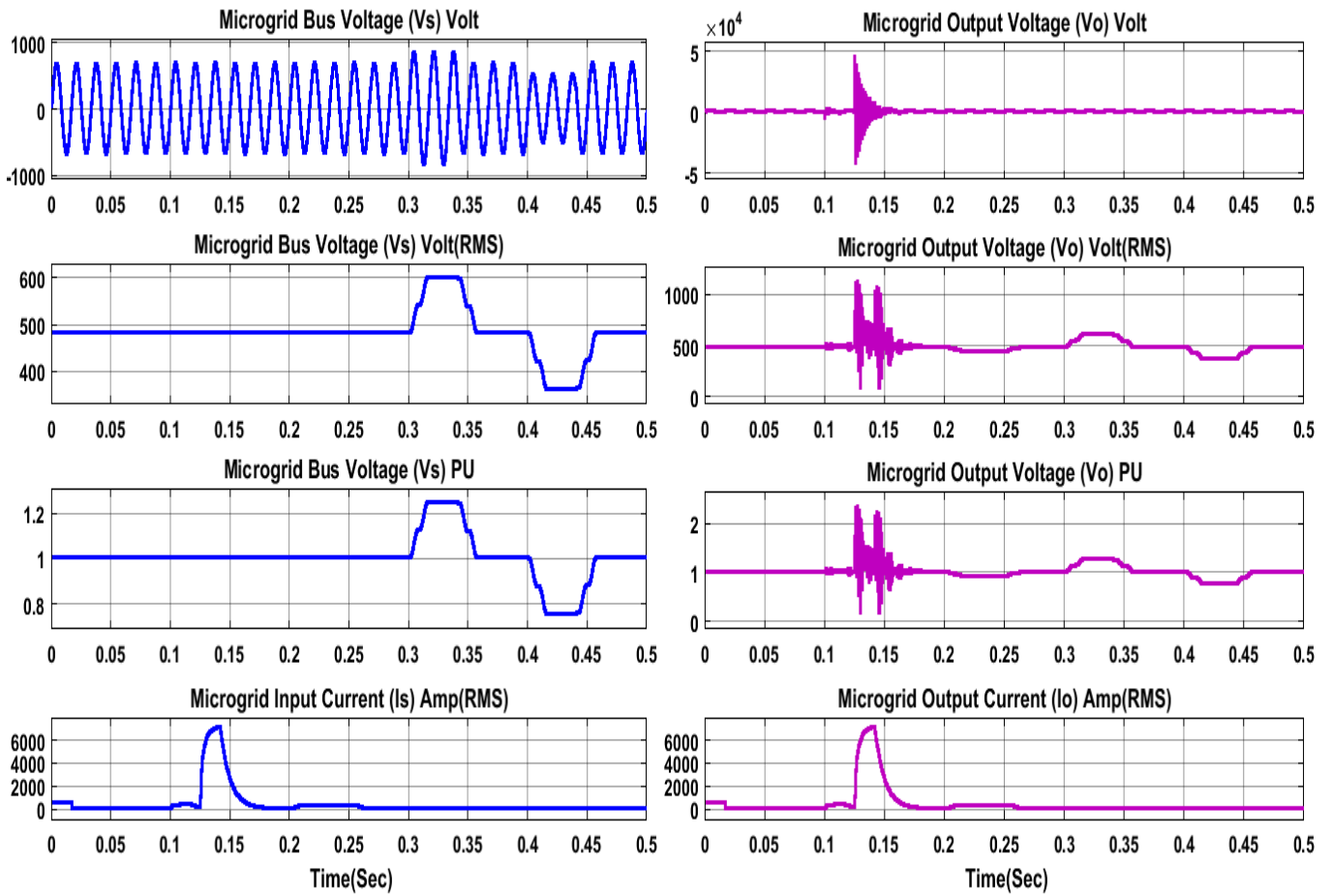


Figure 5:5: Comparison between input and output (voltage and current) of the microgrid system before adopting compensation technique.

Before applying the proposed scheme there was a major irregularity between the input voltage and output voltage across CPL which is represented in in figure 5.4 along with their RMS. And the required power provided by the battery unit to maintain a constant output voltage level is represented in figure 5.3 with respective RMS.

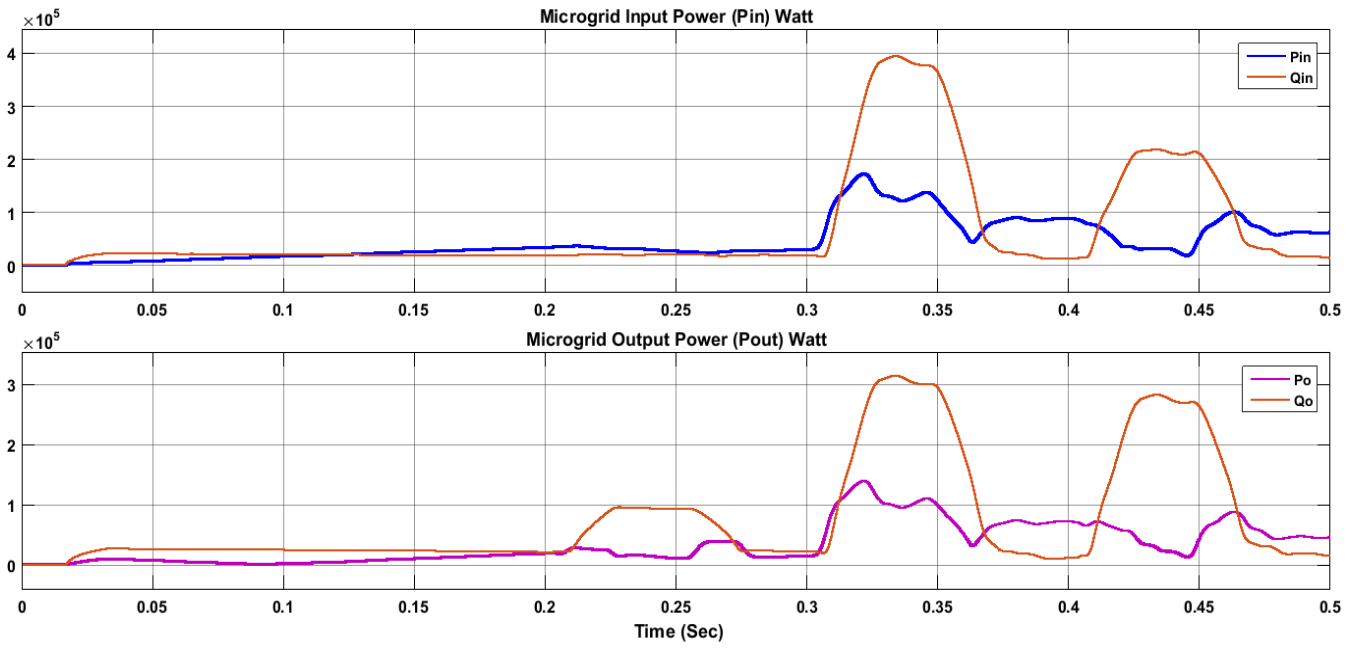


Figure 5:6: Comparison of input and output power (both real and reactive) after adopting the proposed compensation technique.

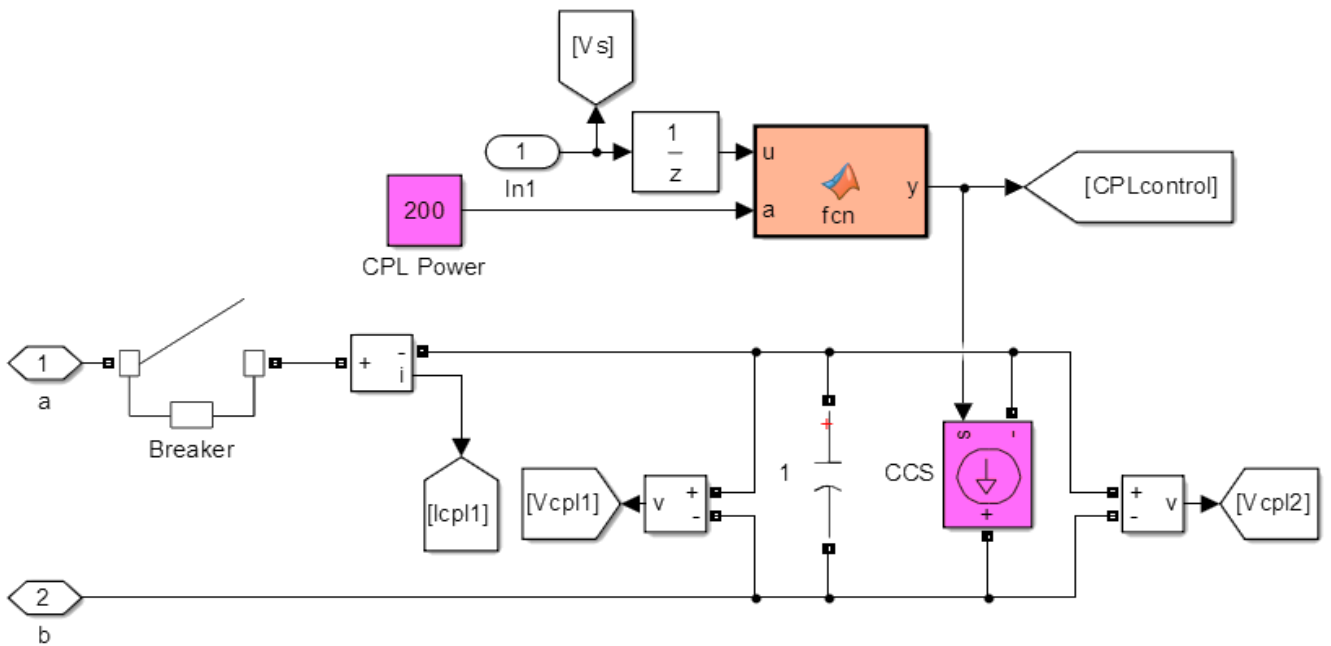


Figure 5:7: Representation of CPL-loaded system with controlled current source.

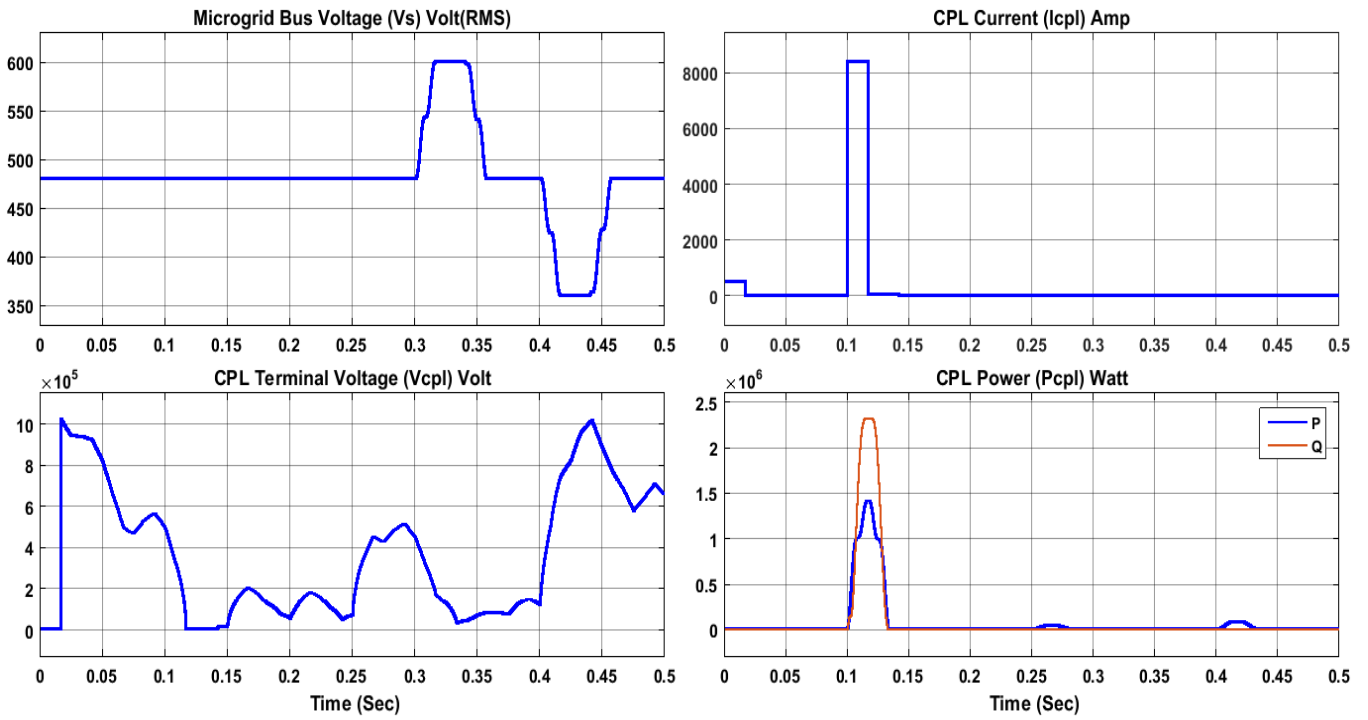


Figure 5:8: Representation of CPL load performance parameters (terminal voltage, current and power)

At figure 5.9, a representation of CVL load performance parameters (terminal voltage, current, and power) has been shown. After that, the reference voltage, microgrid output voltage, error signal, and the control signal regarding the proposed PID controller have been presented at figure 5.10. Later at figure 5.11(a) the block diagram of the proposed controller using PID control technique has been given. Then, at figure 5.11(b), gate signal of the MOSFET/ diode universal bridge has been shown. After that, the steps how the entire controller operates its functions to provide the desire stability of the system have been discussed in brief below.

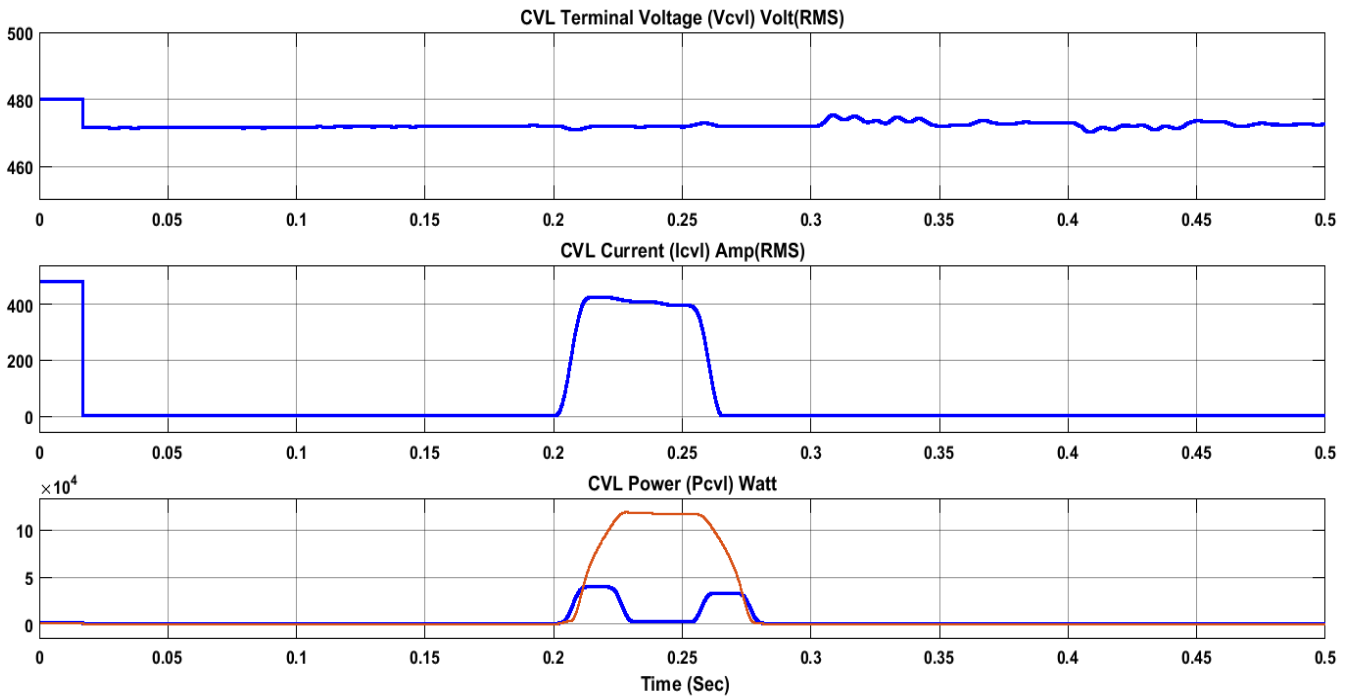


Figure 5:9: Representation of CVL load performance parameters (terminal voltage, current and power)

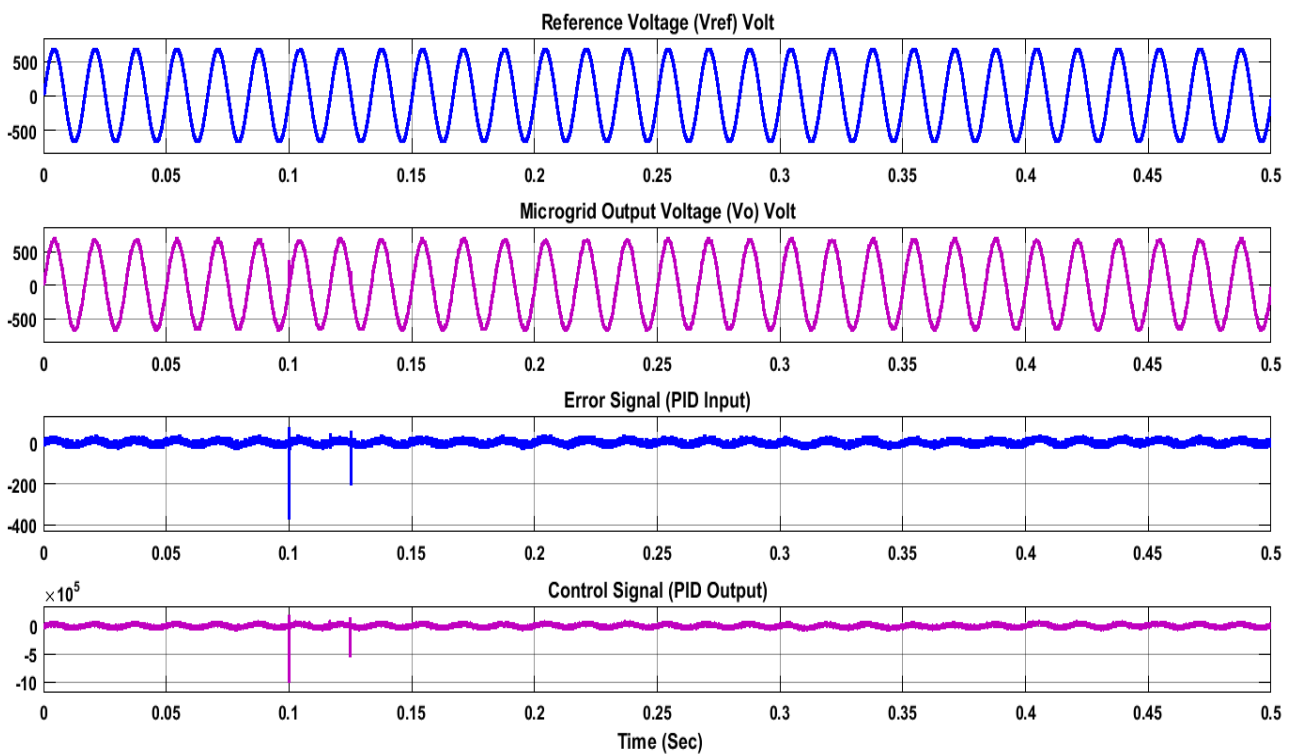
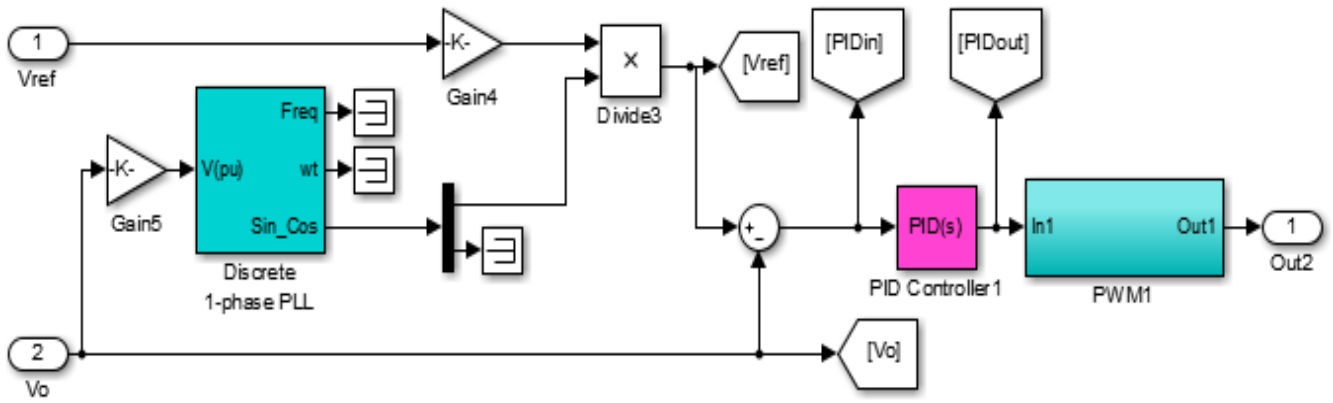
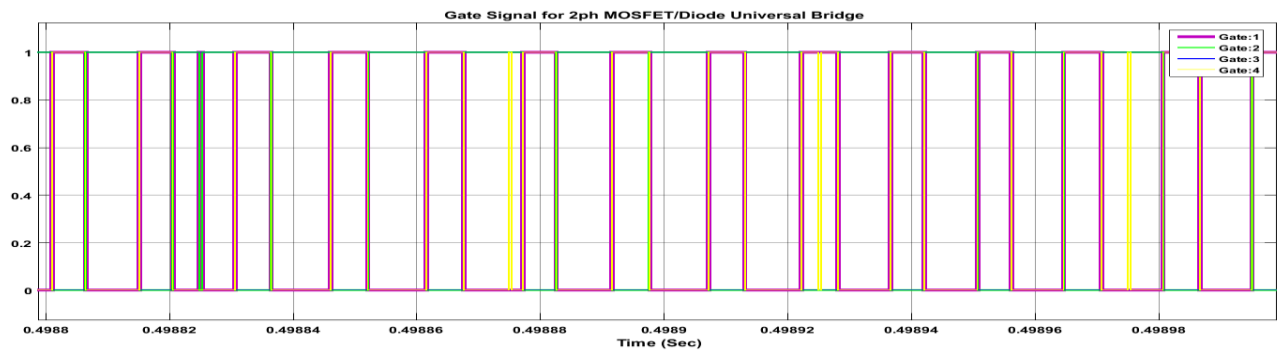


Figure 5:10: Reference voltage, microgrid output voltage, error signal, and the control signal regarding the proposed PID controller.



(a)



(b)

Figure 5:11: (a) Block diagram of the proposed controller using PID control technique, (b) gate signal of the MOSFET/ diode universal bridge.

In the case of the proposed controller, to control output voltages,  $V_o$  has been taken for feedback and considered as input to controller block. Here, the controller has used it for two purposes. First is to find the error, and second is to create the reference to detect the phase. The PLL creates an in-phase pure sine wave, which has been multiplied with the reference constant value ( $480\sqrt{2}$ ). After that, the sine wave of rms 480VAC has been used as a reference, and then  $V_o$  has been subtracted from it to get the error signal. Then, this error signal has been used by the PID controller to generate control output which has been sent to generate PWM. In this case, PWM is controlling the universal bridge. As the battery always has constant voltage, the constant voltage has been passed on to the circuit on the opening of universal bridge. But, the voltage has been controlled by varying the pulse width. In brief, by adopting this proposed PID controller, the microgrid stability has been achieved in the case of CPL instability. In this case, it is evident that the microgrid stability has been retained, albeit the bus voltage

fluctuation of 75% to 125% and step change of CVL load. Hence, the CPL instability has been solved after adopting this proposed PID controller by virtual impedance based compensation technique.

## 5.3 Simulation Results from Sliding Mode Control

### 5.3.1 Sliding Mode Control

Sliding mode control, commonly known as SMC technique, is an advanced nonlinear control strategy that features salient properties of accuracy, robustness, easy tuning, and adjusts the system dynamics by the function of discontinuous control signal forcing the system output to ‘slide’ along with sliding surface or a defined cross-section of the system’s nominal behavior [115]. Here, the state feedback control law, a discontinuous function of time, can shift from one structure to another (in a continuous manner) based on the prevailing location in the space. Therefore, the SMC can be defined as a variable structured control technique. The certain operation mode of the system, as it slides along the predefined boundaries of the control structures, is called the sliding mode. Besides that, the geometrical locus, necessarily consisting of the boundaries, is said to be the sliding surface of the system. Here, Figure 5.12 depicts an instance of the trajectory of a certain system regarding the SMC technique. In this illustration, the sliding surface is defined by  $s = 0$ , and, in this occasion, the sliding mode starts after a finite time while the system trajectories have come to the specified surface.

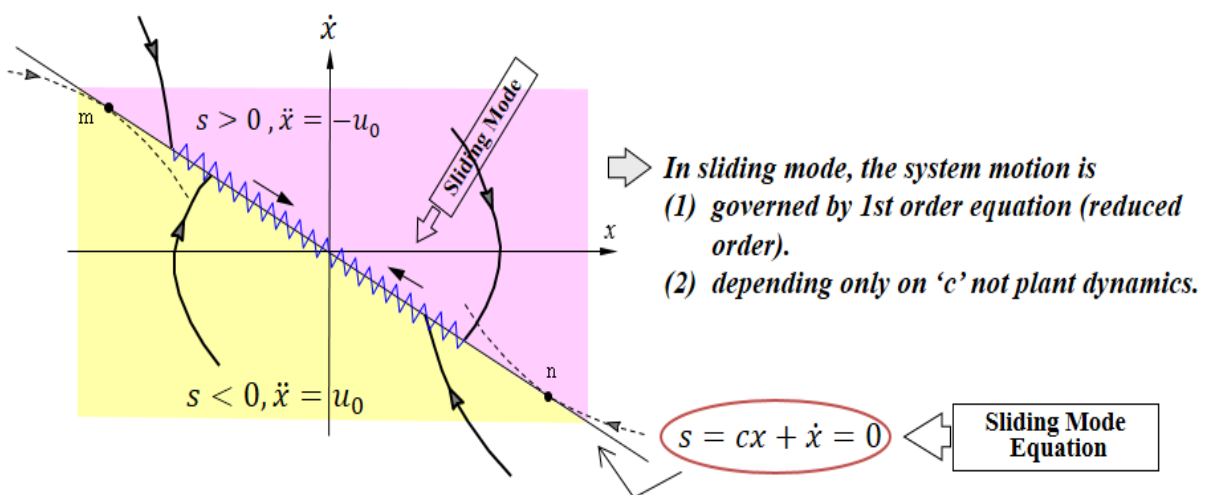


Figure 5.12: Schematic representation of sliding mode control scheme [69].

- State trajectories are toward the switching line  $s=0$
- State trajectories cannot leave and belong to the switching line  $s=0$  [116]

- After sliding mode starts, further motion is governed by  $s = cx + \dot{x} = 0$

## Chattering

The absolute sliding mode remains only while the state trajectory  $x(t)$  of the controlled plant complies with the coveted trajectory at each  $t \geq t_1$  for some value of  $t_1$  [117]. Here, it may need the infinitely rapid switching. But, In case of the practical systems, the switching controller does have a number of inadequacies that actually confine switching up to a definite frequency. In this occasion, then the representative point oscillates within a predefined neighborhood of the switching surface. In particular, such kind of oscillation is said to be the chattering [118]. This phenomenon is presented in figure 5.13.

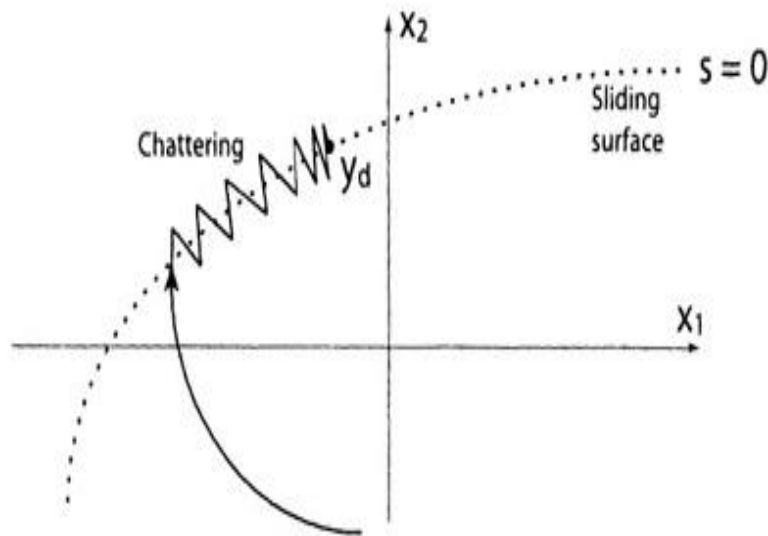


Figure 5:13: Chattering as a result of imperfect control switching [43].

## Chattering Reduction

Control laws which are satisfying sliding condition (The simplified 1<sup>st</sup> order problem of keeping the scalar  $s$  at zero can be achieved by choosing the control law  $u$  such that outside of  $s(t)$  as  $\frac{1}{2} \frac{d}{dt} s^2 \leq -\eta|s|$ , where  $\eta$  is a strictly positive constant) and lead to “perfect” tracking in the face of model

uncertainty, are discontinuous across the surface  $S(t)$ , thus causing control chattering. Chattering is undesirable for the designers because it demands extremely high control activity, and furthermore it involves with the high-frequency dynamics which is neglected in the course of Modeling. Chattering must be reduced (eliminated) for the controller to perform properly. This can be achieved by smoothing out the control discontinuity in a thin boundary layer neighboring the switching surface in equation (5.1)

$$B(t) = \{x, |s(x, t)| \leq \phi\} \quad \phi > 0 \quad (5.1)$$

$$\forall t \geq 0, |\tilde{x}^i(t)| \leq 2\lambda^i \varepsilon, \quad i = 0, \dots, \dots, (n - 1) \quad (5.2)$$

Where,  $\phi$  is boundary layer thickness,

$\varepsilon$  is tracking precision.

## **Selection of Sliding Mode Control over PID Control Technique**

PID control technique is one of the most popular and used linear control technique around the world. But, in case of microgrid applications to retain the desired stability albeit the negative incremental load characteristics of CPL, it has been experienced some inconveniences due to the lack of consistency of accuracy. Unlike the PID controller, sliding mode control technique has been developed into the preferable choice to the researchers because of its success in practical cases, desired consistency, and straight forward firmware implementation. Besides that, in course of sliding mode control technique, it generates discontinuous on/off signal that necessarily forces the system to slide along the desired system's behavior. The SMC controller utilizes a discrete sliding decision rule to retain the desired output. The system, adopting SMC technique, flows through the both of continuous and discrete modes. In this way, it demonstrates a hybrid feedback configuration in practice. Sliding mode control technique has a number of advantages over the conventional proportional- integral-differential (PID) control technique. Hence, in this paper, the sliding mode control technique has been adopted to improve the

stability of the microgrid system in the presence of CPL load. The advantage of SMC control technique listed below to compare between these two techniques [117].

- Characteristically, the microgrid system is significantly nonlinear with the time-varying parameters as well as with the system uncertainties. Hence, using the PID control technique may hamper the system stability due to the possible over linearization of the system. On the other hand, an SMC controller doesn't ignore the system nonlinearity during controller design.
- The efficiency of the entire system depends cardinally on the loading condition. In case of modeling imprecision, SMC controller offers a systematic way to the complication of retaining stability as well as the desired consistent performance.
- The sliding mode control technique is easy to implement. It requires short computational and numerical algorithms to implement in the microcontroller. It is readily compatible with the standard communication protocol such as Ethernet/IP, RS-232, and the Modbus.
- In the case of harsh industrial environment, where the stability as well as the high performance is required despite the presence of high nonlinearity, the lifetime of the hardware components can be reduced considerably in application of PID controller. Unlike PID control technique, SMC offers significantly less equipment and maintenance cost.
- Comparing to PID control technique, SMC offers robust performance against the parametric variations and any disturbance, and better response time to retain microgrid stability.

But, in microgrid applications, the main reason of choosing SMC over PID control technique is its robustness against parametric variation and its faster response in solving instability problem.

## Controller Design

Two steps have to be followed according to the controller design procedure. Initially, it is required to select a feedback control law  $u$  to verify the sliding condition. The control law has to be discontinuous across  $s(t)$  to account for the existence of the modeling imprecision as well as of perturbations. As the consequence of the imperfection of associated control switching, it contributes to chattering (at figure 5.13). In practice, chattering is absolutely undesirable for the system, since this requires special control scheme. Besides that, it may introduce high frequency dynamics that was neglected in the case of modeling purpose. In the next step, the discontinuous control law  $u$  is to be suitably smoothed to attain an optimal condition in course of trade-off between the control bandwidth and tracking precision [117]. Therefore, the first step assures the desired robustness for the parametric uncertainty as well as perturbations, and the second step offers robustness to the high frequency unmodeled dynamics. The illustrated design steps of the SMC controller are discussed for the microgrid system [119]. Here, now, the sliding mode controller simulation platform has been presented at figure 14.

## System Equation

$$\begin{bmatrix} \dot{x}_1 \\ \dot{x}_2 \\ \dot{x}_3 \\ \dot{x}_4 \\ \dot{x}_5 \\ \dot{x}_6 \end{bmatrix} = \begin{bmatrix} \omega x_2 - \frac{R_1}{L_1} x_1 - \frac{x_3}{L_1} + \frac{r_1}{L_1} \\ -\omega x_4 - \frac{R_1}{L_1} x_2 - \frac{x_4}{L_1} + \frac{r_2}{L_1} \\ \omega x_4 + \frac{1}{C} x_1 - \frac{1}{C} \frac{P_1}{x_3} - \frac{1}{C} x_5 \\ -\omega x_3 + \frac{1}{C} x_1 - \frac{1}{C} \frac{P_0}{x_4} - \frac{1}{C} x_6 \\ \omega x_6 + \frac{1}{L} x_3 - \frac{R}{L} x_5 \\ -\omega x_5 + \frac{1}{L} x_4 - \frac{R}{L} x_6 \end{bmatrix} + \begin{bmatrix} 0 & 0 \\ 0 & 0 \\ -\frac{1}{C} & 0 \\ 0 & -\frac{1}{C} \\ 0 & 0 \\ 0 & 0 \end{bmatrix} \begin{bmatrix} u_1 \\ u_2 \end{bmatrix} \quad (5.3)$$

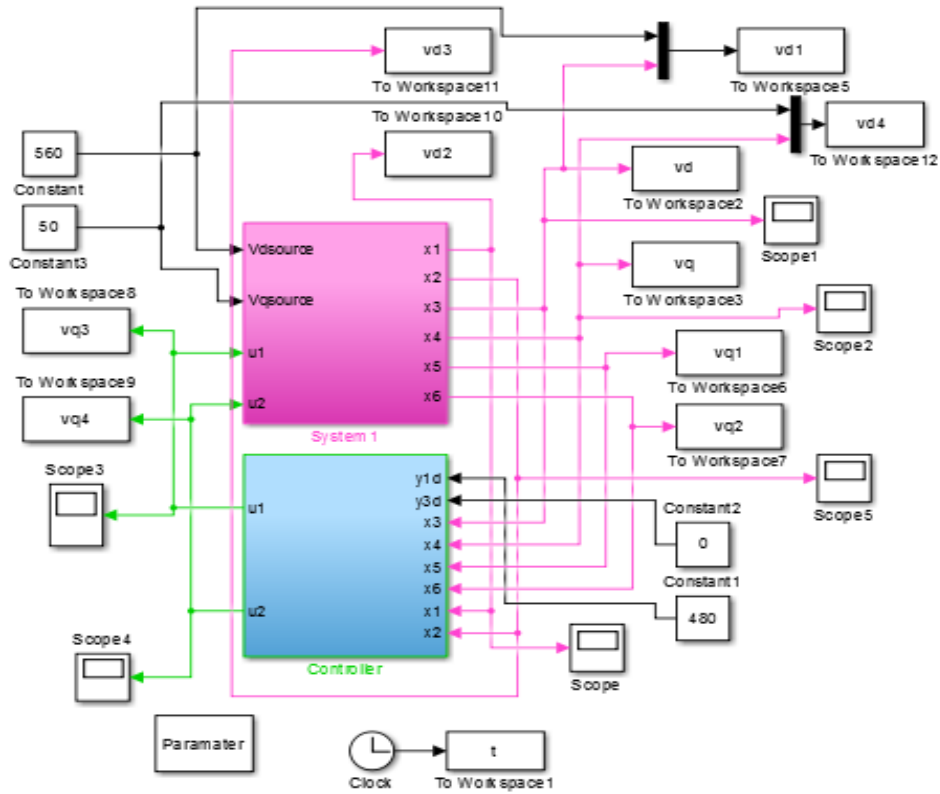


Figure 5:14: Matlab/Simulink schematic model of sliding mode control of microgrid.

Here, we are presenting the modified controller model of microgrid system to implement the proposed storage based virtual impedance stabilization technique using SMC controller.

Control objectives/desired output:

- $Y1 = V_{dC} \approx V_d \approx 480$  Volt
- $Y2 = V_{qC} \approx V_q \approx 0$  (as low as possible) Volt

The general form of a system which is affine in the control(s) is given by equation (5.4) [126,127]:

$$\dot{x} = f(x) + g(x)u \quad (5.4)$$

Let, consider for few key parameters to implement sliding mode control technique

For instance,

$$e_1 = \int (x_3 - x_{3d}) dt \quad (5.5)$$

$$e_2 = \dot{e}_1 = x_3 - x_{3d} \quad (5.6)$$

$$\dot{e}_2 = \dot{x}_3 - \dot{x}_{3d} = f_3(x) + g_3(x)u_1 - \dot{x}_{3d} \quad (5.7)$$

Expanding  $f_3(x)$  and  $g_3(x)$

$$\dot{e}_2 = \omega x_4 + \frac{1}{c}x_1 - \frac{1}{c}\frac{P_0}{x_3} - \frac{1}{c}x_5 - \frac{1}{c}u_1 - \dot{x}_{3d} \quad (5.8)$$

Let the sliding surface be

$$s = e_1 + e_2 \quad (5.9)$$

Then, its derivative will be

$$\dot{s} = \dot{e}_1 + \dot{e}_2 \quad (5.10)$$

$$\dot{s} = e_2 + (\omega x_4 + \frac{1}{c}x_1 - \frac{1}{c}\frac{P_0}{x_3} - \frac{1}{c}x_5 - \frac{1}{c}u_1 - \dot{x}_{3d}) \quad (5.11)$$

Let this be the Lyapunov candidate function

$$V = \frac{1}{2}s^2 \quad (5.12)$$

$$\dot{V} = s\dot{s} = s(e_2 + (\omega x_4 + \frac{1}{c}x_1 - \frac{1}{c}\frac{P_0}{x_3} - \frac{1}{c}x_5 - \frac{1}{c}u_1 - \dot{x}_{3d})) \quad (5.13)$$

We use  $u_1$  as

$$u_1 = -c[-e_2 + \frac{1}{c}x_5 + \dot{x}_{3d} + \frac{1}{c}\frac{P_0}{x_3} - \omega x_4 - \frac{1}{c}x_1 + v]$$

Then, we can obtain

$$\dot{V} = s * v \quad (5.14)$$

The following discontinuous control,  $v$ , will make  $\dot{V}$  to be negative, and consequently, guarantee stability

$$v = -K \text{sat}\left(\frac{s}{\varepsilon}\right); \quad K > 0, \varepsilon > 0 \quad (5.15)$$

Totally, the control input is

$$u_1 = -c[-e_2 + \frac{1}{c}x_5 + \dot{x}_{3d} + \frac{1}{c}\frac{P_0}{x_3} - \omega x_4 - \frac{1}{c}\hat{x}_1 + -Ksat(\frac{s}{\varepsilon})] \quad (5.16)$$

Again,

$$e_3 = \int(x_4 - x_{4d})dt \quad (5.17)$$

$$e_4 = \dot{e}_3 = x_4 - x_{4d} \quad (5.18)$$

$$\dot{e}_4 = \dot{x}_4 - \dot{x}_{4d} = f_4(x) + g_4(x)u_2 - \dot{x}_{4d} \quad (5.19)$$

Expanding  $f_4(x)$  and  $g_4(x)$

$$\dot{e}_4 = -\omega x_3 + \frac{1}{c}x_2 - \frac{1}{c}\frac{Q_0}{x_4} - \frac{1}{c}x_6 - \frac{1}{c}u_2 - \dot{x}_{4d} \quad (5.20)$$

Let, the sliding surface be

$$s = e_3 + e_4 \quad (5.21)$$

Then, its derivative will be

$$\dot{s} = \dot{e}_3 + \dot{e}_4 \quad (5.22)$$

$$\dot{s} = e_4 + \left(-\omega x_3 + \frac{1}{c}x_2 - \frac{1}{c}\frac{Q_0}{x_4} - \frac{1}{c}x_6 - \frac{1}{c}u_2 - \dot{x}_{4d}\right) \quad (5.23)$$

Let this be the Lyapunov candidate function

$$V = \frac{1}{2}s^2 \quad (5.24)$$

$$\dot{V} = s\dot{s} = s\left(e_4 + \left(-\omega x_3 + \frac{1}{c}\hat{x}_2 - \frac{1}{c}\frac{Q_0}{x_4} - \frac{1}{c}x_6 - \frac{1}{c}u_2 - \dot{x}_{4d}\right)\right) \quad (5.25)$$

We use  $u_2$  as

$$u_2 = -c[-e_4 + \omega x_3 - \frac{1}{c}\hat{x}_2 + \frac{1}{c}\frac{Q_0}{x_4} + \frac{1}{c}x_6 + \dot{x}_{4d} + v]$$

Then, we can obtain

$$\dot{V} = s * v \quad (5.26)$$

The following discontinuous control,  $v$ , will make  $\dot{V}$  to be negative, and consequently, guarantee stability

$$v = -Ksat\left(\frac{s}{\varepsilon}\right); \quad K > 0, \varepsilon > 0 \quad (5.27)$$

Totally, the control input is

$$u_2 = -c[-e_4 + \omega x_3 - \frac{1}{c}\hat{x}_2 + \frac{1}{c}\frac{Q_0}{x_4} + \frac{1}{c}x_6 + \dot{x}_{4d} - Ksat\left(\frac{s}{\varepsilon}\right)] \quad (5.28)$$

In the following illustration, figure 5.15, the entire design of the microgrid arrangement loaded with CPLs is depicted for d-q representation. The figure exhibits the undamped oscillation due to the perturbation created by the CPL loads in case of microgrid d axis and q axis bus voltage. This disturbance in both of the output voltages leads to the undesired voltage collapse in the microgrid system.

## Chattering removal

We can remove the chattering by using a sigmoid function. For instance,

```
s = abs(u);
if s <= 0.1
    y = 10*u;
else
    y=sign(u);
end
```

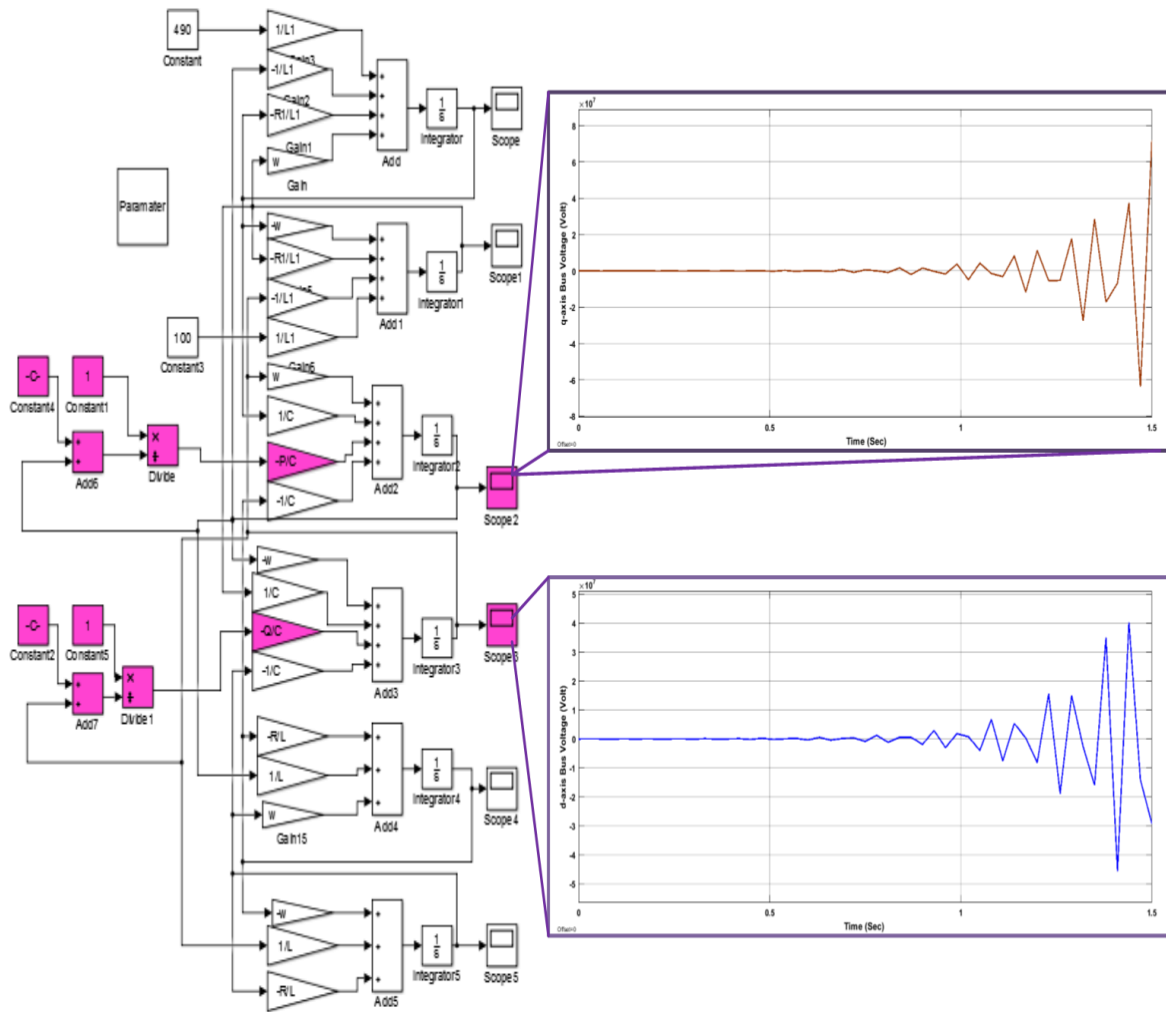


Figure 5:15: The schematic diagram of a microgrid system, which has been made unstable by a CPL while control inputs are absent.

This sigmoid function is like the sign function, but the width of transition is decreased. For this particular implementation, it is decreased to 0.1, which means if the value of  $s$  is less than 0.1 then output will be  $u \cdot 10$ , but if it's more than 0.1, then the output will be the sign function of the input.

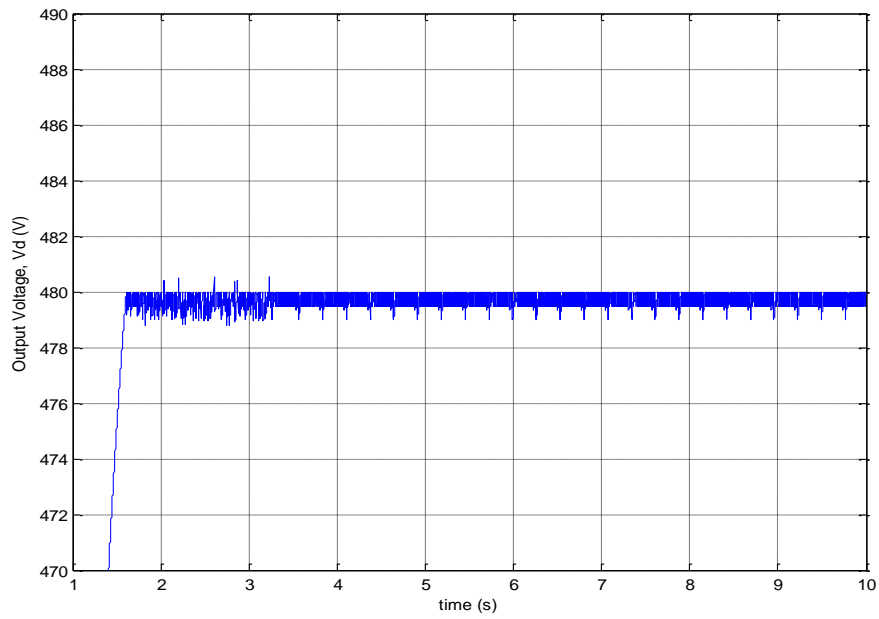


Figure 5:16: The terminal voltage (active) of CPL while using SMC control technique.

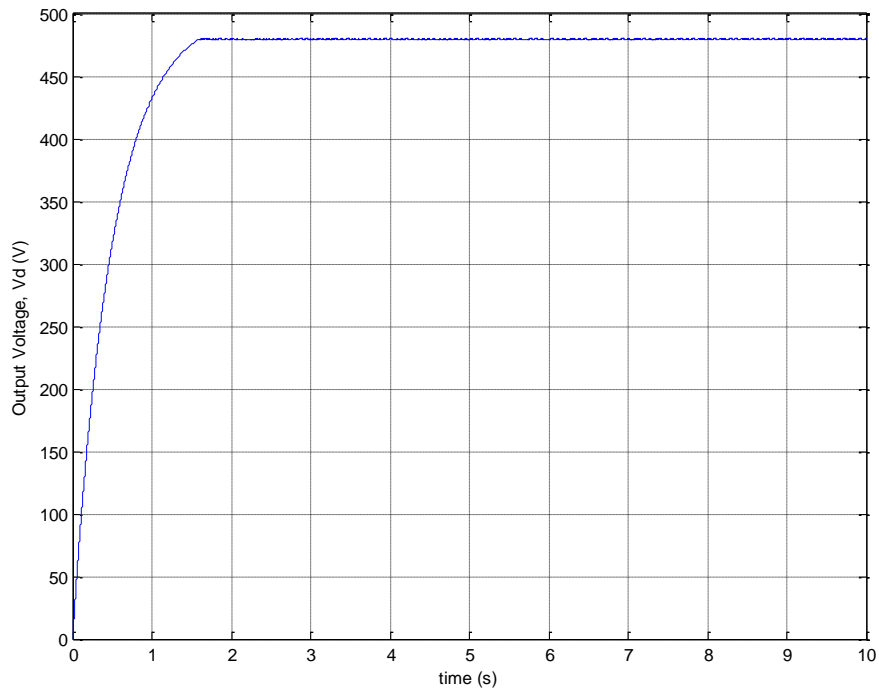


Figure 5:17: The terminal voltage (active) of CPL while using SMC control technique chattering free.

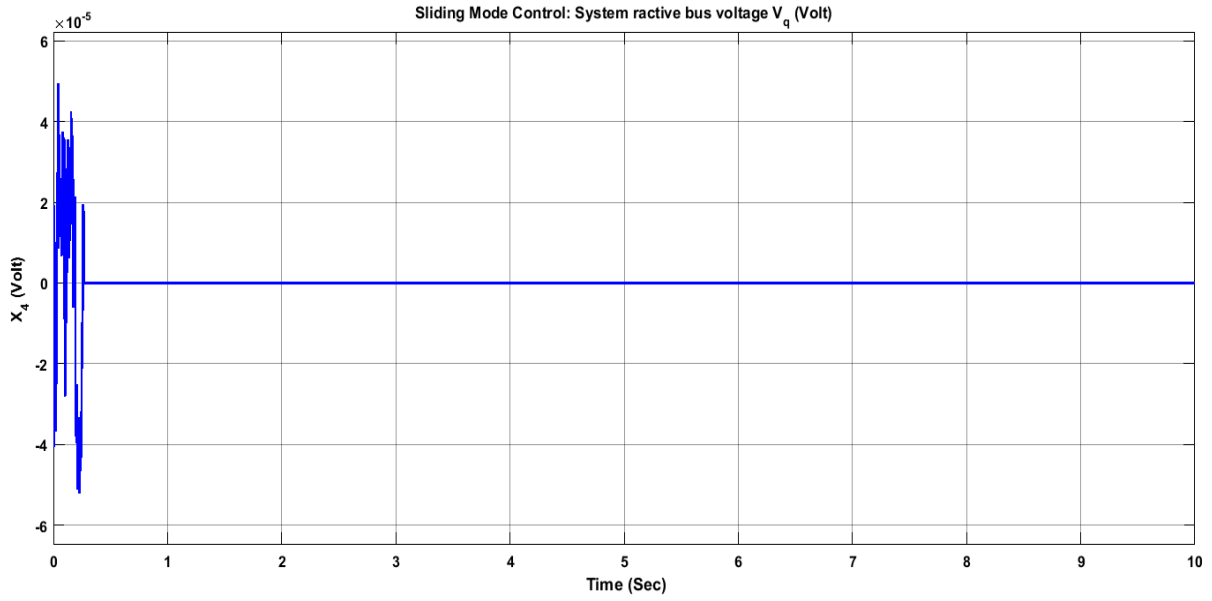


Figure 5:18: The terminal voltage (reactive) of CPL while using SMC control technique.

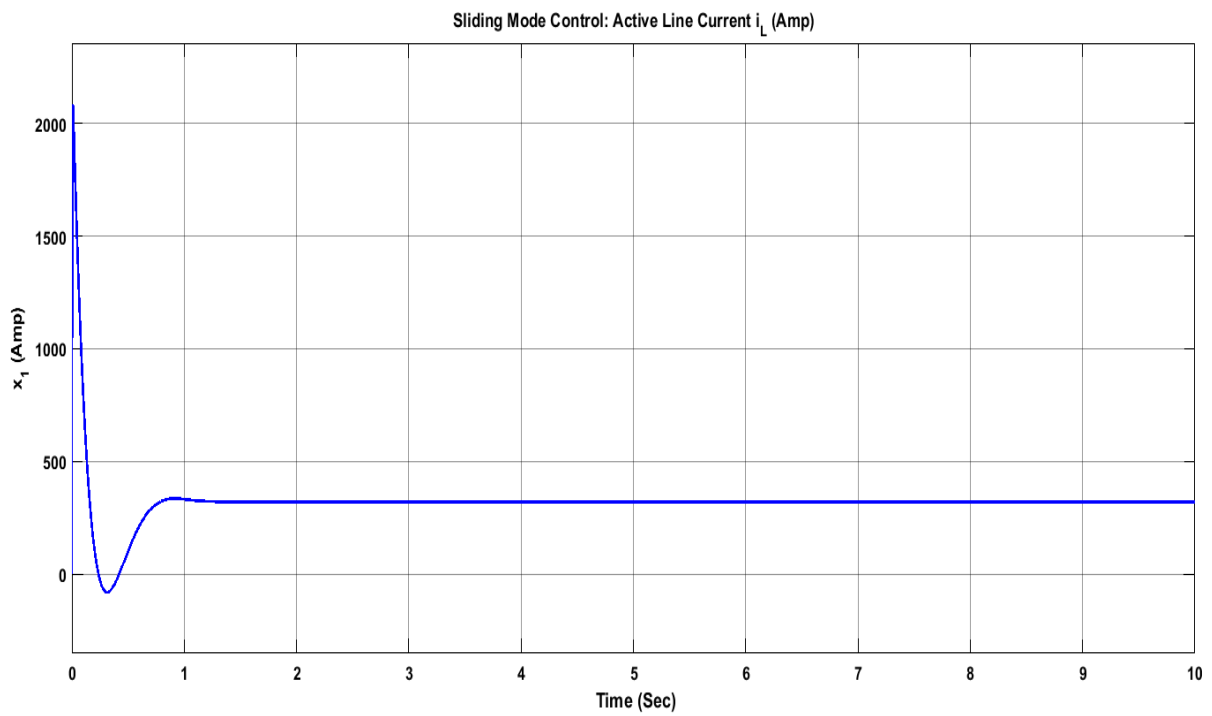


Figure 5:19: Line current  $i_L$  (active) of system while using SMC control technique.

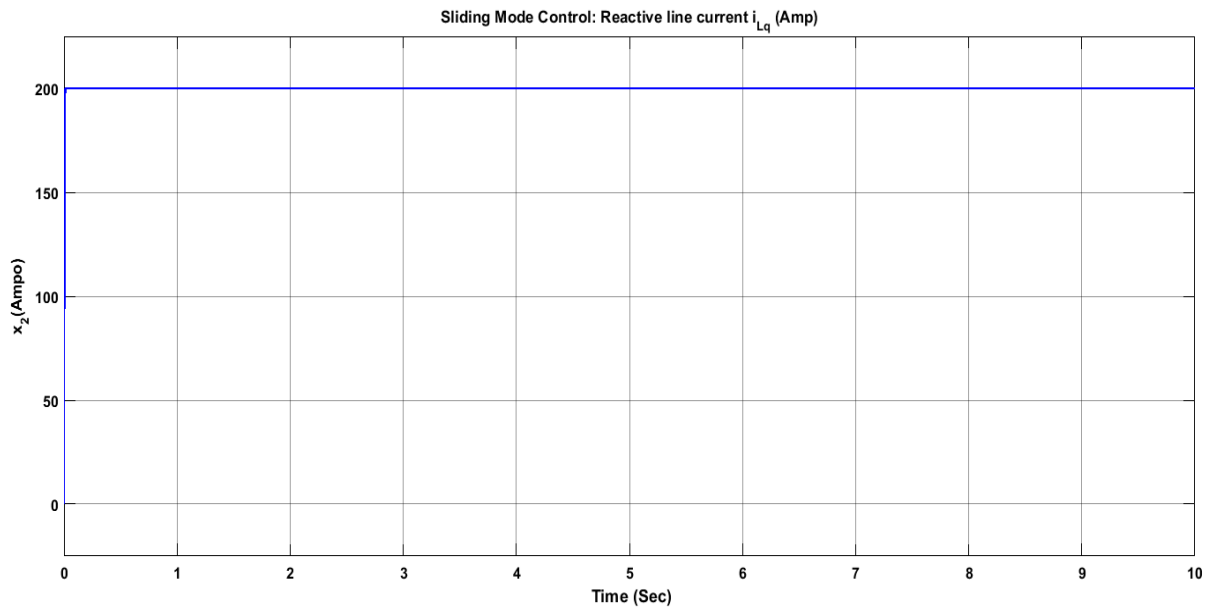


Figure 5:20: Line current  $i_L$  (reactive) of system while using SMC control technique.

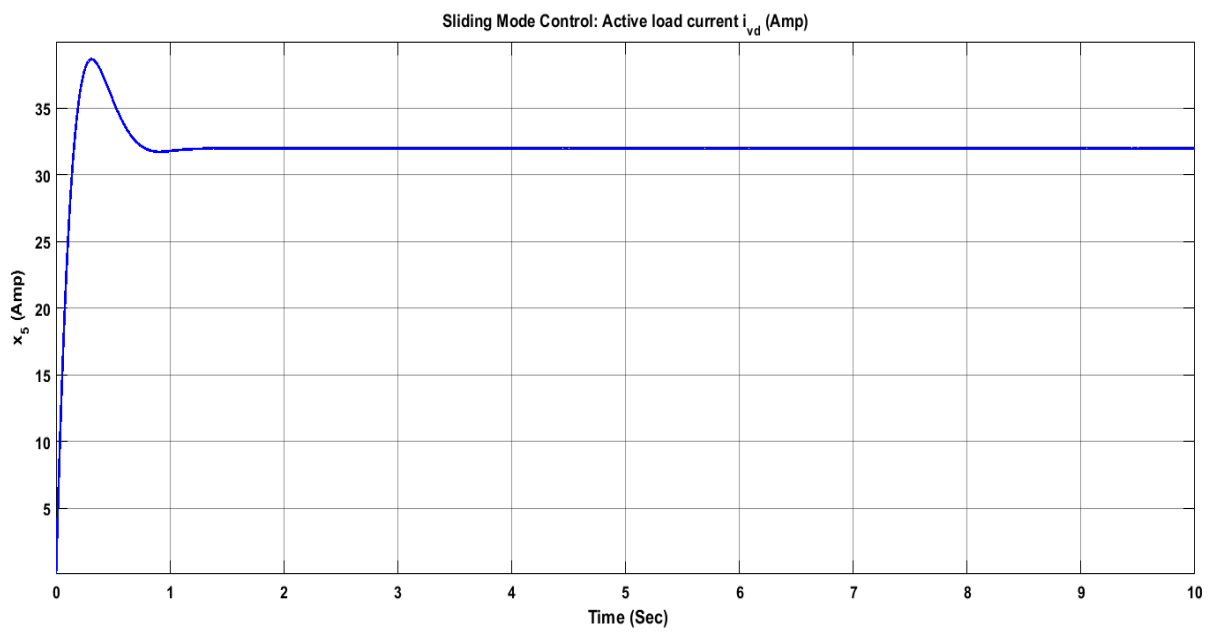


Figure 5:21: CVL current  $i_{CVL}$  (active) of system while using SMC control technique.

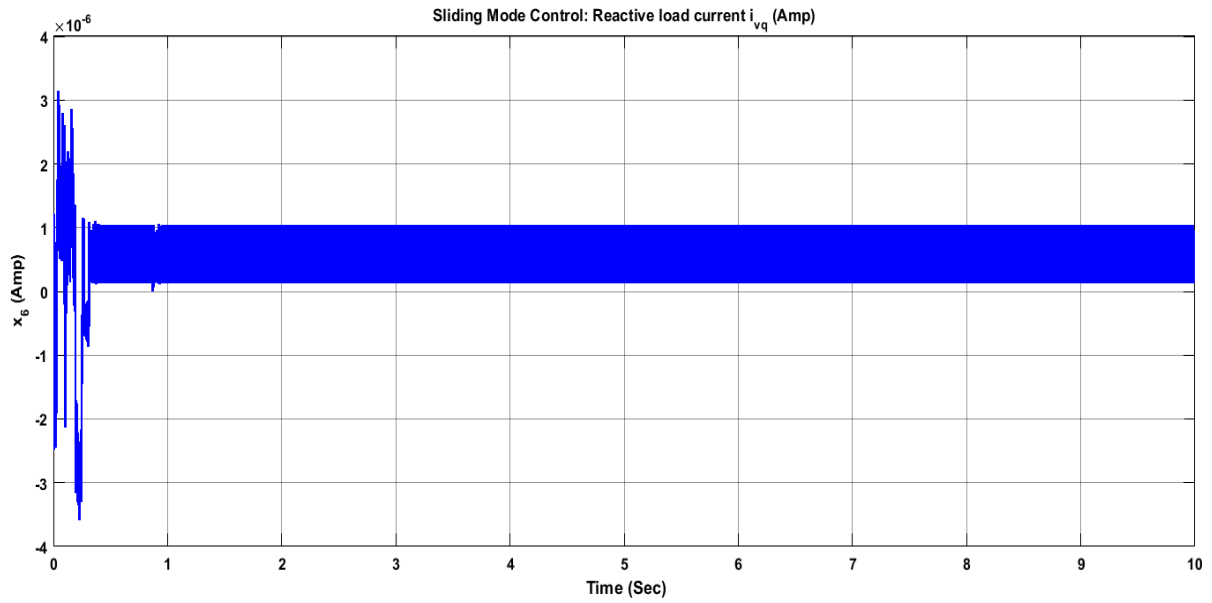


Figure 5:22: CVL current  $i_{CVL}$  (reactive) of system while using SMC control technique.

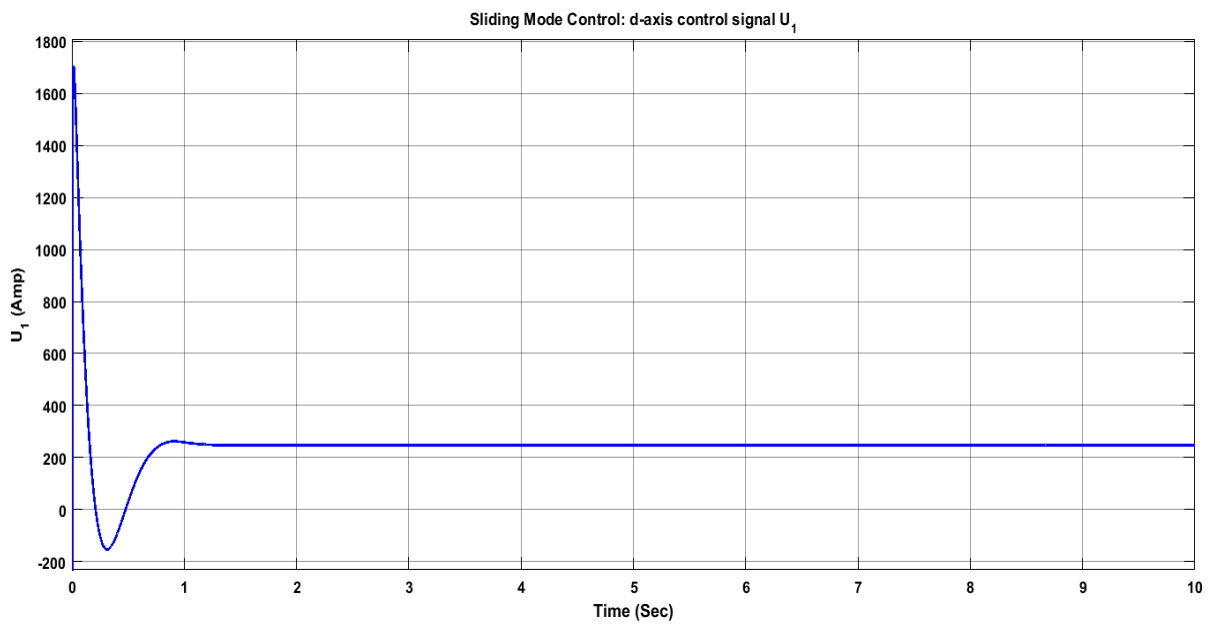


Figure 5:23: Storage current  $i_b$  (active/ d axis current) of system while using SMC control technique.

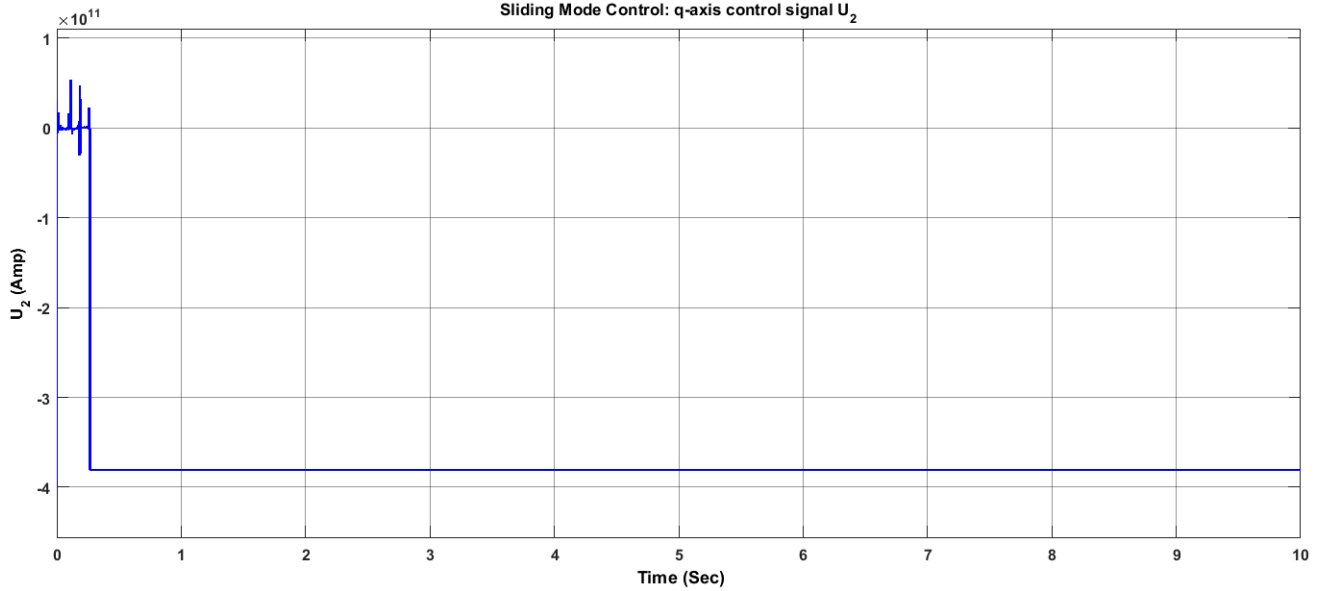


Figure 5:24: Storage current  $i_b$  (reactive/ q axis current) of system while using SMC control technique.

## 5.4 Robustness Analysis of Sliding Mode Controller

### 5.4.1 Sliding Mode Controller, Robustness against Parametric Uncertainties

We can rewrite our state space model equation in below (5.26)

$$\begin{bmatrix} \dot{x}_1 \\ \dot{x}_2 \\ \dot{x}_3 \\ \dot{x}_4 \\ \dot{x}_5 \\ \dot{x}_6 \end{bmatrix} = \begin{bmatrix} \omega x_2 - \frac{R_1}{L_1} x_1 - \frac{x_3}{L_1} \\ -\omega x_1 - \frac{R_1}{L_1} x_2 - \frac{x_4}{L_1} \\ \omega x_4 + \frac{1}{C} x_1 - \frac{1}{C} \frac{P_0}{x_3} - \frac{1}{C} x_5 \\ -\omega x_3 + \frac{1}{C} x_2 - \frac{1}{C} \frac{Q_0}{x_4} - \frac{1}{C} x_6 \\ \omega x_6 + \frac{1}{L} x_3 - \frac{R}{L} x_5 \\ -\omega x_5 + \frac{1}{L} x_4 - \frac{R}{L} x_6 \end{bmatrix} + \begin{bmatrix} 0 \\ 0 \\ -\frac{1}{C} u_1 \\ -\frac{1}{C} u_2 \\ 0 \\ 0 \end{bmatrix} + \begin{bmatrix} r_1 \\ L_1 \\ r_2 \\ L_1 \\ 0 \\ 0 \\ 0 \\ 0 \end{bmatrix} \quad (5.29)$$

Where  $r_1$  and  $r_2$  are unknown parameters that satisfy  $r_1 \leq \delta_{r1}$  and  $r_2 \leq \delta_{r2}$  for some known bounds  $\delta_{r1}$  and  $\delta_{r2}$ . Our goal is to regulate the output active voltage  $x_3$  and reactive voltage  $x_4$  by designing the control laws  $u_1$  and  $u_2$  respectively. As  $x_3$  and  $x_4$  are related to  $r_1$  and  $r_2$  through  $x_1$  and  $x_2$  respectively. So,  $x_1$  and  $x_2$  are also unknown parameters that satisfy  $\Delta x_1 \leq \delta_{x1}$  and  $\Delta x_2 \leq \delta_{x2}$  for some known

bounds  $\delta_{x_1}$  and  $\delta_{x_2}$ . We will design sliding mode control input,  $u_1$  in the first attempt and then we will follow the similar method to design another control input,  $u_2$ .

To make the integral controller, let

$$e_1 = \int (x_3 - x_{3d}) dt \quad (5.30)$$

$$e_2 = \dot{e}_1 = x_3 - x_{3d} \quad (5.31)$$

$$\dot{e}_2 = \dot{x}_3 - \dot{x}_{3d} = f_3(x) + g_3(x)u_1 - \dot{x}_{3d} \quad (5.32)$$

Expanding  $f_3(x)$  and  $g_3(x)$

$$\dot{e}_2 = \omega x_4 + \frac{1}{c} x_1 - \frac{1}{c} \frac{P_0}{x_3} - \frac{1}{c} x_5 - \frac{1}{c} u_1 - \dot{x}_{3d} \quad (5.33)$$

Let the sliding surface be

$$s = e_1 + e_2 \quad (5.34)$$

Then, its derivative will be

$$\dot{s} = \dot{e}_1 + \dot{e}_2 \quad (5.35)$$

$$\dot{s} = e_2 + (\omega x_4 + \frac{1}{c} x_1 - \frac{1}{c} \frac{P_0}{x_3} - \frac{1}{c} x_5 - \frac{1}{c} u_1 - \dot{x}_{3d}) \quad (5.36)$$

The state  $x_1$  is unknown, then we can represent the uncertainty as  $x_1 = \hat{x}_1 + \Delta x_1$  and  $\left\| \frac{1}{c} \Delta x_1 \right\| \leq \frac{1}{c} \delta_{x_1}$

$$= e_2 + \left( -\frac{1}{c} x_5 - \dot{x}_{3d} - \frac{1}{c} \frac{P_0}{x_3} + \omega x_4 + \frac{1}{c} \hat{x}_1 + \frac{1}{c} \Delta x_1 - \frac{1}{c} u_1 \right) \quad (5.37)$$

Let this be the Lyapunov candidate function

$$V = \frac{1}{2} s^2 \quad (5.38)$$

$$\dot{V} = s \dot{s} = s \left( e_2 + \left( -\frac{1}{c} x_5 - \dot{x}_{3d} - \frac{1}{c} \frac{P_0}{x_3} + \omega x_4 + \frac{1}{c} \hat{x}_1 + \frac{1}{c} \Delta x_1 - \frac{1}{c} u_1 \right) \right) \quad (5.39)$$

We use  $u_1$  as

$$u_1 = -c[-e_2 + \frac{1}{c}x_5 + \dot{x}_{3d} + \frac{1}{c}\frac{P_0}{x_3} - \omega x_4 - \frac{1}{c}\hat{x}_1 + v]$$

Then, we can obtain

$$\dot{V} = s(\frac{1}{c}\Delta x_1 + v) \quad (5.40)$$

Considering  $\|\frac{1}{c}\Delta x_1\| \leq \frac{1}{c}\delta_{x1}$ , the following discontinuous control,  $v$ , will make  $\dot{V}$  the negative, and consequently, guarantee stability

$$v = -\frac{1}{c}\delta_{x1} \text{sat}\left(\frac{s}{\varepsilon}\right); \quad \varepsilon > 0 \quad (5.41)$$

Totally, the control input is

$$u_1 = -c[-e_2 + \frac{1}{c}x_5 + \dot{x}_{3d} + \frac{1}{c}\frac{P_0}{x_3} - \omega x_4 - \frac{1}{c}\hat{x}_1 - \frac{1}{c}\delta_{x1} \text{sat}\left(\frac{s}{\varepsilon}\right)] \quad (5.42)$$

Like  $u_1$ , let

$$e_3 = \int (x_4 - x_{4d}) dt \quad (5.43)$$

$$e_4 = \dot{e}_3 = x_4 - x_{4d} \quad (5.44)$$

$$\dot{e}_4 = \dot{x}_4 - \dot{x}_{4d} = f_4(x) + g_4(x)u_2 - \dot{x}_{4d} \quad (5.45)$$

Expanding  $f_4(x)$  and  $g_4(x)$

$$\dot{e}_4 = -\omega x_3 + \frac{1}{c}x_2 - \frac{1}{c}\frac{Q_0}{x_4} - \frac{1}{c}x_6 - \frac{1}{c}u_2 - \dot{x}_{4d} \quad (5.46)$$

Let, the sliding surface be

$$s = e_3 + e_4 \quad (5.47)$$

Then, its derivative will be

$$\dot{s} = \dot{e}_3 + \dot{e}_4 \quad (5.48)$$

$$\dot{s} = e_4 + (-\omega x_3 + \frac{1}{c}x_2 - \frac{1}{c}\frac{Q_0}{x_4} - \frac{1}{c}x_6 - \frac{1}{c}u_2 - \dot{x}_{4d}) \quad (5.49)$$

The state  $x_2$  is unknown, then we can represent the uncertainty as  $x_2 = \hat{x}_2 + \Delta x_2$  and  $\|\frac{1}{c}\Delta x_2\| \leq \frac{1}{c}\delta_{x_2}$

$$= e_4 + (-\omega x_3 + \frac{1}{c}\hat{x}_2 - \frac{1}{c}\frac{Q_0}{x_4} - \frac{1}{c}x_6 - \dot{x}_{4d} + \frac{1}{c}\Delta x_2 - \frac{1}{c}u_2) \quad (5.50)$$

Let this be the Lyapunov candidate function

$$V = \frac{1}{2}s^2 \quad (5.51)$$

$$\dot{V} = s\dot{s} = s(e_4 + (-\omega x_3 + \frac{1}{c}\hat{x}_2 - \frac{1}{c}\frac{Q_0}{x_4} - \frac{1}{c}x_6 - \dot{x}_{4d} + \frac{1}{c}\Delta x_2 - \frac{1}{c}u_2)) \quad (5.52)$$

We use  $u_2$

$$u_2 = -c[-e_4 + \omega x_3 - \frac{1}{c}\hat{x}_2 + \frac{1}{c}\frac{Q_0}{x_4} + \frac{1}{c}x_6 + \dot{x}_{4d} + v]$$

Then, we can obtain

$$\dot{V} = s(\frac{1}{c}\Delta x_2 + v) \quad (5.53)$$

Considering  $\|\frac{1}{c}\Delta x_2\| \leq \frac{1}{c}\delta_{x_2}$ , the following discontinuous control,  $v$ , will make  $\dot{V}$  the negative, and consequently, guarantee stability

$$v = -\frac{1}{c}\delta_{x_2} \text{sat}\left(\frac{s}{\varepsilon}\right); \quad \varepsilon > 0 \quad (5.54)$$

Totally, the control input is

$$u_2 = -c[-e_4 + \omega x_3 - \frac{1}{c}\hat{x}_2 + \frac{1}{c}\frac{Q_0}{x_4} + \frac{1}{c}x_6 + \dot{x}_{4d} - \frac{1}{c}\delta_{x_2} \text{sat}\left(\frac{s}{\varepsilon}\right)] \quad (5.55)$$

## 5.4.2 Sliding Mode Controller Robustness against Parametric Uncertainties Including Uncertainties in Power of CPL

In this section, we will enhance the robustness by considering the uncertainties in active power of CPL ( $P_0$ ) and reactive power of CPL ( $Q_0$ ). When  $P_0$  is unknown in case of designing  $u_1$ , we will also consider  $x_3$  as unknown to avoid any complexity. Similarly, in case of  $u_2$ , we will also consider  $x_4$  as unknown. Although  $P_0$  and  $Q_0$  are unknown, they satisfy  $P_0 \leq \delta_P$  and  $Q_0 \leq \delta_Q$  for some known bounds  $\delta_P$  and  $\delta_Q$ . The variation on CPL power can be summarized as

$$d_P = \Delta_P / \Delta x_3$$

$$d_Q = \Delta_Q / \Delta x_4$$

where  $d_P$  represents the uncertainties of  $P_0$ ,  $d_Q$  represents the uncertainties of  $Q_0$ ,  $\Delta x_3$  is the uncertainties in  $x_3$ , and  $\Delta x_4$  is the uncertainties in  $x_4$ . As  $x_3$  and  $x_4$  are in the denominator, we need lower bounds of these parameters. Also, uncertainty of power is expressed in term of current. We know that  $x_3$  is the voltage of “d-axis” and it satisfies  $\Delta x_3 \leq \delta_{x_3}$  for some known, strictly positive bound  $\delta_{x_3}$ . Similarly,  $x_4$  is the voltage of “q-axis” and it satisfies  $\Delta x_4 \leq \delta_{x_4}$  for some known, strictly positive bound  $\delta_{x_4}$ . Altogether, we have six unknowns with their known bounds. We will design sliding mode control input,  $u_1$  in the first attempt and then we will follow the similar method to design another control input  $u_2$ .

Using the similar method as discussed in last section, let

$$e_1 = \int (x_3 - x_{3d}) dt \tag{5.56}$$

$$e_2 = \dot{e}_1 = x_3 - x_{3d} \tag{5.57}$$

$$\dot{e}_2 = \dot{x}_3 - \dot{x}_{3d} = f_3(x) + g_3(x)u_1 - \dot{x}_{3d} \tag{5.58}$$

Expanding  $f_3(x)$  and  $g_3(x)$

$$\dot{e}_2 = \omega x_4 + \frac{1}{c} x_1 - \frac{1}{c} \frac{P_0}{x_3} - \frac{1}{c} x_5 - \frac{1}{c} u_1 - \dot{x}_{3d} \tag{5.59}$$

Let, the sliding surface be

$$s = e_1 + e_2 \quad (5.60)$$

After differentiating and considering the uncertainties

$$\dot{s} = \dot{e}_1 + \dot{e}_2 \quad (5.61)$$

$$\dot{s} = e_2 + (\omega(\hat{x}_4 + \Delta x_4) + \frac{1}{c}(\hat{x}_1 + \Delta x_1) - \frac{1}{c}(\frac{P_0}{x_3} + d_P) - \frac{1}{c}x_5 - \frac{1}{c}u_1 - \dot{x}_{3d}) \quad (5.62)$$

where

$$x_4 = \hat{x}_4 + \Delta x_4$$

Then we can represent the total parametric uncertainty including uncertainty of CPL power as

$$d = \frac{1}{c}\Delta x_1 + \omega\Delta x_4 - \frac{1}{c}d_P; \quad \|d\| \leq dmax \quad (5.63)$$

where  $dmax$  is the bound of the total disturbance  $d$ .

$$dmax = \frac{1}{c}\delta_{x_1} + \omega\delta_{x_4} - \frac{1}{c}\delta_P / \delta_{x_3} \quad (5.64)$$

Then

$$\dot{s} = e_2 - \frac{1}{c}x_5 - \dot{x}_{3d} + \omega\hat{x}_4 + \frac{1}{c}\hat{x}_1 - \frac{1}{c}\frac{P_0}{x_3} - \frac{1}{c}u_1 + d \quad (5.65)$$

Let this be the Lyapunov candidate function

$$V = \frac{1}{2}s^2 \quad (5.66)$$

$$\dot{V} = s\dot{s} = s(e_2 - \frac{1}{c}x_5 - \dot{x}_{3d} + \omega\hat{x}_4 + \frac{1}{c}\hat{x}_1 - \frac{1}{c}\frac{P_0}{x_3} - \frac{1}{c}u_1 + d) \quad (5.67)$$

We use  $u_1$

$$u_1 = -c[-e_2 + \frac{1}{c}x_5 + \dot{x}_{3d} - \omega\hat{x}_4 - \frac{1}{c}\hat{x}_1 + \frac{1}{c}\frac{P_0}{x_3} + v]$$

Then, we can obtain

$$\dot{V} = s(d + v) \quad (5.68)$$

Considering  $\|d\| \leq dmax$ , the following discontinuous control,  $v$ , will make  $\dot{V}$  the negative, and consequently, guarantee stability

$$v = -dmax * sat\left(\frac{s}{\varepsilon}\right); \quad \varepsilon > 0 \quad (5.69)$$

Totally, the control input is

$$u_1 = -c[-e_2 + \frac{1}{c}x_5 + \dot{x}_{3d} + \frac{1}{c}\frac{P_0}{x_3} - \omega\hat{x}_4 - \frac{1}{c}\hat{x}_1 - dmax * sat\left(\frac{s}{\varepsilon}\right)] \quad (5.70)$$

Similar analysis is also shown here for  $u_2$ , let

$$e_3 = \int(x_4 - x_{4d})dt \quad (5.71)$$

$$e_4 = \dot{e}_3 = x_4 - x_{4d} \quad (5.72)$$

$$\dot{e}_4 = \dot{x}_4 - \dot{x}_{4d} = f_4(x) + g_4(x)u_2 - \dot{x}_{4d} \quad (5.73)$$

Expanding  $f_4(x)$  and  $g_4(x)$

$$\dot{e}_4 = -\omega x_3 + \frac{1}{c}x_2 - \frac{1}{c}\frac{Q_0}{x_4} - \frac{1}{c}x_6 - \frac{1}{c}u_2 - \dot{x}_{4d} \quad (5.74)$$

Let, the sliding surface be

$$s = e_3 + e_4 \quad (5.75)$$

After differentiating and considering the uncertainties

$$\dot{s} = e_4 + \left(-\omega(\hat{x}_3 + \Delta x_3) + \frac{1}{c}(\hat{x}_2 + \Delta x_2) - \frac{1}{c}\left(\frac{Q_0}{x_4} + d_Q\right) - \frac{1}{c}x_6 - \frac{1}{c}u_2 - \dot{x}_{4d}\right) \quad (5.76)$$

where

$$x_3 = \hat{x}_3 + \Delta x_3$$

Then we can represent the total parametric uncertainty, including uncertainty of CPL power as

$$d = \frac{1}{c}\Delta x_2 - \omega\Delta x_3 - \frac{1}{c}d_Q; \quad \|d\| \leq dmax \quad (5.77)$$

where  $dmax$  is the bound of the total disturbance  $d$ .

$$dmax = \frac{1}{c}\delta_{x_2} - \omega\delta_{x_3} - \delta_Q / \delta_{x_4} \quad (5.78)$$

Then

$$\dot{s} = e_3 - \frac{1}{c}x_6 - \dot{x}_{4d} + \omega\hat{x}_3 + \frac{1}{c}\hat{x}_2 - \frac{1}{c}\frac{Q_0}{x_4} - \frac{1}{c}u_2 + d \quad (5.79)$$

Let this be the Lyapunov candidate function

$$V = \frac{1}{2}s^2 \quad (5.80)$$

$$\dot{V} = s\dot{s} = s(e_3 - \frac{1}{c}x_6 - \dot{x}_{4d} + \omega\hat{x}_3 + \frac{1}{c}\hat{x}_2 - \frac{1}{c}\frac{Q_0}{x_4} - \frac{1}{c}u_2 + d) \quad (5.81)$$

We use  $u_2$

$$u_2 = -c[-e_3 + \frac{1}{c}x_6 + \dot{x}_{4d} - \omega\hat{x}_3 - \frac{1}{c}\hat{x}_2 + \frac{1}{c}\frac{Q_0}{x_4} + v]$$

Then, we can obtain

$$\dot{V} = s(d + v) \quad (5.82)$$

Considering  $\|d\| \leq dmax$ , the following discontinuous control,  $v$ , will make  $\dot{V}$  the negative, and consequently, guarantee stability

$$v = -dmax * sat\left(\frac{s}{\varepsilon}\right); \quad \varepsilon > 0 \quad (5.83)$$

Totally, the control input is

$$u_2 = -c\left[-e_3 + \frac{1}{c}x_6 + \dot{x}_{4d} - \omega\hat{x}_3 - \frac{1}{c}\hat{x}_2 + \frac{1}{c}\frac{Q_0}{x_4} - dmax * sat\left(\frac{s}{\varepsilon}\right)\right] \quad (5.84)$$

### 5.4.3 Sliding Mode Controller Robustness against Parametric Uncertainties and Frequency Variations

In this section, we will enhance the robustness to another level by considering the variations in frequency. Although the frequency is unknown, it satisfies  $\omega \leq \delta_\omega$  for some known bound  $\delta_\omega$ . As  $x_3$  and  $x_4$  are also multiplied with  $\omega$ , they are also considered as unknowns.

Using the similar method as discussed in last section, let

$$e_1 = \int (x_3 - x_{3d}) dt \quad (5.85)$$

$$e_2 = \dot{e}_1 = x_3 - x_{3d} \quad (5.86)$$

$$\dot{e}_2 = \dot{x}_3 - \dot{x}_{3d} = f_3(x) + g_3(x)u_1 - \dot{x}_{3d} \quad (5.87)$$

Expanding  $f_3(x)$  and  $g_3(x)$

$$\dot{e}_2 = \omega x_4 + \frac{1}{c} x_1 - \frac{1}{c} \frac{P_0}{x_3} - \frac{1}{c} x_5 - \frac{1}{c} u_1 - \dot{x}_{3d} \quad (5.88)$$

Let, the sliding surface be

$$s = e_1 + e_2 \quad (5.89)$$

After differentiating and considering the parametric uncertainties and frequency variations

$$\dot{s} = \dot{e}_1 + \dot{e}_2 \quad (5.90)$$

$$\dot{s} = e_2 + ((\hat{\omega} + \Delta\omega)(\hat{x}_4 + \Delta x_4) + \frac{1}{c}(\hat{x}_1 + \Delta x_1) - \frac{1}{c}(\frac{P_0}{\hat{x}_3} + d_p) - \frac{1}{c}x_5 - \frac{1}{c}u_1 - \dot{x}_{3d}) \quad (5.91)$$

where

$$\omega = \hat{\omega} + \Delta\omega$$

where  $\Delta\omega$  represents the frequency variation. Then we can represent the total parametric uncertainty and frequency variation as

$$d = \Delta\omega\hat{x}_4 + \Delta\omega\Delta x_4 + \hat{\omega}\Delta x_4 + \frac{1}{c}\Delta x_1 - \frac{1}{c}d_P; \quad \|d\| \leq dmax \quad (5.92)$$

where  $dmax$  is the bound of the total disturbance  $d$ .

$$dmax = \frac{1}{c}\delta_{x_1} + \delta_\omega\hat{x}_4 + \delta_\omega\delta_{x_4} + \hat{\omega}\delta_{x_4} - \frac{1}{c}\delta_P / \delta_{x_3} \quad (5.93)$$

Then

$$\dot{s} = e_2 - \frac{1}{c}x_5 - \dot{x}_{3d} + \hat{\omega}\hat{x}_4 + \frac{1}{c}\hat{x}_1 - \frac{1}{c}\frac{P_0}{x_3} - \frac{1}{c}u_1 + d \quad (5.94)$$

Let this be the Lyapunov candidate function

$$V = \frac{1}{2}s^2 \quad (5.95)$$

$$\dot{V} = s\dot{s} = s(e_2 - \frac{1}{c}x_5 - \dot{x}_{3d} + \hat{\omega}\hat{x}_4 + \frac{1}{c}\hat{x}_1 - \frac{1}{c}\frac{P_0}{x_3} - \frac{1}{c}u_1 + d) \quad (5.96)$$

We use  $u_1$

$$u_1 = -c[-e_2 + \frac{1}{c}x_5 + \dot{x}_{3d} - \hat{\omega}\hat{x}_4 - \frac{1}{c}\hat{x}_1 + \frac{1}{c}\frac{P_0}{x_3} + v]$$

Then, we can obtain

$$\dot{V} = s(d + v) \quad (5.97)$$

Considering  $\|d\| \leq dmax$ , the following discontinuous control,  $v$ , will make  $\dot{V}$  the negative, and consequently, guarantee stability

$$v = -dmax * sat\left(\frac{s}{\varepsilon}\right); \quad \varepsilon > 0 \quad (5.98)$$

Totally, the control input is

$$u_1 = -c[-e_2 + \frac{1}{c}x_5 + \dot{x}_{3d} + \frac{1}{c}\frac{P_0}{x_3} - \hat{\omega}\hat{x}_4 - \frac{1}{c}\hat{x}_1 - dmax * sat\left(\frac{s}{\varepsilon}\right)] \quad (5.99)$$

Similar analysis is also shown here for  $u_2$ , let

$$e_3 = \int(x_4 - x_{4d})dt \quad (5.100)$$

$$e_4 = \dot{e}_3 = x_4 - x_{4d} \quad (5.101)$$

$$\dot{e}_4 = \dot{x}_4 - \dot{x}_{4d} = f_4(x) + g_4(x)u_2 - \dot{x}_{4d} \quad (5.102)$$

Expanding  $f_4(x)$  and  $g_4(x)$

$$\dot{e}_4 = -\omega x_3 + \frac{1}{c}x_2 - \frac{1}{c}\frac{Q_0}{x_4} - \frac{1}{c}x_6 - \frac{1}{c}u_2 - \dot{x}_{4d} \quad (5.103)$$

Let, the sliding surface be

$$s = e_3 + e_4 \quad (5.104)$$

After differentiating and considering the parametric uncertainties and frequency variations

$$\dot{s} = e_4 + \left( -(\hat{\omega} + \Delta\omega)(\hat{x}_3 + \Delta x_3) + \frac{1}{c}(\hat{x}_2 + \Delta x_2) - \frac{1}{c}\left(\frac{Q_0}{\hat{x}_4} + d_Q\right) - \frac{1}{c}x_6 - \frac{1}{c}u_2 - \dot{x}_{4d} \right) \quad (5.105)$$

Then we can represent the total parametric uncertainty and frequency variation as

$$d = -(\Delta\omega\hat{x}_3 + \Delta\omega\Delta x_3 + \hat{\omega}\Delta x_3) + \frac{1}{c}\Delta x_2 - \frac{1}{c}d_Q; \quad \|d\| \leq dmax \quad (5.106)$$

Where  $dmax$  is the bound of the total disturbance  $d$ .

$$dmax = \frac{1}{c}\delta_{x_2} - (\delta_\omega\hat{x}_3 + \delta_\omega\delta_{x_3} + \hat{\omega}\delta_{x_3}) - \frac{1}{c}\delta_Q / \delta_{x_4} \quad (5.107)$$

Then

$$\dot{s} = e_3 - \frac{1}{c}x_6 - \dot{x}_{4d} + \hat{\omega}\hat{x}_3 + \frac{1}{c}\hat{x}_2 - \frac{1}{c}\frac{Q_0}{\hat{x}_4} - \frac{1}{c}u_2 + d \quad (5.108)$$

Let this be the Lyapunov candidate function

$$V = \frac{1}{2}s^2 \quad (5.109)$$

$$\dot{V} = s\dot{s} = s(e_3 - \frac{1}{c}x_6 - \dot{x}_{4d} + \hat{\omega}\hat{x}_3 + \frac{1}{c}\hat{x}_2 - \frac{1}{c}\frac{Q_0}{\hat{x}_4} - \frac{1}{c}u_2 + d) \quad (5.110)$$

We use  $u_2$

$$u_2 = -c[-e_3 + \frac{1}{c}x_6 + \dot{x}_{4d} - \hat{\omega}\hat{x}_3 - \frac{1}{c}\hat{x}_2 + \frac{1}{c}\frac{Q_0}{x_4} + v]$$

Then, we can obtain

$$\dot{V} = s(d + v) \quad (5.111)$$

Considering  $\|d\| \leq dmax$ , the following discontinuous control,  $v$ , will make  $\dot{V}$  the negative, and consequently, guarantee stability

$$v = -dmax * sat\left(\frac{s}{\varepsilon}\right); \quad \varepsilon > 0 \quad (5.112)$$

Totally, the control input is

$$u_2 = -c[-e_3 + \frac{1}{c}x_6 + \dot{x}_{4d} - \hat{\omega}\hat{x}_3 - \frac{1}{c}\hat{x}_2 + \frac{1}{c}\frac{Q_0}{x_4} - dmax * sat\left(\frac{s}{\varepsilon}\right)] \quad (5.113)$$

#### 5.4.4 Sliding Mode Controller Robustness against Parametric Uncertainties, Frequency Variations and Additive White Gaussian Noise (AWGN)

In this section, we will enhance the robustness by introducing a white noise rejection method. From the last section, we can see that we have to measure just two states as all other states are replaced by their bounds. These two parameters are  $x_3$  and  $x_5$  for  $u_1$  and,  $x_4$  and  $x_6$  for  $u_2$ . As we know that multiplicative noise does not affect the stability of the system, we will only consider additive noise. Let, the disturbances added to  $x_3$ ,  $x_4$ ,  $x_5$  and  $x_6$  be  $n_3$ ,  $n_4$ ,  $n_5$  and  $n_6$ . Although all the noises  $n_3$ ,  $n_4$ ,  $n_5$  and  $n_6$  are white, let their maximum possible value be  $\delta_{n3}$ ,  $\delta_{n4}$ ,  $\delta_{n5}$  and  $\delta_{n6}$  respectively.

Using the similar method as discussed in last section, let

$$e_1 = \int(x_3 - x_{3d})dt \quad (5.114)$$

$$e_2 = \dot{e}_1 = x_3 - x_{3d} \quad (5.115)$$

$$\dot{e}_2 = \dot{x}_3 - \dot{x}_{3d} = f_3(x) + g_3(x)u_1 - \dot{x}_{3d} \quad (5.116)$$

Expanding  $f_3(x)$  and  $g_3(x)$

$$\dot{e}_2 = \omega x_4 + \frac{1}{c} x_1 - \frac{1}{c} \frac{P_0}{x_3} - \frac{1}{c} x_5 - \frac{1}{c} u_1 - \dot{x}_{3d} \quad (5.117)$$

Let, the sliding surface be

$$s = e_1 + e_2 \quad (5.118)$$

After differentiating and adding the noises and uncertainties

$$\dot{s} = \dot{e}_1 + \dot{e}_2 \quad (5.119)$$

$$\dot{s} = e_2 + n_3 + ((\omega + \Delta\omega)(x_4 + n_4) + \frac{1}{c}(\hat{x}_1 + \Delta x_1) - \frac{1}{c}(\frac{P_0}{x_3} + d_P) - \frac{1}{c}(x_5 + n_5) - \frac{1}{c}u_1 - \dot{x}_{3d}) \quad (5.120)$$

where  $n_3$ ,  $n_4$ , and  $n_5$  are noises on  $x_3$ ,  $x_4$ , and  $x_5$ , respectively. Then we can represent the total parametric uncertainty and noises as

$$d = n_3 + \Delta\omega n_4 + \Delta\omega x_4 + \omega n_4 + \frac{1}{c} \Delta x_1 - \frac{1}{c} n_5 - \frac{1}{c} d_P; \quad \|d\| \leq dmax \quad (5.121)$$

where  $dmax$  is the bound of the total disturbance  $d$ .

$$dmax = \frac{1}{c} \delta_{x1} + \delta_{n3} + \delta_\omega \delta_{n4} + \delta_\omega \delta_{x4} + \omega \delta_{n4} - \frac{1}{c} \delta_{n5} - \frac{1}{c} \delta_P / \delta_{x3} \quad (5.122)$$

Then

$$\dot{s} = e_2 - \frac{1}{c} x_5 - \dot{x}_{3d} + \omega x_4 + \frac{1}{c} \hat{x}_1 - \frac{1}{c} \frac{P_0}{x_3} - \frac{1}{c} u_1 + d \quad (5.123)$$

Let this be the Lyapunov candidate function

$$V = \frac{1}{2} s^2 \quad (5.124)$$

$$\dot{V} = s\dot{s} = s(e_2 - \frac{1}{c} x_5 - \dot{x}_{3d} + \omega x_4 + \frac{1}{c} \hat{x}_1 - \frac{1}{c} \frac{P_0}{x_3} - \frac{1}{c} u_1 + d) \quad (5.125)$$

We use  $u_1$

$$u_1 = -c[-e_2 + \frac{1}{c} x_5 + \dot{x}_{3d} - \omega x_4 - \frac{1}{c} \hat{x}_1 + \frac{1}{c} \frac{P_0}{x_3} + v]$$

Then, we can obtain

$$\dot{V} = s(d + v) \quad (5.126)$$

Considering  $\|d\| \leq dmax$ , the following discontinuous control,  $v$ , will make  $\dot{V}$  the negative, and consequently, guarantee stability

$$v = -dmax * sat\left(\frac{s}{\varepsilon}\right); \quad \varepsilon > 0 \quad (5.127)$$

Totally, the control input is

$$u_1 = -c[-e_2 + \frac{1}{c}x_5 + \dot{x}_{3d} + \frac{1}{c}\frac{P_0}{x_3} - \omega x_4 - \frac{1}{c}\hat{x}_1 - dmax * sat\left(\frac{s}{\varepsilon}\right)] \quad (5.128)$$

Similar analysis is also shown here for  $u_2$ ; let

$$e_3 = \int (x_4 - x_{4d}) dt \quad (5.129)$$

$$e_4 = \dot{e}_3 = x_4 - x_{4d} \quad (5.130)$$

$$\dot{e}_4 = \dot{x}_4 - \dot{x}_{4d} = f_4(x) + g_4(x)u_2 - \dot{x}_{4d} \quad (5.131)$$

Expanding  $f_4(x)$  and  $g_4(x)$

$$\dot{e}_4 = -\omega x_3 + \frac{1}{c}x_2 - \frac{1}{c}\frac{Q_0}{x_4} - \frac{1}{c}x_6 - \frac{1}{c}u_2 - \dot{x}_{4d} \quad (5.132)$$

Let, the sliding surface be

$$s = e_3 + e_4 \quad (5.133)$$

After differentiating and adding the noises and uncertainties

$$\dot{s} = e_4 + n_4 + \left( -(\omega + \Delta\omega)(x_3 + n_3) + \frac{1}{c}(\hat{x}_2 + \Delta x_2) - \frac{1}{c}\left(\frac{Q_0}{x_4} + d_Q\right) - \frac{1}{c}(x_6 + n_6) - \frac{1}{c}u_2 - \dot{x}_{4d} \right) \quad (5.134)$$

where  $n_6$  is the noise on  $x_6$ . Then we can represent the total parametric uncertainty and noises as

$$d = n_4 - \omega n_3 - \Delta \omega n_3 - \Delta \omega x_3 + \frac{1}{c} \Delta x_2 - \frac{1}{c} n_6 - \frac{1}{c} d_Q; \quad \|d\| \leq dmax \quad (5.135)$$

where  $dmax$  is the bound of the total disturbance  $d$ .

$$dmax = \frac{1}{c} \delta_{x_2} - \delta_\omega \delta_{x_3} - \delta_\omega \delta_{n_3} - \omega \delta_{n_3} + \delta_{n_4} - \frac{1}{c} \delta_{n_6} - \frac{1}{c} \delta_Q / \delta_{x_4} \quad (5.136)$$

Then

$$\dot{s} = e_3 - \frac{1}{c} x_6 - \dot{x}_{4d} + \omega x_3 + \frac{1}{c} \hat{x}_2 - \frac{1}{c} \frac{Q_0}{x_4} - \frac{1}{c} u_2 + d \quad (5.137)$$

Let this be the Lyapunov candidate function

$$V = \frac{1}{2} s^2 \quad (5.138)$$

$$\dot{V} = s \dot{s} = s(e_3 - \frac{1}{c} x_6 - \dot{x}_{4d} + \omega x_3 + \frac{1}{c} \hat{x}_2 - \frac{1}{c} \frac{Q_0}{x_4} - \frac{1}{c} u_2 + d) \quad (5.139)$$

We use  $u_2$

$$u_2 = -c[-e_3 + \frac{1}{c} x_6 + \dot{x}_{4d} - \omega x_3 - \frac{1}{c} \hat{x}_2 + \frac{1}{c} \frac{Q_0}{x_4} + v]$$

Then, we can obtain

$$\dot{V} = s(d + v) \quad (5.140)$$

Considering  $\|d\| \leq dmax$ , the following discontinuous control,  $v$ , will make  $\dot{V}$  the negative, and consequently, guarantee stability

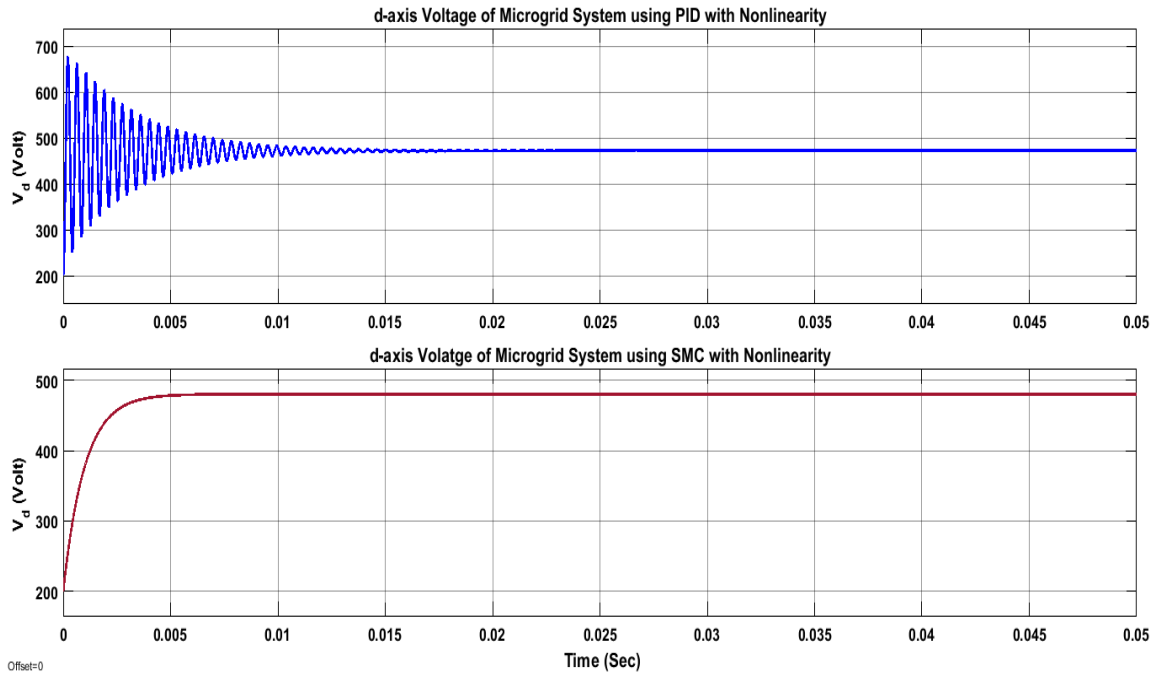
$$v = -dmax * sat\left(\frac{s}{\varepsilon}\right); \quad \varepsilon > 0 \quad (5.141)$$

Totally, the control input is

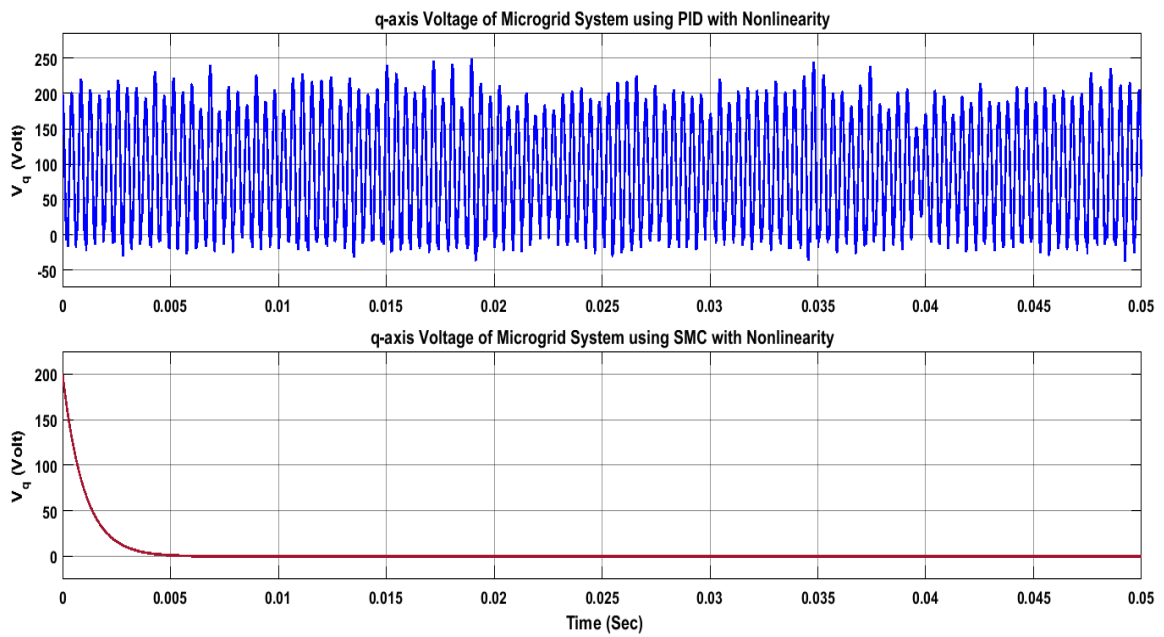
$$u_2 = -c[-e_3 + \frac{1}{c} x_6 + \dot{x}_{4d} - \omega x_3 - \frac{1}{c} \hat{x}_2 + \frac{1}{c} \frac{Q_0}{x_4} - dmax * sat\left(\frac{s}{\varepsilon}\right)] \quad (5.142)$$

In this section, a sliding mode controller (SMC) has been selected over a PID controller due to considerably better performance. At figure 5.25, performance comparison between PID (blue) and

SMC (red) has been shown in case of (a) real axis output voltage, (b) in case of reactive axis output voltage for nonlinear system applications. It has been seen that PID controller experienced initial chattering rather than stabilized d-axis output voltage in face of nonlinearity. In case q-axis output voltage, the PID controller doesn't experience appreciable stabilization, but continuous chattering. On the other hand, the SMC experienced quick and firm output voltage stabilization in face of microgrid nonlinearity. After that, performance comparison between PID and SMC has been presented at figure 5.26 in the case of (a) real axis output voltage, and (b) reactive axis output voltage considering parametric uncertainties. Here, it is evident that the chattering range of the PID controller is considerably more than that of sliding mode controller. Hence, in the case of parametric uncertainties, SMC shows significantly better performance than PID controller. Then, in figure 5.27, performance comparison between the PID and SMC has been illustrated in the case of (a) real axis output voltage, and (b) reactive axis output voltage considering noise rejection. Here, the Sliding Mode Controller handled the instability issue quite fairly. Hence, to improve the microgrid stability in the presence of dense CPL, an SMC has been chosen over a PID controller in load side compensation technique.

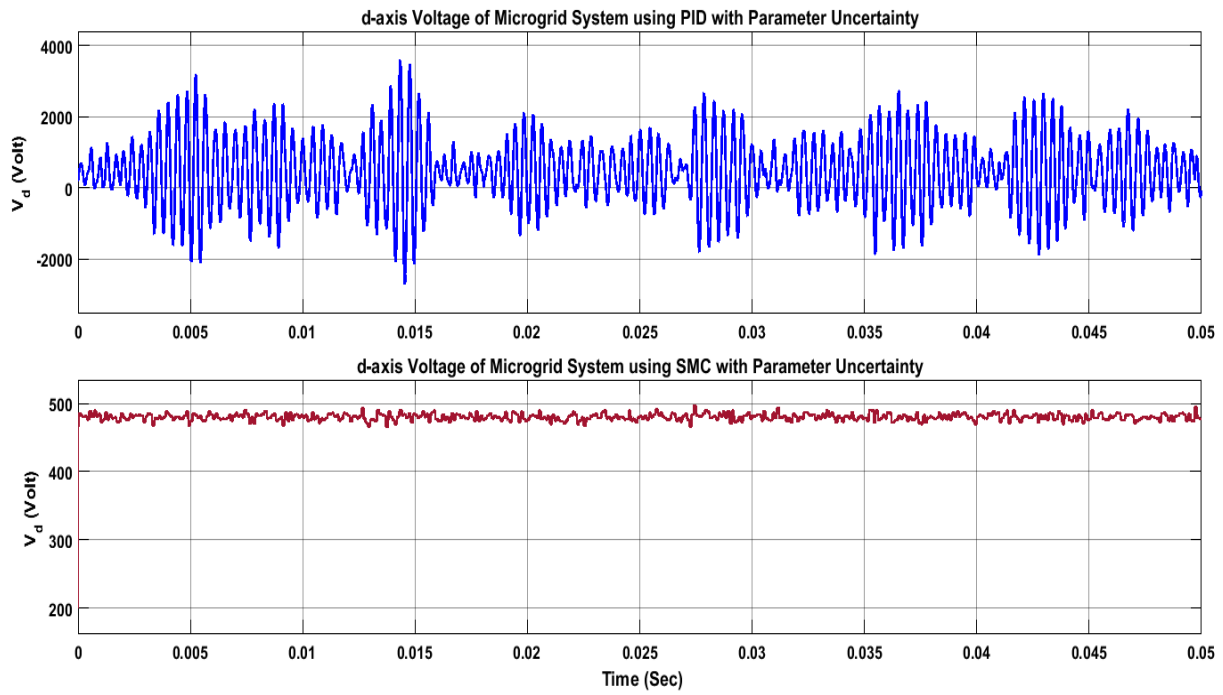


(a)

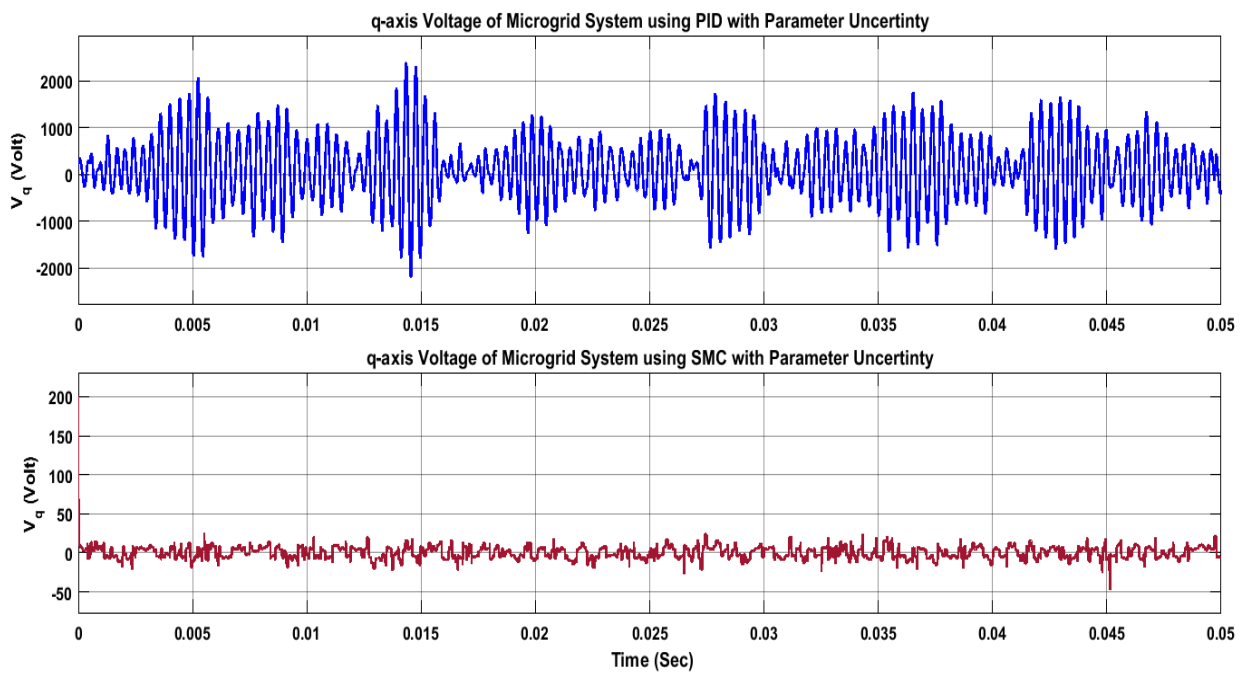


(b)

Figure 5:25: Performance comparison between PID (blue) and SMC (red) in the case of (a) real axis output voltage ( $V_d$ ), (b) reactive axis output voltage ( $V_q$ ) for nonlinear system applications.

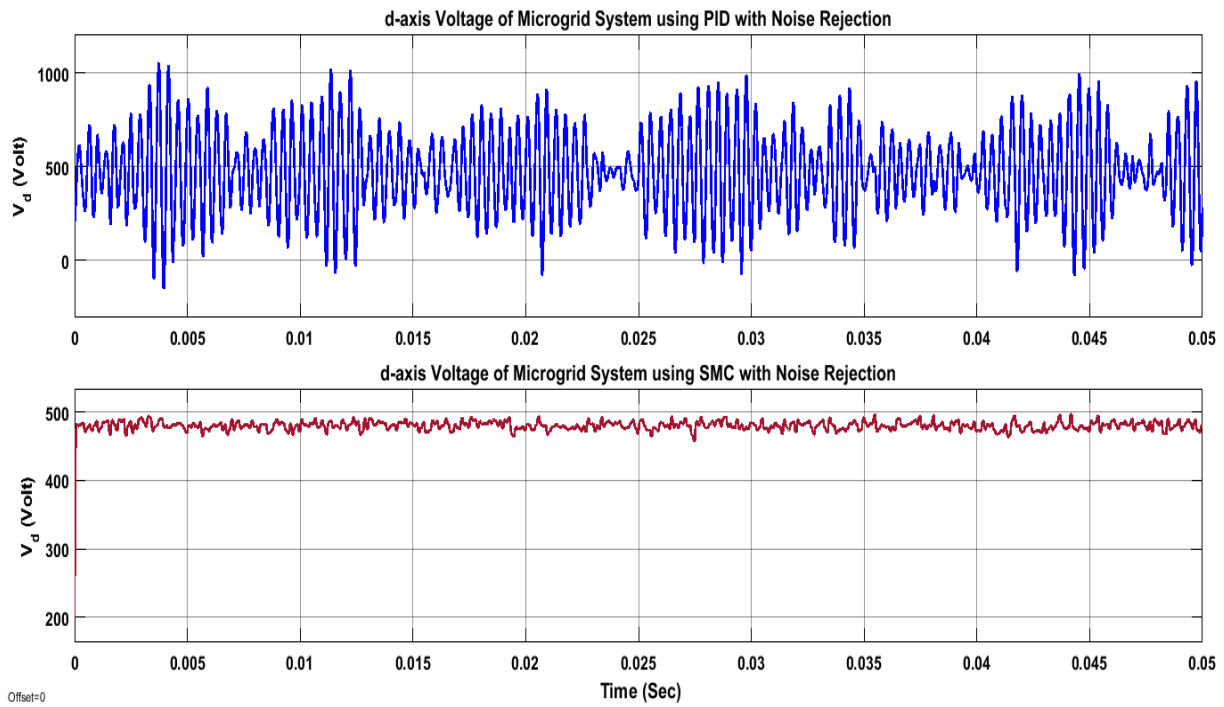


(a)

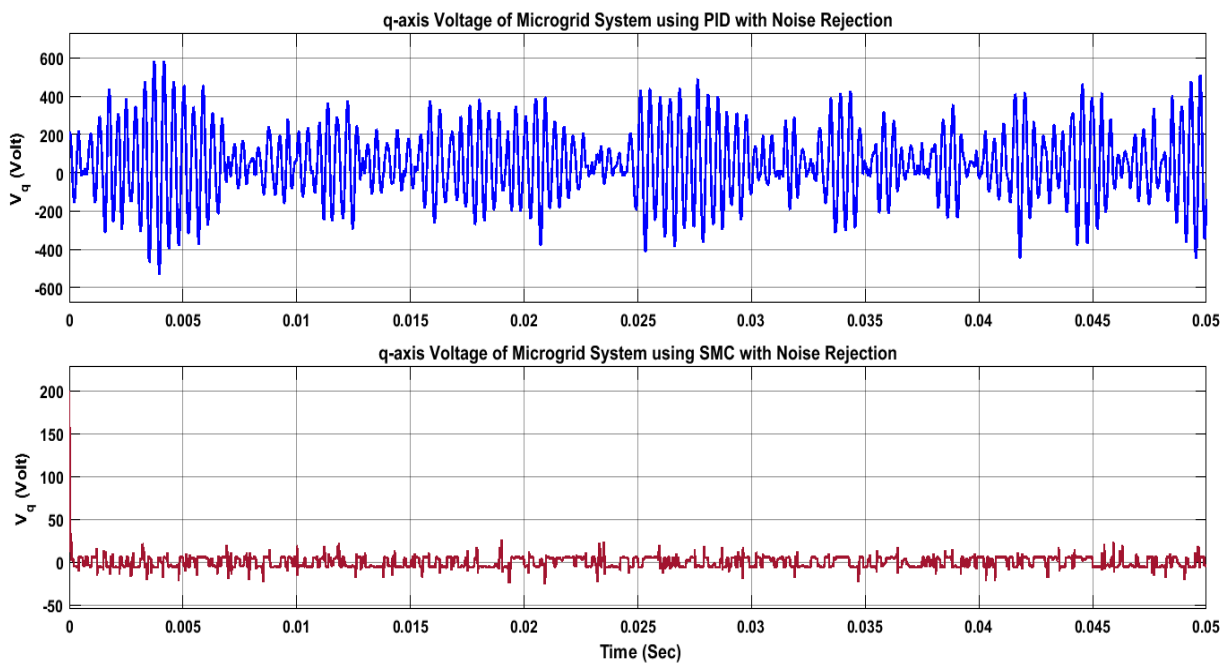


(b)

Figure 5:26: Performance comparison between PID (blue) and SMC (red) in the case of (a) real axis output voltage ( $V_d$ ), (b) reactive axis output voltage ( $V_q$ ) considering parametric uncertainties.



(a)



(b)

Figure 5:27: Performance comparison between PID (blue) and SMC (red) in the case of (a) real axis output voltage ( $V_d$ ), (b) reactive axis output voltage ( $V_q$ ) considering noise rejection.

Performance comparison between robustness analysis against parametric variation and robustness analysis against parametric uncertainties, frequency variation and additive gaussian noise using SMC control technique based on boundary conditions have been analyzed here in figure 5.28 to figure 5.35.

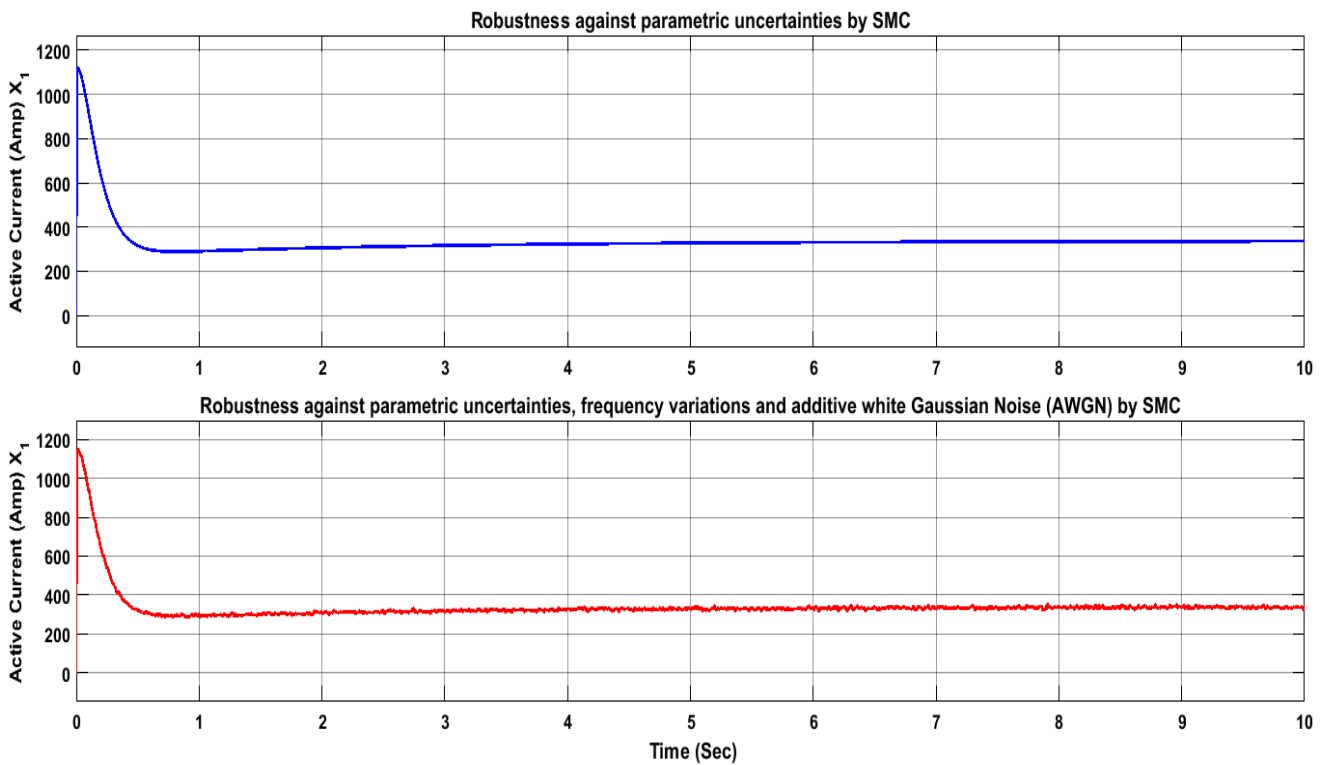


Figure 5:28: d-axis current comparison between robustness analysis against parametric variation and robustness analysis against parametric uncertainties, frequency variation, and additive gaussian noise using SMC control technique based on boundary conditions.

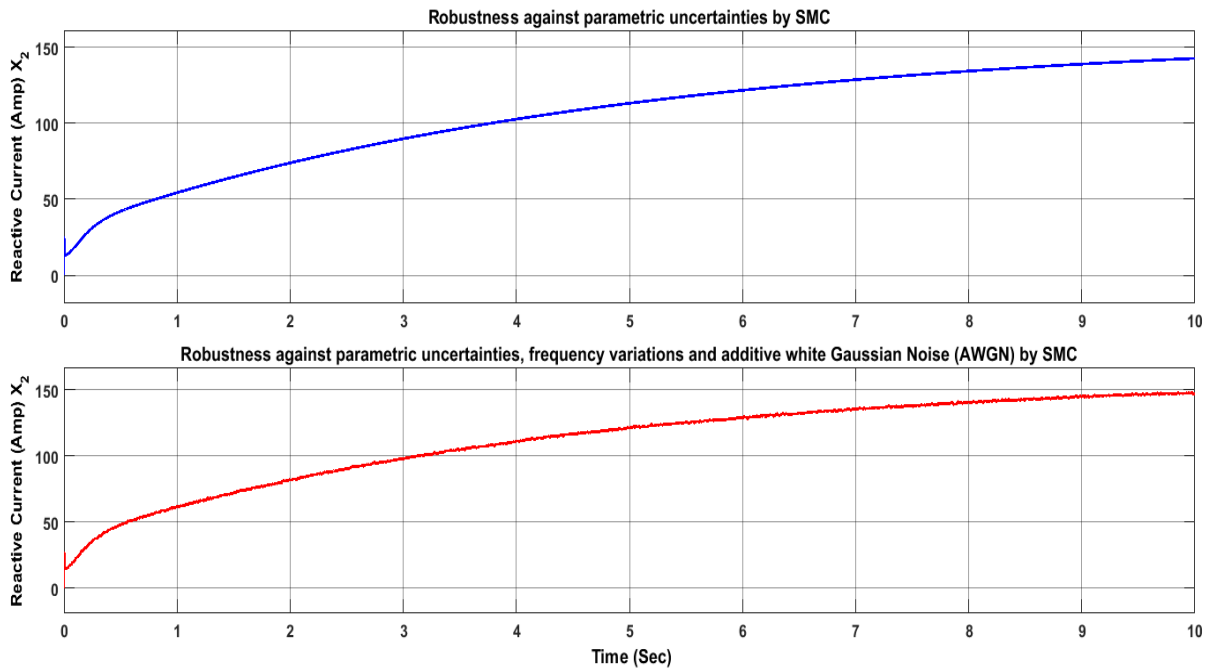


Figure 5:29: q-axis current comparison between robustness analysis against parametric variation and robustness analysis against parametric uncertainties, frequency variation, and additive gaussian noise using SMC control technique based on boundary conditions.

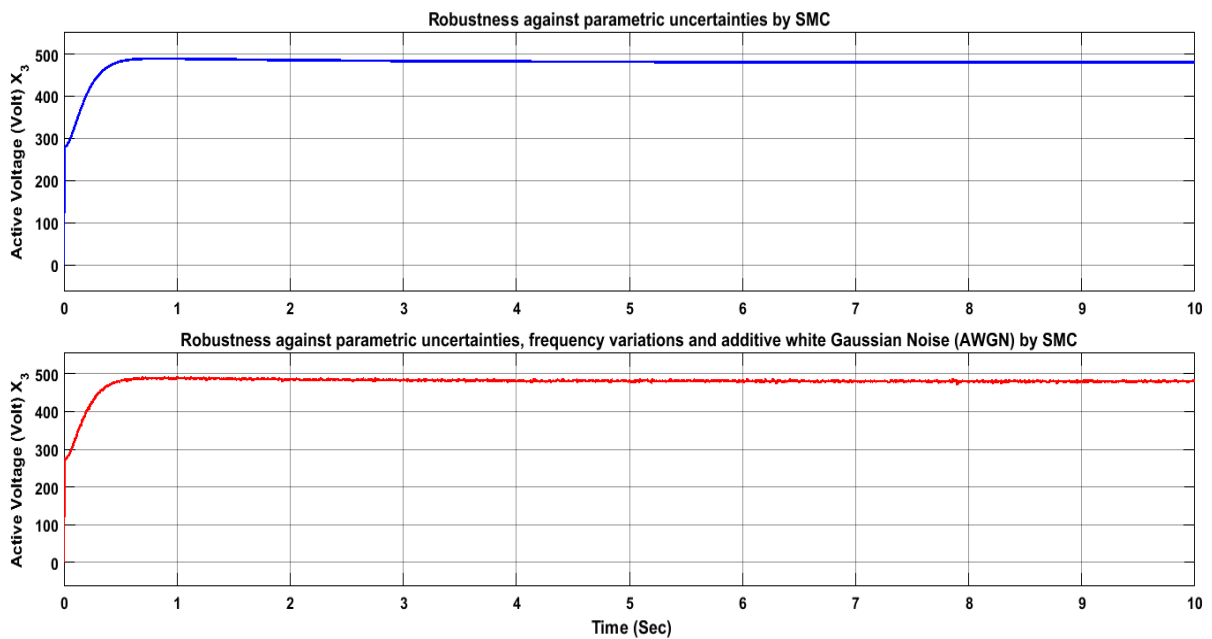


Figure 5:30: d-axis bus voltage comparison between robustness analysis against parametric variation and robustness analysis against parametric uncertainties, frequency variation, and additive gaussian noise using SMC control technique based on boundary conditions.

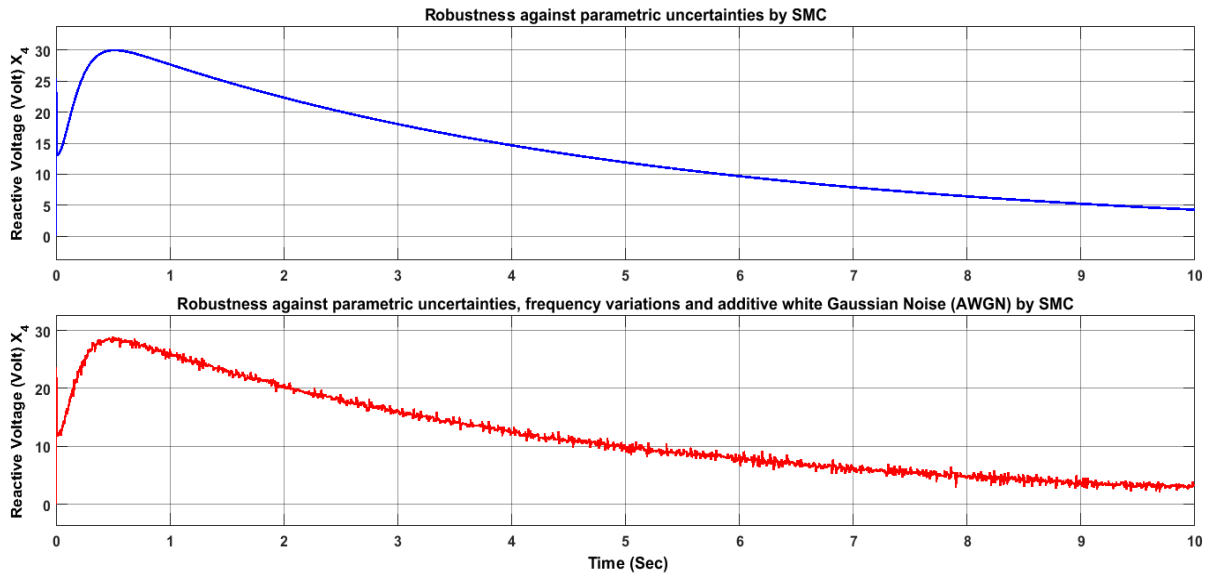


Figure 5:31: q-axis bus voltage comparison between robustness analysis against parametric variation and robustness analysis against parametric uncertainties, frequency variation, and additive gaussian noise using SMC control technique based on boundary conditions.

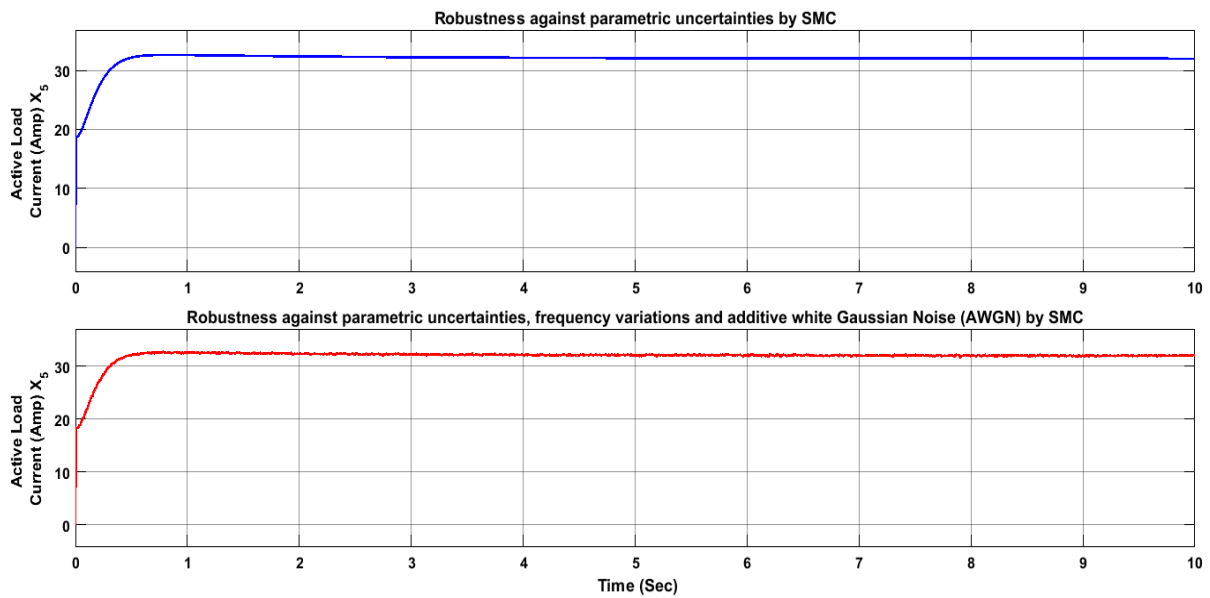


Figure 5:32: d-axis current (CVL load) comparison between robustness analysis against parametric variation and robustness analysis against parametric uncertainties, frequency variation, and additive gaussian noise using SMC control technique based on boundary conditions.

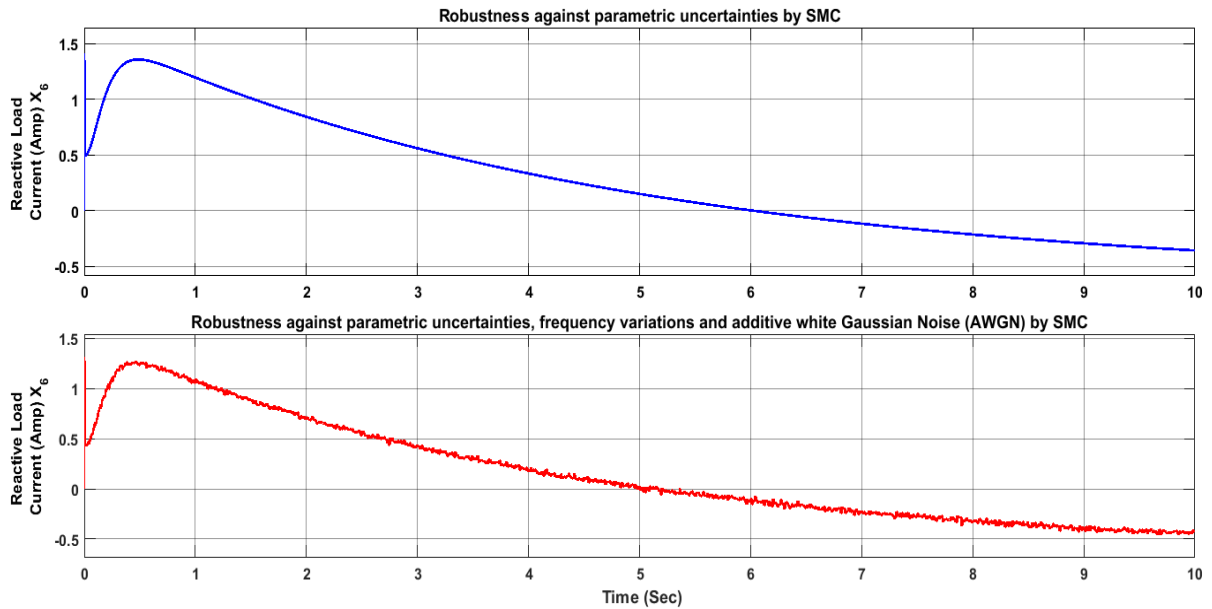


Figure 5:33: q-axis current (CVL load) comparison between robustness analysis against parametric variation and robustness analysis against parametric uncertainties, frequency variation, and additive gaussian noise using SMC control technique based on boundary conditions.

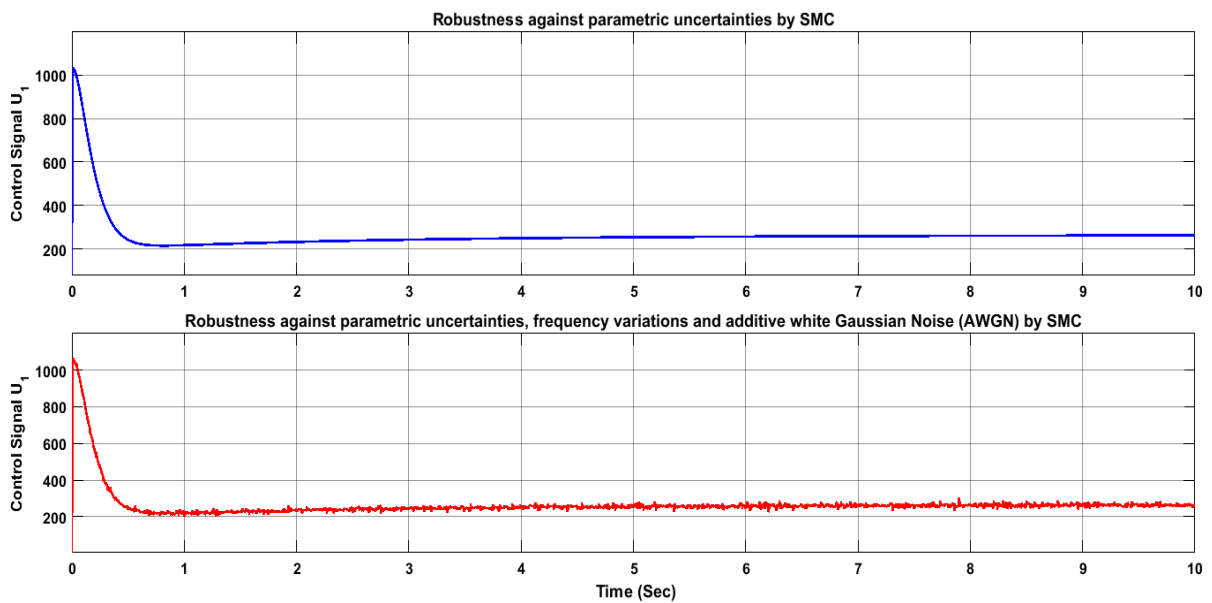


Figure 5:34: d-axis current compensation (d-axis control signal) comparison between robustness analysis against parametric variation and robustness analysis against parametric uncertainties, frequency variation, and additive gaussian noise using SMC control technique based on boundary conditions.

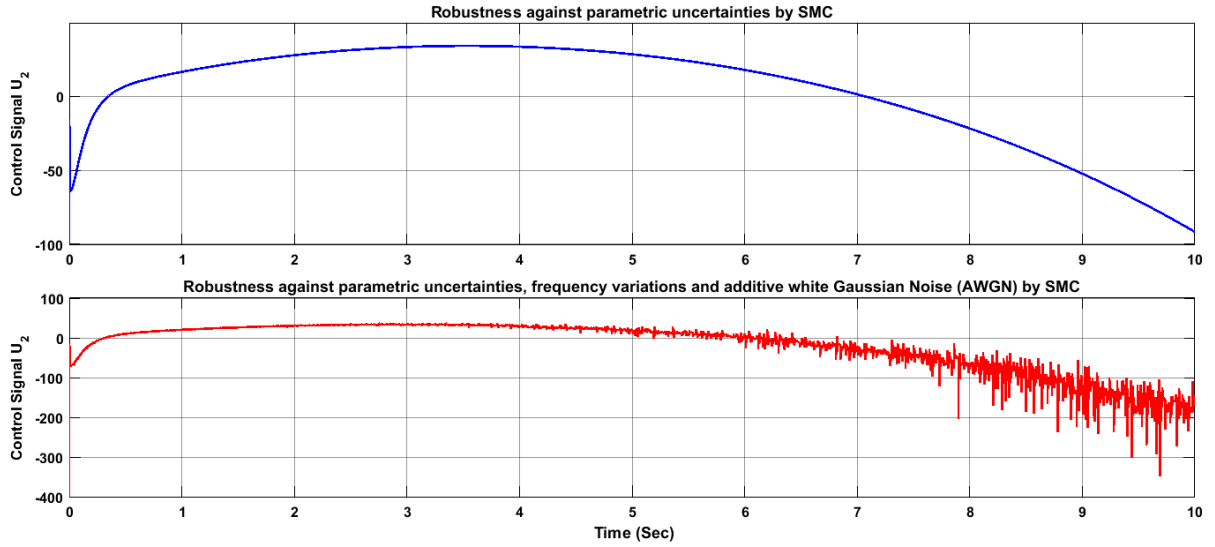


Figure 5:35: q-axis current compensation (q-axis control signal) comparison between robustness analysis against parametric variation and robustness analysis against parametric uncertainties, frequency variation, and additive gaussian noise using SMC control technique based on boundary conditions.

Here, we can also define some numerical values of bounds and the perturbed parameters for robustness analysis.

**For  $u_1$**

Let,  $\omega = 60\text{Hz}$ ,  $x_3 = 600\text{V}$ ,  $x_4 = 10\text{V}$ ,  $\Delta x_1 = 200\text{A}$ ,  $\Delta x_2 = 200\text{A}$ ,  $n_3 = 50\text{V}$ ,  $n_4 = 50\text{V}$ ,  $n_5 = 30\text{A}$ ,  $n_6 = 30\text{A}$ ,  $\Delta\omega = 10\text{Hz}$ ,  $d_p = 50\text{A}$ , and  $d_Q = 20\text{A}$ . Also, we have the numerical value of bounds;  $\delta_{x1} = 4000\text{A}$ ,  $\delta_{x4} = 100\text{V}$ ,  $\delta_\omega = 70\text{Hz}$ ,  $\delta_P = 30\text{kW}$ ,  $\delta_Q = 20\text{Var}$ ,  $\delta_{n3} = \delta_{n4} = \delta_{n5} = \delta_{n6} = 100\text{A}$ ,  $\rho_{x3} = 200\text{V}$ , and  $\varepsilon = 100$ .

$$\dot{V} = s(d + v) = s(n_3 + \Delta\omega n_4 + \Delta\omega x_4 + \omega n_4 + \frac{1}{c}\Delta x_1 - \frac{1}{c}n_5 - \frac{1}{c}d_p - \left[ \frac{1}{c}\delta_{x1} + \delta_{n3} + \delta_\omega \delta_{n4} + \delta_\omega \delta_{x4} + \omega \delta_{n4} - \frac{1}{c}\delta_{n5} - \frac{\delta_P}{C\delta_{x3}} \right] \text{sat} \left( \frac{s}{\varepsilon} \right)) \quad (5.143)$$

$$\dot{V} = s \left[ 50 + (10)(50) + (10)(10) + (60)(50) + \frac{1}{c}(200) - \frac{1}{c}(30) - \frac{1}{c}(50) - \left[ \frac{1}{c}4000 + 100 + (70)(100) + (70)(100) + (65)(100) - \frac{1}{c}100 - \frac{1}{c} \left( \frac{30000}{200} \right) \right] \text{sat} \left( \frac{s}{100} \right) \right] \quad (5.144)$$

$$\dot{V} = s \left[ 18.004 \times 10^6 - [375.021 \times 10^6] \text{sat} \left( \frac{s}{100} \right) \right] \quad (5.145)$$

Now, if s is either positive or negative, we will get  $\dot{V} \leq 0$ .

**For  $u_2$**

$$\dot{V} = s(d + v) = s \left[ n_4 - \omega n_3 - \Delta \omega n_3 - \Delta \omega x_3 + \frac{1}{c} \Delta x_2 - \frac{1}{c} n_6 - \frac{1}{c} d_Q - \left[ \frac{1}{c} \delta_{x2} + \delta_{n4} - \frac{1}{c} \delta_{n6} - \delta_{\omega} \delta_{x3} - \delta_{\omega} \delta_{n3} - \omega \delta_{n3} - \delta_Q / \delta_{x4} \right] \text{sat} \left( \frac{s}{100} \right) \right] \quad (5.146)$$

$$\dot{V} = s \left[ 50 - (60)(50) - (10)(600) - (10)(50) + \frac{1}{c}(200) - \frac{1}{c}(30) - \frac{1}{c}(20) - \left[ \frac{1}{c} 1000 + 100 - (70)(1000) - (70)(100) - (65)(100) - \frac{1}{c} 100 - \frac{1}{c} \left( \frac{20}{1} \right) \right] \text{sat} \left( \frac{s}{100} \right) \right] \quad (5.147)$$

$$\dot{V} = s \left[ 14.99 \times 10^6 - [79.916 \times 10^6] \text{sat} \left( \frac{s}{100} \right) \right] \quad (5.148)$$

Now, if s is either positive or negative, we will get  $\dot{V} \leq 0$

So, as derivative of Lyapunov function is negative, our system will remain stable even in the case of perturbing.

Table 5-1: Boundary Conditions.

Name	Symbol	Range	Range
Frequency	$\omega$	$\rho_{\omega}$ to $\delta_{\omega}$	50 to 70
Power	P	$\rho_P$ to $\delta_P$	10 to 30kW
Var	Q	$\rho_Q$ to $\delta_Q$	0 to 2 kVar
$x_1$	$i_{dL}$	$\rho_{x1}$ to $\delta_{x1}$	1000 to 4000 Amp
$x_2$	$i_{qL}$	$\rho_{x2}$ to $\delta_{x2}$	10 to 1000 Amp
$x_3$	$v_{dc}$	$\rho_{x3}$ to $\delta_{x3}$	200 to 1000 V
$x_4$	$v_{qc}$	$\rho_{x4}$ to $\delta_{x4}$	1 to 100 V

## 5.5 Performance Analysis of Lyapunov Redesign Control Technique

Lyapunov functions, one of the most significant scalar functions in this course, is adopted to confirm the stability of the equilibrium of an Ordinary Differential Equation. In simplified manner, Lyapunov function is nothing but a function which takes the positive values in most of the cases and the values decrease along each trajectory of ordinary differential equation (ODE) [120]. The main function of the Lyapunov function-based stability analysis of the ODEs is that the certain solution (either analytical, or numerical, or both) of ODE is not necessitated. In the course of the nonlinear control, the method of Lyapunov Redesign deals with the design where the stabilizing state feedback controller can be readily constructed with the demonstration of Lyapunov function  $V$ .

Definition of Lyapunov candidate function  $V$

Let  $V: R^n \rightarrow R$  be a continuous scalar function [121].

$V$  is a Lyapunov candidate function; if it is a locally positive definite function, i.e.

$$V(0) = 0$$

$$V(x) > 0 \quad \forall x \in U \setminus \{0\} \tag{5.148}$$

With  $U$  being a neighborhood region around  $x = 0$ .

Consider the system

$$\dot{x} = f(t, x) + G(t, x)[u + \delta(t, x, u)] \tag{5.149}$$

Where,  $x \in R^n$  is the state vector and  $u \in R^p$  is the vector of inputs. The functions  $f, G$  and  $\delta$  are defined for  $(t, x, u) \in [0, \infty) \times D \times R^p$ , where  $D \subset R^n$  is a domain that contains the origin. A nominal model for this system can be written as in equation (5.150)

$$\dot{x} = f(t, x) + G(t, x)u \tag{5.150}$$

And the control law as in equation (5.151)

$$u = u_0 + v \quad (5.151)$$

It stabilizes the system. The design of  $v$  is called Lyapunov redesign.

### **Selection of Lyapunov Redesign Control over PID control technique**

PID control technique is one of the most popular and used linear control techniques around the world. But, in case of microgrid applications to retain the desired stability albeit the negative incremental load characteristics of CPL, it has some disadvantages due to the lack of consistency of accuracy. Unlike the PID controller, Lyapunov redesign control technique has become the preferable choice to researchers because of its success in practical cases, desired consistency, and straightforward firmware implementation. Lyapunov redesign control technique generates discontinuous on/off signals that necessarily forces the system to slide along the desired system's behavior. LRC controller utilizes a discrete sliding decision rule to retain the desired output. According to this, the system, adopting LRC technique, flows through both continuous and discrete modes. In this way, it demonstrates a hybrid feedback configuration in practice. Lyapunov Redesign control technique has a number of advantages over the conventional proportional- integral-differential (PID) control technique. Hence, in this paper, the LRC technique has been adopted to improve the stability of the microgrid system in the presence of CPL load. The advantages of LRC control technique listed below.

- Characteristically, the microgrid system is significantly nonlinear with the time-varying parameters as well as with the system uncertainties. Hence, using a PID control technique may hamper the system stability due to the possible over linearization of the system. On the other hand, an LRC controller doesn't ignore the system nonlinearity during controller design.
- The efficiency of the entire system depends cardinally on the loading conditions. In case of modeling imprecision, an LRC controller offers a systematic way to the complication of retaining stability as well as the desired consistent performance.
- Compared to PID control technique, LRC offers robust performance against the parametric variations and any disturbance, and better response time to retain microgrid stability.

In microgrid applications, the main reason of choosing LRC over PID control technique is its robustness against parametric variation and its faster response in solving instability problem.

Figure 5.44, 5.45, and 5.46 are represented in the result segment to verify the distinct advantage of LRC over PID control techniques in microgrid applications.

## Advantages

- Closed loop stability can be guaranteed.
- Robustness can be assured against the variation of system's parameters.

In sliding mode controller (SMC) design, the gain of controller for example  $K_1$ ,  $K_2$  are constant, but in Lyapunov redesign we use Lyapunov function to design the gain of controller and the saturation function is different here. That means  $K_1$ ,  $K_2$  have replaced with functions; that is why we have a better result in latter techniques.

In case of implementation of Lyapunov Redesign in microgrid control scheme, let's consider

$$e_1 = \int (x_3 - x_{3d}) dt \quad (5.153)$$

$$e_2 = \dot{e}_1 = x_3 - x_{3d} \quad (5.154)$$

$$\dot{e}_2 = \dot{x}_3 - \dot{x}_{3d} = f_3(x) + g_3(x)u_1 - \dot{x}_{3d} \quad (5.155)$$

Expanding  $f_3(x)$  and  $g_3(x)$

$$\dot{e}_2 = \omega x_4 + \frac{1}{c} x_1 - \frac{1}{c} \frac{P_0}{x_3} - \frac{1}{c} x_5 - \frac{1}{c} u_1 - \dot{x}_{3d} \quad (5.156)$$

We get the linear state space as

$$\dot{e} = \begin{bmatrix} 0 & 1 \\ -k_1 & -k_2 \end{bmatrix} e \quad (5.157)$$

Now, we define the desired Eigen values for the linearized system

Desired Eigen values -10, -10

Here, now, the Lyapunov Redesign Controller Simulation Platform has been presented at figure 5.36.

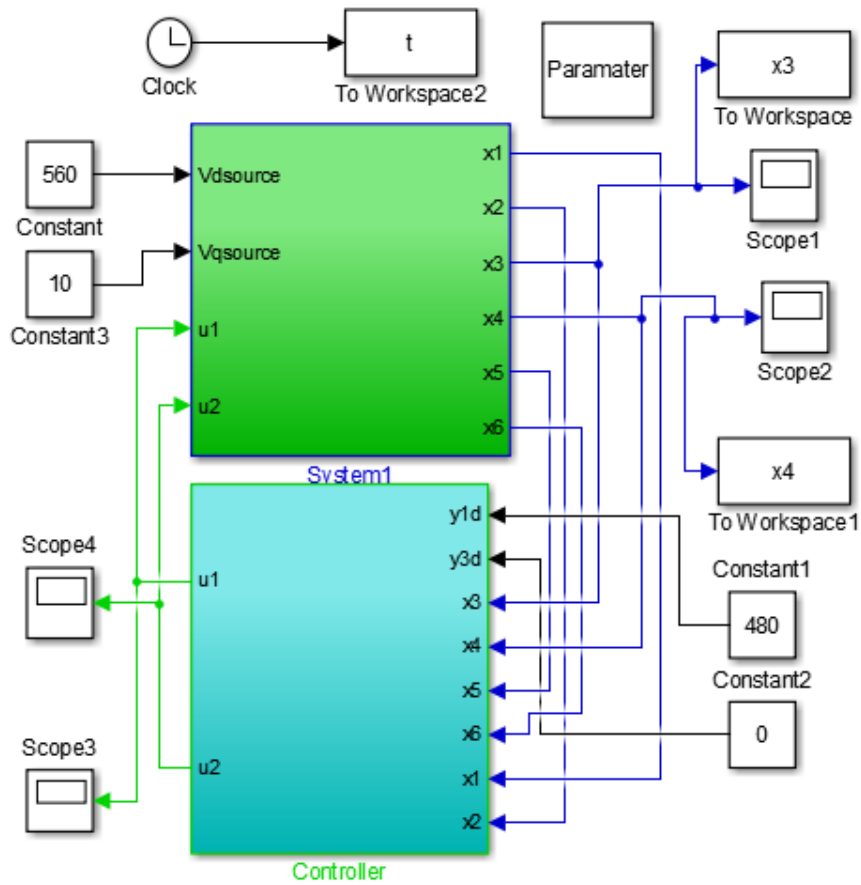


Figure 5:36: Matlab/Simulink schematic model of Lyapunov redesign control of microgrid.

### Derivation of gain $k_1$ , $k_2$ for Lyapunov redesign:

$$\dot{e} = \begin{bmatrix} 0 & 1 \\ -k_1 & -k_2 \end{bmatrix} e \quad (5.158)$$

Generalized Eigen values of matrix “A”

$$sI - A = \begin{bmatrix} s & -1 \\ k_1 & s + k_2 \end{bmatrix} \quad (5.159)$$

$$|sI - A| = s(s + k_2) + k_1 = s^2 + k_2s + k_1 \quad (5.160)$$

Desired Eigen values  $-10, -10$

Characteristic polynomial (desired)

$$(s + 10)(s + 10) = s^2 + 20s + 100 \quad (5.161)$$

Comparing equation (5.160) and (5.161)

$$k_2 = 20, k_1 = 100$$

So, the values of  $k_1$  and  $k_2$  will become +100 to +20 respectively.

$$\dot{e} = \begin{bmatrix} 0 & 1 \\ -100 & -20 \end{bmatrix} e \quad (5.162)$$

$$A = \begin{bmatrix} 0 & 1 \\ -100 & -20 \end{bmatrix} \quad (5.163)$$

$$PA + A^T P = -I; \quad \text{where } P = P^{-1} \quad (5.164)$$

$$P = \begin{bmatrix} \frac{21}{8} & \frac{1}{200} \\ \frac{1}{200} & \frac{101}{4000} \end{bmatrix} \quad (5.165)$$

$$V(z) = e^T P e \quad (5.166)$$

$$w = 2e^T P G = 2[e_1 \quad e_2] \begin{bmatrix} \frac{21}{8} & \frac{1}{200} \\ \frac{1}{200} & \frac{101}{4000} \end{bmatrix} \begin{bmatrix} 0 \\ 1 \end{bmatrix} \quad (5.167)$$

$$w = \frac{1}{100} e_1 + \frac{101}{2000} e_2 \quad (5.168)$$

Then, we can choose the Lyapunov function for the nominal system or disturbance-free system be

$$V = \frac{1}{2} e_2^2 \quad (5.169)$$

$$\dot{V} = e_2 \dot{e}_2 = e_2 \left( \omega x_4 + \frac{1}{c} x_1 - \frac{1}{c} \frac{P_0}{x_3} - \frac{1}{c} x_5 - \frac{1}{c} u_0 - \dot{x}_{3d} \right) \quad (5.170)$$

if we choose

$$u_0 = -c \left[ \frac{1}{c} \frac{P_0}{x_3} - \dot{x}_{3d} - \omega x_4 + \frac{1}{c} x_5 + \dot{x}_{3d} - k_1 e_1 - k_2 e_2 \right]$$

then,  $\dot{V} < 0$ . The terms  $[-k_1 e_1 - k_2 e_2]$  guarantee the global stability of the nominal system which is absent in SMC method.

Redesigning the Lyapunov function,

$$V = \frac{1}{2} e_2^2 \quad (5.171)$$

$$\dot{V} = e_2 \dot{e}_2 = e_2 \left( \left( \omega x_4 + \frac{1}{c} x_1 - \frac{1}{c} \frac{P_0}{x_3} - \frac{1}{c} x_5 - \frac{1}{c} u_0 - \dot{x}_{3d} \right) + \left( \frac{1}{c} v \right) \right) \quad (5.172)$$

If  $\left[ \omega x_4 + \frac{1}{c} x_1 - \frac{1}{c} \frac{P_0}{x_3} - \frac{1}{c} x_5 - \frac{1}{c} u_0 - \dot{x}_{3d} \right]$  is assured to be negative, then the discontinuous control can be designed as

$$v = -c * K * \text{sat} \left( \frac{K * w}{\mu} \right); \quad \text{where } K > 0, \mu > 0 \quad (5.173)$$

Then, the overall input is

$$u_1 = -c \left[ \frac{1}{c} \frac{P_0}{x_3} + \dot{x}_{3d} - \omega x_4 + \frac{1}{c} x_5 - 100e_1 - 20e_2 - K * \text{sat} \left( \frac{K \left( \frac{1}{100} e_1 + \frac{101}{2000} e_2 \right)}{\mu} \right) \right] \quad (5.174)$$

Hence, there is  $\mu > 0$  such that for  $\mu < \mu^*$  origin of the closed-loop system is globally asymptotically stable according to absolute stability theorem.

Similarly, when we design a controller for  $u_2$  with same desired points we get

$$u_2 = -c \left[ \frac{1}{c} \frac{P_0}{x_4} + \dot{x}_{4d} + \omega x_3 + \frac{1}{c} x_6 - 100e_3 - 20e_4 - K * \text{Sat} \left( \frac{K \left( \frac{1}{100} e_3 + \frac{101}{2000} e_4 \right)}{\mu} \right) \right] \quad (5.175)$$

Here,  $K > 0, \mu > 0$ ,

Where,

$$e_3 = x_4 - x_{4d} \quad (5.176)$$

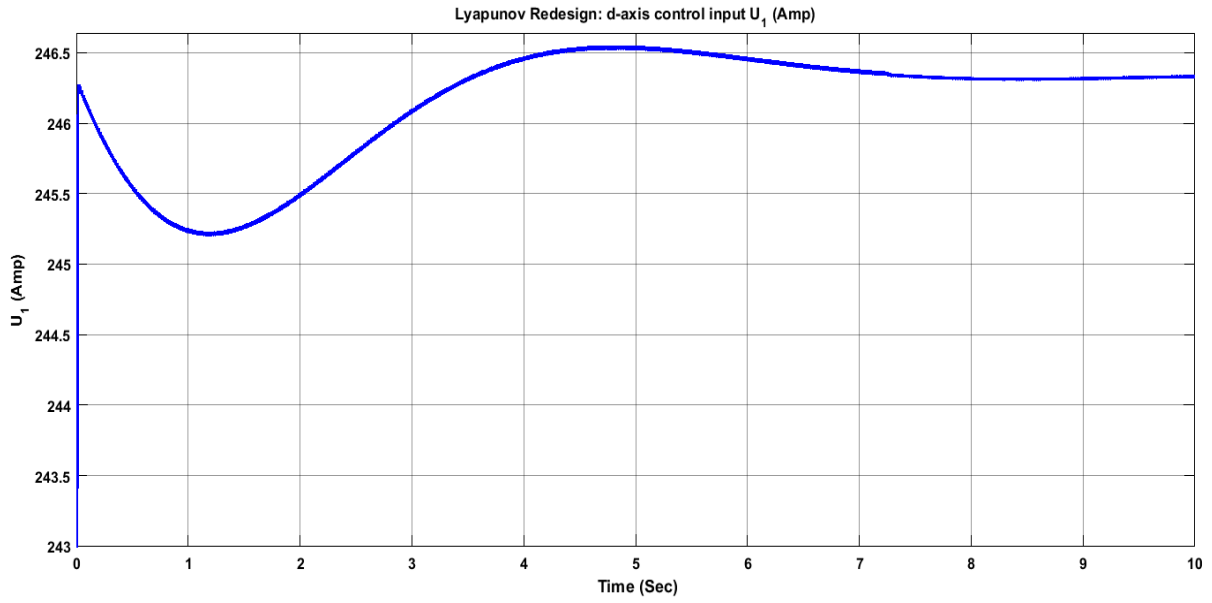


Figure 5:37: Control signal of system while using Lyapunov redesign control technique.

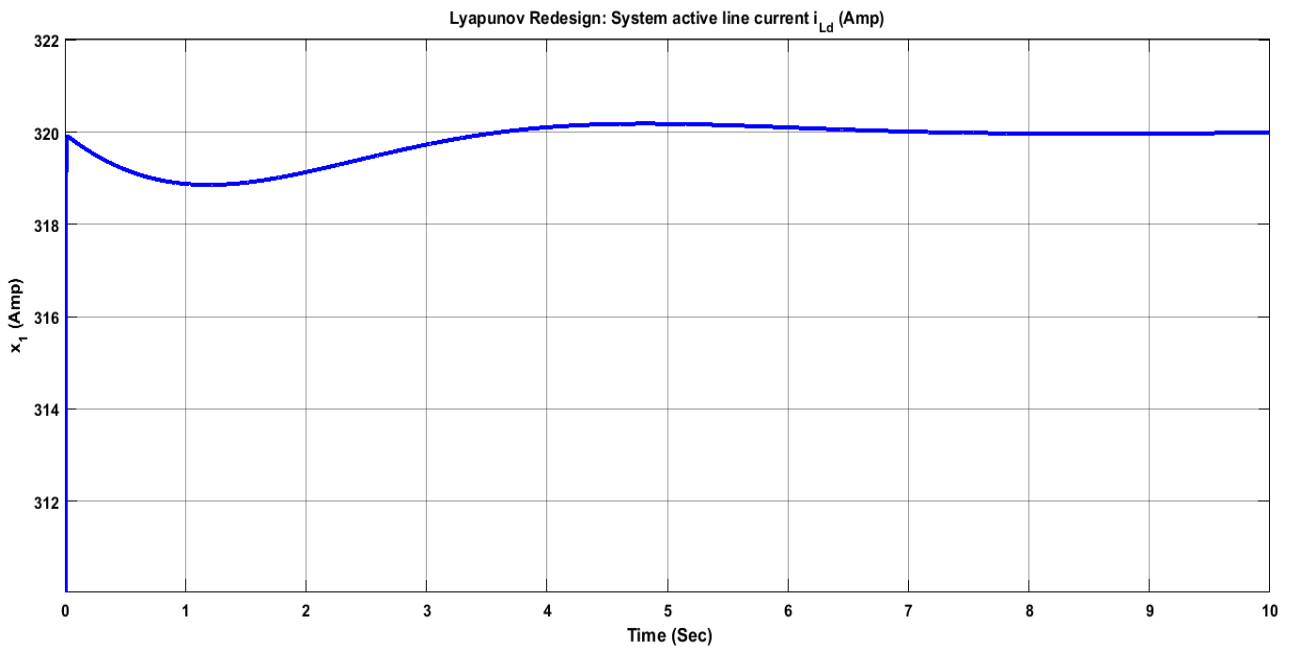


Figure 5:38: d axis current of  $i_L$  while using Lyapunov redesign control technique.

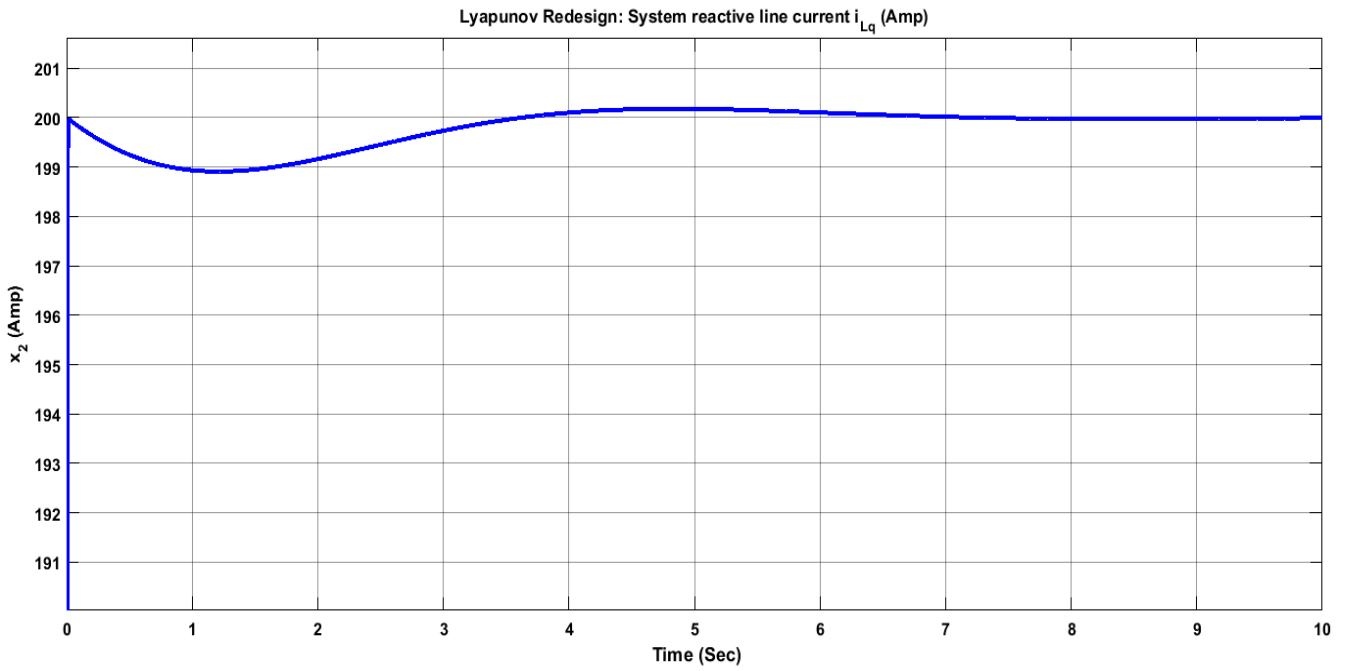


Figure 5:39: q axis current of  $i_L$  while using Lyapunov redesign control technique.

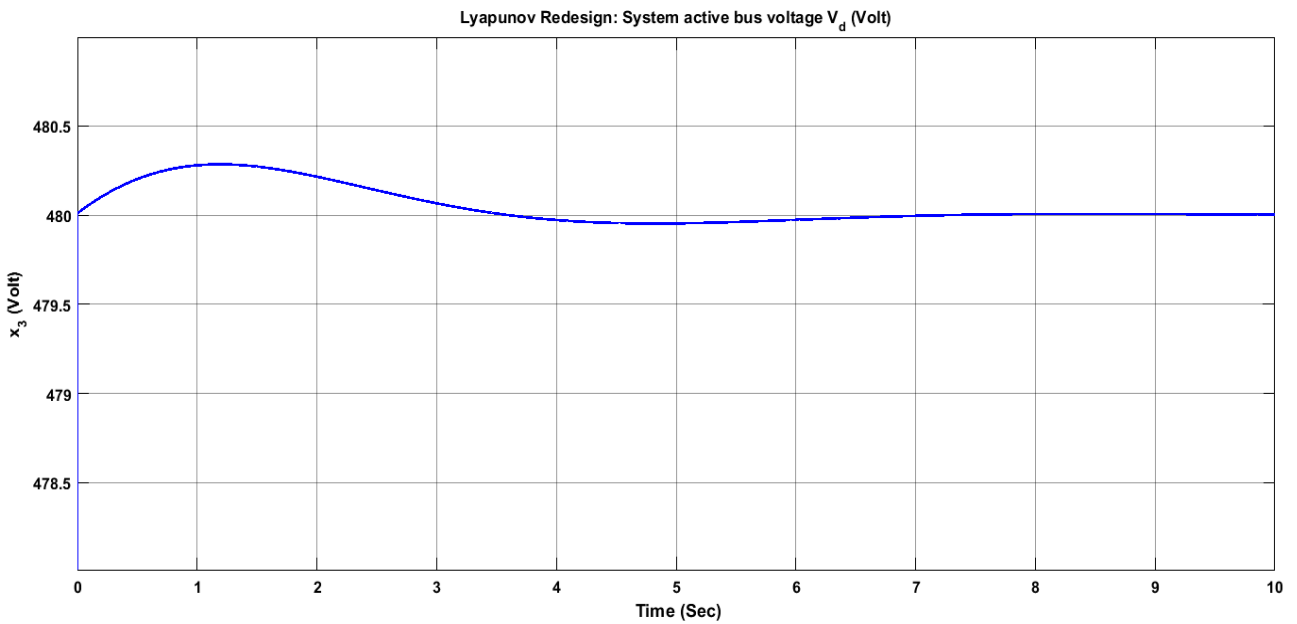


Figure 5:40: The d axis terminal voltage of CPL while using Lyapunov redesign control technique.

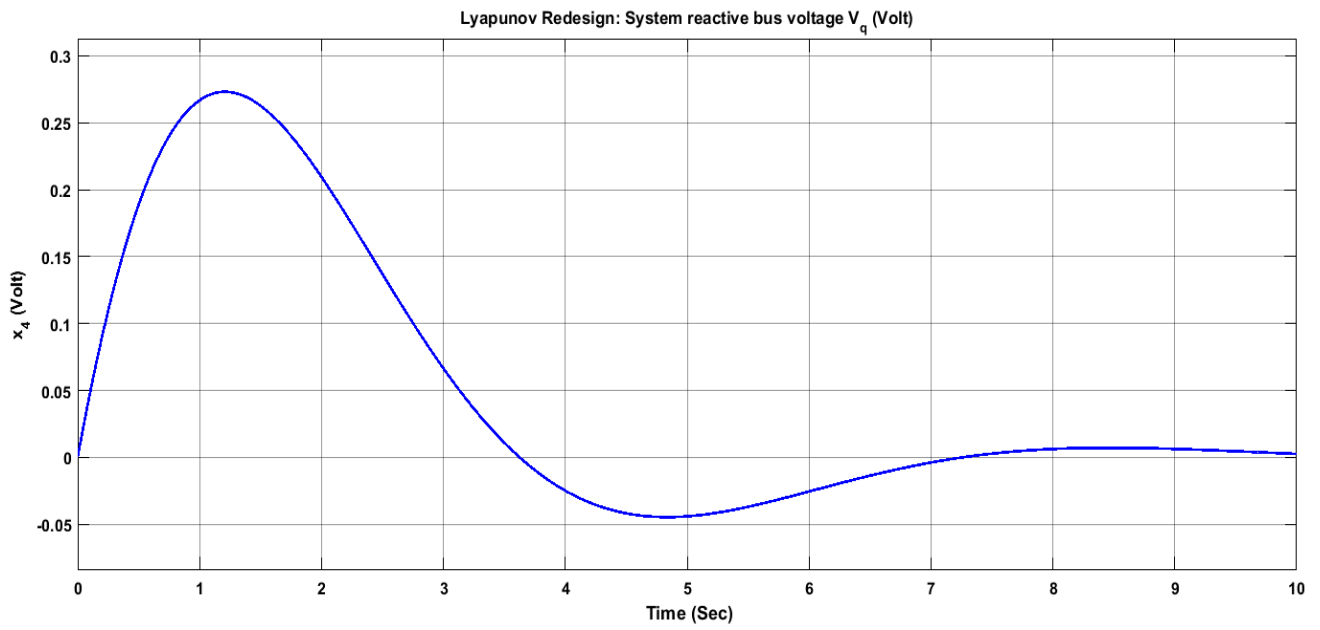


Figure 5:41: The q axis terminal voltage of CPL while using Lyapunov redesign control technique.

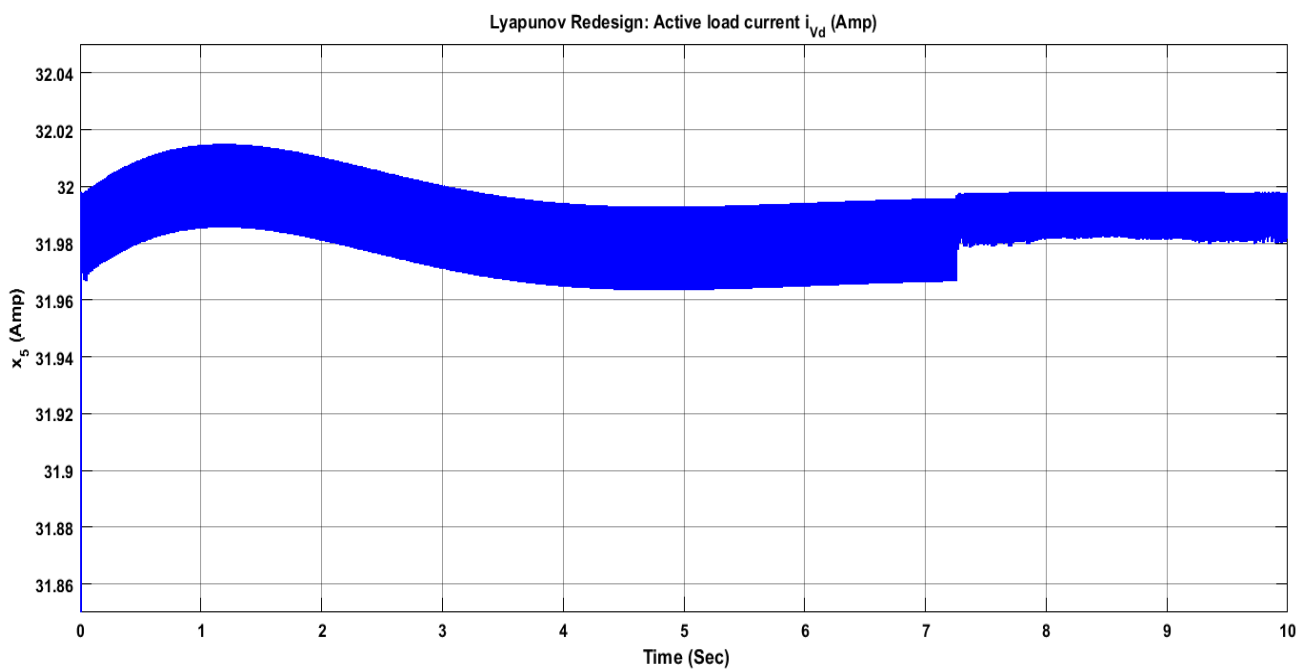


Figure 5:42: d axis current of CVL while using Lyapunov redesign control technique.

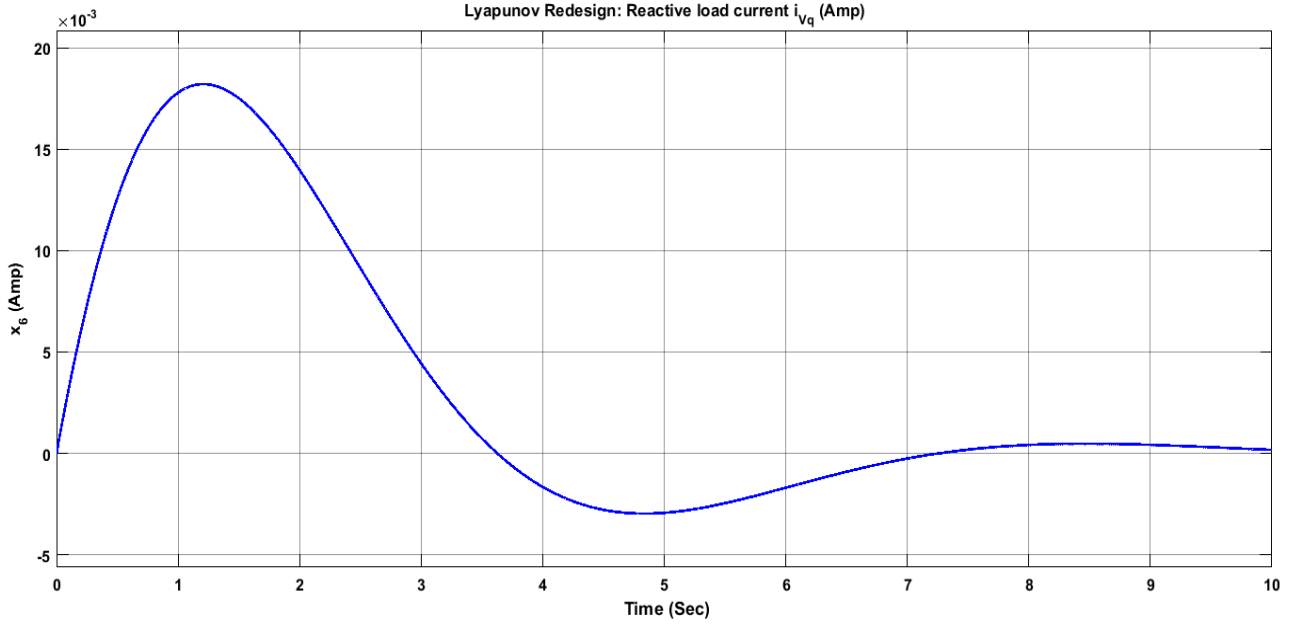


Figure 5:43: q axis current of CVL while using Lyapunov redesign control technique.

### 5.5.1 Lyapunov Redesign, Robustness against Parametric Uncertainties

$$\begin{bmatrix} \dot{x}_1 \\ \dot{x}_2 \\ \dot{x}_3 \\ \dot{x}_4 \\ \dot{x}_5 \\ \dot{x}_6 \end{bmatrix} = \begin{bmatrix} \omega x_2 - \frac{R_1}{L_1} x_1 - \frac{x_3}{L_1} \\ -\omega x_1 - \frac{R_1}{L_1} x_2 - \frac{x_4}{L_1} \\ \omega x_4 + \frac{1}{C} x_1 - \frac{1}{C} \frac{P_0}{x_3} - \frac{1}{C} x_5 \\ -\omega x_3 + \frac{1}{C} x_2 - \frac{1}{C} \frac{Q_0}{x_4} - \frac{1}{C} x_6 \\ \omega x_6 + \frac{1}{L} x_3 - \frac{R}{L} x_5 \\ -\omega x_5 + \frac{1}{L} x_4 - \frac{R}{L} x_6 \end{bmatrix} + \begin{bmatrix} 0 \\ 0 \\ -\frac{1}{C} u_1 \\ -\frac{1}{C} u_2 \\ 0 \\ 0 \end{bmatrix} + \begin{bmatrix} r_1 \\ \frac{r_2}{L_1} \\ 0 \\ 0 \\ 0 \\ 0 \end{bmatrix} \quad (5.175)$$

Where,  $r_1$  and  $r_2$  are unknown parameters that satisfy  $r_1 \leq \delta_{r_1}$  and  $r_2 \leq \delta_{r_2}$  for some known bounds  $\delta_{r_1}$  and  $\delta_{r_2}$ . Our goal is to regulate the output active voltage  $x_3$  and reactive voltage  $x_4$  by designing the control laws  $u_1$  and  $u_2$  respectively. As  $x_3$  and  $x_4$  are related to  $r_1$  and  $r_2$  through  $x_1$  and  $x_2$  respectively, so  $x_1$  and  $x_2$  are also unknown parameters that satisfy  $\Delta x_1 \leq \delta_{x_1}$  and  $\Delta x_2 \leq \delta_{x_2}$  for the unknown bounds  $\delta_{x_1}$  and  $\delta_{x_2}$ . We will design Lyapunov redesign control input,  $u_1$  in the first attempt and then we will follow the similar method to design another control input,  $u_2$ .

To make the integral controller, let's introduce new state variables such that

$$\dot{y}_1 = y_2 \quad (5.177)$$

$$\dot{y}_2 = \dot{x}_3 = f_3(x) + g_3(x)u_1 \quad (5.178)$$

Then, the error between  $y_1$  and the desired state is in equation (5.179) to (5.183)

To make the integral controller, let

$$e_1 = \int (x_3 - x_{3d}) dt \quad (5.179)$$

$$e_2 = \dot{e}_1 = x_3 - x_{3d} \quad (5.180)$$

$$\dot{e}_2 = \dot{x}_3 - \dot{x}_{3d} = f_3(x) + g_3(x)u_1 - \dot{x}_{3d} \quad (5.181)$$

Expanding  $f_3(x)$  and  $g_3(x)$

$$\dot{e}_2 = \omega x_4 + \frac{1}{c} x_1 - \frac{1}{c} \frac{P_0}{x_3} - \frac{1}{c} x_5 - \frac{1}{c} u_1 - \dot{x}_{3d} \quad (5.182)$$

The state  $x_1$  is unknown, then we can represent the uncertainty as  $x_1 = \hat{x}_1 + \Delta x_1$  and  $\left\| \frac{1}{c} \Delta x_1 \right\| \leq \frac{1}{c} \delta_{x1}$

$$\dot{e}_2 = \omega x_4 + \frac{1}{c} \hat{x}_1 + \frac{1}{c} \Delta x_1 - \frac{1}{c} \frac{P_0}{x_3} - \frac{1}{c} x_5 - \frac{1}{c} u_1 - \dot{x}_{3d} \quad (5.183)$$

Following the methodology of Lyapunov redesign, the overall input is

$$u_1 = u_0 + v \quad (5.184)$$

where  $u_0$  is the nominal stabilizing controller and  $v$  to handle the disturbances.

We get the linear state space of error as in equation (5.185)

$$\dot{e} = \begin{bmatrix} 0 & 1 \\ -k_1 & -k_2 \end{bmatrix} e \quad (5.185)$$

Now, we define the desired Eigen values for the linearized system

Desired Eigen values would be -10, -10

Let, (5.185) be written as  $\dot{e} = Ae$  and  $A = \begin{bmatrix} 0 & 1 \\ -k_1 & -k_2 \end{bmatrix}$

Generalized Eigen values of matrix “A”

$$sI - A = \begin{bmatrix} s & -1 \\ k_1 & s + k_2 \end{bmatrix} \quad (5.186)$$

$$|sI - A| = s^2 + k_2s + k_1 \quad (5.187)$$

Characteristic polynomial (desired)

$$(s + 10)(s + 10) = s^2 + 20s + 100 \quad (5.188)$$

Comparing equation (5.187) and (5.188)

$$k_2 = 20, k_1 = 100$$

So, the values of  $k_1$  and  $k_2$  will become +100 and +20 respectively.

$$\dot{e} = \begin{bmatrix} 0 & 1 \\ -100 & -20 \end{bmatrix} e \quad (5.189)$$

$$A = \begin{bmatrix} 0 & 1 \\ -100 & -20 \end{bmatrix} \quad (5.190)$$

$$PA + A^T P = -I \quad (5.191)$$

$$P = \begin{bmatrix} \frac{21}{8} & \frac{1}{200} \\ \frac{1}{200} & \frac{101}{4000} \end{bmatrix} \quad (5.192)$$

$$V(e) = e^T P e \quad (5.193)$$

$$w = 2e^T P G = 2[e_1 \quad e_2] \begin{bmatrix} \frac{21}{8} & \frac{1}{200} \\ \frac{1}{200} & \frac{101}{4000} \end{bmatrix} \begin{bmatrix} 0 \\ 1 \end{bmatrix} \quad (5.194)$$

$$w = \frac{1}{100} e_1 + \frac{101}{2000} e_2 \quad (5.195)$$

Then, we can choose the Lyapunov function for the nominal system or disturbance-free system be

$$V = \frac{1}{2} e_2^2 \quad (5.196)$$

$$\dot{V} = e_2 \dot{e}_2 = e_2 \left( \omega x_4 + \frac{1}{c} x_1 - \frac{1}{c} \frac{P_0}{x_3} - \frac{1}{c} x_5 - \frac{1}{c} u_0 - \dot{x}_{3d} \right) \quad (5.197)$$

if we choose

$$u_0 = -c \left[ \frac{1}{c} \frac{P_0}{x_3} + \dot{x}_{3d} - \omega x_4 + \frac{1}{c} x_5 + \dot{x}_{3d} - k_1 e_1 - k_2 e_2 \right]$$

then,  $\dot{V} < 0$ . The terms  $[-k_1 e_1 - k_2 e_2]$  guarantee the global stability of the nominal system which is absent in SMC method.

The overall system is stabilized using the discontinuous control in the presence of disturbances.

Redesigning the Lyapunov function in the presence of disturbances,

$$V = \frac{1}{2} e_2^2 \quad (5.198)$$

$$\dot{V} = e_2 \dot{e}_2 = e_2 \left( \left( \omega x_4 + \frac{1}{c} x_1 - \frac{1}{c} \frac{P_0}{x_3} - \frac{1}{c} x_5 - \frac{1}{c} u_0 - \dot{x}_{3d} \right) + \left( \frac{1}{c} v + d \right) \right) \quad (5.199)$$

If  $\left[ \omega x_4 + \frac{1}{c} x_1 - \frac{1}{c} \frac{P_0}{x_3} - \frac{1}{c} x_5 - \frac{1}{c} u_0 - \dot{x}_{3d} \right]$  is assured to be negative, then the discontinuous control can be designed as

$$v = -\delta_{x1} \left( \frac{\delta_{x1} * w}{\mu} \right) \quad (5.200)$$

Then, the overall input is

$$u_1 = -c \left[ \frac{1}{c} \frac{P_0}{x_3} + \dot{x}_{3d} - \omega x_4 + \frac{1}{c} x_5 - 100e_1 - 20e_2 - \delta_{x1} \text{Sat} \left( \frac{\delta_{x1} \left( \frac{1}{100} e_1 + \frac{101}{2000} e_2 \right)}{\mu} \right) \right] \quad (5.201)$$

Hence, there is  $\mu > 0$  such that for  $\mu < \mu^*$  origin of the closed-loop system is globally asymptotically stable according to absolute stability theorem.

Similarly, when we design a controller for  $u_2$  with same desired points, we have equation (5.202).

$$u_2 = -c \left[ \frac{1}{c} \frac{Q_0}{x_4} + \omega x_3 + \frac{1}{c} x_6 + \dot{x}_{4d} - 100e_3 - 20e_4 - \delta_{x2} \text{Sat} \left( \frac{\delta_{x2} \left( \frac{1}{100} e_3 + \frac{101}{2000} e_4 \right)}{\mu} \right) \right] \quad (5.202)$$

Where,

$$e_3 = \int (x_4 - x_{4d}) dt \quad (5.203)$$

$$e_4 = \dot{e}_3 = x_4 - x_{4d} \quad (5.204)$$

$$x_2 = \hat{x}_2 + \Delta x_2 ; \left\| \frac{1}{c} \Delta x_2 \right\| \leq \frac{1}{c} \delta_{x2} \quad (5.205)$$

### 5.5.2 Lyapunov Redesign Controller Robustness against Parametric Uncertainties Including Uncertainties in Power of CPL

In this section, we will enhance the robustness by considering the uncertainties in active power of CPL,  $P_0$  and reactive power of CPL,  $Q_0$ . When  $P_0$  is unknown in case of designing  $u_1$ , we will also consider  $x_3$  as unknown to avoid any complexity. Similarly, in case of  $u_2$  we will also consider  $x_4$  as unknown. Although  $P_0$  and  $Q_0$  are unknown but they satisfy  $P_0 \leq \delta_P$  and  $Q_0 \leq \delta_Q$  for some known bounds  $\delta_P$  and  $\delta_Q$ . The variation on CPL power can be summarized as

$$d_P = \Delta_P / \Delta x_3$$

$$d_Q = \Delta_Q / \Delta x_4$$

where  $d_P$  represents the uncertainties of  $P_0$ ,  $d_Q$  represents the uncertainties of  $Q_0$ ,  $\Delta x_3$  is the uncertainties in  $x_3$ , and  $\Delta x_4$  is the uncertainties in  $x_4$ . As  $x_3$  and  $x_4$  are in the denominator, so we need lower bounds of these parameters. Also, this is expressed in current value. We know that  $x_3$  is the voltage of “d-side” and it satisfies  $\Delta x_3 \leq \delta_{x3}$  for some known, strictly positive bound  $\delta_{x3}$ . Similarly,  $x_4$  is the voltage of “q-side” and it satisfies  $\Delta x_4 \leq \delta_{x4}$  for some known, strictly positive bound  $\delta_{x4}$ . Altogether, we have six unknowns with their known bounds. We will design Sliding Mode Control input,  $u_1$  in the first attempt and then we will follow the similar method to design another control input  $u_2$ .

Using the similar method as discussed in last section, we introduce new state variables

$$e_1 = \int (x_3 - x_{3d}) dt \quad (5.206)$$

$$e_2 = \dot{e}_1 = x_3 - x_{3d} \quad (5.207)$$

$$\dot{e}_2 = \dot{x}_3 - \dot{x}_{3d} = f_3(x) + g_3(x)u_1 - \dot{x}_{3d} \quad (5.208)$$

Expanding  $f_3(x)$  and  $g_3(x)$

$$\dot{e}_2 = \omega x_4 + \frac{1}{c} x_1 - \frac{1}{c} \frac{P_0}{x_3} - \frac{1}{c} x_5 - \frac{1}{c} u_1 - \dot{x}_{3d} \quad (5.209)$$

Considering the uncertainties

$$\dot{e}_2 = \omega(\hat{x}_4 + \Delta x_4) + \frac{1}{c}(\hat{x}_1 + \Delta x_1) - \frac{1}{c}\left(\frac{P_0}{x_3} + d_P\right) - \frac{1}{c}x_5 - \frac{1}{c}u_1 - \dot{x}_{3d} \quad (5.210)$$

where

$$x_4 = \hat{x}_4 + \Delta x_4$$

Then we can represent the total parametric uncertainty including uncertainty of CPL power as

$$d = \frac{1}{c}\Delta x_1 + \omega\Delta x_4 - \frac{1}{c}d_P; \quad \|d\| \leq d_{max} \quad (5.211)$$

where  $d_{max}$  is the bound of the total disturbance  $d$ .

$$d_{max} = \frac{1}{c}\delta_{x1} + \omega\delta_{x4} - \frac{1}{c}\delta_P / \delta_{x3} \quad (5.212)$$

Following the methodology of Lyapunov redesign, the overall input is

$$u_1 = u_0 + v \quad (5.213)$$

where  $u_0$  is the nominal stabilizing controller and  $v$  to handle the disturbances.

We get the linear state space of error as in equation (5.214)

$$\dot{e} = \begin{bmatrix} 0 & 1 \\ -k_1 & -k_2 \end{bmatrix} e \quad (5.214)$$

Now, we define the desired Eigen values for the linearized system

Desired Eigen values would be -10, -10

$$\text{Let, (5.214) be written as } \dot{e} = Ae \text{ and } A = \begin{bmatrix} 0 & 1 \\ -k_1 & -k_2 \end{bmatrix}$$

Generalized Eigen values of matrix “A”

$$sI - A = \begin{bmatrix} s & -1 \\ k_1 & s + k_2 \end{bmatrix} \quad (5.215)$$

$$|sI - A| = s^2 + k_2s + k_1 \quad (5.216)$$

Characteristic polynomial (desired)

$$(s + 10)(s + 10) = s^2 + 20s + 100 \quad (5.217)$$

Comparing equation (5.216) and (5.217)

$$k_2 = 20, k_1 = 100$$

So, the values of  $k_1$  and  $k_2$  will become +100 and +20 respectively.

$$\dot{e} = \begin{bmatrix} 0 & 1 \\ -100 & -20 \end{bmatrix} e \quad (5.218)$$

$$A = \begin{bmatrix} 0 & 1 \\ -100 & -20 \end{bmatrix} \quad (5.219)$$

$$PA + A^T P = -I \quad (5.220)$$

$$P = \begin{bmatrix} \frac{21}{8} & \frac{1}{200} \\ \frac{1}{200} & \frac{101}{4000} \end{bmatrix} \quad (5.221)$$

$$V(e) = e^T P e \quad (5.222)$$

$$w = 2e^T P G = 2[e_1 \quad e_2] \begin{bmatrix} \frac{21}{8} & \frac{1}{200} \\ \frac{1}{200} & \frac{101}{4000} \end{bmatrix} \begin{bmatrix} 0 \\ 1 \end{bmatrix} \quad (5.223)$$

$$w = \frac{1}{100} e_1 + \frac{101}{2000} e_2 \quad (5.224)$$

Then, we can choose the Lyapunov function for the nominal system or disturbance-free system be

$$V = \frac{1}{2} e_2^2 \quad (5.225)$$

$$\dot{V} = e_2 \dot{e}_2 = e_2 \left( \omega \hat{x}_4 + \frac{1}{c} x_1 - \frac{1}{c} \frac{P_0}{x_3} - \frac{1}{c} x_5 - \frac{1}{c} u_0 - \dot{x}_{3d} \right) \quad (5.226)$$

if we choose

$$u_0 = -c \left[ \frac{1}{c} \frac{P_0}{x_3} - \omega \hat{x}_4 + \frac{1}{c} x_5 + \dot{x}_{3d} - k_1 e_1 - k_2 e_2 \right]$$

then,  $\dot{V} < 0$ . The terms  $[-k_1 e_1 - k_2 e_2]$  guarantee the global stability of the nominal system which is absent in SMC method.

The overall system is stabilized using the discontinuous control in the presence of disturbances.

Redesigning the Lyapunov function in the presence of disturbances,

$$V = \frac{1}{2} e_2^2 \quad (5.227)$$

$$\dot{V} = e_2 \dot{e}_2 = e_2 \left( \left( \omega \hat{x}_4 + \frac{1}{c} x_1 - \frac{1}{c} \frac{P_0}{x_3} - \frac{1}{c} x_5 - \frac{1}{c} u_0 - \dot{x}_{3d} \right) + \left( \frac{1}{c} v + d \right) \right) \quad (5.228)$$

If  $\left[ \omega \hat{x}_4 + \frac{1}{c} x_1 - \frac{1}{c} \frac{P_0}{x_3} - \frac{1}{c} x_5 - \frac{1}{c} u_0 - \dot{x}_{3d} \right]$  is assured to be negative, then the discontinuous control can be designed as

$$v = -c * dmax * sat\left(\frac{dmax*w}{\mu}\right) \quad (5.229)$$

Then, the overall input is

$$u_1 = -c \left[ \frac{1}{c} \frac{P_0}{x_3} - \omega \hat{x}_4 + \frac{1}{c} x_5 + \dot{x}_{3d} - 100e_1 - 20e_2 - dmax * sat\left(\frac{dmax\left(\frac{1}{100}e_1 + \frac{101}{2000}e_2\right)}{\mu}\right) \right] \quad (5.230)$$

Hence, there is  $\mu > 0$  such that for  $\mu < \mu^*$  origin of the closed-loop system is globally asymptotically stable according to absolute stability theorem.

Similarly, when we design a controller for  $u_2$  with same desired points, we have equation (5.231).

$$u_2 = -c \left[ \frac{1}{c} \frac{Q_0}{x_4} + \omega \hat{x}_3 + \frac{1}{c} x_6 + \dot{x}_{4d} - 100e_3 - 20e_4 - dmax * sat \left( \frac{dmax \left( \frac{1}{100} e_3 + \frac{101}{2000} e_4 \right)}{\mu} \right) \right] \quad (5.231)$$

Where,

$$e_3 = \int (x_4 - x_{4d}) dt \quad (5.232)$$

$$e_4 = \dot{e}_3 = x_4 - x_{4d} \quad (5.233)$$

$$d = \frac{1}{c} \Delta x_2 - \omega \Delta x_3 - \frac{1}{c} d_Q; \quad \|d\| \leq dmax = \frac{1}{c} \delta_{x_2} - \omega \delta_{x_3} - \delta_Q / \delta_{x_4} \quad (5.234)$$

where

$$x_3 = \hat{x}_3 + \Delta x_3$$

### 5.5.3 Lyapunov Redesign, Robustness against Parametric Uncertainties and Frequency Variations

In this section, we will enhance robustness to another level by considering the variations in frequency. Although the frequency is unknown, it satisfies  $\omega \leq \delta_\omega$  for some known bound  $\delta_\omega$ . As  $x_3$  and  $x_4$  are also multiplied with  $\omega$ , so they are also considered as unknowns.

Using the similar method as discussed in last section, we introduce new state variables.

$$e_1 = \int (x_3 - x_{3d}) dt \quad (5.235)$$

$$e_2 = \dot{e}_1 = x_3 - x_{3d} \quad (5.236)$$

$$\dot{e}_2 = \dot{x}_3 - \dot{x}_{3d} = f_3(x) + g_3(x)u_1 - \dot{x}_{3d} \quad (5.237)$$

Expanding  $f_3(x)$  and  $g_3(x)$

$$\dot{e}_2 = \omega x_4 + \frac{1}{c} x_1 - \frac{1}{c} \frac{P_0}{x_3} - \frac{1}{c} x_5 - \frac{1}{c} u_1 - \dot{x}_{3d} \quad (5.238)$$

Considering the parametric uncertainties and frequency variations

$$\dot{e}_2 = (\hat{\omega} + \Delta\omega)(\hat{x}_4 + \Delta x_4) + \frac{1}{c}(\hat{x}_1 + \Delta x_1) - \frac{1}{c}\left(\frac{P_0}{x_3} + d_p\right) - \frac{1}{c}x_5 - \frac{1}{c}u_1 - \dot{x}_{3d} \quad (5.239)$$

where

$$\omega = \hat{\omega} + \Delta\omega$$

where  $\Delta\omega$  represents the frequency variation. Then we can represent the total parametric uncertainty and frequency variation as

$$d = \Delta\omega\hat{x}_4 + \Delta\omega\Delta x_4 + \hat{\omega}\Delta x_4 + \frac{1}{c}\Delta x_1 - \frac{1}{c}d_p; \quad \|d\| \leq dmax \quad (5.240)$$

where  $dmax$  is the bound of the total disturbance  $d$ .

$$dmax = \frac{1}{c}\delta_{x1} + \delta_{\omega}\hat{x}_4 + \delta_{\omega}\delta_{x4} + \hat{\omega}\delta_{x4} - \frac{1}{c}\delta_p / \delta_{x3} \quad (5.241)$$

Following the methodology of Lyapunov redesign, the overall input is

$$u_1 = u_0 + v \quad (5.242)$$

where  $u_0$  is the nominal stabilizing controller and  $v$  to handle the disturbances.

We get the linear state space of error as in equation (5.243)

$$\dot{e} = \begin{bmatrix} 0 & 1 \\ -k_1 & -k_2 \end{bmatrix} e \quad (5.243)$$

Now, we define the desired Eigen values for the linearized system

Desired Eigen values would be -10, -10

$$\text{Let, (5.243) be written as } \dot{e} = Ae \text{ and } A = \begin{bmatrix} 0 & 1 \\ -k_1 & -k_2 \end{bmatrix}$$

Generalized Eigen values of matrix “A”

$$sI - A = \begin{bmatrix} s & -1 \\ k_1 & s + k_2 \end{bmatrix} \quad (5.244)$$

$$|sI - A| = s^2 + k_2s + k_1 \quad (5.245)$$

Characteristic polynomial (desired)

$$(s + 10)(s + 10) = s^2 + 20s + 100 \quad (5.246)$$

Comparing equation (5.245) and (5.246)

$$k_2 = 20, k_1 = 100$$

So, the values of  $k_1$  and  $k_2$  will become +100 and +20 respectively.

$$\dot{e} = \begin{bmatrix} 0 & 1 \\ -100 & -20 \end{bmatrix} e \quad (5.247)$$

$$A = \begin{bmatrix} 0 & 1 \\ -100 & -20 \end{bmatrix} \quad (5.248)$$

$$PA + A^T P = -I \quad (5.249)$$

$$P = \begin{bmatrix} \frac{21}{8} & \frac{1}{200} \\ \frac{1}{200} & \frac{101}{4000} \end{bmatrix} \quad (5.250)$$

$$V(e) = e^T P e \quad (5.251)$$

$$w = 2e^T P G = 2[e_1 \quad e_2] \begin{bmatrix} \frac{21}{8} & \frac{1}{200} \\ \frac{1}{200} & \frac{101}{4000} \end{bmatrix} \begin{bmatrix} 0 \\ 1 \end{bmatrix} \quad (5.252)$$

$$w = \frac{1}{100} e_1 + \frac{101}{2000} e_2 \quad (5.253)$$

Then, we can choose the Lyapunov function for the nominal system or disturbance-free system be

$$V = \frac{1}{2} e_2^2 \quad (5.254)$$

$$\dot{V} = e_2 \dot{e}_2 = e_2 \left( \hat{\omega} \hat{x}_4 + \frac{1}{c} x_1 - \frac{1}{c} \frac{P_0}{x_3} - \frac{1}{c} x_5 - \frac{1}{c} u_0 - \dot{x}_{3d} \right) \quad (5.255)$$

if we choose

$$u_0 = -c \left[ \frac{1}{c} \frac{P_0}{x_3} - \dot{x}_{3d} - \widehat{\omega} \widehat{x}_4 + \frac{1}{c} x_5 + \dot{x}_{3d} - k_1 e_1 - k_2 e_2 \right]$$

then,  $\dot{V} < 0$ . The terms  $[-k_1 e_1 - k_2 e_2]$  guarantee the global stability of the nominal system which is absent in SMC method.

The overall system is stabilized using the discontinuous control in the presence of disturbances.

Redesigning the Lyapunov function in the presence of disturbances,

$$V = \frac{1}{2} e_2^2 \quad (5.256)$$

$$\dot{V} = e_2 \dot{e}_2 = e_2 \left( \widehat{\omega} \widehat{x}_4 + \frac{1}{c} x_1 - \frac{1}{c} \frac{P_0}{x_3} - \frac{1}{c} x_5 - \frac{1}{c} u_0 - \dot{x}_{3d} \right) + \left( \frac{1}{c} v + d \right) \quad (5.257)$$

If  $\left[ \widehat{\omega} \widehat{x}_4 + \frac{1}{c} x_1 - \frac{1}{c} \frac{P_0}{x_3} - \frac{1}{c} x_5 - \frac{1}{c} u_0 - \dot{x}_{3d} \right]$  is assured to be negative, then the discontinuous control can be designed as

$$v = -c * dmax * sat\left(\frac{dmax*w}{\mu}\right) \quad (5.258)$$

Then, the overall input is

$$u_1 = -c \left[ \frac{1}{c} \frac{P_0}{x_3} - \widehat{\omega} \widehat{x}_4 + \frac{1}{c} x_5 + \dot{x}_{3d} - 100e_1 - 20e_2 - dmax * sat\left(\frac{dmax\left(\frac{1}{100}e_1 + \frac{101}{2000}e_2\right)}{\mu}\right) \right] \quad (5.259)$$

Hence, there is  $\mu > 0$  such that for  $\mu < \mu^*$  origin of the closed-loop system is globally asymptotically stable according to absolute stability theorem.

Similarly, when we design a controller for  $u_2$  with same desired points, we have equation (5.260).

$$u_2 = -c \left[ \frac{1}{c} \frac{Q_0}{x_4} + \widehat{\omega} \widehat{x}_3 + \frac{1}{c} x_6 + \dot{x}_{4d} - 100e_3 - 20e_4 - dmax * sat\left(\frac{dmax\left(\frac{1}{100}e_3 + \frac{101}{2000}e_4\right)}{\mu}\right) \right] \quad (5.260)$$

Where,

$$e_3 = \int (x_4 - x_{4d}) dt \quad (5.261)$$

$$e_4 = \dot{e}_3 = x_4 - x_{4d} \quad (5.262)$$

$$d = -(\Delta\omega\hat{x}_3 + \Delta\omega\Delta x_3 + \hat{\omega}\Delta x_3) + \frac{1}{c}\Delta x_2 - \frac{1}{c}d_Q; \quad \|d\| \leq d_{max} = \frac{1}{c}\delta_{x2} - (\delta_\omega\hat{x}_3 + \delta_\omega\delta_{x3} + \hat{\omega}\delta_{x3}) - \frac{1}{c}\delta_Q/\delta_{x4} \quad (5.263)$$

#### 5.5.4 Lyapunov Redesign Control Technique for Robustness against Parametric Uncertainties, Frequency Variations and Additive White Gaussian Noise (AWGN)

In this section, we will enhance robustness by introducing white noise rejection. From last section 5.5.3, we can see that we have to measure just one state as all other states are replaced by their bounds. This parameter is  $x_5$  for  $u_1$  and  $x_6$  for  $u_2$ . As we know that multiplicative noise does not affect the stability of the system, so we will only consider additive noise. Let, the disturbances added to  $x_5$  and  $x_6$  be  $n_5$  and  $n_6$  respectively. Although, all the noises;  $n_5$  and  $n_6$  are white but we know their maximum possible value be  $\delta_{n5}$  and  $\delta_{n6}$  respectively.

Using the similar method as discussed in last section, we introduce new state variables.

$$e_1 = \int (x_3 - x_{3d}) dt \quad (5.264)$$

$$e_2 = \dot{e}_1 = x_3 - x_{3d} \quad (5.265)$$

$$\dot{e}_2 = \dot{x}_3 - \dot{x}_{3d} = f_3(x) + g_3(x)u_1 - \dot{x}_{3d} \quad (5.266)$$

Expanding  $f_3(x)$  and  $g_3(x)$

$$\dot{e}_2 = \omega x_4 + \frac{1}{c}x_1 - \frac{1}{c}\frac{P_0}{x_3} - \frac{1}{c}x_5 - \frac{1}{c}u_1 - \dot{x}_{3d} \quad (5.267)$$

Considering the parametric uncertainties, noises and frequency variations

$$\dot{e}_2 = (\omega + \Delta\omega)(x_4 + n_4) + \frac{1}{c}\hat{x}_1 + \frac{1}{c}\Delta x_1 - \frac{1}{c}\frac{P_0}{x_3} - \frac{1}{c}d_P - \frac{1}{c}(x_5 + n_5) - \frac{1}{c}u_1 - \dot{x}_{3d} \quad (5.268)$$

where  $n_3$ ,  $n_4$ , and  $n_5$  are noises on  $x_3$ ,  $x_4$ , and  $x_5$ , respectively. Then we can represent the total parametric uncertainty and frequency variation as

$$d = \Delta\omega n_4 + \Delta\omega x_4 + \omega n_4 + \frac{1}{c}\Delta x_1 - \frac{1}{c}n_5 - \frac{1}{c}d_p; \quad \|d\| \leq dmax \quad (5.269)$$

where  $dmax$  is the bound of the total disturbance  $d$ .

$$dmax = \frac{1}{c}\delta_{x1} + \delta_\omega\delta_{n4} + \delta_\omega\delta_{x4} + \omega\delta_{n4} - \frac{1}{c}\delta_{n5} - \frac{1}{c}\delta_p / \delta_{x3} \quad (5.270)$$

Following the methodology of Lyapunov redesign, the overall input is

$$u_1 = u_0 + v \quad (5.271)$$

where  $u_0$  is the nominal stabilizing controller and  $v$  to handle the disturbances.

We get the linear state space of error as in equation (5.272)

$$\dot{e} = \begin{bmatrix} 0 & 1 \\ -k_1 & -k_2 \end{bmatrix} e \quad (5.272)$$

Now, we define the desired Eigen values for the linearized system

Desired Eigen values would be -10, -10

$$\text{Let, (5.272) be written as } \dot{e} = Ae \text{ and } A = \begin{bmatrix} 0 & 1 \\ -k_1 & -k_2 \end{bmatrix}$$

Generalized Eigen values of matrix “A”

$$sI - A = \begin{bmatrix} s & -1 \\ k_1 & s + k_2 \end{bmatrix} \quad (5.273)$$

$$|sI - A| = s^2 + k_2s + k_1 \quad (5.274)$$

Characteristic polynomial (desired)

$$(s + 10)(s + 10) = s^2 + 20s + 100 \quad (5.275)$$

Comparing equation (5.274) and (5.275)

$$k_2 = 20, k_1 = 100$$

So, the values of  $k_1$  and  $k_2$  will become +100 and +20 respectively.

$$\dot{e} = \begin{bmatrix} 0 & 1 \\ -100 & -20 \end{bmatrix} e \quad (5.276)$$

$$A = \begin{bmatrix} 0 & 1 \\ -100 & -20 \end{bmatrix} \quad (5.277)$$

$$PA + A^T P = -I \quad (5.278)$$

$$P = \begin{bmatrix} \frac{21}{8} & \frac{1}{200} \\ \frac{1}{200} & \frac{101}{4000} \end{bmatrix} \quad (5.279)$$

$$V(e) = e^T P e \quad (5.280)$$

$$w = 2e^T P G = 2[e_1 \quad e_2] \begin{bmatrix} \frac{21}{8} & \frac{1}{200} \\ \frac{1}{200} & \frac{101}{4000} \end{bmatrix} \begin{bmatrix} 0 \\ 1 \end{bmatrix} \quad (5.281)$$

$$w = \frac{1}{100} e_1 + \frac{101}{2000} e_2 \quad (5.282)$$

Then, we can let the Lyapunov function for the nominal system or disturbance-free system be

$$V = \frac{1}{2} e_2^2 \quad (5.283)$$

$$\dot{V} = e_2 \dot{e}_2 = e_2 \left( \omega x_4 + \frac{1}{c} x_1 - \frac{1}{c} \frac{P_0}{x_3} - \frac{1}{c} x_5 - \frac{1}{c} u_0 - \dot{x}_{3d} \right) \quad (5.284)$$

if we choose

$$u_0 = -c \left[ \frac{1}{c} \frac{P_0}{x_3} - \omega x_4 + \frac{1}{c} x_5 + \dot{x}_{3d} - k_1 e_1 - k_2 e_2 \right] \quad (5.285)$$

then,  $\dot{V} < 0$ . The terms  $[-k_1 e_1 - k_2 e_2]$  guarantee the global stability of the nominal system which is absent in SMC method.

The overall system is stabilized using the discontinuous control in the presence of disturbances.

Redesigning the Lyapunov function in the presence of disturbances,

$$V = \frac{1}{2} e_2^2 \quad (5.286)$$

$$\dot{V} = e_2 \dot{e}_2 = e_2 \left( \left( \omega x_4 + \frac{1}{c} x_1 - \frac{1}{c} \frac{P_0}{x_3} - \frac{1}{c} x_5 - \frac{1}{c} u_0 - \dot{x}_{3d} \right) + \left( \frac{1}{c} v + d \right) \right) \quad (5.287)$$

If  $\left[ \omega x_4 + \frac{1}{c} x_1 - \frac{1}{c} \frac{P_0}{x_3} - \frac{1}{c} x_5 - \frac{1}{c} u_0 - \dot{x}_{3d} \right]$  is assured to be negative, then the discontinuous control can be designed as

$$v = -c * dmax * sat\left(\frac{dmax*w}{\mu}\right) \quad (5.288)$$

Then, the overall input is

$$u_1 = -c \left[ \frac{1}{c} \frac{P_0}{x_3} - \omega x_4 + \frac{1}{c} x_5 + \dot{x}_{3d} - 100e_1 - 20e_2 - dmax * sat\left(\frac{dmax\left(\frac{1}{100}e_1 + \frac{101}{2000}e_2\right)}{\mu}\right) \right] \quad (5.289)$$

Hence, there is  $\mu > 0$  such that for  $\mu < \mu^*$  origin of the closed-loop system is globally asymptotically stable according to absolute stability theorem.

Similarly, when we design a controller for  $u_2$  with same desired points, we have equation (5.290).

$$u_2 = -c \left[ \frac{1}{c} \frac{Q_0}{x_4} + \omega x_3 + \frac{1}{c} x_6 + \dot{x}_{4d} - 100e_3 - 20e_4 - dmax * sat\left(\frac{dmax\left(\frac{1}{100}e_3 + \frac{101}{2000}e_4\right)}{\mu}\right) \right] \quad (5.290)$$

Where,

$$e_3 = \int (x_4 - x_{4d}) dt \quad (5.291)$$

$$e_4 = \dot{e}_3 = x_4 - x_{4d} \quad (5.292)$$

$$d = -\omega n_3 - \Delta \omega n_3 - \Delta \omega x_3 + \frac{1}{c} \Delta x_2 - \frac{1}{c} n_6 - \frac{1}{c} d_Q; \quad \|d\| \leq dmax = \frac{1}{c} \delta_{x_2} - \delta_\omega \delta_{x_3} - \delta_\omega \delta_{n_3} - \omega \delta_{n_3} - \frac{1}{c} \delta_{n_6} - \frac{1}{c} \delta_Q / \delta_{x_4} \quad (5.293)$$

where  $n_6$  represents the noise on  $x_6$ .

So, as derivative of Lyapunov function is negative, our system will remain stable even in the case of perturbations. Moreover, here we can also define some numerical values of bounds and the perturbed parameters for robustness analysis.

**For  $u_1$**

Let,  $\omega = 60\text{Hz}$ ,  $x_3 = 600\text{V}$ ,  $x_4 = 10\text{V}$ ,  $\Delta x_1 = 200\text{A}$ ,  $\Delta x_2 = 200\text{A}$ ,  $n_3 = 50\text{V}$ ,  $n_4 = 50\text{V}$ ,  $n_5 = 30\text{A}$ ,  $n_6 = 30\text{A}$ ,  $\Delta\omega = 10\text{Hz}$ ,  $d_p = 50\text{A}$ , and  $d_Q = 20\text{A}$ . Also, we have the numerical value of bounds;  $\delta_{x_1} = 4000\text{A}$ ,  $\delta_{x_4} = 100\text{V}$ ,  $\delta_\omega = 70\text{Hz}$ ,  $\delta_p = 30\text{kW}$ ,  $\delta_Q = 20\text{Var}$ ,  $\delta_{n_3} = \delta_{n_4} = \delta_{n_5} = \delta_{n_6} = 100\text{A}$ ,  $\rho_{x_3} = 200\text{V}$ , and  $\mu = 100$ .

$$\dot{V} = e_2 \left( \left( \omega x_4 + \frac{1}{c} x_1 - \frac{1}{c} \frac{P_0}{x_3} - \frac{1}{c} x_5 - \frac{1}{c} u_0 - \dot{x}_{3d} \right) + \left( \frac{1}{c} v + d \right) \right) \quad (5.294)$$

$$= e_2 \left( (-100e_1 - 20e_2) + \left( \frac{1}{c} v + d \right) \right)$$

$$= (-100e_1 - 20e_2) + (-d_{max} * \text{sat} \left( \frac{d_{max} * w}{\mu} \right) + \Delta\omega n_4 + \Delta\omega x_4 + \omega n_4 + \frac{1}{c} \Delta x_1 - \frac{1}{c} n_5 - \frac{1}{c} d_p)$$

$$= (-100e_1 - 20e_2) - \left( \frac{1}{c} \delta_{x_1} + \delta_\omega \delta_{n_4} + \delta_\omega \delta_{x_4} + \omega \delta_{n_4} - \frac{1}{c} \delta_{n_5} - \frac{\delta_p}{\delta_{x_3}} \right) \text{sat} \left( \frac{d_{max} * \left( \frac{1}{100} e_1 + \frac{101}{2000} e_2 \right)}{\mu} \right) +$$

$$\left( \Delta\omega n_4 + \Delta\omega x_4 + \omega n_4 + \frac{1}{c} \Delta x_1 - \frac{1}{c} n_5 - \frac{1}{c} d_p \right)$$

$$\dot{V} = (-10(600 - 480)(1) - 20(600 - 480)) - \left[ \frac{1}{c} 4000 + 100 + (70)(100) + (70)(100) + \right.$$

$$(65)(100) - \frac{1}{c} 100 -$$

$$\left. \frac{1}{c} \left( \frac{30000}{200} \right) \right] \text{sat} \left( \frac{\left( \left( \frac{1}{c} 4000 + 100 + (70)(100) + (70)(100) + (65)(100) - \frac{1}{c} 100 - \frac{1}{c} \left( \frac{30000}{200} \right) \right) \left( \frac{1}{100} (600 - 480) + \frac{101}{2000} (600 - 480) \right) \right)}{100} \right) +$$

$$\left[ 30 + (10)(50) + (10)(10) + (60)(50) + \frac{1}{c} (200) - \frac{1}{c} (30) - \frac{1}{c} (50) \right]$$

$$\dot{V} = s \left[ 15.005 \times 10^6 - [375.021 \times 10^6] \text{sat} \left( \frac{260.639 \times 10^6}{100} \right) \right] \quad (5.295)$$

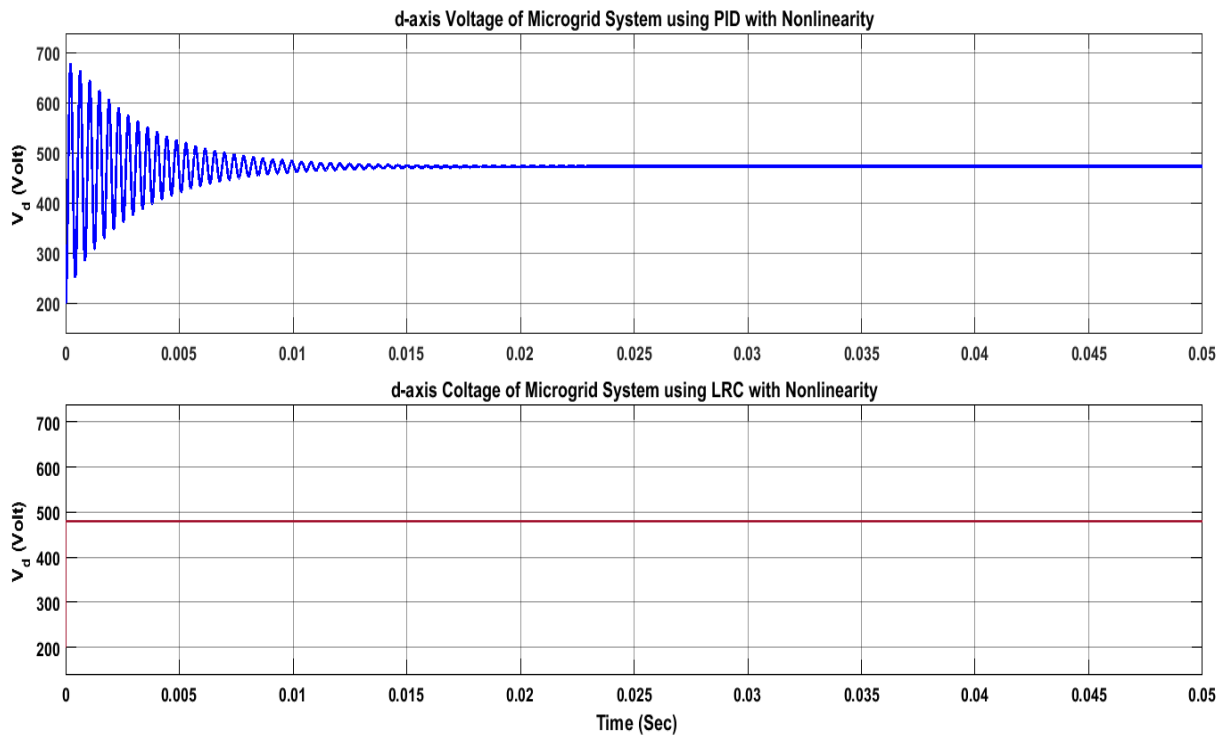
Now even though there are disturbances present in the system, we will get  $\dot{V} \leq 0$ . Hence, system is globally stable.

**For  $u_2$**

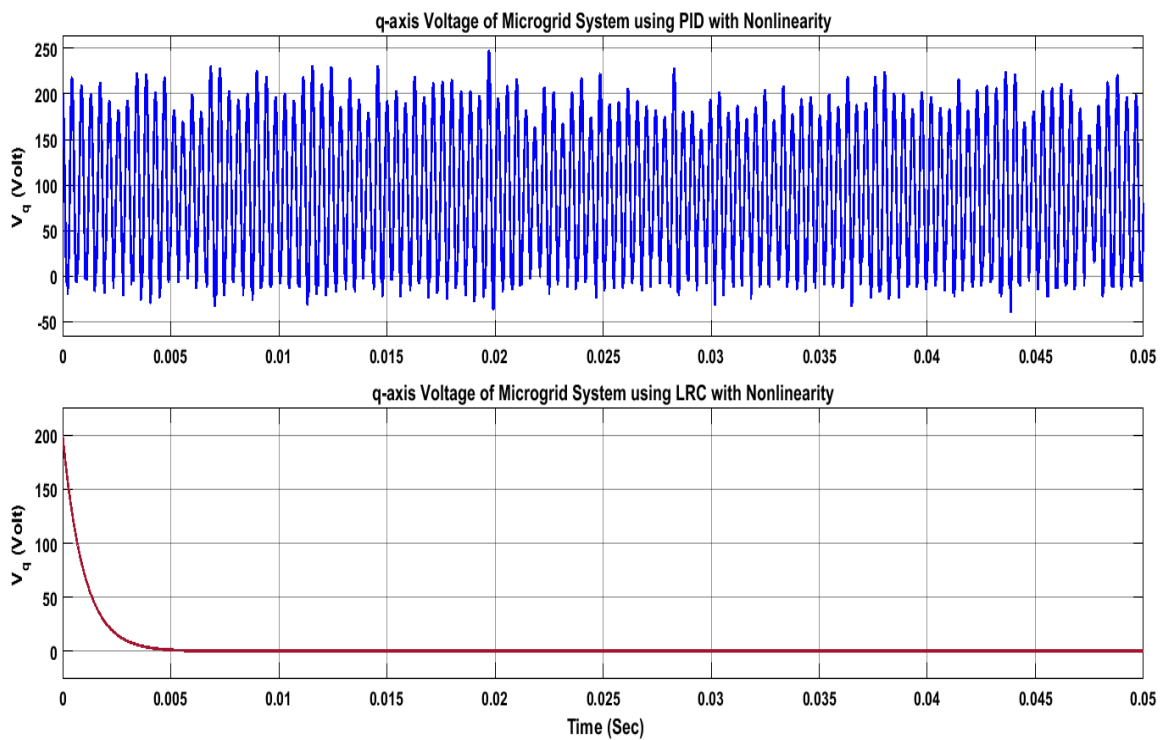
$$\begin{aligned}
\dot{V} &= e_4 \left( (-100e_3 - 20e_4) + \left( \frac{1}{c}v + d \right) \right) \tag{5.296} \\
&= (-100e_3 - 20e_4) + (-dmax * sat \left( \frac{dmax*w}{\mu} \right) + \Delta\omega n_3 + \Delta\omega x_3 + \omega n_3 + \frac{1}{c}\Delta x_2 - \frac{1}{c}n_6 - \frac{1}{c}d_Q) \\
&= \\
&(-100e_3 - 20e_4) - \left( \frac{1}{c}\delta_{x2} - \delta_\omega \delta_{x3} - \delta_\omega \delta_{n3} - \omega \delta_{n3} - \frac{1}{c}\delta_{n6} - \frac{1}{c}\delta_Q / \delta_{x4} \right) sat \left( \frac{dmax * \left( \frac{1}{100}e_3 + \frac{101}{2000}e_4 \right)}{\mu} \right) + \\
&(\Delta\omega n_4 + \Delta\omega x_4 + \omega n_4 + \frac{1}{c}\Delta x_1 - \frac{1}{c}n_5 - \frac{1}{c}d_P) \\
\dot{V} &= (-100(0 - 10)(1) - 20(0 - 10)) - \left[ 100 - (70)(1000) - (70)(100) - (65)(100) - \frac{1}{c}100 - \right. \\
&\left. \frac{1}{c} \left( \frac{20}{1} \right) \right] sat \left( \frac{\left( \frac{1}{c}1000 + 100 - (70)(1000) - (70)(100) - (65)(100) - \frac{1}{c}100 - \frac{1}{c} \left( \frac{20}{1} \right) \right) \left( \frac{1}{100}(0-10) + \frac{101}{2000}(0-10) \right)}{100} \right) + \left[ 50 - \right. \\
&\left. (60)(50) - (10)(600) - (10)(50) + \frac{1}{c}(200) - \frac{1}{c}(30) - \frac{1}{c}(20) \right] \\
\dot{V} &= s \left[ 14.99 \times 10^6 - [79.916 \times 10^6] sat \left( \frac{48.349 \times 10^6}{100} \right) \right] \tag{5.297}
\end{aligned}$$

Now even though there are disturbances present in the system, we will get  $\dot{V} \leq 0$ . Hence, the system is globally stable. In this section, a Lyapunov redesign controller (LRC) has been selected over a PID controller due to considerably better performance. At figure 5.44, performance comparisons between PID (blue) and LRC (red) have been shown in the case of (a) real axis output voltage (Vd), and (b) reactive axis output voltage (Vq) for nonlinear system applications. It has been seen that PID controller experienced initial chattering rather than stabilized d-axis output voltage in face of nonlinearity. In case q-axis output voltage, a PID controller doesn't experience appreciable stabilization, but continuous chattering. On the other hand, Lyapunov redesign controller experienced quick and firm output voltage stabilization in face of microgrid nonlinearity. Performance comparisons between the PID and LRC

have been presented at figure 5.45 in the case of (a) real axis output voltage ( $V_d$ ), and (b) reactive axis output voltage ( $V_q$ ) considering parametric uncertainties. Here, it is evident that the chattering range of the PID controller is considerably more than that of Lyapunov Redesign controller. Hence, in the case of parametric uncertainties, LRC shows significantly better performance than PID controller. Then, in figure 5.46, performance comparisons between the PID and LRC have been illustrated in the case of (a) real axis output voltage ( $V_d$ ), and (b) reactive axis output voltage ( $V_q$ ) considering noise rejection. Here, the Lyapunov Redesign controller handled the instability issue well. Hence, to improve the microgrid stability in the presence of dense CPL, Lyapunov Redesign Controller has been chosen over PID controller in load side compensation technique.

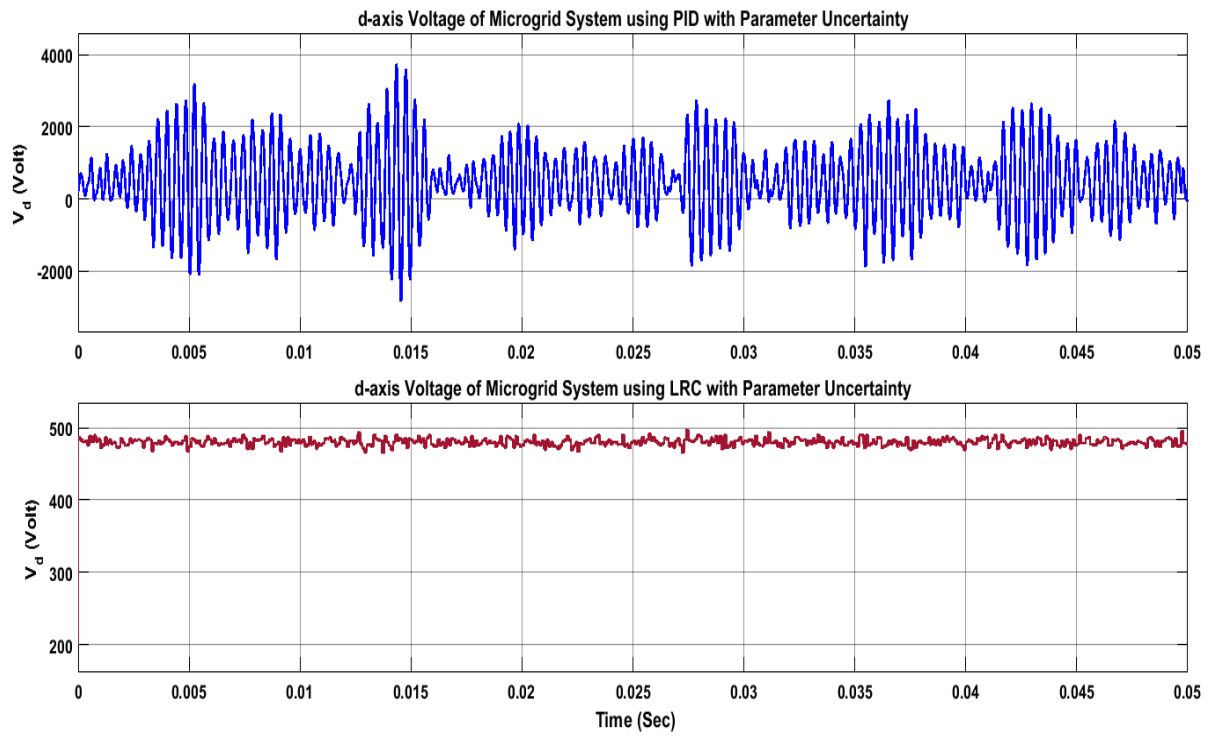


(a)

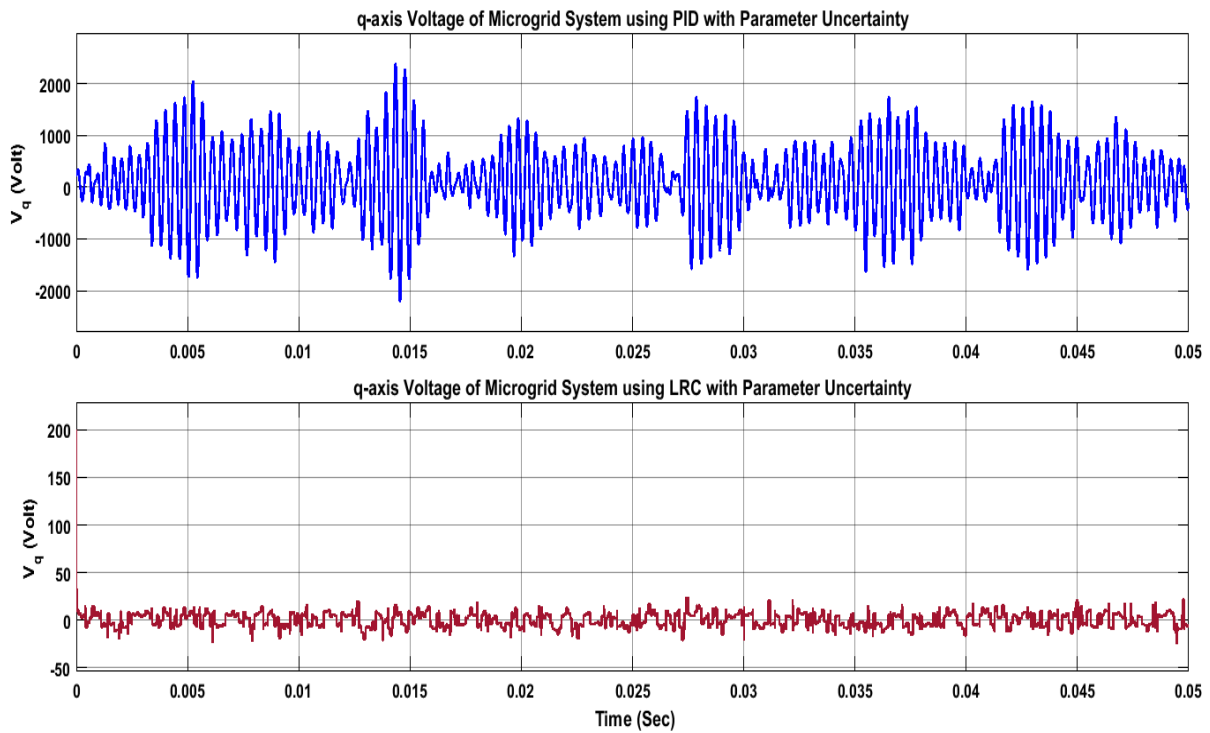


(b)

Figure 5:44: Performance comparison between the PID (blue) and LRC (red) in the case of (a) real axis output voltage ( $V_d$ ), (b) reactive axis output voltage ( $V_q$ ) for nonlinear system applications.

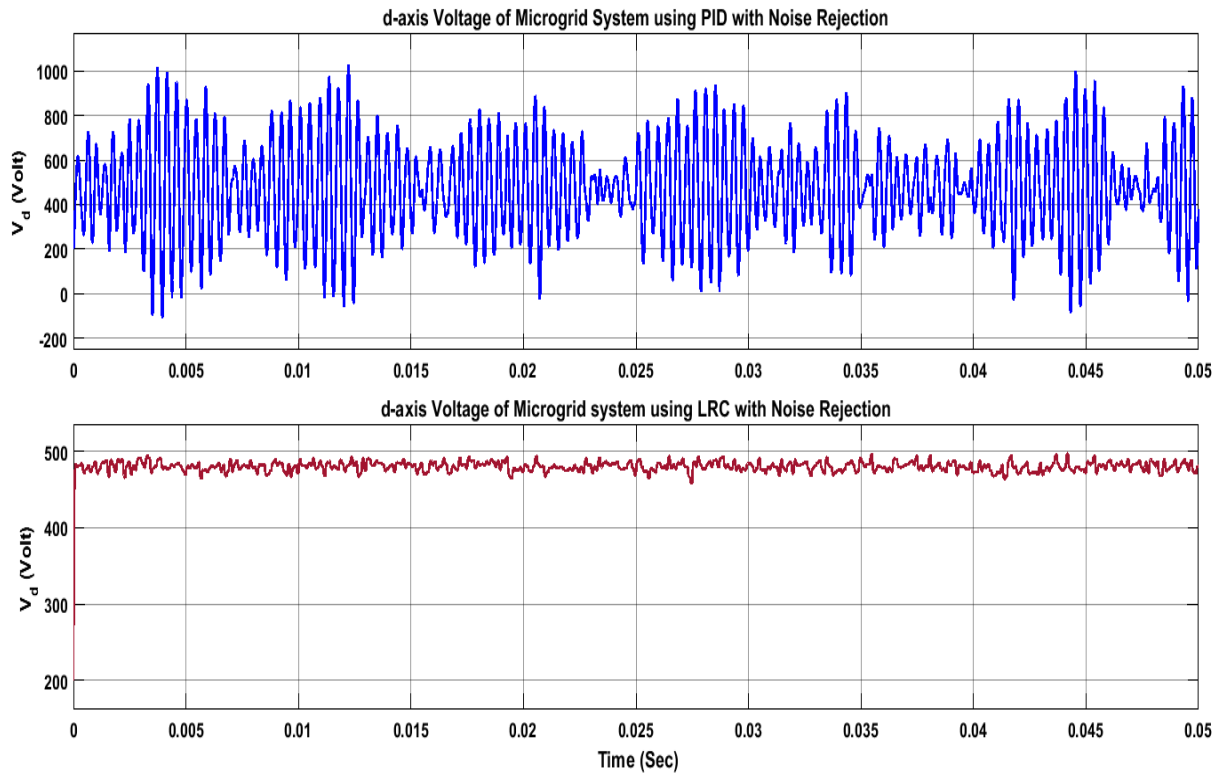


(a)

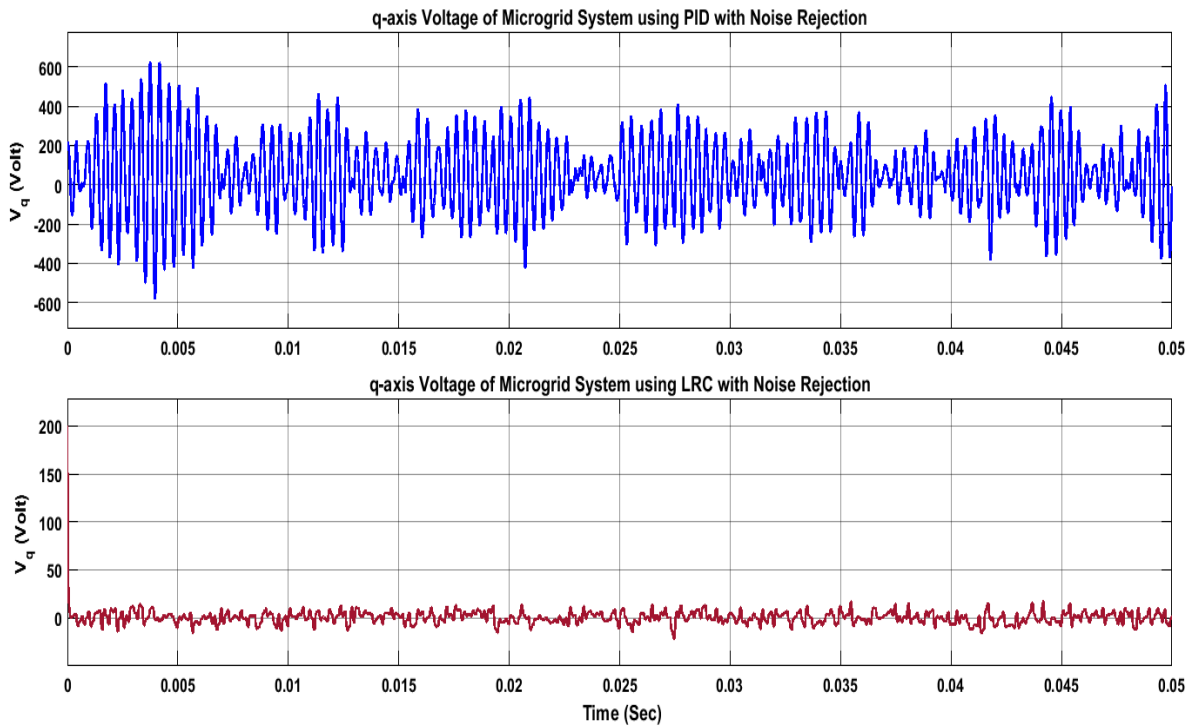


(b)

Figure 5:45: Performance comparison between the PID (blue) and LRC (red) in the case of (a) real axis output voltage ( $V_d$ ), (b) reactive axis output voltage ( $V_q$ ) considering parametric uncertainties.



(a)



(b)

Figure 5:46: Performance comparison between the PID (blue) and LRC (red) in the case of (a) real axis output voltage ( $V_d$ ), (b) reactive axis output voltage ( $V_q$ ) considering noise rejection.

A performance comparison between robustness analysis against parametric variation and robustness analysis against parametric uncertainties, frequency variation and additive Gaussian noise using Lyapunov Redesign control technique have been analyzed here in figure 5.47 to figure 5.54 based on boundary conditions.

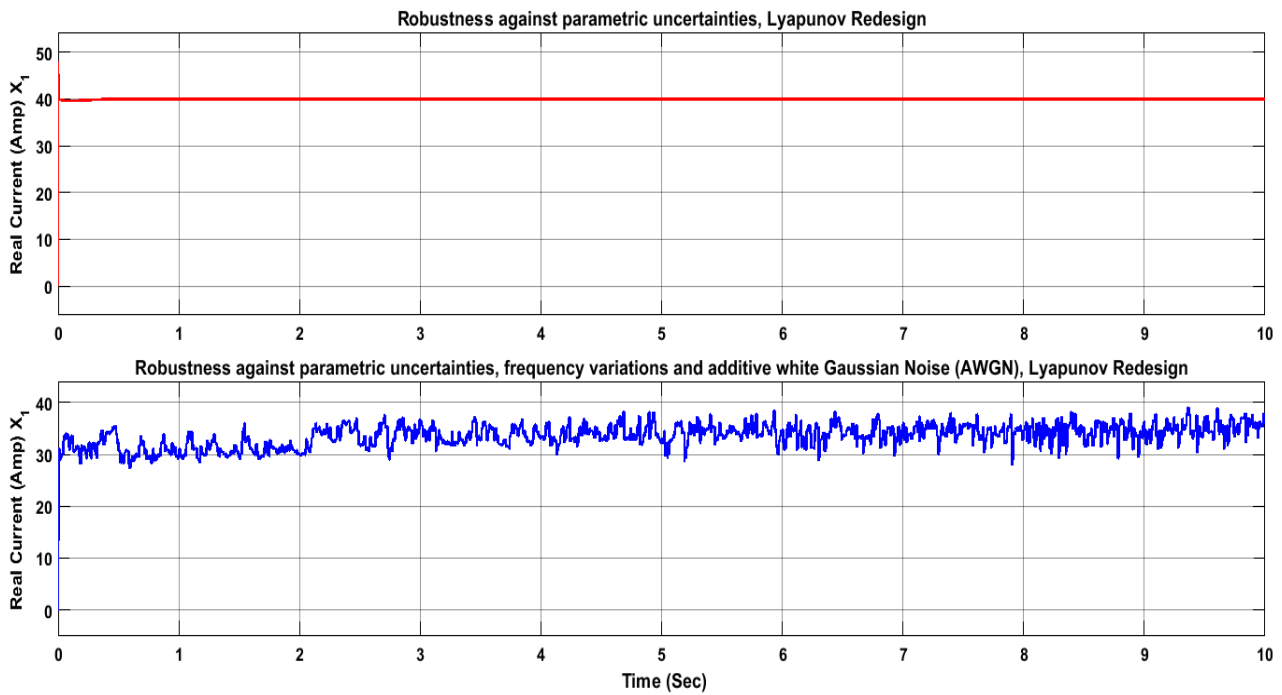


Figure 5:47: d-axis current comparisons between robustness analysis against parametric variation and robustness analysis against parametric uncertainties, frequency variation, and additive gaussian noise using Lyapunov redesign control technique based on boundary conditions.

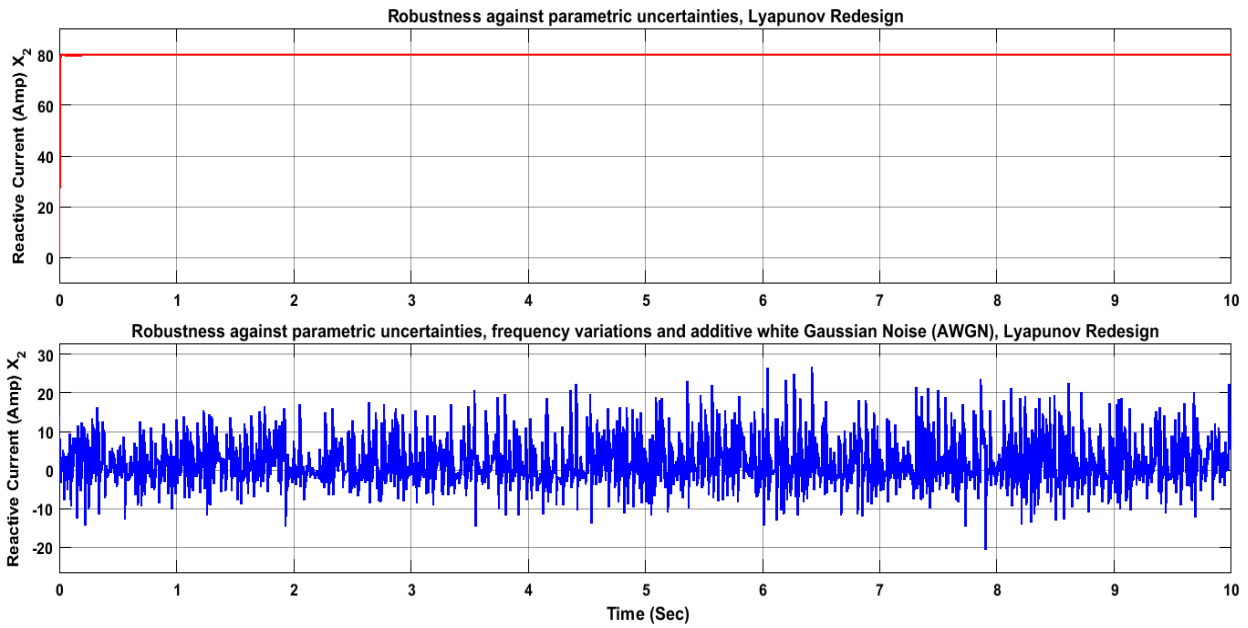


Figure 5:48: q-axis current comparisons between robustness analysis against parametric variation and robustness analysis against parametric uncertainties, frequency variation, and additive gaussian noise using Lyapunov redesign control technique based on boundary conditions.

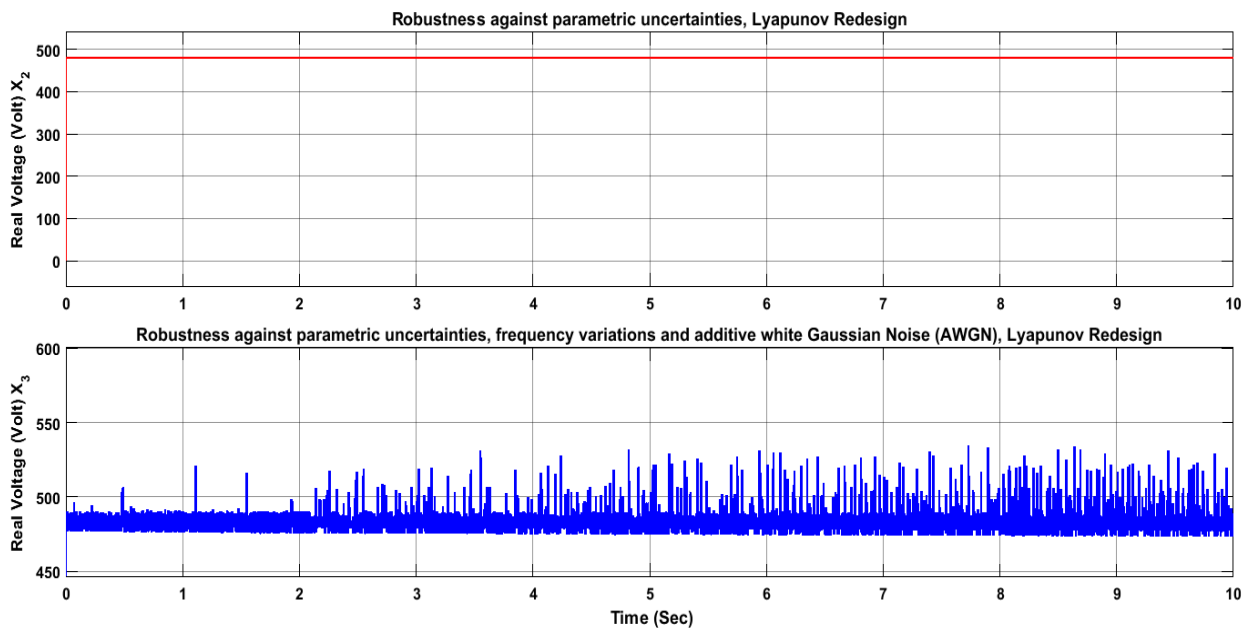


Figure 5:49: d-axis bus voltage comparisons between robustness analysis against parametric variation and robustness analysis against parametric uncertainties, frequency variation, and additive gaussian noise using Lyapunov redesign control technique based on boundary conditions.

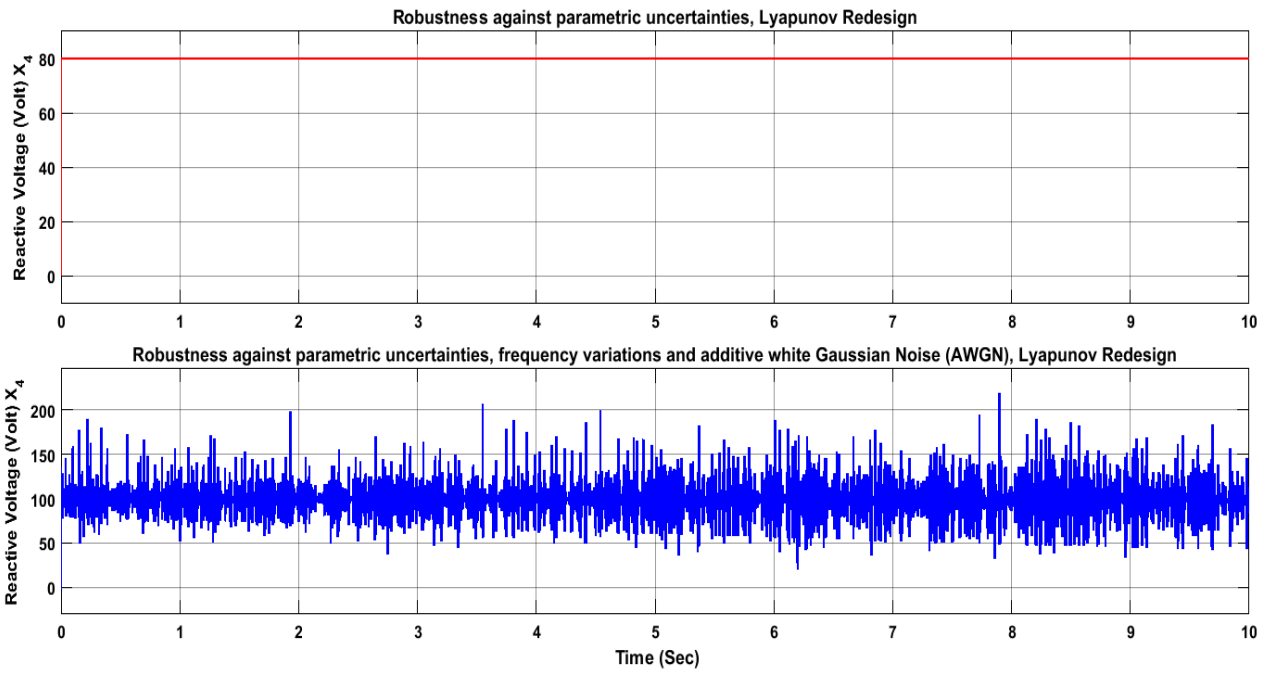


Figure 5:50: q-axis bus voltage comparisons between robustness analysis against parametric variation and robustness analysis against parametric uncertainties, frequency variation, and additive gaussian noise using Lyapunov redesign control technique based on boundary conditions.

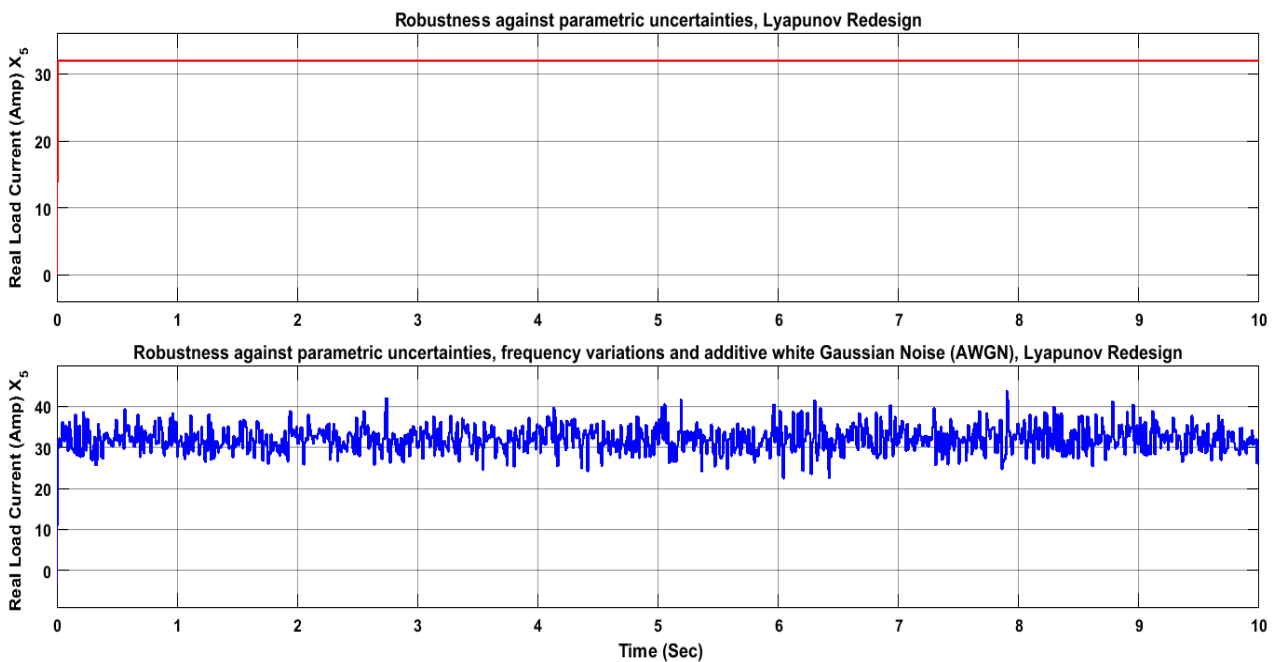


Figure 5:51: d-axis current (CVL load) comparisons between robustness analysis against parametric variation and robustness analysis against parametric uncertainties, frequency variation, and additive gaussian noise using Lyapunov redesign control technique based on boundary conditions.

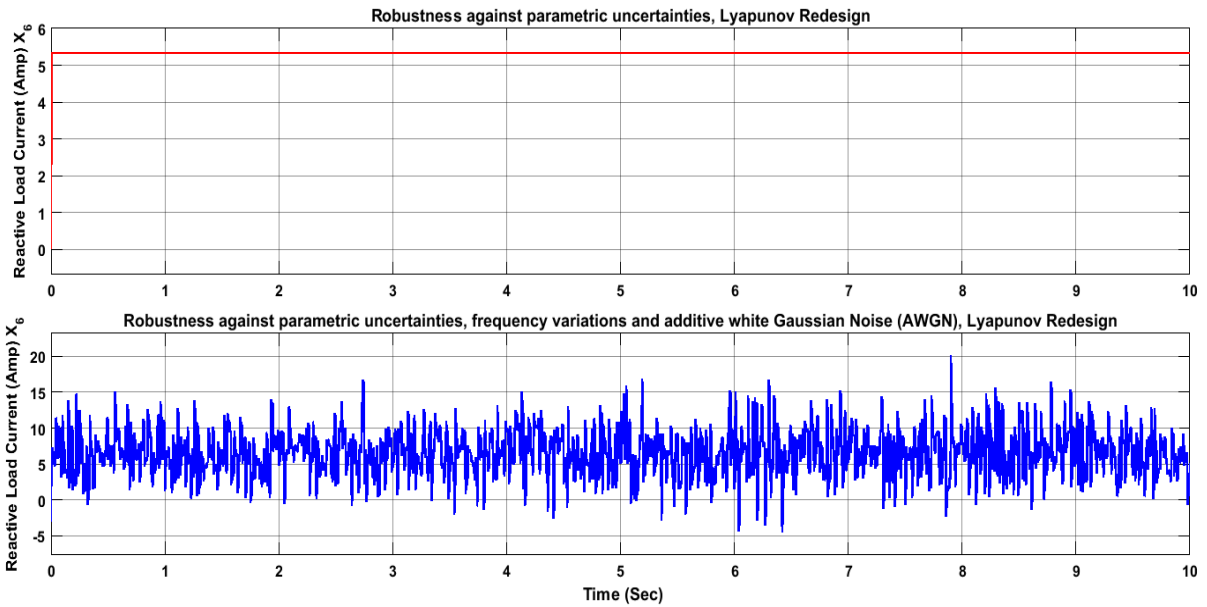


Figure 5:52: q-axis current (CVL load) comparisons between robustness analysis against parametric variation and robustness analysis against parametric uncertainties, frequency variation, and additive gaussian noise using Lyapunov redesign control technique based on boundary conditions.

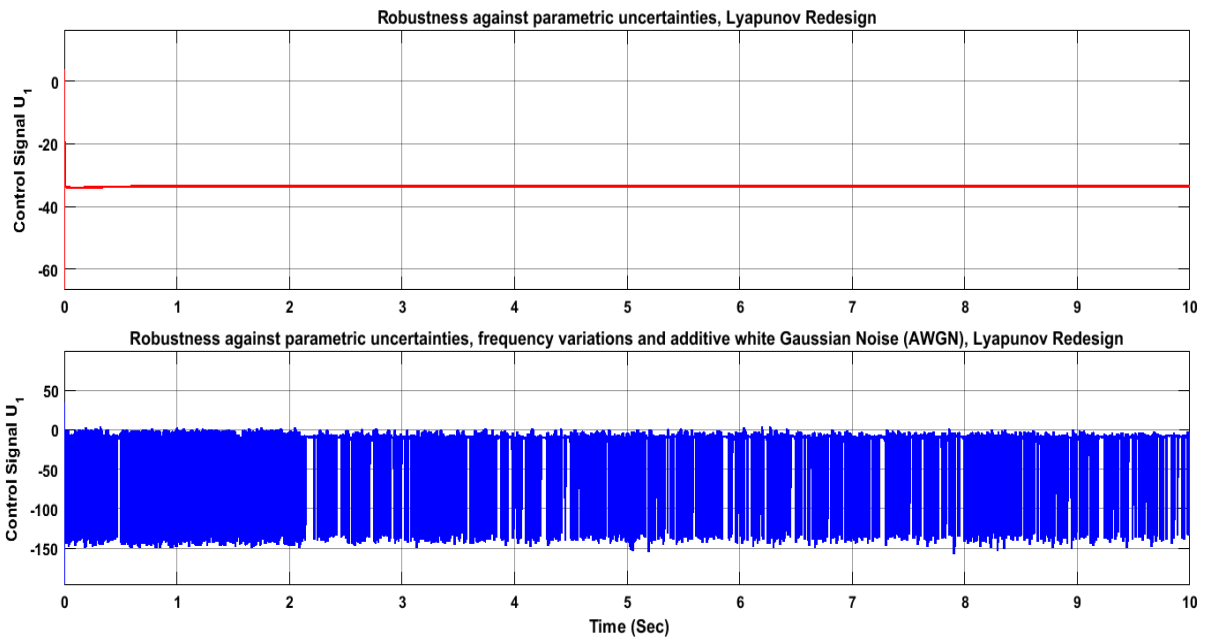


Figure 5:53: d-axis current compensation (d-axis control signal) comparisons between robustness analysis against parametric variation and robustness analysis against parametric uncertainties, frequency variation, and additive gaussian noise using Lyapunov redesign control technique based on boundary conditions.

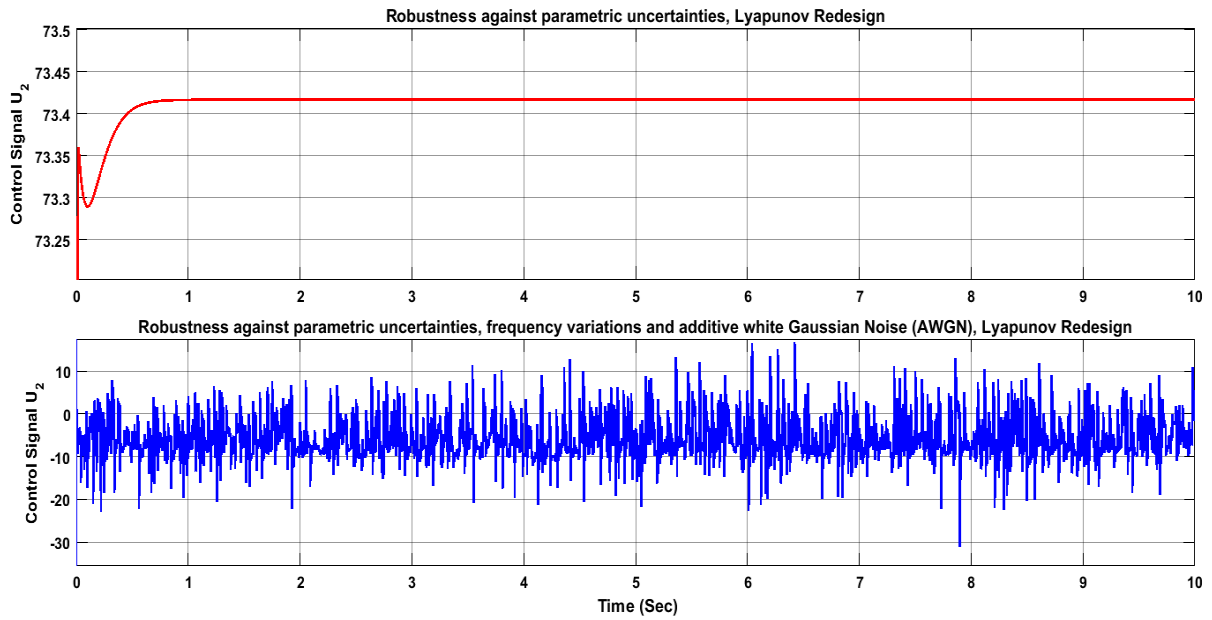


Figure 5:54: q-axis current compensation (q-axis control signal) comparisons between robustness analysis against parametric variation and robustness analysis against parametric uncertainties, frequency variation, and additive gaussian noise using Lyapunov redesign control technique based on boundary conditions.

## Comparative Analysis between SMC and LRC with CPL Power Variation

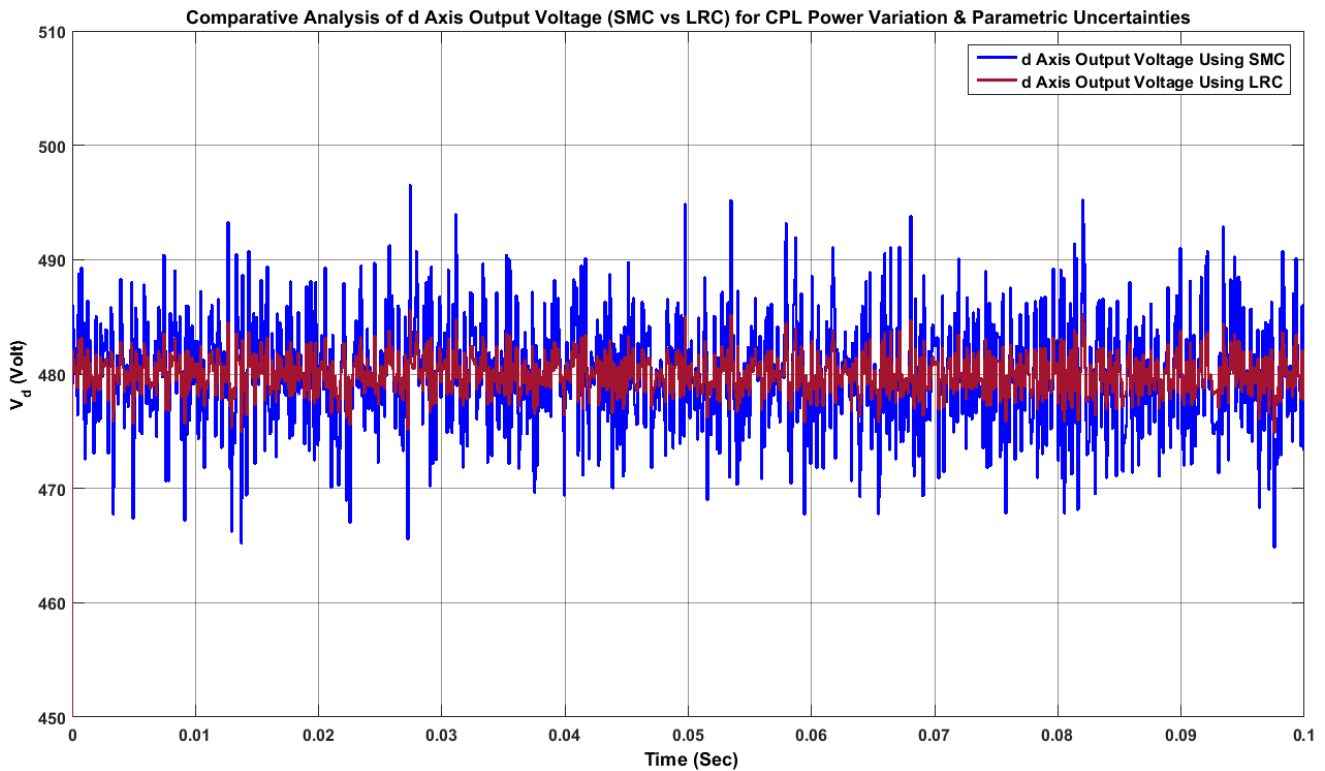
Here, the comparative performance analysis will be presented between SMC and LRC techniques that will justify why the Lyapunov Redesign Control technique shows better robustness than the previous one in microgrid applications with dense CPL-loaded conditions. The parameters and the parametric values regarding the comparative analysis varying the CPL power have been presented in table 5-2.

Table 5-2: Table of Parameters

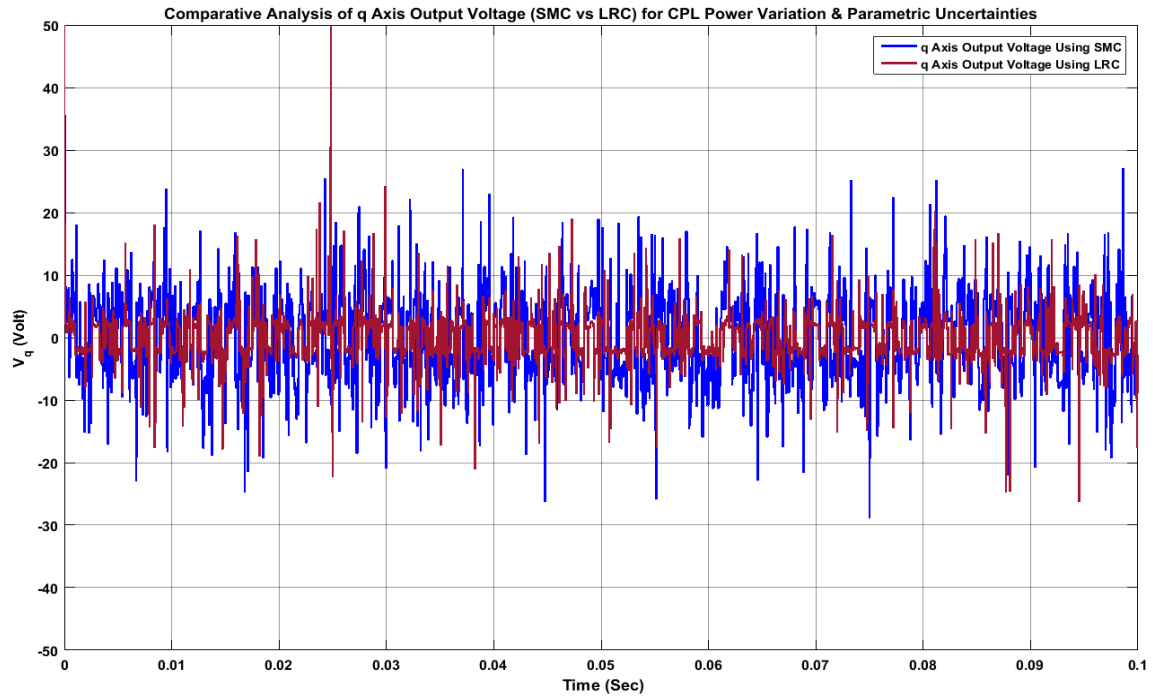
Parameter	Value	Parameter	Value
$\omega$	60 Hz	$\delta_{x4}$	100 V
$X_3$	600 V	$\delta_p$	30 kW
$X_4$	50 V	$\delta_Q$	2 kVar
$d_p$	50 A	$\rho_{x3}$	200V
$d_Q$	20 A	$\varepsilon$	100
$\delta_{x3}$	1000 A	$R_{eq}$	0.25 Ohm
$L_{eq}$	0.5e-3 H	$C_{eq}$	10e-6 F
$R_{CVL}$	15 Ohm	$L_{CVL}$	5e-3 H
$R_B$	10 Ohm	$C_B$	1e-6 F
$L_B$	1e-3 H		

In figure 5.55(a) and 5.55(b), performance comparisons have been illustrated between SMC (blue) and LRC (red) in case of d- axis output voltage and q- axis output voltage respectively considering CPL power variation and parametric uncertainties. For d-axis output voltage, the control objective has been considered 480 volt. From figure 5.55(a), it is evident that the LRC controller shows considerably better performance than that of the SMC controller and the output is retained as close as the control objective. In case of q-axis output voltage, the control objective has been considered as low as possible and negligible in practice. In figure 5.55(b), the q-axis output voltage fluctuates more in case of SMC

controller than that of LRC controller. Hence, the LRC offers appreciable stability considering the CPL power variation and parametric uncertainties. In figure 5.56(a) and 5.56(b), performance comparisons have been presented between SMC (blue) and LRC (red) in the case of d-axis control input current ( $U_1$ ) and q-axis control input current ( $U_2$ ) respectively considering CPL power variation and parametric uncertainties. Here, the more the fluctuation in control input current, the more the stress will be imposed on the storage system to compensate, consequently degrading the storage performance and overall life time. This situation, in practice, makes harder to retain microgrid stability. From figure 5.56(a) and 5.56(b), both real and reactive axis control input current have been experienced more fluctuation in the case of SMC controller, which hampers the system's stability. LRC controller shows relatively less fluctuation that ascertains desired stability. Therefore, from the comparative analysis presented here, Lyapunov Redesign controller shows better performance to retain system stability in face of CPL power variation. Hence, LRC controller is preferred to be adopted for storage based load side compensation technique to improve microgrid stability in the presence of dense CPL loads.

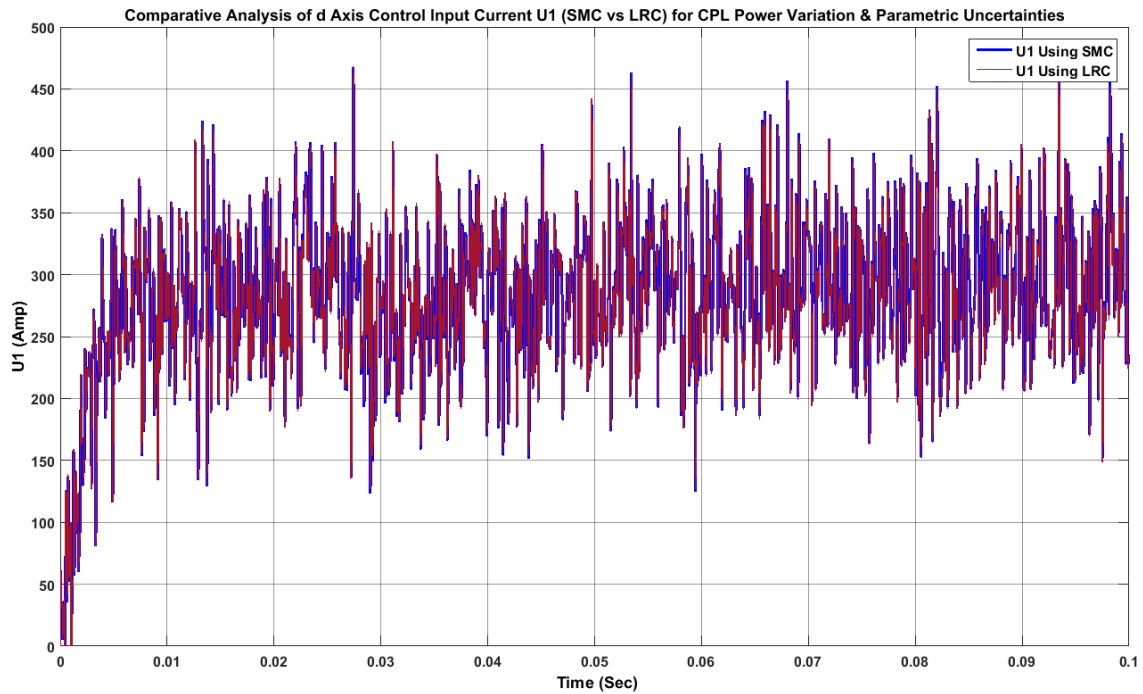


(a)

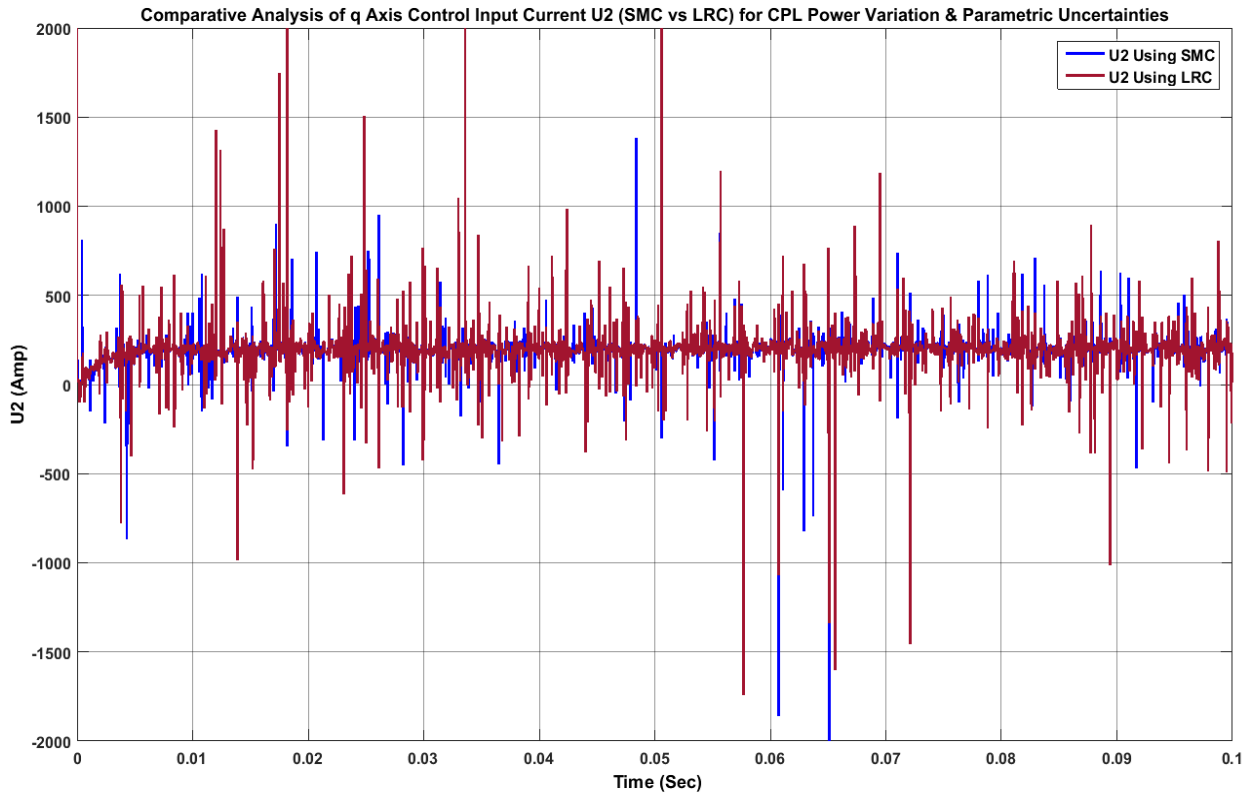


(b)

Figure 5:55: Performance comparison between the SMC (blue) and LRC (red) in the case of (a) d- axis output voltage, (b) q- axis output voltage considering CPL power variation and parametric uncertainties.



(a)



(b)

Figure 5:56: Performance comparison between the SMC (blue) and LRC (red) in the case of (a) d-axis control input current (U1), (b) q-axis control input current (U2) considering CPL power variation and parametric uncertainties

## 5.6 Conclusion

In a nutshell, this research demonstrates a comprehensive analysis on the impact due to instability by CPL loads and introduces a robust solution of active and passive damping based on virtual impedance. In particular, the loading limits of the constant power load and the constant voltage load connected in a parallel manner are attained to determine the desired stability of a regular AC microgrid in the case of islanding mode or grid connected mode applications. As has been experienced, because of negative incremental characteristics of CPL, the loading fluctuation is narrowed and it is challenging to control the system stability of the microgrid operation in the case of transient conditions such as CVL load shedding or CPL power rise. In practice, this suggested active damping technique extends the loading limit, hence,

stabilizes the entire system. Besides that, the corresponding transfer functions as well as the stability criteria are developed and analyzed with necessary illustrations. In latter segment of this chapter, the PID control technique is delineated to ensure the required stability. After that, to adopt the nonlinear control technique for robustness, the SMC and Lyapunov Redesign technique are introduced and described with proper illustrations. Next, a comprehensive robustness analysis is accomplished for instability several cases to justify the efficiency of the SMC and Lyapunov Redesign technique. After that, SMC and LRC controller robustness analysis are presented with the variation of CPL power. Next, the comparative analysis between the SMC controller and LRC controller robustness is illustrated which ascertains that Lyapunov Redesign controller performs better than the previous one to retain microgrid stability in dense CPL-loaded condition. To verify the performance of these approaches, the simulation results, using linear and nonlinear control techniques, demonstrated on virtual platform are presented in occasion of transient cases.

## **Chapter 6 : Extended Research**

### **6.1 Introduction**

The storage unit, a necessary tool to retain microgrid stability, assures the required power when it is needed by compensation technique. However, the storage system only comprised of battery units doesn't experience a sound functionality in microgrid arrangement in the case of highly variable distributed energy systems like renewable energy sources. In this particular case, by function, the storage unit is to provide high power density with quick charging/discharging time and the ultracapacitor/supercapacitor is to compensate the transient demand for a short period of time. In this chapter, the hybrid energy storage system (HESS), with a battery unit as well as an ultracapacitor unit, has been introduced to reduce the deficiency in the case of using either battery-only or ultracapacitor-only storage systems and offer the combined features with higher energy and higher power density.

### **6.2 Ultracapacitor as Energy Compensation Element**

#### **6.2.1 What is Ultracapacitor?**

EDLCs (elaborated as Electrochemical Double Layer Capacitors), commonly familiar as ultracapacitors, are electrochemical capacitors which possess exceptionally high energy power density feature compared to the conventional capacitors [122] which offer the required surges of power even when the battery is functioning in the system, thus, improving microgrid's performance [71].

### 6.2.2 Ultracapacitor vs Battery Performance

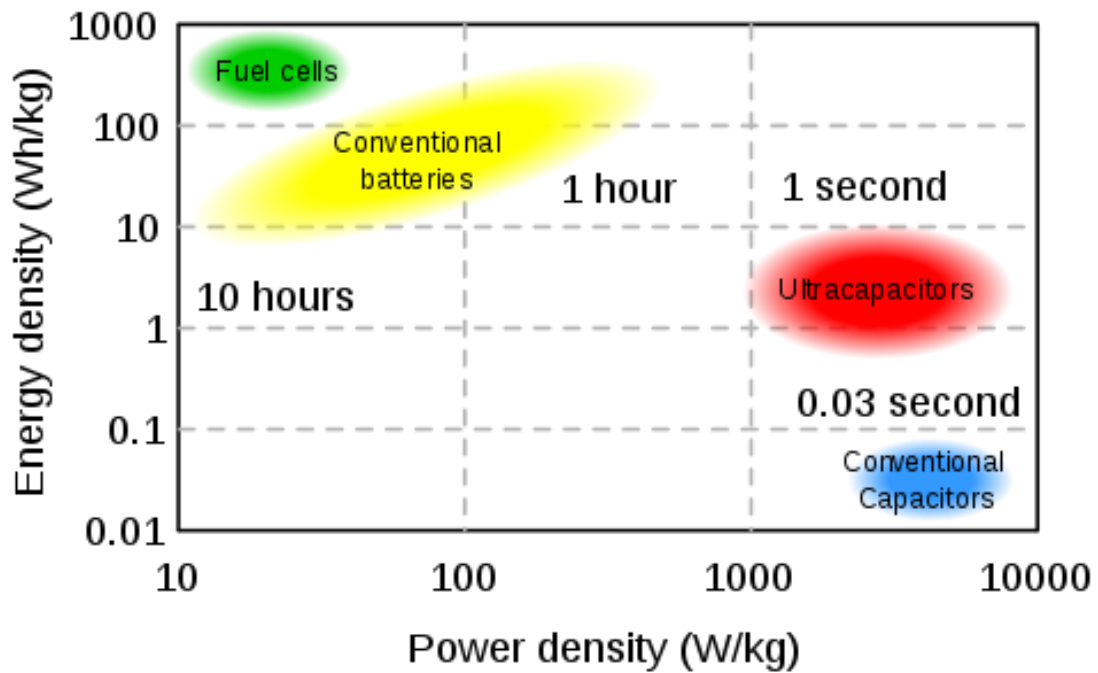


Figure 6:1: Comparisons of various electrochemical storage devices in energy density, power density and charging time [106].

From figure 6.1, it can be interpreted that the ultracapacitors range in between the conventional batteries and the conventional capacitors in terms of energy density and power density. Hence, they are usually installed for the applications where batteries have a shortfall when transient high power is required. Moreover, to handle the situation of transient high power requirement, conventional capacitors cannot be used because they lack expected energy. On the other hand, an ultracapacitor offers a high power density along with adequate energy density for the most transient high power applications [122]. From the view of purpose and application, ultracapacitors are with the batteries considering the necessary storage parameters compared in the chart below: Table 6-1.

### 6.3 Conventional Energy Storage System for Microgrid Applications

Since CPLs have negatively incremental load characteristics, CPL-loaded microgrids experience transient spikes or sudden peaks in bus voltage response. In practice, though CVL power range is of KW or MW and CPL power is of 533 W, the transient peaks created by CPL loads are significantly higher than those of the previous one (as observed in figure 6.13). For instance, microgrid bus voltage is illustrated in figure 6.2 without any compensation (in the presence of CPL). To handle this issue, an energy storage system is used in microgrid applications. Here, in this chapter, two kinds of conventional energy storage systems are delineated in the case of microgrid applications. First, the battery-only compensator is presented here with the regarding simulation platform and performance graphs in several cases. Similarly, the ultracapacitor-only compensator is described here with necessary detail for microgrid applications. Furthermore, the advantages and limitations of each storage system will be described.

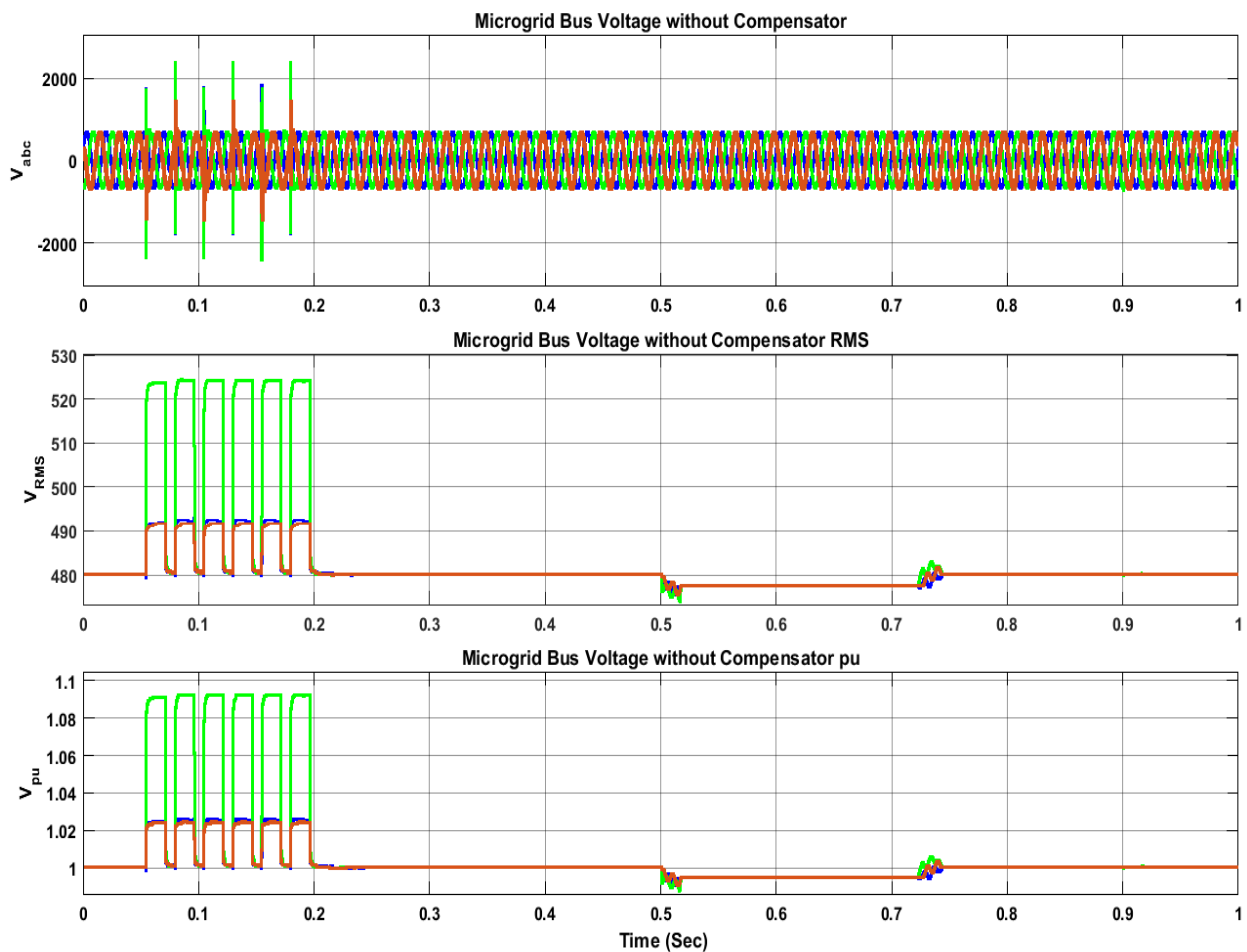


Figure 6:2: Microgrid bus voltage without any compensation (in the presence of CPL).

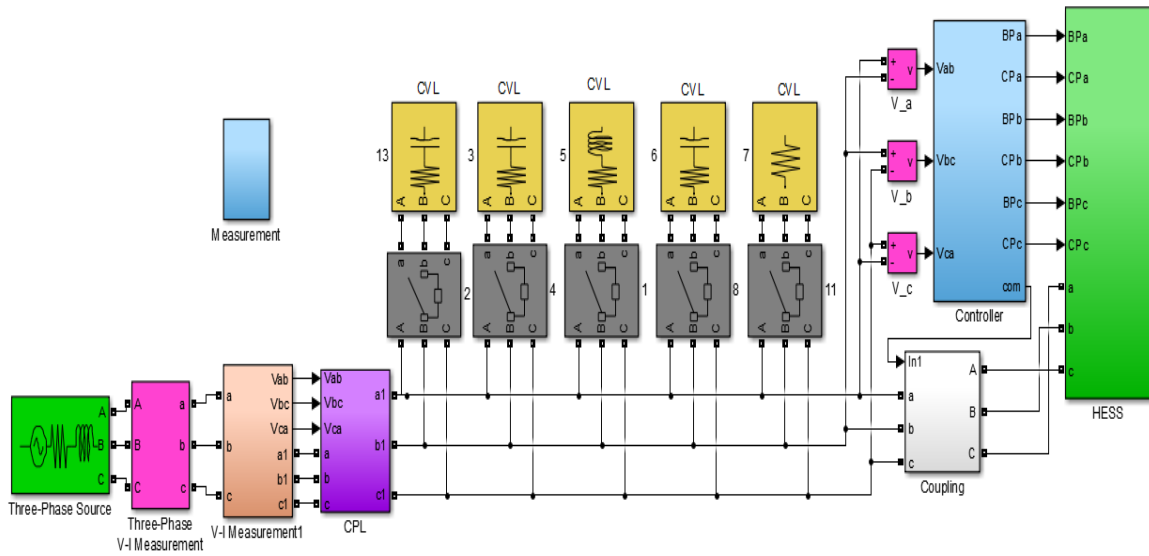


Figure 6:3: Simulation platform for entire microgrid system using compensator unit in Matlab/Simulink.

Table 6-1: Battery vs Ultracapacitor Parameters [82].

Parameters	Ultracapacitors	Batteries
Energy Storage	W-s of Energy	W-Hr of Energies
Charge Methods	Voltage across terminals i.e. from a battery	Current and Voltage
Power Delivered	Rapid discharge linear or exponential voltage decay	Constant voltage over long time period
Charge/Discharge Time	ms to s	1 to 10 Hrs
Form Factor	Small	Large
Weight	1-2g	1g to > 10kg
Energy Density	1 to 5 Wh/kg	8 to 600 Wh/kg
Power Density	High, > 4000W/kg	Low, 100 to 3000W/kg
Operating Voltage	2.3V to 2.75V/Cell	1.2V to 4.2V/Cell
Lifetime	>100k cycles	150 to 1500 cycles
Operating Temperature	-40 to +85 °C	-20 to +65 °C

### 6.3.1 Battery-Only Compensator

When microgrid voltage tends to fluctuate from the stable voltage range, a battery delivers the required compensation to stabilize the microgrid voltage. In figure 6.3, a simulation platform is presented for the entire microgrid system using a compensator unit (here, battery as compensator unit) in Matlab/Simulink. In figure 6.6(a), the representation of the battery power support and the power demand for a certain period of time is illustrated to comprehend the practical scenario. In the next figure, at 6.6(b), the power demand and the respective power support by the battery-only compensator in transient cases are illustrated. To illustrate the characteristic of battery-only compensator, the instance of battery terminal voltage, current, SOC, and power are presented in figure 6.4 (in the presence of CPL). In figure 6.18, the comparative analysis and the terminal voltage responses are presented in the case of the battery only compensator.

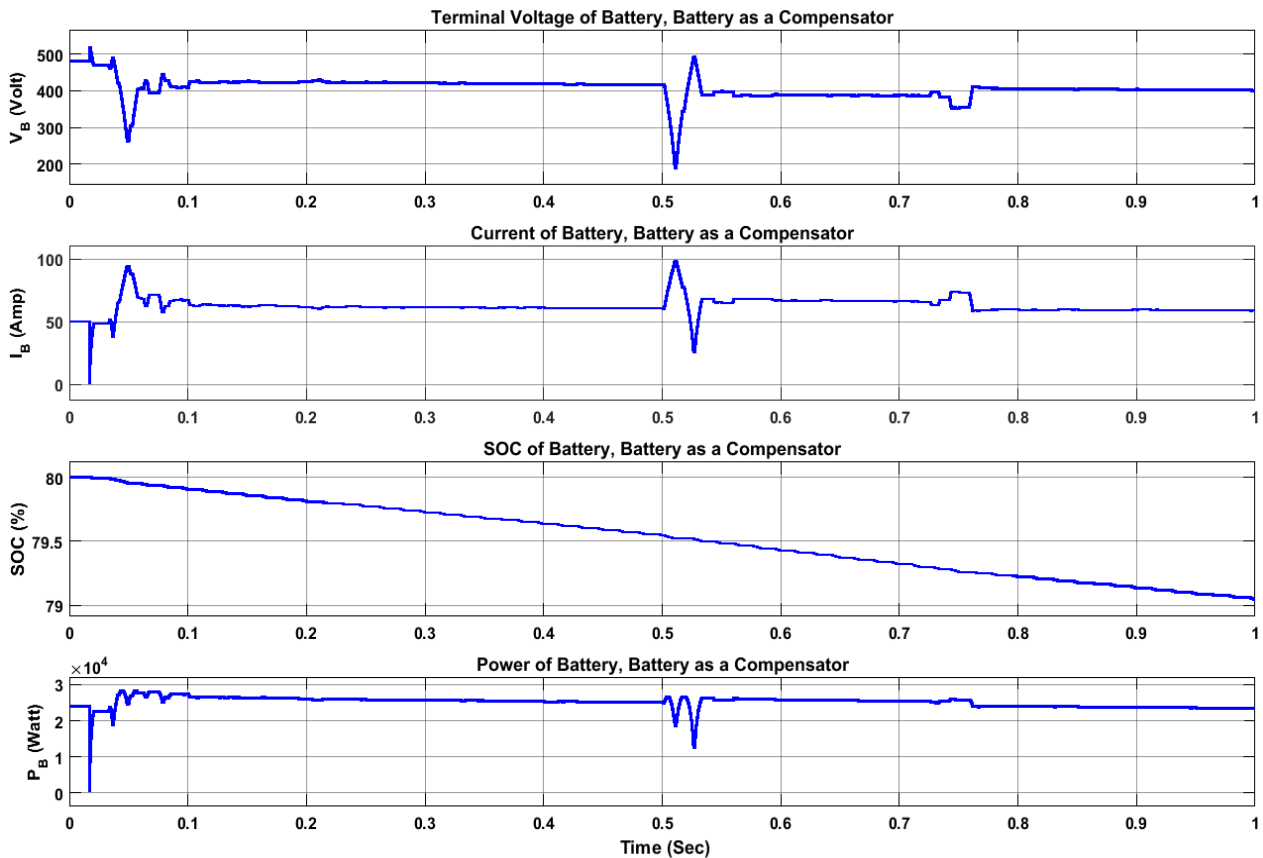


Figure 6:4: The characteristics of the battery terminal voltage, current, SOC, and power (in the presence of CPL) when battery-only is used as compensator.

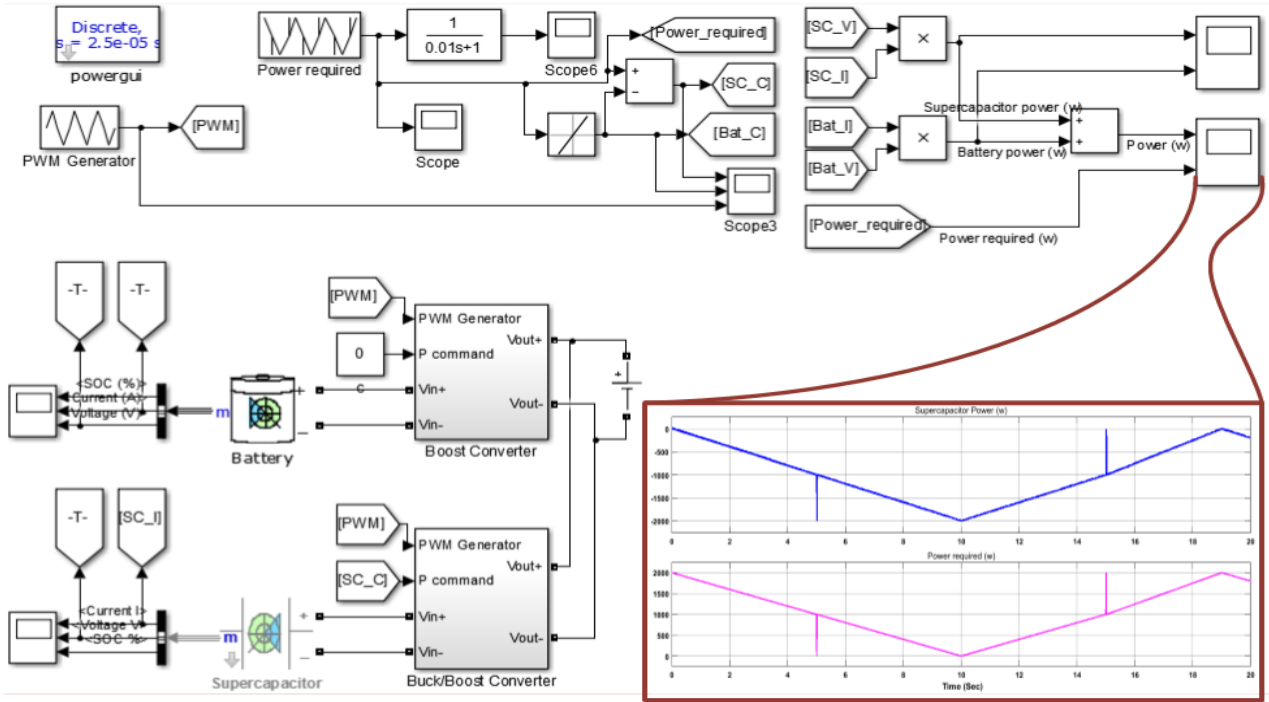
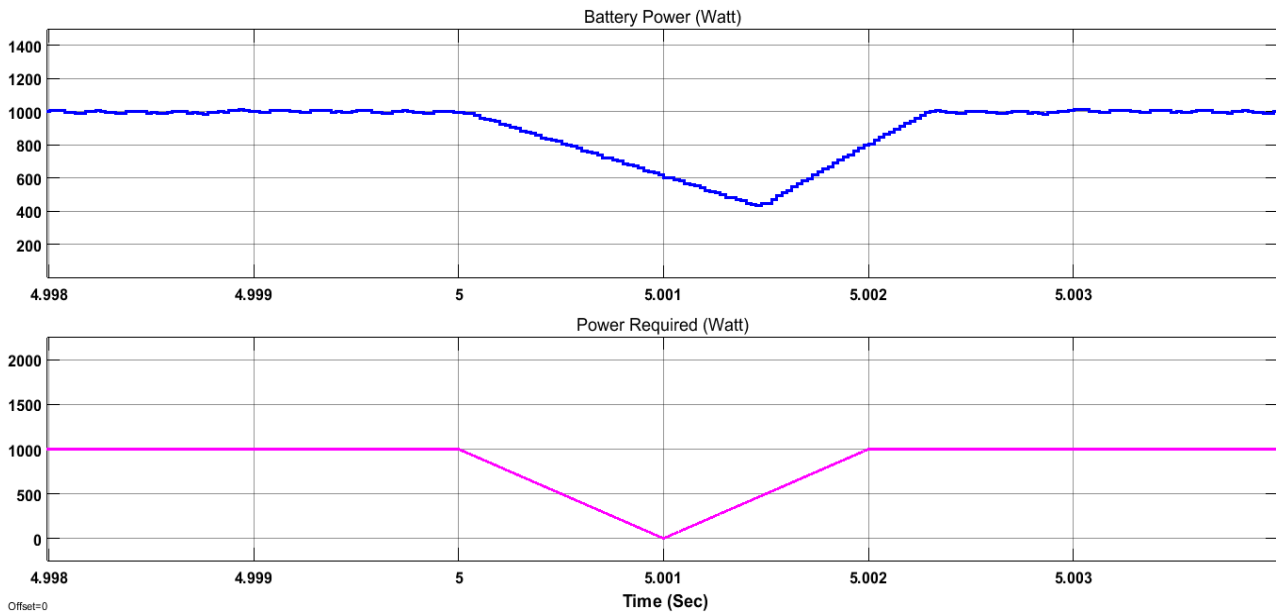
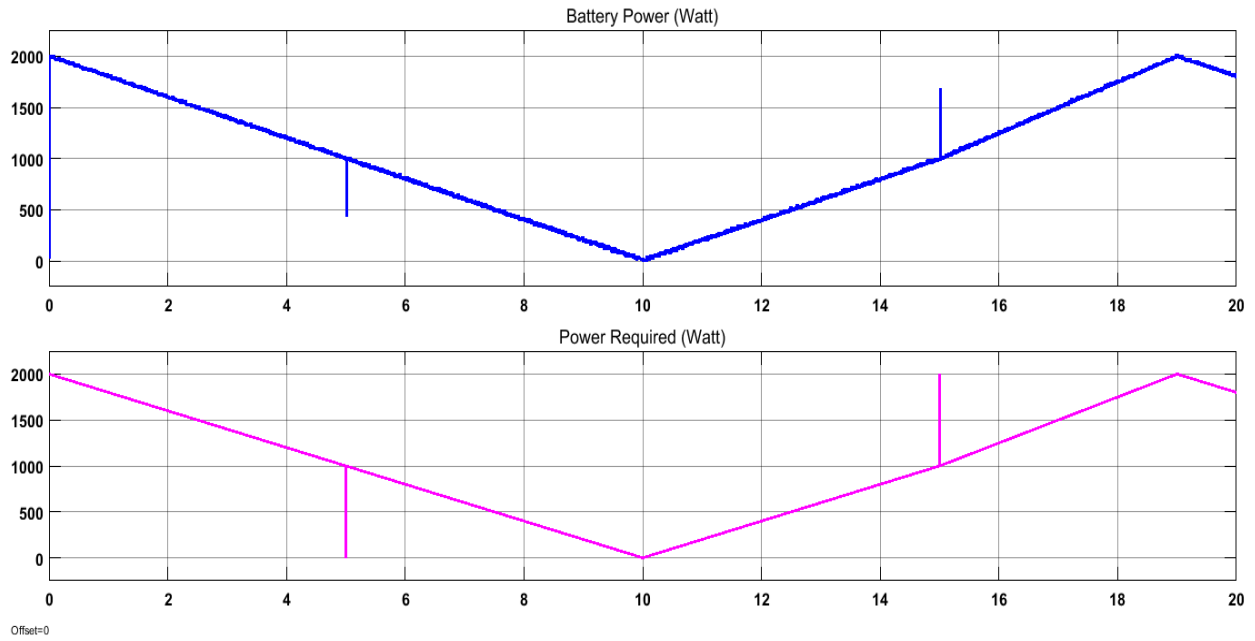


Figure 6:5: The simulation platform for performance comparisons between battery-only compensator and ultracapacitor-only compensator.



(a)



(b)

Figure 6:6: (a) Representation of the battery power support and the power demand, (b) representation of the transient power demand and respective battery support.

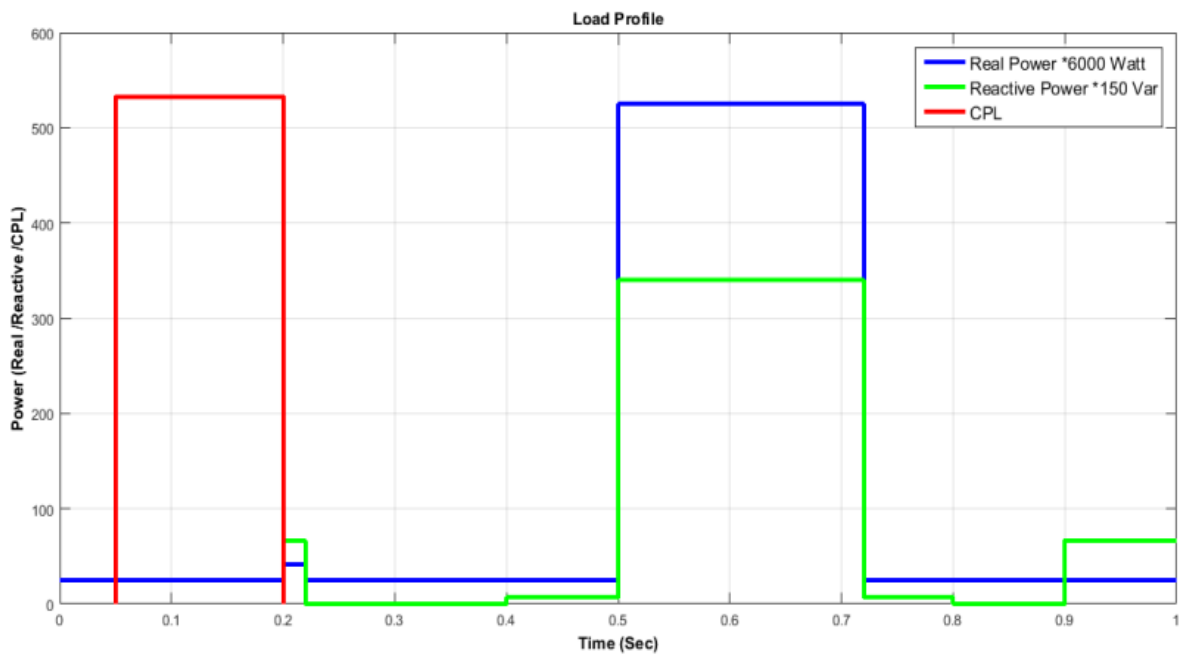


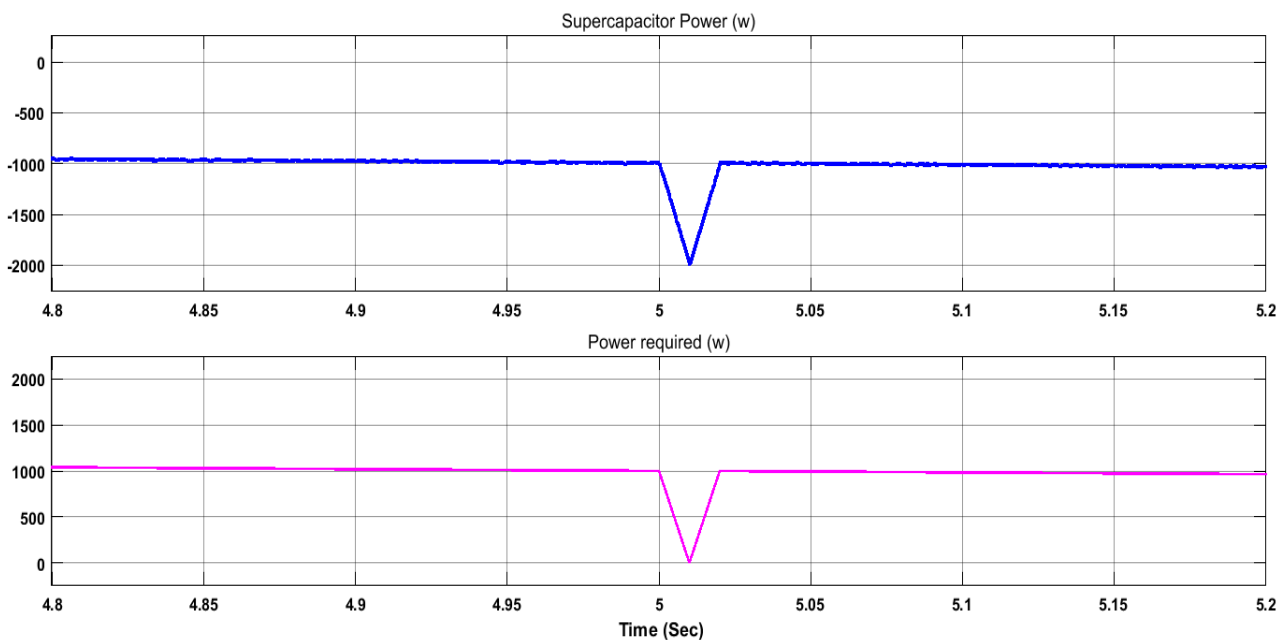
Figure 6:7: Load profile of CPL-loaded microgrid system.

As is evident from the above graphical representations, the battery-only compensator can supply the nominal power efficiently for a longer period without charging-discharging backward and forward, but, in

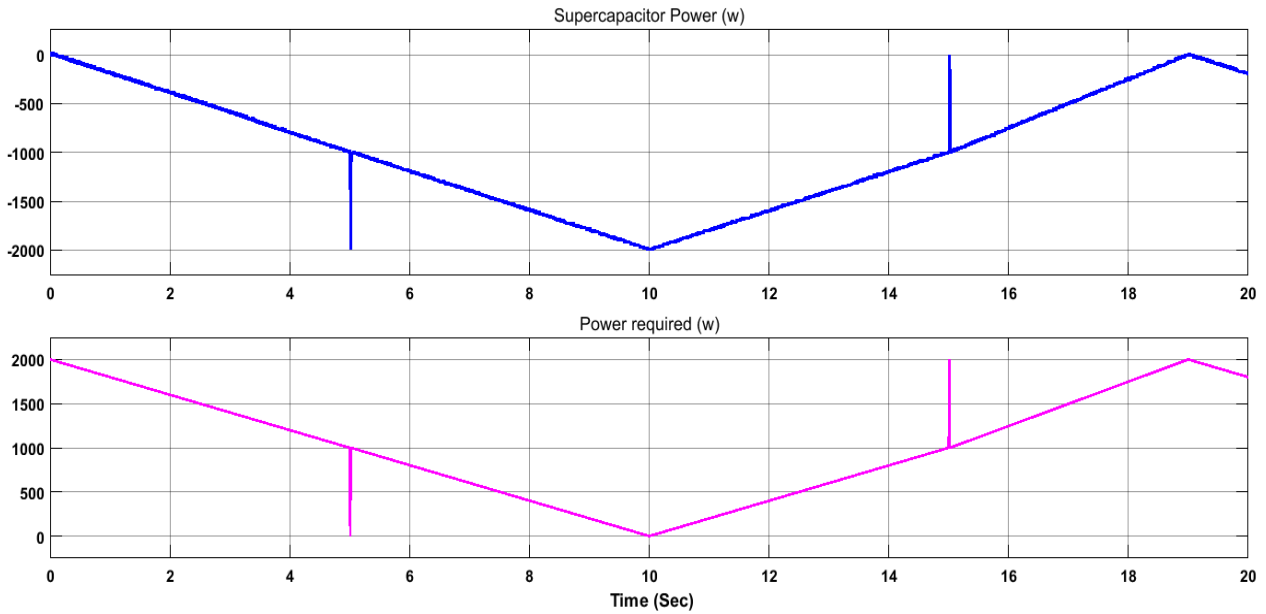
another occasion, it's ineffective when it comes to feeding transient demand. Due to the large response time and low power density, a battery needs longer time to retain stability. As can be seen from figure 6.6, to retain microgrid stability, the transient spikes must be handled effectively. Hence, ultracapacitor-only compensator is used as compensator unit to mitigate microgrid instability. The load profile of the microgrid system is presented in figure 6.7 in the presence of CPL loads.

### 6.3.2 Ultracapacitor-Only Compensator

When microgrid voltage tends to fluctuate from the stable voltage range, an ultracapacitor delivers the required compensation to stabilize the microgrid voltage. In figure 6.3, simulation platform is presented for the entire microgrid system using compensator unit (here, ultracapacitor as compensator unit) in Matlab/Simulink.



(a)



(b)

Figure 6:8: (a) Representation of the ultracapacitor power support and power demand, (b) representation of the transient power demand and respective ultracapacitor support.

In figure 6.8(a), the representations of the ultracapacitor power support and the power demand for a certain period of time are illustrated to comprehend the practical scenario. In figure 6.8(b), the power demand and the respective power support by the ultracapacitor-only compensator in transient cases are illustrated. To illustrate the characteristics of the ultracapacitor-only compensator, the instance of ultracapacitor terminal voltage, current, SOC, and power are presented in figure 6.9 (in the presence of CPL). In figure 6.18, in the comparative analysis, the terminal voltage response is presented in case of the ultracapacitor-only compensator. Due to the higher power density and fast response time, the ultracapacitor can stabilize the switching overshoot within 0.02 sec and the grid voltage remains within stable zone of 0.95 to 1.05 per unit, which is standard stable zone of microgrid and the performance is much better than that of the battery-only compensator. The ultracapacitor-only compensator exhibits poor energy density but high discharging rate; therefore this compensation technique needs to charge up frequently. On the other hand, in the case of transient load fluctuation, the ultracapacitor-only compensator represents excellent performance. After the handling the transient demand, it goes to charging mode again. Hence, a hybrid energy storage system comprised of both the battery unit and the

ultracapacitor unit is proposed as compensator to retain the microgrid stability, to handle CPL transients effectively, and provide uninterrupted nominal support.

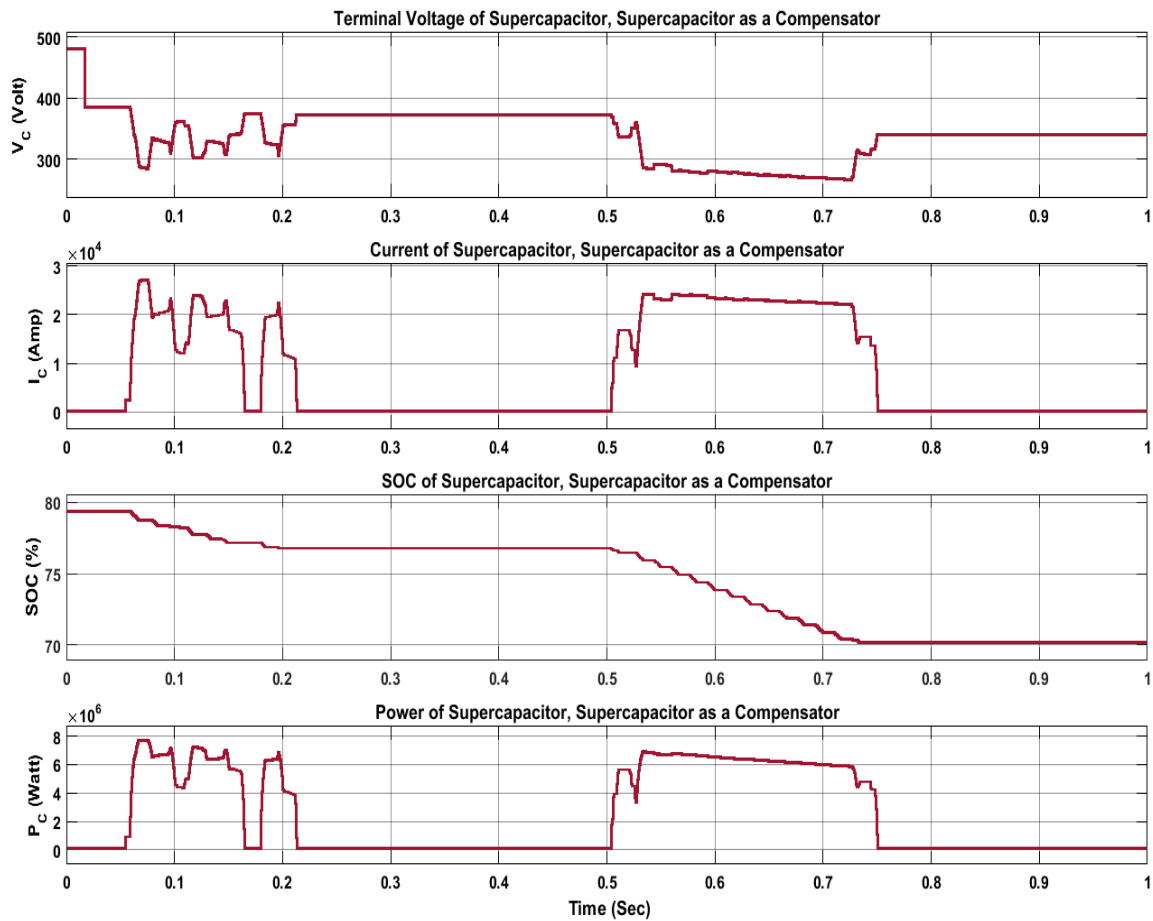


Figure 6:9: Characteristics of the ultracapacitor terminal voltage, current, SOC, and power (in the presence of CPL) when ultracapacitor-only is used as compensator.

## 6.4 Proposed Hybrid Energy Storage for Microgrid

To take the advantage of the highest energy density for an electrochemical battery and the highest power density for an ultracapacitor (according to figure 6.1 and Table 6.1), a hybrid energy storage system is proposed in this segment. A comprehensive energy management control algorithm is presented in figure 6.12 to retain the microgrid stability and to handle CPL transients effectively. The main advantages of a Hybrid Energy Storage System are

- Cutback of overall costs considered to a single storage system (because of decoupling the regarding energy and power, and battery, alone, has to manage the nominal power support)
- Increase of entire system performance
- Increase the storage lifetime (lessen the dynamic stress as well as ensure optimized operation)

The combination of battery and ultracapacitor units is selected as a hybrid energy storage system unit for microgrid applications (as illustrated in figure 6.10) with a flexible and smart energy management control algorithm. Figure 6.11 represents the basic structure of Hybrid Energy Storage System for microgrids.

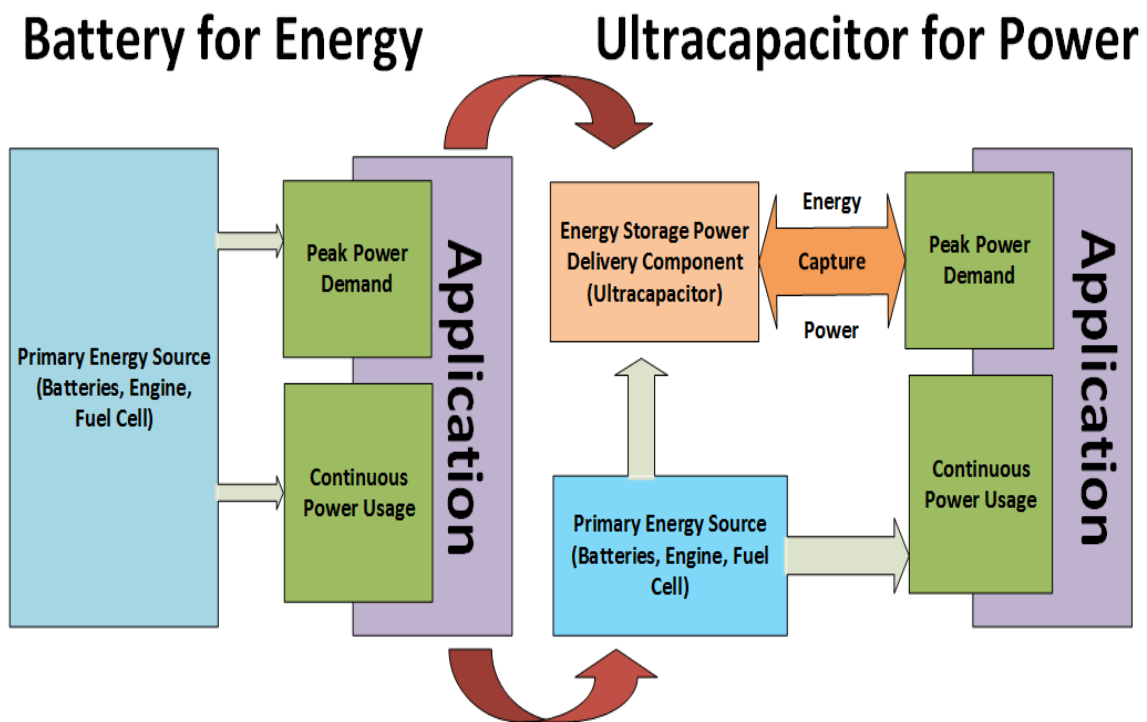


Figure 6:10: Hybrid energy storage system for microgrid [73].

The battery will initiate compensation according to the algorithm when terminal voltage remains within 0.99 and 1.01 pu. If the voltage tends to fluctuate from this zone (either upper or lower), the ultracapacitor will initiate compensation. To illustrate the characteristic of HESS compensator, the instances of HESS terminal voltage, current, SOC, and power are presented in figure 6.17 (in the presence of CPL). Microgrid overall current, frequency, and power are represented in figure 6.14, 6.15 and 6.16 respectively for a clear perspective.

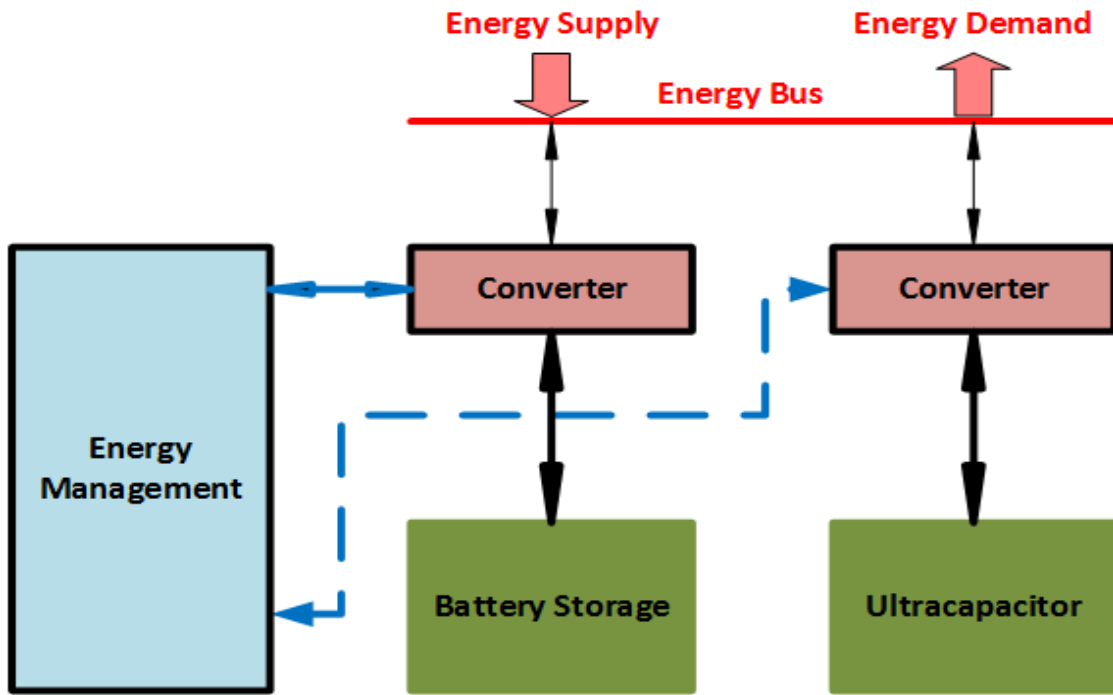


Figure 6:11: Basic structure of hybrid energy storage system.

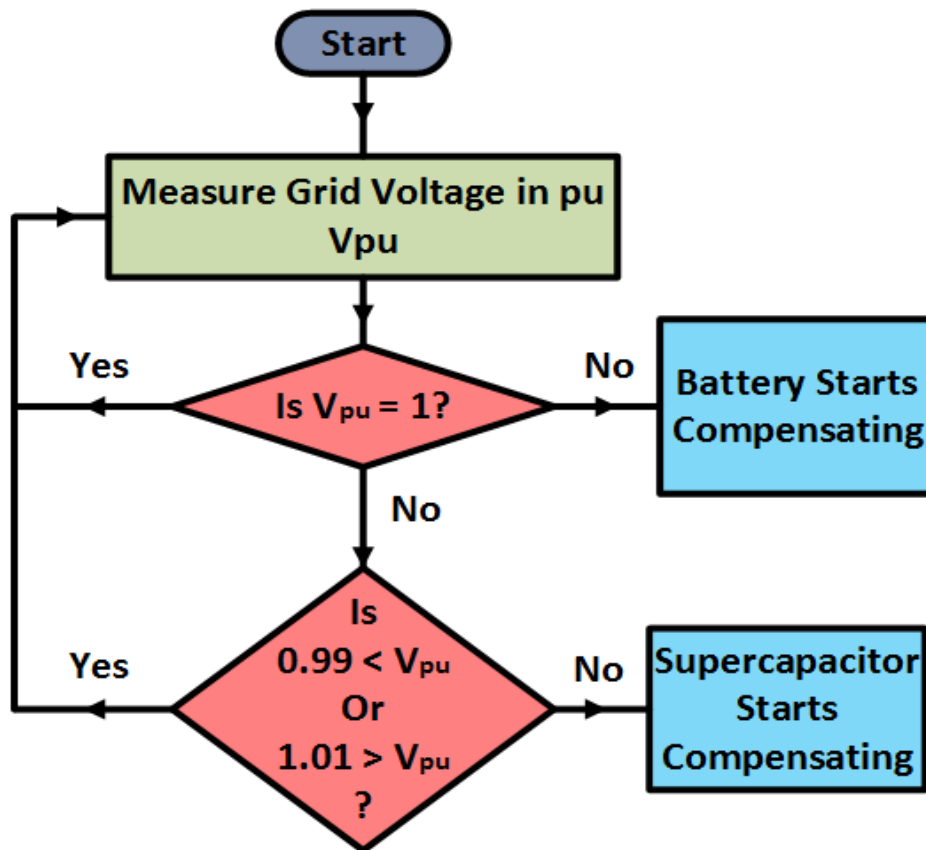


Figure 6:12: Energy management algorithm form hybrid energy storage system (in the presence of CPL).

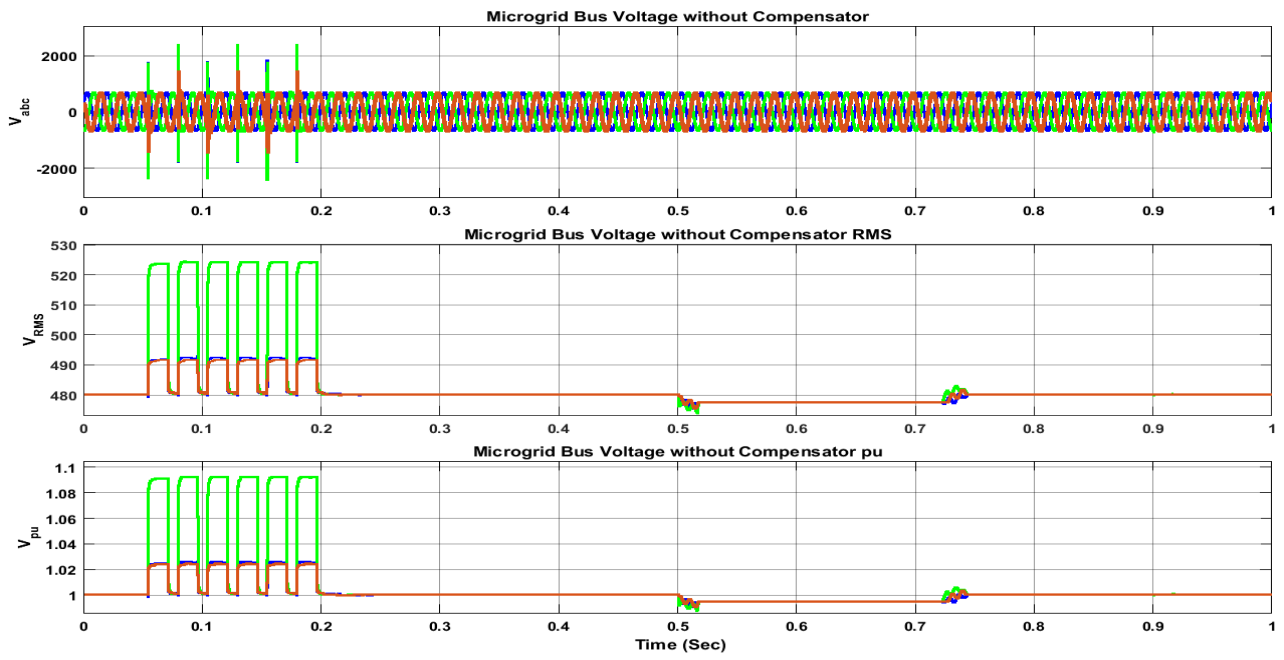


Figure 6:13: Microgrid bus voltage (in the presence of hybrid energy CPL) when storage system is used as compensator.

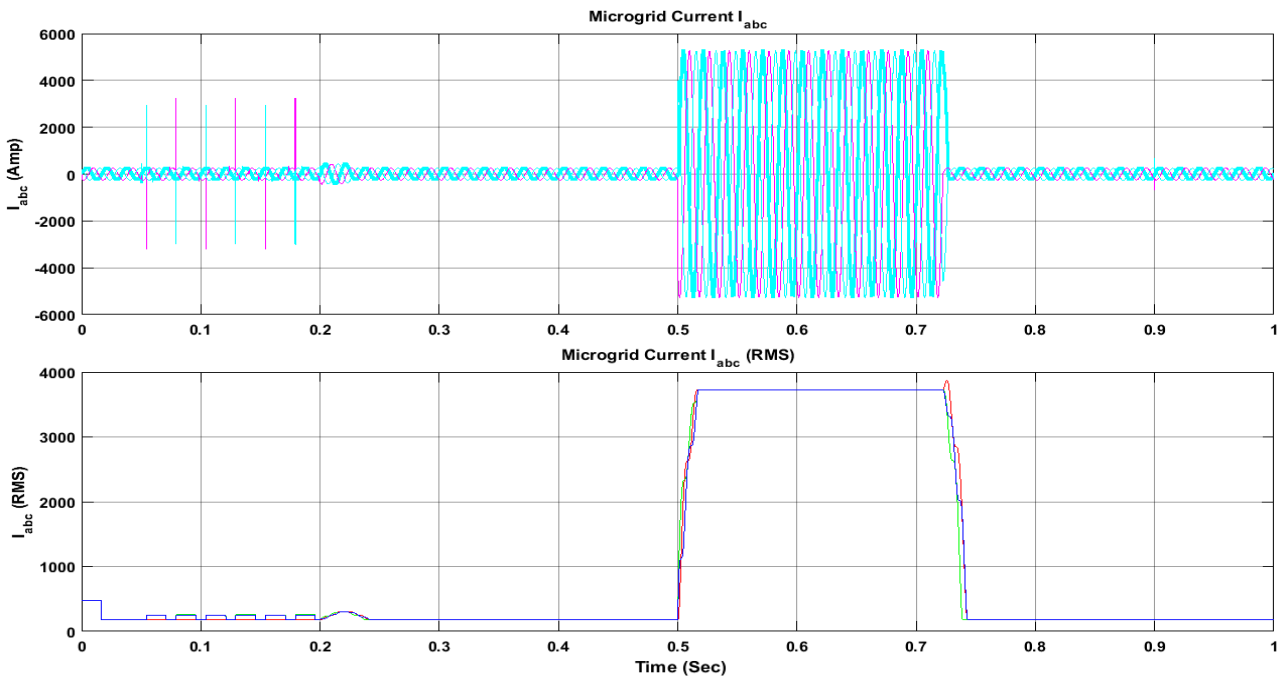


Figure 6:14: Microgrid current (in the presence of CPL) when hybrid energy storage system is used as compensator.

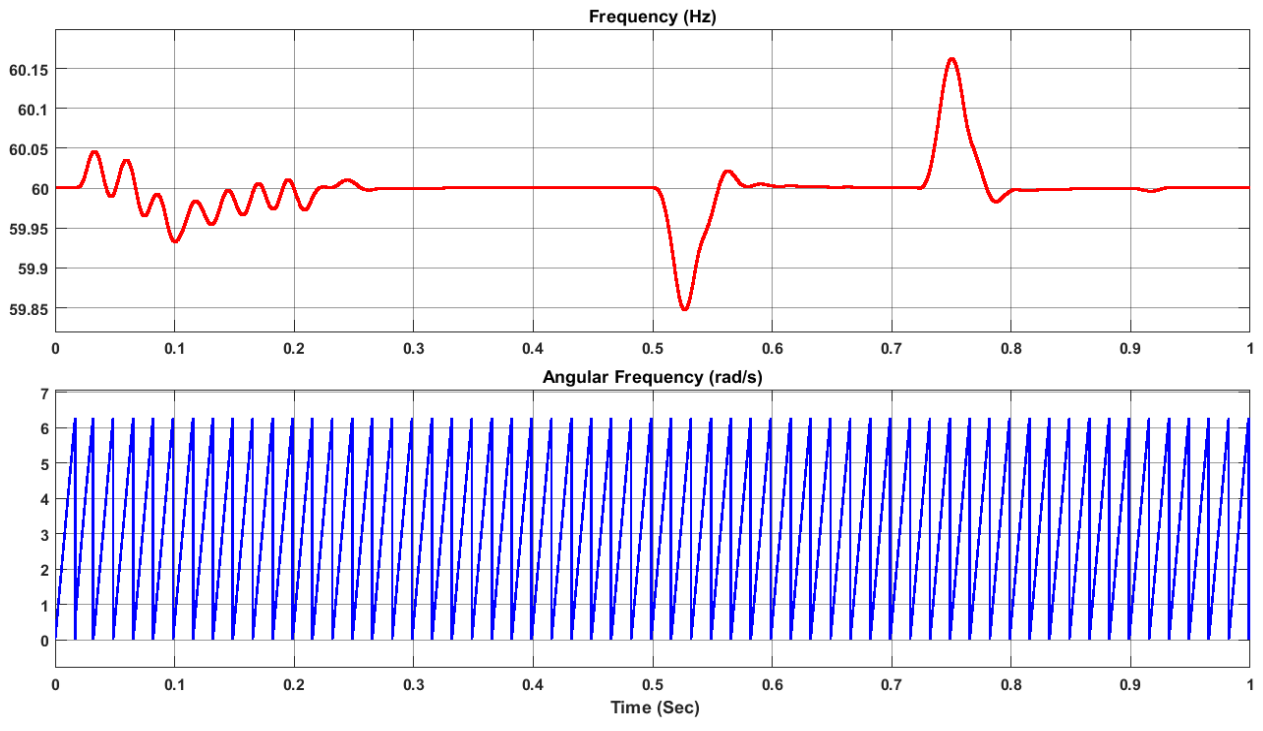


Figure 6:15: Microgrid frequency (in the presence of CPL) when hybrid energy storage system is used as compensator.

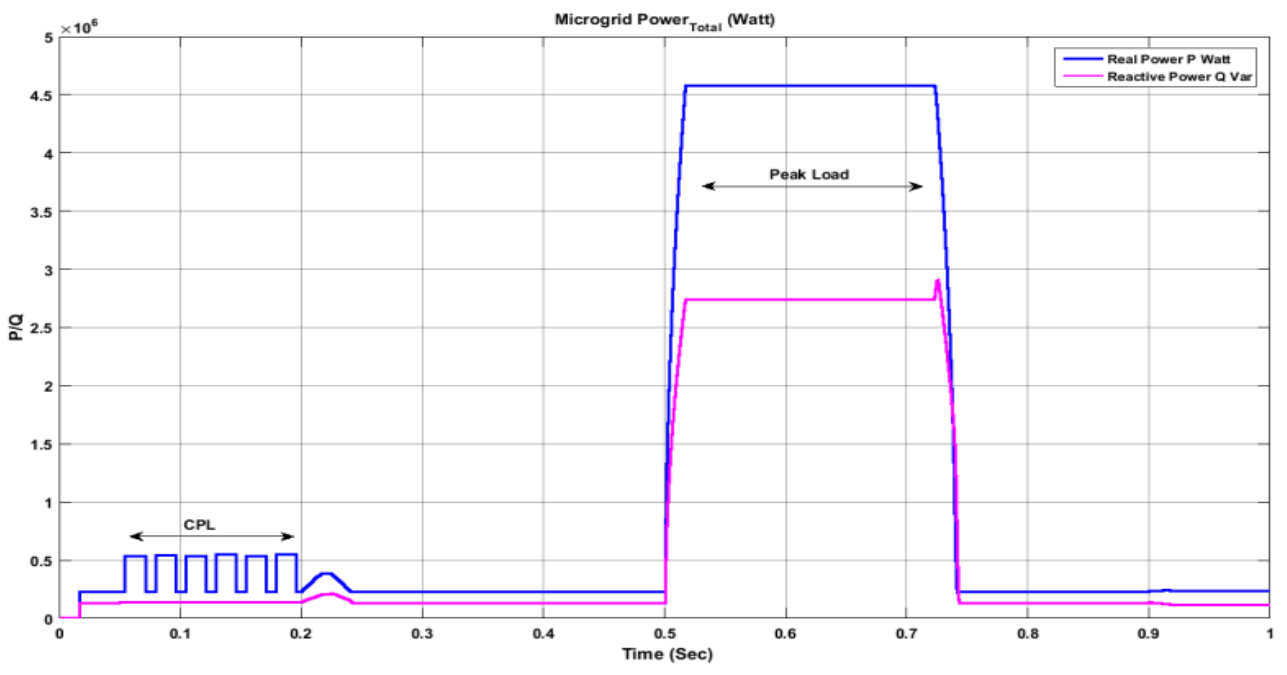


Figure 6:16: Microgrid power (in the presence of CPL) when hybrid energy storage system is used as compensator.

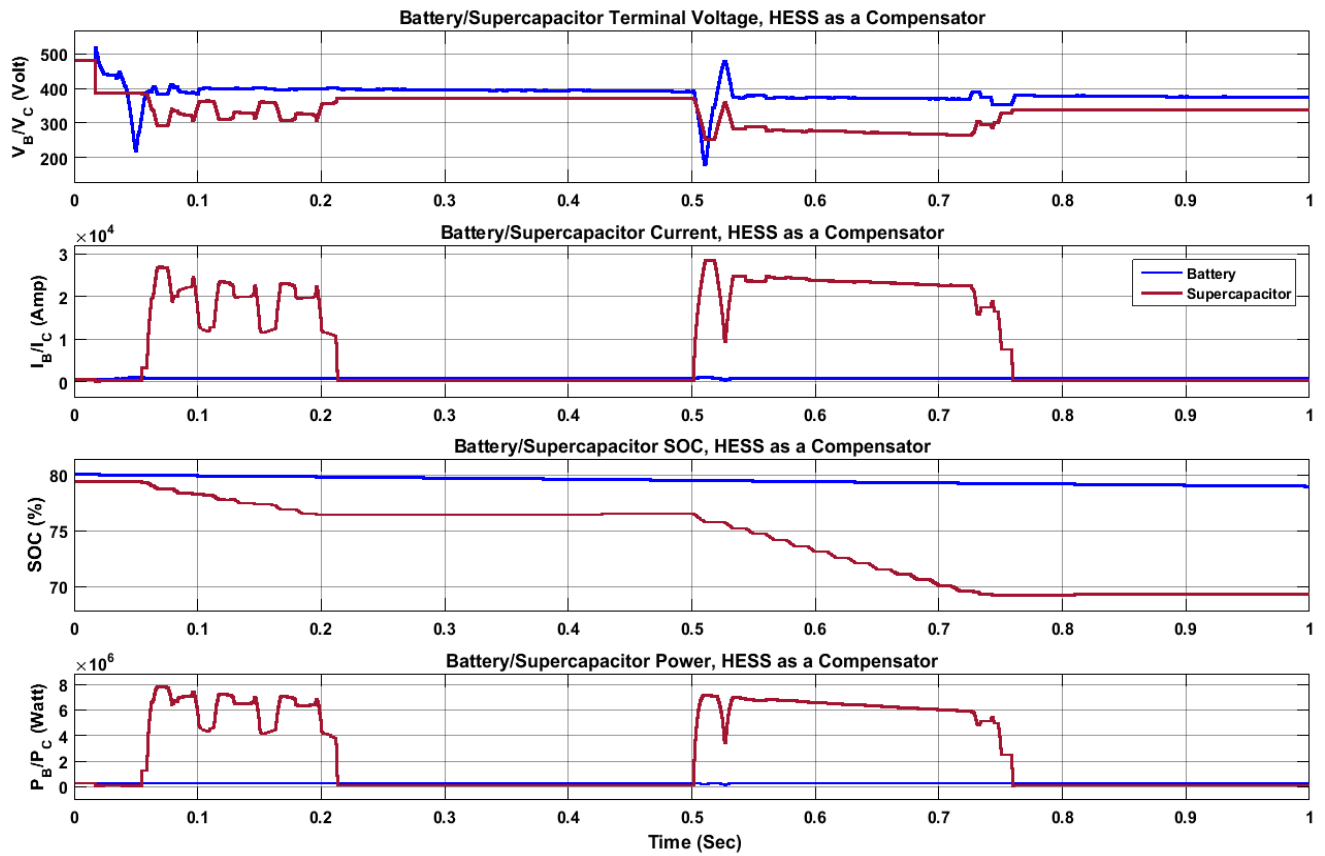


Figure 6:17: Characteristics of the HESS terminal voltage, current, SOC, and power (in the presence of CPL) when hybrid energy storage system is used as compensator.

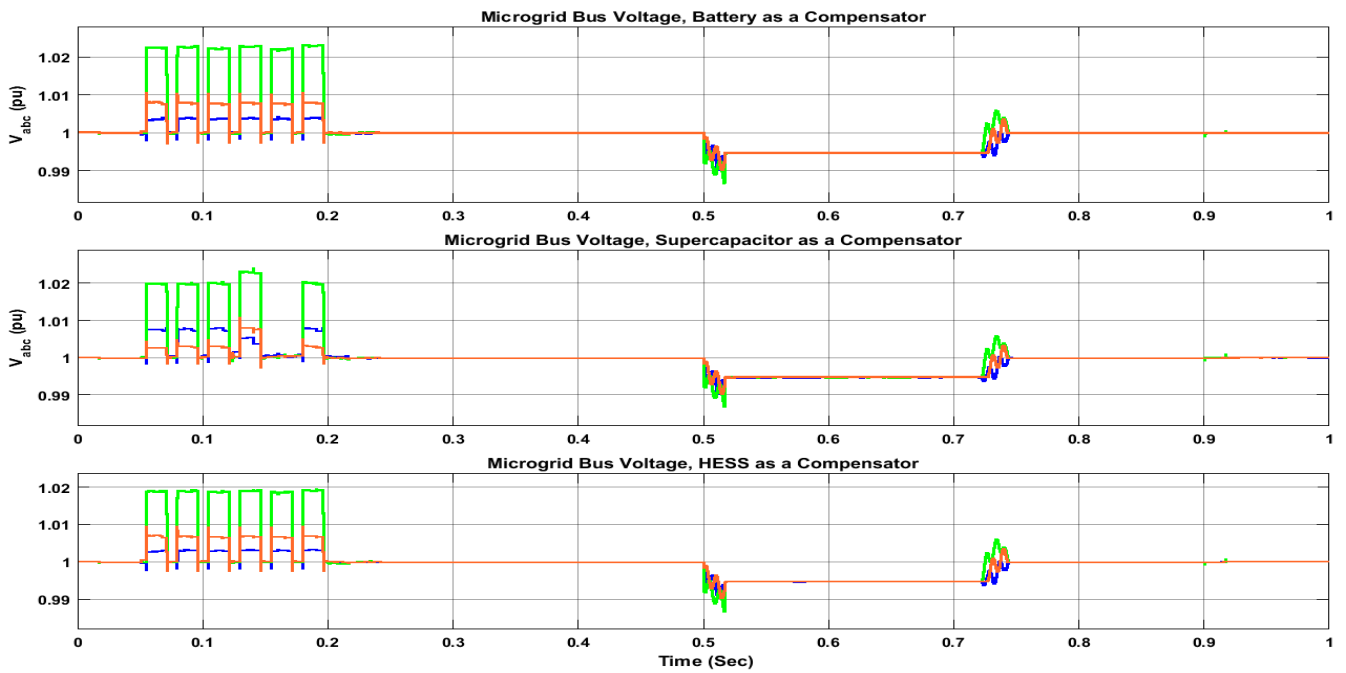


Figure 6:18: Performance comparisons of microgrid bus voltage (in the presence of CPL) among battery-only compensator, ultracapacitor-only compensator, HESS compensator.

From figure 6.17, it can be observed that the high energy density from the battery unit and the power density from the ultracapacitor unit support both long-term slow SOC-demanding applications and transient fast load switching overshoot. In figure 6.18, the comparative analysis is presented on the performance of handling/compensating the transient spikes among the battery-only compensator, ultracapacitor-only compensator, and hybrid energy storage system as compensator. From this, it can be seen that the transient peak that occurred in the microgrid system has been compensated up to 1.023 pu in the case of the battery-only compensator, compensated up to 1.02 pu in the case of the ultracapacitor-only compensator, and compensated up to 1.017 pu in the case of the hybrid energy storage system. So, it is evident that HESS can handle the transient spikes most efficiently among these three cases.

## **6.5 Performance Evaluation and Findings**

A Hybrid Energy Storage System has been developed into one of the promising tools to retain stability and ensure stability in the microgrid arrangement. In renewable energy-based power supply policy, instability is one of the major concerns for system designers. In this section, a short overview of typical Hybrid Energy Storage System applications, energy storage coupling architectures, and basic energy management concepts are presented to show how stability can be managed in the transient high power requirement scenario. To identify the distinct advantages of the Hybrid Energy Storage Systems, a number of comprehensive analysis results have been presented with similar load profiles and energy management algorithms for only battery as storage and only ultracapacitor as storage condition. The key findings of this extended research can be outlined as

- Battery size is scaled down significantly because the transient load/peak load demand is eventually compensated by the ultracapacitor. Consequentially, the installation cost of additional battery units can be minimized; figure 6.6(a) implies the phenomenon.
- Generally, for a long-term slow SOC demanding applications, high energy density batteries are desirable. But, the high energy density battery unit cannot sustain at the time of load switching when

transient overshoot arises. In consequence, its life cycle reduces dramatically. To solve this dilemma, an ultracapacitor with high power density can be installed there to ensure longer power sustainability; figure 6.8 indicates that particular characteristic.

- A battery takes longer reaction time (charging/discharging) while, on the other hand, an ultracapacitor reacts instantly compared to the battery. In the case of transient power demand, an ultracapacitor reacts instantly and assists battery in the process.
- By using this approach, System efficiency can be increased. Besides that, the microgrid voltage can be stabilized within 0.02 sec and the switching overshoot can be limited to below 1.02 per unit voltage in Hybrid Energy Storage System (HESS) as shown in figure 6.13. Moreover, similar characteristics have been shown for only battery and for only ultracapacitor, but HESS has been improved significantly in this particular outcome.
- In renewable energy-based microgrid arrangement, the transient high power requirement is one of the major concerns for system designers to ensure stability. Sometimes, consumers of this power supply system experience sudden blackout and brownout, when the storage cannot supply the required transient peak. In this occasion, a Hybrid Energy Storage System offers the most reliable operation to handle the scenario.

## Chapter 7 : Summary

### 7.1 Salient Accomplishments

In this dissertation, a detailed mathematical model of microgrid with CPL and CVL load has been developed considering the variation of the system parameters. Here, microgrid has been represented as an arrangement where the  $V_{\text{Output}}$  and stability margin vary with the change of  $R_{\text{eq}}$ ,  $L_{\text{eq}}$ , and  $C_{\text{eq}}$ . In this occasion, the stability margin/criteria for CPL load have been determined considering the parameter variation with the assistance of the Routh-Hurwitz stability criterion and Lyapunov stability criterion. Besides that, the system analysis has been performed by dq axis modeling and then determined the nonlinear state space model to implement the nonlinear control strategies. In this approach, active and reactive power can be controlled independently by controlling the dq components. In the case of linear control technique, a PID controller has been implemented as a comprehensive solution. On the other hand, for nonlinear control, SMC and LRC techniques have been implemented to control the entire system. After that, a comparative analysis has been presented between SMC and LRC controller robustness by varying CPL power. From this analysis, it is evident that a Lyapunov redesign controller performs better than the previous one (SMC) to retain microgrid stability in dense CPL-loaded condition. Besides that, a storage system has been proposed to handle CPL instability. In this particular case, the load side compensation has been achieved by using a storage-based virtual impedance method where compensation is provided through the d-axis and q-axis current. After that, robustness and disturbance analysis with noise rejection (White Noise or Harmonics) have been performed both analytically and graphically. Robustness of the system has been analyzed by using the Sliding Mode Control technique and Lyapunov Redesign Control technique considering the uncertainty of system parameters such as frequency, CPL power, CVL power, and bus voltage variations.

In the later part of this dissertation, CPL instability compensator module (Hybrid Energy Storage System) was described which is basically a portable device consisting of both ultracapacitor and battery. Generally, for a long term slow SOC demanding applications, high energy density batteries are desirable.

But, the high energy density battery unit cannot sustain at the time of load switching when transient overshoot arises. In consequence, its life cycle reduces dramatically. To solve this dilemma, an ultracapacitor with high power density can be installed to ensure longer power sustainability. An ultracapacitor contributes also in transient power demand where battery handles the nominal power requirements. Sometimes, consumers of this power supply system experience sudden black out and brown out when the storage cannot supply the required transient peak. On this occasion, Hybrid Energy Storage System offers the most reliable operation to handle the scenario. Apart from that, battery size is scaled down significantly because the transient load/peak load demand is eventually compensated by the ultracapacitor. Consequentially, the installation cost of additional battery units can be minimized.

## **7.2 Discussion and Conclusion**

In the beginning of this dissertation, the instability due to the impact of the negatively incremental resistivity was discussed in the case of constant power load of the microgrid system. After that, among all the possible solutions, virtual impedance-based hybrid storage system has been proposed where real or reactive current would be injected to ensure desired stability. To justify the proposed methodology, the performance of this technique has been analyzed in the virtual platform performing necessary simulations. In that case, the system is linearized, albeit the inherent non-linearity of the system and linear controller such as the PID has been implemented to analyze the impact of the proposed compensation technique. After that, to ensure more accuracy in the analysis, two standard nonlinear control techniques have also been implemented considering the certain non-linearity nature of the system. Robustness, frequency uncertainty, noise rejection, and boundary conditions have been analyzed by necessary simulation results. Finally, to eliminate the possibility of sudden black out and brown out in the system and to reduce the storage installation cost, Hybrid Energy Storage System (HESS), consisting of battery plus ultracapacitor, has been introduced. The advantages of this system over the conventional storage technique have been verified by the comprehensive simulation results performed in Matlab/Simulink.

## 7.3 Future Work

### 7.3.1 Selection of Storage System Based on Microgrid Capacity and Operating Specification

Since the microgrid system has different types based on operation and capacity, a specifically modeled storage system might not perform efficiently in all categories or operating conditions. According to the microgrid types/category and system specified requirement, the requirement of storage system will vary. As the storage system varies (such as Mechanical, Electrical, and Electrochemical), the storage system parameters also varies. It is important to figure out the appropriate storage system for specific applications which is required to be addressed. As we can see in Table 7.1, the characteristics of microgrids also change with their types such as facility microgrids, remote microgrids, and utility/industrial microgrids. The regulation and the geographical area are the two most important parameters in CPL loads analysis in microgrid. With the variation of those parameters, the proportion of CPL load makes changes to the system. Hence, based on the application of microgrid, researchers need to select the appropriate compensation technologies. A further detailed study is required to address those parameters.

Table 7-1: Detailed Classification of Microgrid [18].

Classification	Utilities Impact	Responsibility	Operational Mode	Geographical Span	Power Quality	Remarks
Facility Microgrid	Little impact on utilities	For complement mostly for viral systems	International or Unintentional island mode	2 miles	High	Making greater of renewable energy, increasing energy efficiency, reducing pollution, greenhouse gas emission & high power quality reliability for sensitive loads as well to single business-entity
Remote Microgrid	No impact on utilities	Independent system for isolated electrification	Islanded Mode only	30 miles	Relaxed	Mostly decentralized control & maximum power use is limited for the customers
Utility Microgrid	Massive impact on utilities	For support of power system	Grid tie mode	15 miles	Medium	Providing high power quality & reliability to sensitive local loads, contributing to utility stability & robustness as well

## Grid Energy Storage Technologies and Applications

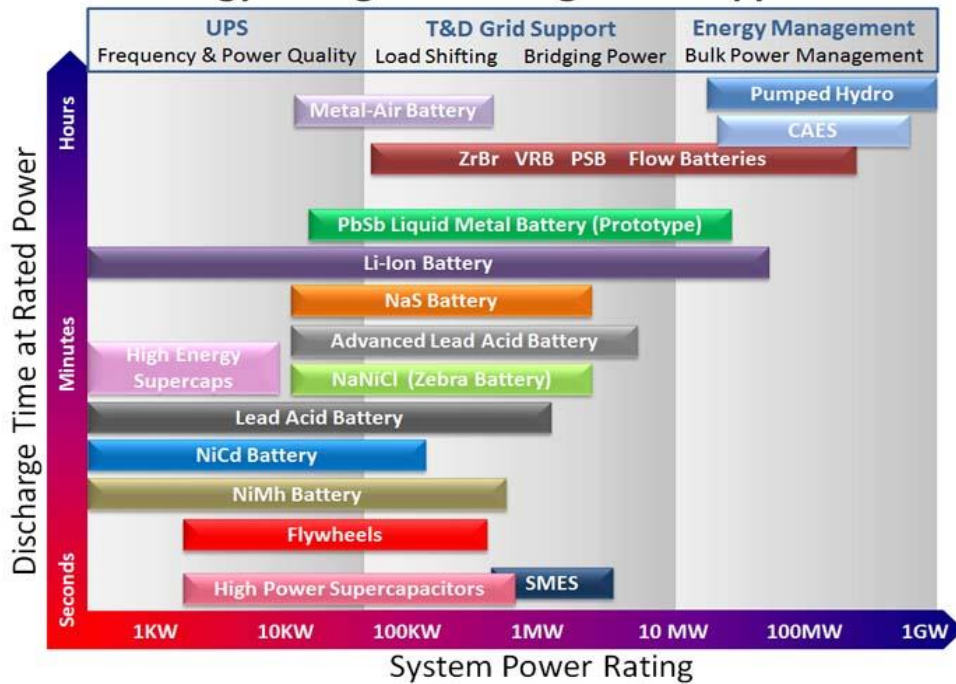


Figure 7:1: Grid energy storage technology and applications [82].

### 7.3.1.1 Applications Summary

For stabilization and compensation purposes of electric utility, comparatively faster responding technologies are recommended. While intermediate response technologies can be implemented for load tracking, the comparatively slower response technologies can be used for the buffer storage. Batteries can provide a wide range of support to all of these applications. Besides that, they facilitate not only the supply of power within one second when required, but also store the additional power when the supply surpasses the demand. The combination of these attributes makes the battery more viable for an extensive range of grid applications or islanded applications. Figure 7.1 shows the characteristics of a range of energy storage systems and their appropriateness for performing in the case of UPS, T&D grid support and energy management. In the most of the cases, the energy storage systems have fast response time. The given figure shows the power handling capacity of each system and the duration for which this power can be sustained. For example, in industrial microgrid applications, the reactive power demand is higher; in that case HESS system would be the better

choice. A further study is required in detail to select appropriate compensation technology in microgrid applications.

Table 7-2: Reactive Power Compensator in Microgrid Technology [81].

	Synchronous Condenser	Static Compensator		Self-Commutated Compensator	Supercapacitor/ Ultracapacitor
		TCR (with shunt capacitors if necessary)	TSC (with TCR if necessary)		
<b>Low</b>	Good	Very Good	Good, very good with TCR	Excellent	Excellent
<b>Control Flexibility</b>	Good	Very Good	Good, very good with TCR	Excellent	Excellent
<b>Reactive Power Capability</b>	Leading/Lagging	Lagging/Leading indirect	Lagging/Leading indirect	Leading/Lagging	Lagging
<b>Control</b>	Continuous	Continuous	Discontinuous (cont. with TCR)	Continuous	Continuous
<b>Response Time</b>	Slow	Fast, 0.5 to 2 cycles	Fast, 0.5 to 2 cycles	Very fast but depends on the control system and switching frequency	Very fast but depends on the control system and switching frequency
<b>Harmonics</b>	Very Good	Very high (large size filters are needed)	Good, filters are necessary with TCR	Good, but depends on switching pattern	Good
<b>Losses</b>	Moderate	Good, but increase in lagging mode	Good, but increase in leading mode	Very good, but increase with switching frequency	Very good
<b>Phase Balancing Ability</b>	Limited	Good	Limited	Very good with 1-phase units, limited with 3-phase units	Very Good
<b>Cost</b>	High	Moderate	Moderate	Low to moderate	Medium to high

### 7.3.2 Load-ability Calculation of “Microgrid with CPL” Using Droop control strategy

By tracing the maximum real power of microgrid geometrically, the droop-control may be applied to microgrids with the loads being constant power loads (CPLs). This control approach might be more efficient in balancing bus voltage and withstanding the microgrid stability within a very fast response time.

Maximum loading limit of the microgrid can be determined from the geometrical approach and the stability analysis, which is required to optimize the size of compensation element. Based on various aspects, the different types of reactive power compensators in microgrid technology are shown in table 7.2.

### 7.3.2.1 Droop Control

Droop control, down scaling the conventional grid control concept to the low voltage grid, is one of the promising approaches to adopt in microgrid systems to retain the desired stability. In this technique, by fine-tuning the voltage amplitude and the phase angle, the required transmission power control is attained. In particular on inductive transmission lines, the active power and reactive power basically depend on the power angle and the voltage inequality respectively. Therefore, active power can be controlled by adjusting the power angle and reactive power by fine-tuning the voltage difference. As droop control is one of the comprehensive control techniques in microgrid application, researchers should investigate it in CPL instability analysis [125].

### 7.3.2.2 Stability Analysis Using Popov's Stability Criterion

The highly nonlinear behavior of microgrid with the loads being constant power loads (CPLs) can be derived more efficiently by using advanced control theory such as Popov's nonlinear theory. From those more specific and detail derivations, robust and adaptive nonlinear controllers can be designed to stabilize the microgrid bus voltage and to implement reactive power compensation methodologies in an efficient way.

### 7.3.3 Reviewing the Feeder Side and by Adding Intermediate Circuitry Methodologies for CPL Compensation on Microgrid

Further investigation of CPL compensation technologies in feeder side in addition to adding intermediate circuitry (e.g. FACTS device) can be performed using storage-based compensation or reactive power compensation techniques. Performance of those technologies for CPL compensation can be compared for all

the possible compensation position and a standard and efficient method can be suggested for prototype testing. A comprehensive mathematical analysis and simulation environment could also be developed to support the suggested methodologies. Moreover, feeder side and intermediate side along with load side strategy for CPL compensation on microgrid applications can be investigated.

## Bibliography

- [1] Jusoh, A.B., "The instability effect of constant power loads," *Power and Energy Conference, 2004. PECon 2004. Proceedings. National*, vol., no., pp.175, 179, 29-30 Nov. 2004
- [2] Ariyasinghe, D.P.; Vilathgamuwa, D.M., "Stability analysis of microgrids with constant power loads," *Sustainable Energy Technologies, 2008. ICSET 2008. IEEE International Conference on*, vol., no., pp.279, 284, 24-27 Nov. 2008
- [3] Kwasinski, A.; Onwuchekwa, C.N., "Effects of instantaneous constant-power loads on DC microgrids for sustainable power systems," *Power Electronics Conference (IPEC), 2010 International*, vol., no., pp.862, 869, 21-24 June 2010
- [4] Magne, P.; Nahid-Mobarakeh, B.; Pierfederici, S., "A design method for a fault-tolerant multi-agent stabilizing system for DC microgrids with Constant Power Loads," *Transportation Electrification Conference and Expo (ITEC), 2012 IEEE* , vol., no., pp.1,6, 18-20 June 2012
- [5] Huddy, S.R.; Skufca, J.D., "Amplitude Death Solutions for Stabilization of DC Microgrids with Instantaneous Constant-Power Loads," *Power Electronics, IEEE Transactions on*, vol.28, no.1, pp.247, 253, Jan. 2013
- [6] Singh, S.; Fulwani, D., "Constant power loads: A solution using sliding mode control," *Industrial Electronics Society, IECON 2014 - 40th Annual Conference of the IEEE* , vol., no., pp.1989,1995, Oct. 29 2014-Nov. 1 2014
- [7] Rahimi, Amir M., "Addressing negative impedance instability problem of constant power loads: Comprehensive view encompassing entire system from the load to the source," *Dissertation, Illinois Institute of Technology: ProQuest/UMI*, 2009. (Publication No. 3370877)
- [8] Molinas, M.; Moltoni, D.; Fascendini, G.; Suul, J.A.; Undeland, T., "Constant power loads in AC distribution systems: An investigation of stability," *Industrial Electronics, 2008. ISIE 2008. IEEE International Symposium on*, vol., no., pp.1531,1536, June 30 2008-July 2 2008
- [9] Vilathgamuwa, D.M.; Zhang, X.N.; Jayasinghe, S.D.G.; Bhangu, B.S.; Gajanayake, C.J.; King Jet Tseng, "Virtual resistance based active damping solution for constant power instability in AC microgrids," *IECON 2011 - 37th Annual Conference on IEEE Industrial Electronics Society* , vol., no., pp.3646,3651, 7-10 Nov. 2011
- [10] Leon, A.E.; Solsona, I.A.; Valla, M.I., "Observer-based nonlinear controller for a three-phase Voltage-Source Converter feeding a constant power load," *Industrial Electronics, 2008. ISIE 2008. IEEE International Symposium on*, vol., no., pp.124, 129, June 30 2008-July 2 2008
- [11] Emadi, A.; Khaligh, A.; Rivetta, C.H.; Williamson, G.A., "Constant power loads and negative impedance instability in automotive systems: definition, modeling, stability, and control of power electronic converters and motor drives," *Vehicular Technology, IEEE Transactions on*, vol.55, no.4, pp.1112, 1125, July 2006

- [12] Jesse Leonard, "Nonlinear Modeling of DC Constant Power Loads with Frequency Domain Volterra Kernels" UMI Number: 3681743, Published by ProQuest LLC (2015)
- [13] Alireza Khaligh, "Digital Control of DC/DC Converters Driving Constant Power Loads in Vehicular Systems" UMI Number: 3220880, Chicago, Illinois May 2006.
- [14] Xiaonan Lu; Kai Sun; Lipei Huang; Guerrero, J.M.; Vasquez, J.C.; Yan Xing, "Virtual impedance based stability improvement for DC microgrids with constant power loads," *Energy Conversion Congress and Exposition (ECCE), 2014 IEEE* , vol., no., pp.2670,2675, 14-18 Sept. 2014 doi: 10.1109/ECCE.2014.6953759
- [15] Fei Zhao; Ningning Li; Zhenggang Yin; Xisheng Tang, "Small-signal modeling and stability analysis of DC microgrid with multiple type of loads," *Power System Technology (POWERCON), 2014 International Conference on* , vol., no., pp.3309,3315, 20-22 Oct. 2014 doi: 10.1109/POWERCON.2014.6993873
- [16] Sanchez, S.; Molinas, M., "Assessment of a stability analysis tool for constant power loads in DC-grids," *Power Electronics and Motion Control Conference (EPE/PEMC), 2012 15th International* , vol., no., pp.DS3b.2-1,DS3b.2-5, 4-6 Sept. 2012 doi: 10.1109/EPEPEMC.2012.6397317
- [17] Jelani, N.; Molinas, M., "Stability investigation of control system for power electronic converter acting as load interface in AC distribution system," *Industrial Electronics (ISIE), 2011 IEEE International Symposium on* , vol., no., pp.408,413, 27-30 June 2011 doi: 10.1109/ISIE.2011.5984193
- [18] Eklas Hossain, Ersan Kabalci, Ramazan Bayindir and Ronald Perez "Microgrid testbeds around the world: State of art", *Energy Conversion and Management* 86 (2014) 132–153
- [19] Eklas Hossain, Ersan Kabalci, Ramazan Bayindir and Ronald Perez "A Comprehensive Study on Microgrid Technology", *International Journal of Renewable Energy Research*, Vol.4, No.4, 2014 1094–1107
- [20] George J. Roth "Stability Analysis Of A Constant Power Load Serviced By A Buck Converter As The Source Impedance Varies" Naval Postgraduate School September 2012
- [21] Acevedo, S.S.; Molinas, M., "Assessing the validity of a propose stability analysis method in a three phase system with constant power load," *Power Electronics for Distributed Generation Systems (PEDG), 2012 3rd IEEE International Symposium on* , vol., no., pp.41,45, 25-28 June 2012 doi: 10.1109/PEDG.2012.6253977
- [22] Zeng Liu; Jinjun Liu; Weihan Bao; Yalin Zhao; Fangcheng Liu, "A novel stability criterion of AC power system with constant power load," *Applied Power Electronics Conference and Exposition (APEC), 2012 Twenty-Seventh Annual IEEE* , vol., no., pp.1946,1950, 5-9 Feb. 2012 doi: 10.1109/APEC.2012.6166089
- [23] Yanjun Dong; Wentao Liu; Zhaohui Gao; Xiaobin Zhang, "Study of a simulation model of AC Constant Power Load," *TENCON 2008 - 2008 IEEE Region 10 Conference* , vol., no., pp.1,5, 19-21 Nov. 2008 doi: 10.1109/TENCON.2008.4766537

- [24] Rahimi, A.M.; Williamson, G.A.; Emadi, A., "Loop-Cancellation Technique: A Novel Nonlinear Feedback to Overcome the Destabilizing Effect of Constant-Power Loads," *Vehicular Technology, IEEE Transactions on* , vol.59, no.2, pp.650,661, Feb. 2010 doi: 10.1109/TVT.2009.2037429
- [25] Kwasinski, A.; Onwuchekwa, C.N., "Dynamic Behavior and Stabilization of DC Microgrids With Instantaneous Constant-Power Loads," *Power Electronics, IEEE Transactions on* , vol.26, no.3, pp.822,834, March 2011 doi: 10.1109/TPEL.2010.2091285
- [26] Areerak, K-N.; Bozhko, S.V.; Asher, G.M.; Thomas, D.W.P., "DQ-transformation approach for modelling and stability analysis of AC-DC power system with controlled PWM rectifier and constant power loads," *Power Electronics and Motion Control Conference, 2008. EPE-PEMC 2008. 13th* , vol., no., pp.2049,2054, 1-3 Sept. 2008 doi: 10.1109/EPEPEMC.2008.4635567
- [27] Karimipour, D.; Salmasi, F.R., "Stability Analysis of AC Microgrids With Constant Power Loads Based on Popov's Absolute Stability Criterion," *Circuits and Systems II: Express Briefs, IEEE Transactions on* , vol.62, no.7, pp.696,700, July 2015 doi: 10.1109/TCSII.2015.2406353
- [28] Areerak, K-N.; Bozhko, S.V.; Asher, G.M.; Thomas, D.W.P., "Stability analysis and modelling of AC-DC system with mixed load using DQ-transformation method," *Industrial Electronics, 2008. ISIE 2008. IEEE International Symposium on* , vol., no., pp.19,24, June 30 2008-July 2 2008 doi: 10.1109/ISIE.2008.4676898
- [29] Carmeli, M.S.; Forlani, D.; Grillo, S.; Pinetti, R.; Ragaini, E.; Tironi, E., "A stabilization method for DC networks with constant-power loads," *Energy Conference and Exhibition (ENERGYCON), 2012 IEEE International* , vol., no., pp.617,622, 9-12 Sept. 2012 doi: 10.1109/EnergyCon.2012.6348226
- [30] Hamache, D.; Fayaz, A.; Godoy, E.; Karimi, C., "Stabilization of a DC electrical network via backstepping approach," *Industrial Electronics (ISIE), 2014 IEEE 23rd International Symposium on* , vol., no., pp.242,247, 1-4 June 2014 doi: 10.1109/ISIE.2014.6864618
- [31] Cupelli, M.; Mirz, M.; Monti, A., "Application of backstepping to MVDC ship power systems with constant power loads," *Electrical Systems for Aircraft, Railway, Ship Propulsion and Road Vehicles (ESARS), 2015 International Conference on* , vol., no., pp.1,6, 3-5 March 2015 doi: 10.1109/ESARS.2015.7101469
- [32] Herrera, L.; Jin Wang, "Stability analysis and controller design of DC microgrids with constant power loads," *Applied Power Electronics Conference and Exposition (APEC), 2015 IEEE* , vol., no., pp.691,696, 15-19 March 2015 doi: 10.1109/APEC.2015.7104425
- [33] Yue Zhao; Wei Qiao, "A third-order sliding-mode controller for DC/DC converters with constant power loads," *Industry Applications Society Annual Meeting (IAS), 2011 IEEE* , vol., no., pp.1,8, 9-13 Oct. 2011 doi: 10.1109/IAS.2011.6074347
- [34] Hailian Xie; Angquist, L.; Nee, H.-P., "Active Power Compensation of Voltage Source Converters with Energy Storage Capacitors," *Power Systems Conference and Exposition, 2006. PSCE '06. 2006 IEEE PES*, vol., no., pp.1012,1019, Oct. 29 2006-Nov. 1 2006 doi: 10.1109/PSCE.2006.296450

- [35] Sanchez, S.; Ortega, R.; Griño, R.; Bergna, G.; Molinas, M., "Conditions for Existence of Equilibria of Systems With Constant Power Loads," *Circuits and Systems I: Regular Papers, IEEE Transactions on* , vol.61, no.7, pp.2204,2211, July 2014 doi: 10.1109/TCSI.2013.2295953
- [36] Gehrke, C.S.; de Almeida, G.R.P.; Correa, M.B.R.; Oliveira, A.C.; Lima, A.M.N., "Improving energy quality by voltage compensation and active power injection," *Power Electronics Conference (COBEP), 2011 Brazilian* , vol., no., pp.795,800, 11-15 Sept. 2011 doi: 10.1109/COBEP.2011.6085313
- [37] Marx, D.; Magne, P.; Nahid-Mobarakeh, B.; Pierfederici, S.; Davat, B., "Large Signal Stability Analysis Tools in DC Power Systems With Constant Power Loads and Variable Power Loads—A Review," *Power Electronics, IEEE Transactions on* , vol.27, no.4, pp.1773,1787, April 2012 doi: 10.1109/TPEL.2011.2170202
- [38] Magne, P.; Marx, D.; Nahid-Mobarakeh, B.; Pierfederici, S., "Large-Signal Stabilization of a DC-Link Supplying a Constant Power Load Using a Virtual Capacitor: Impact on the Domain of Attraction," *Industry Applications, IEEE Transactions on* , vol.48, no.3, pp.878,887, May-June 2012 doi: 10.1109/TIA.2012.2191250
- [39] Liutanakul, P.; Awan, A.-B.; Pierfederici, S.; Nahid-Mobarakeh, B.; Meibody-Tabar, F., "Linear Stabilization of a DC Bus Supplying a Constant Power Load: A General Design Approach," *Power Electronics, IEEE Transactions on* , vol.25, no.2, pp.475,488, Feb. 2010 doi: 10.1109/TPEL.2009.2025274
- [40] Stramosk, V.; Pagano, D.J., "Nonlinear control of a bidirectional dc-dc converter operating with boost-type Constant-Power Loads," *Power Electronics Conference (COBEP), 2013 Brazilian* , vol., no., pp.305,310, 27-31 Oct. 2013 doi: 10.1109/COBEP.2013.6785132
- [41] Jelani, N.; Molinas, M.; Bolognani, S., "Reactive Power Ancillary Service by Constant Power Loads in Distributed AC Systems," *Power Delivery, IEEE Transactions on* , vol.28, no.2, pp.920,927, April 2013 doi: 10.1109/TPWRD.2012.2235861
- [42] Anun, M.; Ordonez, M.; Galiano, I.; Oggier, G., "Bidirectional power flow with constant power load in electric vehicles: A non-linear strategy for Buck+Boost cascade converters," *Applied Power Electronics Conference and Exposition (APEC), 2014 Twenty-Ninth Annual IEEE* , vol., no., pp.1697,1703, 16-20 March 2014 doi: 10.1109/APEC.2014.6803534
- [43] Singh, S.; Fulwani, D.; Kumar, V., "Robust sliding-mode control of dc/dc boost converter feeding a constant power load," *Power Electronics, IET* , vol.8, no.7, pp.1230,1237, 7 2015 doi: 10.1049/iet-pel.2014.0534
- [44] Abhyankar, S.G.; Flueck, A.J., "Simulating voltage collapse dynamics for power systems with constant power load models," *Power and Energy Society General Meeting - Conversion and Delivery of Electrical Energy in the 21st Century, 2008 IEEE* , vol., no., pp.1,6, 20-24 July 2008 doi: 10.1109/PES.2008.4596587

- [45] Agarwal, Atul; Deekshitha, Koyinni; Singh, Suresh; Fulwani, Deepak, "Sliding mode control of a bidirectional DC/DC converter with constant power load," *DC Microgrids (ICDCM), 2015 IEEE First International Conference on* , vol., no., pp.287,292, 7-10 June 2015 doi: 10.1109/ICDCM.2015.7152056
- [46] Mingfei Wu; Lu, D.D.-C., "A Novel Stabilization Method of LC Input Filter With Constant Power Loads Without Load Performance Compromise in DC Microgrids," *Industrial Electronics, IEEE Transactions on* , vol.62, no.7, pp.4552,4562, July 2015 doi: 10.1109/TIE.2014.2367005
- [47] Yue Zhao; Wei Qiao; Daiyun Ha, "A Sliding-Mode Duty-Ratio Controller for DC/DC Buck Converters With Constant Power Loads," *Industry Applications, IEEE Transactions on* , vol.50, no.2, pp.1448,1458, March-April 2014 doi: 10.1109/TIA.2013.2273751
- [48] Jianwu Zeng; Zhe Zhang; Wei Qiao, "An interconnection-damping-assignment passivity-based controller for a DC-DC boost converter with a constant power load," *Industry Applications Society Annual Meeting (IAS), 2012 IEEE* , vol., no., pp.1,7, 7-11 Oct. 2012 doi: 10.1109/IAS.2012.6374043
- [49] Onwuchekwa, C.N.; Kwasinski, A., "Analysis of Boundary Control for Buck Converters With Instantaneous Constant-Power Loads," *Power Electronics, IEEE Transactions on* , vol.25, no.8, pp.2018,2032, Aug. 2010 doi: 10.1109/TPEL.2010.2045658
- [50] Jelani, N.; Molinas, M., "Asymmetrical Fault Ride Through as Ancillary Service by Constant Power Loads in Grid-Connected Wind Farm," *Power Electronics, IEEE Transactions on* , vol.30, no.3, pp.1704,1713, March 2015 doi: 10.1109/TPEL.2014.2320949
- [51] Anun, M.; Ordonez, M.; Zurbriggen, I.G.; Oggier, G.G., "Circular Switching Surface Technique: High-Performance Constant Power Load Stabilization for Electric Vehicle Systems," *Power Electronics, IEEE Transactions on* , vol.30, no.8, pp.4560,4572, Aug. 2015 doi: 10.1109/TPEL.2014.2358259
- [52] Cespedes, M.; Lei Xing; Jian Sun, "Constant-Power Load System Stabilization by Passive Damping," *Power Electronics, IEEE Transactions on* , vol.26, no.7, pp.1832,1836, July 2011 doi: 10.1109/TPEL.2011.2151880
- [53] Yushan Li; Vannorsdel, K.R.; Zirger, A.J.; Norris, M.; Maksimovic, D., "Current Mode Control for Boost Converters With Constant Power Loads," *Circuits and Systems I: Regular Papers, IEEE Transactions on* , vol.59, no.1, pp.198,206, Jan. 2012 doi: 10.1109/TCSI.2011.2161364
- [54] Rahimi, A.M.; Emadi, A., "Discontinuous-Conduction Mode DC/DC Converters Feeding Constant-Power Loads," *Industrial Electronics, IEEE Transactions on* , vol.57, no.4, pp.1318,1329, April 2010 doi: 10.1109/TIE.2009.2029514
- [55] Magne, P.; Nahid-Mobarakeh, B.; Pierfederici, S., "Dynamic Consideration of DC Microgrids With Constant Power Loads and Active Damping System—A Design Method for Fault-Tolerant Stabilizing System," *Emerging and Selected Topics in Power Electronics, IEEE Journal of* , vol.2, no.3, pp.562,570, Sept. 2014 doi: 10.1109/JESTPE.2014.2305979
- [56] Bottrell, N.; Prodanovic, M.; Green, T.C., "Dynamic Stability of a Microgrid With an Active Load," *Power Electronics, IEEE Transactions on* , vol.28, no.11, pp.5107,5119, Nov. 2013 doi: 10.1109/TPEL.2013.2241455

- [57] Zeng Liu; Jinjun Liu; Weihan Bao; Yalin Zhao, "Infinity-Norm of Impedance-Based Stability Criterion for Three-Phase AC Distributed Power Systems With Constant Power Loads," *Power Electronics, IEEE Transactions on*, vol.30, no.6, pp.3030,3043, June 2015 doi: 10.1109/TPEL.2014.2331419
- [58] Griffo, A.; Jiabin Wang, "Large Signal Stability Analysis of 'More Electric' Aircraft Power Systems with Constant Power Loads," *Aerospace and Electronic Systems, IEEE Transactions on*, vol.48, no.1, pp.477,489, Jan. 2012 doi: 10.1109/TAES.2012.6129649
- [59] Sulligoi, G.; Bosich, D.; Giadrossi, G.; Lin Zhu; Cupelli, M.; Monti, A., "Multiconverter Medium Voltage DC Power Systems on Ships: Constant-Power Loads Instability Solution Using Linearization via State Feedback Control," *Smart Grid, IEEE Transactions on*, vol.5, no.5, pp.2543,2552, Sept. 2014 doi: 10.1109/TSG.2014.2305904
- [60] Xinan Zhang; Vilathgamuwa, D.M.; King-Jet Tseng; Bhangu, B.S.; Gajanayake, C.J., "Power Buffer With Model Predictive Control for Stability of Vehicular Power Systems With Constant Power Loads," *Power Electronics, IEEE Transactions on*, vol.28, no.12, pp.5804,5812, Dec. 2013 doi: 10.1109/TPEL.2012.2233761
- [61] Wook-Jin Lee; Yeongrack Son; Jung-Ik Ha, "Single-Phase Active Power Filtering Method Using Diode-Rectifier-Fed Motor Drive," *Industry Applications, IEEE Transactions on*, vol.51, no.3, pp.2227,2236, May-June 2015 doi: 10.1109/TIA.2014.2365629
- [62] Bo Wen; Boroyevich, D.; Burgos, R.; Mattavelli, P.; Shen, Z., "Small-Signal Stability Analysis of Three-Phase AC Systems in the Presence of Constant Power Loads Based on Measured d-q Frame Impedances," *Power Electronics, IEEE Transactions on*, vol.30, no.10, pp.5952,5963, Oct. 2015 doi: 10.1109/TPEL.2014.2378731
- [63] Xinbo Liu; Yuanjun Zhou; Wei Zhang; Shuohan Ma, "Stability Criteria for Constant Power Loads With Multistage Filters," *Vehicular Technology, IEEE Transactions on*, vol.60, no.5, pp.2042,2049, Jun 2011 doi: 10.1109/TVT.2011.2148133
- [64] Du, W.; Zhang, J.; Zhang, Y.; Qian, Z., "Stability Criterion for Cascaded System With Constant Power Load," *Power Electronics, IEEE Transactions on*, vol.28, no.4, pp.1843,1851, April 2013 doi: 10.1109/TPEL.2012.2211619v
- [65] Hamache, D.; Fayaz, A.; Godoy, E.; Karimi, C., "Stabilization of a DC electrical network by damping injection," *Environmental Friendly Energies and Applications (EFEA), 2014 3rd International Symposium on*, vol., no., pp.1,6, 19-21 Nov. 2014 doi: 10.1109/EFEA.2014.7059990
- [66] Fanghua Zhang; Yangguang Yan, "Start-Up Process and Step Response of a DC-DC Converter Loaded by Constant Power Loads," *Industrial Electronics, IEEE Transactions on*, vol.58, no.1, pp.298,304, Jan. 2011 doi: 10.1109/TIE.2010.2045316
- [67] Kondratiev, I.; Dougal, R., "General Synergetic Control Strategies for Arbitrary Number of Paralleled Buck Converters Feeding Constant Power Load: Implementation of Dynamic Current

- Sharing," *Industrial Electronics, 2006 IEEE International Symposium on* , vol.1, no., pp.257,261, 9-13 July 2006 doi: 10.1109/ISIE.2006.295602
- [68] Kondratiev, I.; Santi, E.; Dougal, R.; Veselov, G., "Synergetic control for DC-DC buck converters with constant power load," *Power Electronics Specialists Conference, 2004. PESC 04. 2004 IEEE 35th Annual*, vol.5, no., pp.3758,3764 Vol.5, 20-25 June 2004 doi: 10.1109/PESC.2004.1355139
- [69] Santi, E.; Li, D.; Monti, A.; Stankovic, A.M., "A Geometric Approach to Large-signal Stability of Switching Converters under Sliding Mode Control and Synergetic Control," *Power Electronics Specialists Conference, 2005. PESC '05. IEEE 36th* , vol., no., pp.1389,1395, 16-16 June 2005 doi: 10.1109/PESC.2005.1581811
- [70] Sebastian, J.; Hernando, M.M.; Villegas, P.; Diaz, J.; Fontan, A., "Input current shaper based on the series connection of a voltage source and a loss-free resistor," *Applied Power Electronics Conference and Exposition, 1998. APEC '98. Conference Proceedings 1998., Thirteenth Annual* , vol.1, no., pp.461,467 vol.1, 15-19 Feb 1998 doi: 10.1109/APEC.1998.647730
- [71]. Tingyou Ming; Weiwen Deng; Jian Wu; Qiao Zhang, "A hierarchical energy management strategy for battery-supercapacitor hybrid energy storage system of electric vehicle," in *Transportation Electrification Asia-Pacific (ITEC Asia-Pacific), 2014 IEEE Conference and Expo* , vol., no., pp.1-5, Aug. 31 2014-Sept. 3 2014
- [72]. Haihua Zhou; Bhattacharya, T.; Duong Tran; Siew, T.S.T.; Khambadkone, A.M., "Composite Energy Storage System Involving Battery and Ultracapacitor With Dynamic Energy Management in Microgrid Applications," in *Power Electronics, IEEE Transactions on* , vol.26, no.3, pp.923-930, March 2011
- [73]. Etxeberria, A.; Vechiu, I.; Camblong, H.; Vinassa, J.M., "Hybrid Energy Storage Systems for renewable Energy Sources Integration in microgrids: A review," in *IPEC, 2010 Conference Proceedings*, vol., no., pp.532-537, 27-29 Oct. 2010
- [74]. Zhang Guoju; Tang Xisheng; Qi Zhiping, "Research on Battery Supercapacitor Hybrid Storage and its application in MicroGrid," in *Power and Energy Engineering Conference (APPEEC), 2010 Asia-Pacific* , vol., no., pp.1-4, 28-31 March 2010
- [75]. Tummuru, N.R.; Mishra, M.K.; Srinivas, S., "Dynamic Energy Management of Renewable Grid Integrated Hybrid Energy Storage System," in *Industrial Electronics, IEEE Transactions on*, vol.62, no.12, pp.7728-7737, Dec. 2015
- [76]. M Glavin, P Chan, S Armstrong, and W Hurley, "A stand-alone photovoltaic supercapacitor battery hybrid energy storage system," in *Proc. 13th Power Electron. Motion Control Conf., 2008 (EPE-PEMC 2008)*, pp. 1688–1695
- [77]. Vechiu I, Etxeberria A, Camblong H, Baudoin S, Kreckelbergh S. Hybrid energy storage system with unique power electronic interface for microgrids. In: *Innovative Smart Grid Technologies Europe (ISGT EUROPE), 2013 4th IEEE/PES; 2013*. p. 1–5

- [78]. Duong Tran; Haihua Zhou; Khambadkone, A.M., "Energy management and dynamic control in Composite Energy Storage System for micro-grid applications," in *IECON 2010 - 36th Annual Conference on IEEE Industrial Electronics Society* , vol., no., pp.1818-1824, 7-10 Nov. 2010
- [79]. Tan, X., Li, Q. and Wang, H. "Advances and trends of energy storage technology in Microgrid. *International Journal of Electrical Power & Energy Systems*, "44(1), pp.179-191
- [80]. Tao Ma; Hongxing Y;Lin Lu,"Development of hybrid battery–supercapacitor energy storage for remote area renewable energy system"Renewable Energy Research Group (RERG), Department of Building Services Engineering, The Hong Kong Polytechnic University, Hong Kong, Volume 153, 1 September 2015, Pages 56–62
- [81] J. Dixon, L. Moran, J. Rodriguez and R. Domke, "Reactive Power Compensation Technologies: State-of-the-Art Review," in *Proceedings of the IEEE*, vol. 93, no. 12, pp. 2144-2164, Dec. 2005. doi: 10.1109/JPROC.2005.859937
- [82] [http://www.mpoweruk.com/grid\\_storage.htm](http://www.mpoweruk.com/grid_storage.htm) “grid Energy Storage Technology and Applications”
- [83] S. Sanchez Acevedo and M. Molinas, "Evaluation of non-active current compensation in smart grids," *2012 3rd IEEE PES Innovative Smart Grid Technologies Europe (ISGT Europe)*, Berlin, 2012, pp. 1-8.doi: 10.1109/ISGTEurope.2012.6465746
- [84] A. Emadi, "Modeling of power electronic loads in AC distribution systems using the generalized State-space averaging method," in *IEEE Transactions on Industrial Electronics*, vol. 51, no. 5, pp. 992-1000, Oct. 2004. doi: 10.1109/TIE.2004.834950
- [85] M. F. Romlie, C. Klumpner, M. Rashed, M. Odavic and G. Asher, "Analysis of stability aspects of a large constant power load in a local grid," *Power Electronics and Applications (EPE), 2013 15th European Conference on*, Lille, 2013, pp. 1-11. doi: 10.1109/EPE.2013.6634481
- [86] P. J. M. Heskes, J. M. A. Myrzik and W. L. Kling, "Power electronic loads with negative differential impedance in a low voltage distribution system," *Electricity Distribution - Part 1, 2009. CIRED 2009. 20th International Conference and Exhibition on*, Prague, Czech Republic, 2009, pp. 1-4. doi: 10.1049/cp.2009.0830
- [87] N. Jelani and M. Molinas, "Shunt active filtering by constant power load in microgrid based on IRP p-q and CPC reference signal generation schemes," *Power System Technology (POWERCON), 2012 IEEE International Conference on*, Auckland, 2012, pp. 1-6. doi: 10.1109/PowerCon.2012.6401438
- [88] E. Lenz and D. J. Pagano, "Nonlinear control of a three-phase power converter with constant power load in a microgrid," *2013 Brazilian Power Electronics Conference*, Gramado, 2013, pp. 368-373. doi: 10.1109/COBEP.2013.6785142
- [89] P. N. A. M. Yunus, A. Jusoh and M. K. Hamzah, "AC-DC Single Phase Matrix Converter with a constant power load (CPL)," *Industrial Electronics and Applications (ISIEA), 2012 IEEE Symposium on*, Bandung, 2012, pp. 275-280. doi: 10.1109/ISIEA.2012.6496643

- [90] M. K. Zadeh, B. Zahedi, M. Molinas and L. E. Norum, "Centralized stabilizer for marine DC microgrid," *Industrial Electronics Society, IECON 2013 - 39th Annual Conference of the IEEE*, Vienna, 2013, pp. 3359-3363. doi: 10.1109/IECON.2013.6699667
- [91] S. Singh and D. Fulwani, "On design of a robust controller to mitigate CPL effect — A DC microgrid application," *Industrial Technology (ICIT), 2014 IEEE International Conference on*, Busan, 2014, pp. 448-454. doi: 10.1109/ICIT.2014.6894982
- [92] S. Sanchez and M. Molinas, "Large Signal Stability Analysis at the Common Coupling Point of a DC Microgrid: A Grid Impedance Estimation Approach Based on a Recursive Method," in *IEEE Transactions on Energy Conversion*, vol. 30, no. 1, pp. 122-131, March 2015. doi: 10.1109/TEC.2014.2359993
- [93] M. Srinivasan and A. Kwasinski, "Decentralized control of a vehicular microgrid with constant power loads," *Electric Vehicle Conference (IEVC), 2014 IEEE International*, Florence, 2014, pp. 1-8. doi: 10.1109/IEVC.2014.7056222
- [94] M. Cupelli, M. Mirz and A. Monti, "A comparison of backstepping and LQG control for stabilizing MVDC microgrids with Constant Power Loads," *PowerTech, 2015 IEEE Eindhoven*, Eindhoven, 2015, pp. 1-6. doi: 10.1109/PTC.2015.7232564
- [95] A. B. Awan, S. Pierfederici, B. Nahid-Mobarakeh and F. Meibody-Tabar, "Active stabilization of a poorly damped input filter supplying a constant power load," *2009 IEEE Energy Conversion Congress and Exposition*, San Jose, CA, 2009, pp. 2991-2997. doi: 10.1109/ECCE.2009.5316102
- [96] M. Ashourloo, A. Khorsandi and H. Mokhtari, "Stabilization of DC microgrids with constant-power loads by an active damping method," *Power Electronics, Drive Systems and Technologies Conference (PEDSTC), 2013 4th*, Tehran, 2013, pp. 471-475. doi: 10.1109/PEDSTC.2013.6506754
- [97] M. Cupelli, M. Moghimi, A. Riccobono and A. Monti, "A comparison between synergetic control and feedback linearization for stabilizing MVDC microgrids with constant power load," *IEEE PES Innovative Smart Grid Technologies, Europe*, Istanbul, 2014, pp. 1-6. doi: 10.1109/ISGTEurope.2014.7028870
- [98] S. Liu, W. Zhu, Y. Cheng and B. Xing, "Modeling and small-signal stability analysis of an islanded DC microgrid with dynamic loads," *Environment and Electrical Engineering (EEEIC), 2015 IEEE 15th International Conference on*, Rome, 2015, pp. 866-871. doi: 10.1109/EEEIC.2015.7165277
- [99] A. R. Gautam, S. Singh and D. Fulwani, "DC bus voltage regulation in the presence of constant power load using sliding mode controlled dc-dc Bi-directional converter interfaced storage unit," *DC Microgrids (ICDCM), 2015 IEEE First International Conference on*, Atlanta, GA, 2015, pp. 257-262. doi: 10.1109/ICDCM.2015.7152050
- [100] S. Singh and D. Fulwani, "Voltage regulation and stabilization of DC/DC buck converter under constant power loading," *Power Electronics, Drives and Energy Systems (PEDES), 2014 IEEE International Conference on*, Mumbai, 2014, pp. 1-6. doi: 10.1109/PEDES.2014.7042054
- [101] S. Islam and S. Anand, "Eigenvalue sensitivity analysis of microgrid with constant power loads," *Power Electronics, Drives and Energy Systems (PEDES), 2014 IEEE International Conference on*, Mumbai, 2014, pp. 1-6. doi: 10.1109/PEDES.2014.7041967

- [102] X. Lu, K. Sun, J. M. Guerrero, J. C. Vasquez, L. Huang and J. Wang, "Stability Enhancement Based on Virtual Impedance for DC Microgrids With Constant Power Loads," in *IEEE Transactions on Smart Grid*, vol. 6, no. 6, pp. 2770-2783, Nov. 2015. doi: 10.1109/TSG.2015.2455017
- [103] M. Su; Z. Liu; Y. Sun; H. Han; X. Hou, "Stability Analysis and Stabilization methods of DC Microgrid with Multiple Parallel-Connected DC-DC Converters loaded by CPLs," in *IEEE Transactions on Smart Grid*, vol. PP, no. 99, pp. 1-1 doi: 10.1109/TSG.2016.2546551
- [104] M. Srinivasan and A. Kwasinski, "Calculation of loadability in a droop controlled DC microgrid with constant power loads," *2015 IEEE 6th International Symposium on Power Electronics for Distributed Generation Systems (PEDG)*, Aachen, 2015, pp. 1-7. doi: 10.1109/PEDG.2015.7223067
- [105] G. Cezar, R. Rajagopal and B. Zhang, "Stability of interconnected DC converters," *2015 54th IEEE Conference on Decision and Control (CDC)*, Osaka, 2015, pp. 9-14. doi: 10.1109/CDC.2015.7402080
- [106] <http://berc.berkeley.edu/storage-wars-batteries-vs-supercapacitors/>
- [107] A. Bidram and A. Davoudi, "Hierarchical Structure of Microgrids Control System," in *IEEE Transactions on Smart Grid*, vol. 3, no. 4, pp. 1963-1976, Dec. 2012. doi: 10.1109/TSG.2012.2197425
- [108] S. Kim and S. S. Williamson, "Negative impedance instability compensation in buck converter using state space pole placement control," *Electrical & Computer Engineering (CCECE)*, 2012 25th IEEE Canadian Conference on, Montreal, QC, 2012, pp. 1-5. doi: 10.1109/CCECE.2012.6335049
- [109] A. Khaligh, A. M. Rahimi and A. Emadi, "Negative Impedance Stabilizing Pulse Adjustment Control Technique for DC/DC Converters Operating in Discontinuous Conduction Mode and Driving Constant Power Loads," in *IEEE Transactions on Vehicular Technology*, vol. 56, no. 4, pp. 2005-2016, July 2007. doi: 10.1109/TVT.2007.897248
- [110] A. Khaligh, A. M. Rahimi and A. Emadi, "Negative Impedance Stabilizing Pulse Adjustment Control Technique for DC/DC Converters Operating in Discontinuous Conduction Mode and Driving Constant Power Loads," in *IEEE Transactions on Vehicular Technology*, vol. 56, no. 4, pp. 2005-2016, July 2007. doi: 10.1109/TVT.2007.897248
- [111] *Vehicular Electric Power Systems Land, Sea, Air, and Space Vehicles* Edited by Mehrdad Ehsani, Ali Emadi, and John M. Miller CRC Press 2003 Print ISBN: 978-0-8247-4751-0 eBook ISBN: 978-0-203-91346-8 DOI: 10.1201/9780203913468.ch12
- [112] Heskes, P. J. M., Myrzik, J. M. A. and Kling, Wil. L. (2011), Impact of distribution system's nonlinear loads with constant power on grid voltage. *Euro. Trans. Electr. Power*, 21: 698–711. doi: 10.1002/etep.470
- [113] Remus Teodorescu, Marco Liserre, Pedro Rodriguez, *Grid Converters for Photovoltaic and Wind Power Systems*, John Wiley & Sons, Jul 28, 2011, ISBN: 978-0-470-05751-3

- [114] [http://www.openelectrical.org/wiki/index.php?title=Dq0\\_Transform](http://www.openelectrical.org/wiki/index.php?title=Dq0_Transform)
- [115] Ganjefar S, Sarajchi M, Mahmoud Hoseini SS. Teleoperation Systems Design Using Singular Perturbation Method and Sliding Mode Controllers. ASME. J. Dyn. Sys., Meas., Control. 2014;136(5):051005-051005-8. doi:10.1115/1.4027164
- [116] Y.Z. Elhalwagy, M. Tarbouchi, Fuzzy logic sliding mode control for command guidance law design, ISA Transactions, Volume 43, Issue 2, April 2004, Pages 231-242, ISSN 0019-0578, [http://dx.doi.org/10.1016/S0019-0578\(07\)60033-0](http://dx.doi.org/10.1016/S0019-0578(07)60033-0)
- [117] [https://theses.lib.vt.edu/theses/available/etd5440202339731121/unrestricted/CHAP4\\_DOC.pdf](https://theses.lib.vt.edu/theses/available/etd5440202339731121/unrestricted/CHAP4_DOC.pdf)
- [118] Torchani, A. Sellami and G. Garcia, "Sliding mode control of saturated systems with norm bounded uncertainty," 2012 16th IEEE Mediterranean Electrotechnical Conference, Yasmine Hammamet, 2012, pp. 15-18. doi: 10.1109/MELCON.2012.6196369
- [119] D. Wang, Q. Zhang and A. Wang, "Robust nonlinear control design for ionic polymer metal composite based on sliding mode approach," Control (CONTROL), 2014 UKACC International Conference on, Loughborough, 2014, pp. 519-524. doi: 10.1109/CONTROL.2014.6915194
- [120] [https://en.wikipedia.org/wiki/Lyapunov\\_function](https://en.wikipedia.org/wiki/Lyapunov_function)
- [121] Freeman, Randy A.; Petar V. Kokotović (2008). Robust Nonlinear Control Design (illustrated, reprint ed.). Birkhäuser. p. 257. ISBN 0-8176-4758-9. Retrieved 2009-03-04
- [122] [https://www.tecategroup.com/ultracapacitors-supercapacitors/ultracapacitor\\_FAQ.php](https://www.tecategroup.com/ultracapacitors-supercapacitors/ultracapacitor_FAQ.php)
- [123] Mendis, N., K. M. Muttaqi, and S. Perera. "Active power management of a super capacitor battery hybrid energy storage system for standalone operation of DFIG based wind turbines", 2012 IEEE Industry Applications Society Annual Meeting, 2012
- [124] Thilo Bocklisch, Hybrid Energy Storage Systems for Renewable Energy Applications, Energy Procedia, Volume 73, June 2015, Pages 103-111, ISSN 1876-6102, <http://dx.doi.org/10.1016/j.egypro.2015.07.582>
- [125] R. Majumder, A. Ghosh, G. Ledwich and F. Zare, "Operation and control of hybrid microgrid with angle droop controller," TENCON 2010 - 2010 IEEE Region 10 Conference, Fukuoka, 2010, pp. 509-515. doi: 10.1109/TENCON.2010.5686716
- [126] H. K. Khalil, Nonlinear Systems, 3rd ed. Upper Saddle River, NJ, USA: Prentice-Hall, 2002.
- [127] Farrell, Jay A., and Marios M. Polycarpou. Adaptive approximation based control: unifying neural, fuzzy and traditional adaptive approximation approaches. Vol. 48. John Wiley & Sons, 2006.

## Appendix: A

### Stability Margin Analysis

#### Parametric Sensitivity of $R_p$ ; $R_v$

```
clc;
close all;
Leq= 9.337e-5;
Ceq= 1.274e-9;
Req=0.001273 ;
Po= 3200;
Rv=0:1:50;
Pb= 20000;
Rb = 12.5;
%Pcpl = 20000;
m=Req*Ceq/Leq
V= 480;
%V=0.1:0.01:100;
%RB = (Rv*V.^2)./(Pcpl*Rv - V.^2 + m*Rv*V.^2)
%figure;
%plot(RB,V)
% Rp = Pb./V.^2;
% figure;
% plot(Rp,V)
Pcpl = (V^2)./Rb + m*V^2 + (V^2)./Rv;
figure;
plot(Pcpl,Rv,'r')
hold on;
% Leq2 = 1*10^-11;
% Req2 = 1000;
% m1=Req*Ceq/Leq2;
% Pcpl = (V^2)/Rb + m1*V^2 + (V^2)./Rv;
% plot(Pcpl,Rv,'b');
Pcpl2 = m*V^2 + (V^2)./Rv;
plot(Pcpl2,Rv,'b')
grid on
```

#### $R_B$

```
clc;
close all;
Leq= 9.337e-5;
Ceq= 1.274e-9;
Req=0.001273 ;
Po= 3200;
Rcvl=72;
Pb=10000;
%Rb = 50;
```

```

Pcpl = 20000;
m=Req*Ceq/Leq;

V=0.1:0.01:10;
RB = (Rcv1*V^2)/(Pcpl*Rcv1 - V^2 + m*Rcv1*V^2)
plot(RB,V)

```

## Pole Zero Movement

```

clear all;
clc;
close all;
s = tf('s');
Req = 0.25;
Leq= 0.5e-3;
Ceq= 10e-6;
Po = 20e3;
R= 15;
L= 5e-3;
Rcpl = 20;
Rb = 0;
Cb = 1e-6;
Lb = 1e-3;
RBS = (1/Rb);
nominal
Voo= 317;
p=Po/(Voo^2);
%L = 0:1*10^-4:10*10^-3
C0 = Cb*Ceq*L*Lb*Leq*Rcpl
C1 = (Cb*L*Lb*Leq*Rcpl - Cb*L*Lb*Leq + Cb*Ceq*L*Lb*Rcpl*Req + Cb*Ceq*L*Leq*Rb*Rcpl +
Cb*Ceq*Lb*Leq*R*Rcpl)
C2 = (Cb*L*Leq*Rcpl - Cb*L*Leq*Rb - Cb*Lb*Leq*R - Cb*L*Lb*Req + Ceq*L*Leq*Rcpl +
Cb*Lb*Leq*Rcpl + Cb*L*Lb*Rcpl*Req + Cb*L*Leq*Rb*Rcpl + Cb*Lb*Leq*R*Rcpl +
Cb*Ceq*L*Rb*Rcpl*Req + Cb*Ceq*Lb*R*Rcpl*Req + Cb*Ceq*Leq*R*Rb*Rcpl)
C3 = (L*Leq*Rcpl - L*Leq - Cb*L*Rb*Req - Cb*Lb*R*Req - Cb*Leq*R*Rb + Cb*L*Rcpl*Req +
Cb*Leq*R*Rcpl + Ceq*L*Rcpl*Req + Ceq*Leq*R*Rcpl + Cb*Lb*Rcpl*Req + Cb*Leq*Rb*Rcpl +
Cb*L*Rb*Rcpl*Req + Cb*Lb*R*Rcpl*Req + Cb*Leq*R*Rb*Rcpl + Cb*Ceq*R*Rb*Rcpl*Req)
C4 = (Leq*Rcpl - Leq*R - L*Req + L*Rcpl*Req + Leq*R*Rcpl - Cb*R*Rb*Req + Cb*R*Rcpl*Req +
Ceq*R*Rcpl*Req + Cb*Rb*Rcpl*Req + Cb*R*Rb*Rcpl*Req)
C5 = -R*Req + Rcpl*Req + R*Rcpl*Req
den = [C0 C1 C2 C3 C4 C5]
m = roots(den)
m1 = real(m(1,1))
hold on
plot(m1,0,'*')
%grid on
%axis([-1.6*10^4 -0.15*10^4 -0.01 0.01])

```

## Transfer Function

```

clear all;
clc;
close all;
% s = tf('s');
v = 480;
L = 5e-3;
Rb = 10;
Cb = 1e-6;
Lb = 1e-3;
Req = 0.25;
Leq = 0.5e-3;
Ceq = 10e-6;
Po = 20e3;
R = 0:0.1:15;
Rcpl4 = (Cb*L*Lb*Leq)/(Cb*L*Lb*Leq + Cb*Ceq*L*Lb*Req + Cb*Ceq*L*Leq*Rb +
Cb*Ceq*Lb*Leq*R)
Pcpl1 = v^2*((Cb*L*Lb*Leq + Cb*Ceq*L*Lb*Req + Cb*Ceq*L*Leq*Rb +
Cb*Ceq*Lb*Leq*R)/(Cb*L*Lb*Leq))
figure;
plot(Pcpl1,R,'b')
hold on;
% Rcpl3 = (Cb*L*Lb*Req + Cb*L*Leq*Rb + Cb*Lb*Leq*R)/(Cb*L*Leq + Ceq*L*Leq + Cb*Lb*Leq +
Cb*L*Lb*Req + Cb*L*Leq*Rb + Cb*Lb*Leq*R + Cb*Ceq*L*Rb*Req + Cb*Ceq*Lb*R*Req +
Cb*Ceq*Leq*R*Rb);
Pcpl2 = v^2*((Cb*L*Leq + Ceq*L*Leq + Cb*Lb*Leq + Cb*L*Lb*Req + Cb*L*Leq*Rb + Cb*Lb*Leq*R
+ Cb*Ceq*L*Rb*Req + Cb*Ceq*Lb*R*Req + Cb*Ceq*Leq*R*Rb)/(Cb*L*Lb*Req + Cb*L*Leq*Rb +
Cb*Lb*Leq*R));
plot(Pcpl2,R,'r')
hold on;
% Rcpl2 = (L*Leq + Cb*L*Rb*Req + Cb*Lb*R*Req + Cb*Leq*R*Rb)/(L*Leq + Cb*L*Req + Cb*Leq*R
+ Ceq*L*Req + Ceq*Leq*R + Cb*Lb*Req + Cb*Leq*Rb + Cb*L*Rb*Req + Cb*Lb*R*Req +
Cb*Leq*R*Rb + Cb*Ceq*R*Rb*Req);
Pcpl3 = v^2*((L*Leq + Cb*L*Req + Cb*Leq*R + Ceq*L*Req + Ceq*Leq*R + Cb*Lb*Req + Cb*Leq*Rb
+ Cb*L*Rb*Req + Cb*Lb*R*Req + Cb*Leq*R*Rb + Cb*Ceq*R*Rb*Req)/(L*Leq + Cb*L*Rb*Req +
Cb*Lb*R*Req + Cb*Leq*R*Rb));
plot(Pcpl3,R,'g')
hold on;
% Rcpl1 = (L*Req + Leq*R + Cb*R*Rb*Req)/(Leq + L*Req + Leq*R + Cb*R*Req + Ceq*R*Req +
Cb*Rb*Req + Cb*R*Rb*Req)
Pcpl4 = v^2*((Leq + L*Req + Leq*R + Cb*R*Req + Ceq*R*Req + Cb*Rb*Req +
Cb*R*Rb*Req)/(L*Req + Leq*R + Cb*R*Rb*Req))
plot(Pcpl4,R,'*')

```

## Stability Analysis Root-locus

```

clear all;
clc;

```

```

close all;
s = tf('s');
Req = 0.25;
Leq= 0.5e-3;
Ceq= 10e-6;
Po = 20e3;
R= 15;
L= 5e-3;
RCPL = 20;
%RB = 15;
%RBS = (1/RB);
nominal
Voo= 317;
p=Po/(Voo^2);
for RB = -15:1:15
num =[L R]
C1= Leq*Ceq*L
C2= Leq*Ceq*R - Leq*L/RCPL + Leq*L/RB + Leq*L + L*Ceq*Req
C3= Leq + Leq*R - Leq*R/RCPL + Leq*R/RB + Ceq*R*Req - L*Req/RCPL + L*Req/RB + L*Req
C4= Req - R*Req/RCPL + R*Req/RB + R*Req
den = [C1 C2 C3 C4]
sys = tf(num,den)
%r = rlocus(sys)
r=roots(den)
hold on
plot(r,0, '*')
%grid on
axis([-9*10^4 -4*10^4 -0.01 0.01])
end

```

## Stability Margin Analysis

```

clear all;
clc;
close all;
%s = tf('s');
v = 480;
L= 5e-3;
RB = 10;
Rb = 0;
Cb = 1e-6;
Lb = 1e-3
Req = 0.25;
Leq = 0.5e-3;
Ceq= 10e-6;
Po = 20e3;
R= 0:0.1:15;
RCPL = 20;
RBS = (1/Rb);
Pcpl1 = v^2*((L + Leq + Ceq*Req*R)/(L*Req + Leq*R));

```

```

plot(Pcpl1,R);
hold on;
Pcpl2 = v^2*((Leq*(RB+R*RB+R) + Req*(Ceq*R*RB + L + L*RB))./(Leq*R + Req*L));
plot(Pcpl2,R,'r')
hold on;
Pcpl3 = v^2*((Cb*L*Leq + Ceq*L*Leq + Cb*Lb*Leq + Cb*L*Lb*Req + Cb*L*Leq*Rb + Cb*Lb*Leq*R
+ Cb*Ceq*L*Rb*Req + Cb*Ceq*Lb*R*Req + Cb*Ceq*Leq*R*Rb)./(Cb*L*Lb*Req + Cb*L*Leq*Rb +
Cb*Lb*Leq*R));
plot(Pcpl3,R,'g')
xlabel('P_C_P_L')
ylabel('R_C_V_L')
%title('Impact of L_C_V_L on Stability')
%axis([0 1.4*10^7 0 15])

```

## Energy Management Algorithm

### Hybrid Energy Storage System

```

function y = fcn(u1,u2,u3)
%#codegen
    if (u1==1)&&(u2==1)&&(u3==1);
        y = 0;
    else y = 1;
        end
    end

%#Hybrid Energy Storage System Connects with Energy Bus

function [BPa,CPa,BPb,CPb,BPc,CPc] = fcn(u1,u2,u3,a,b,c)
%#codegen
if ( u1==1);
BPa = a*0;
else BPa = a;
end
if (0.99<u 1);
    CPa = a*0;
else CPa = a;
end
if (u2==1);
BPb = b*0;
else BPb = b;
end
if (0.99< u2);
    CPb = b*0;
else CPb = b;
end
if ( u3==1);
BPc = c*0;
else BPc = c;

```

```

end
if (0.99< u3);
    CPc = c*0;
else CPc = c;
end
end
end

```

## Load Profile

```

clc;
%r1 real power is scaled down to 6000 times of actual value
%q1 reactive power is scaled down to 150 times of its actual value
t1 = [0 0.05 0.05 0.2 0.2 0.22 0.22 0.4 0.4 0.5 0.5 0.72 0.72 0.8 0.8 0.9 0.9 1];
r1 = [150 150 150 150 250 250 150 150 151 151 3151 3151 151 151 151 151 151.1 151.1];
q1 = [nan nan nan nan 100 100 0 0 10 10 510 510 10 10 0 0 100 100];
cpl = [nan 0 533 533 0 nan nan];
figure;
plot(t1,r1/6);
hold on;
plot(t1,q1/1.5,'r')
hold on;
plot(t1,cpl,'g')
title('Load Profile')
xlabel('Time(Sec)');
ylabel('Power(Real/Reactive/CPL)')
grid on;

```

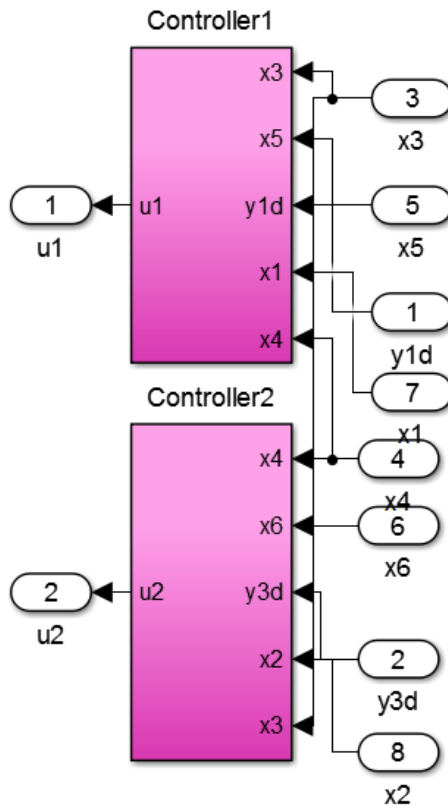
## Appendix: B

### Boundary Conditions:

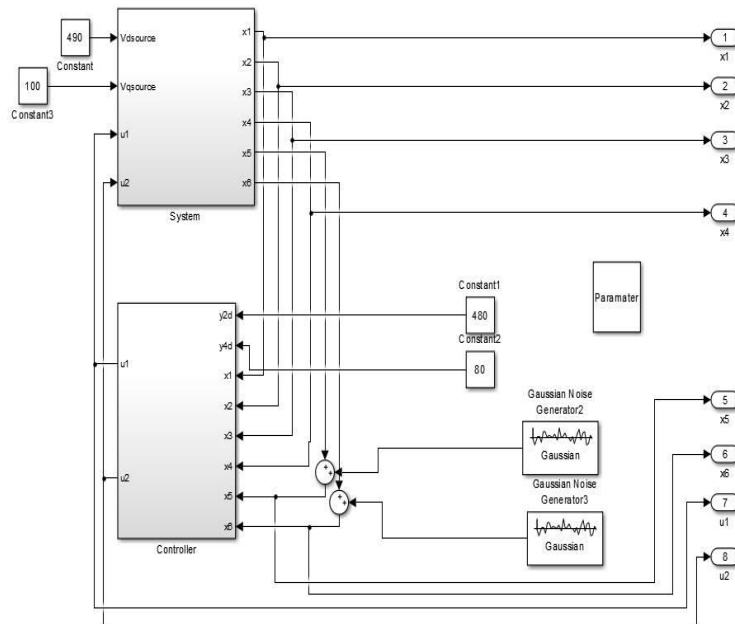
Name	Symbol	Range	Range
Frequency	$\omega$	$\rho_{\omega}$ to $\delta_{\omega}$	50 to 70
Power	P	$\rho_P$ to $\delta_P$	10 to 30kW
Var	Q	$\rho_Q$ to $\delta_Q$	0 to 2 kVar
$x_1$	$i_{dL}$	$\rho_{x1}$ to $\delta_{x1}$	1000 to 4000 Amp
$x_2$	$i_{qL}$	$\rho_{x2}$ to $\delta_{x2}$	10 to 1000 Amp
$x_3$	$v_{dc}$	$\rho_{x3}$ to $\delta_{x3}$	200 to 1000 V
$x_4$	$v_{qc}$	$\rho_{x4}$ to $\delta_{x4}$	1 to 100 V

# Appendix: C

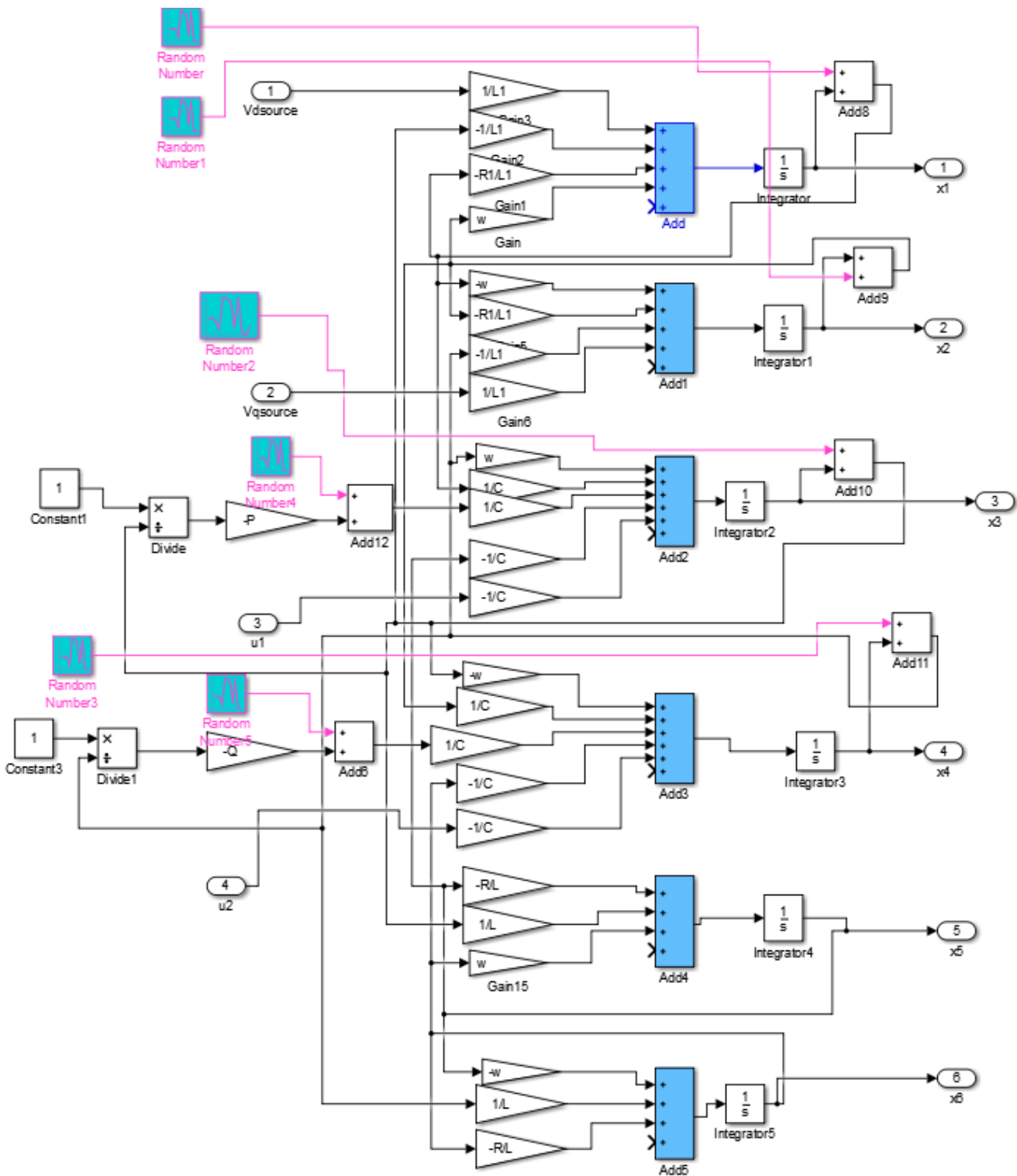
## Lyapunov Redesign Schematic Diagram



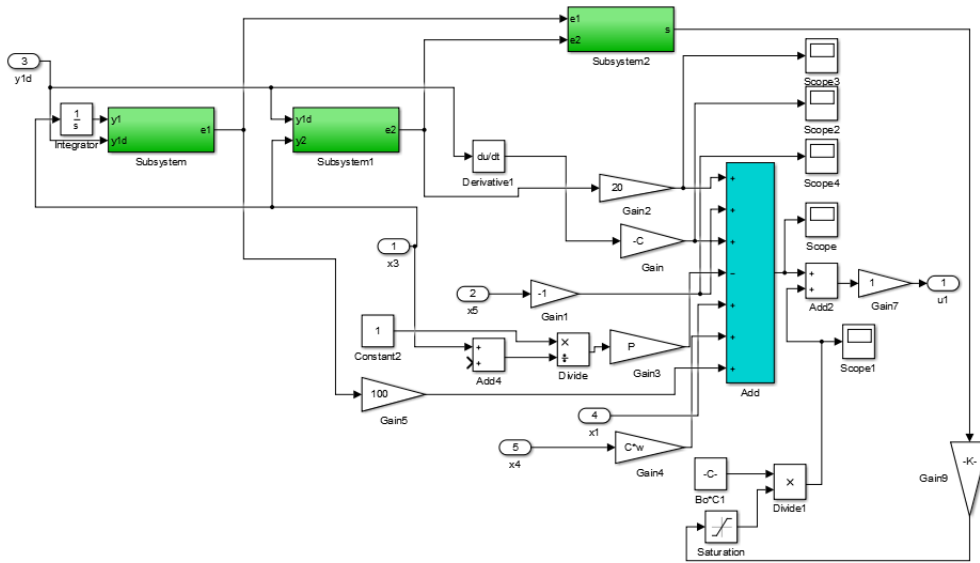
## Lyapunov Redesign Schematic Diagram for Noise Rejection



## Schematic Diagram for Microgrid System

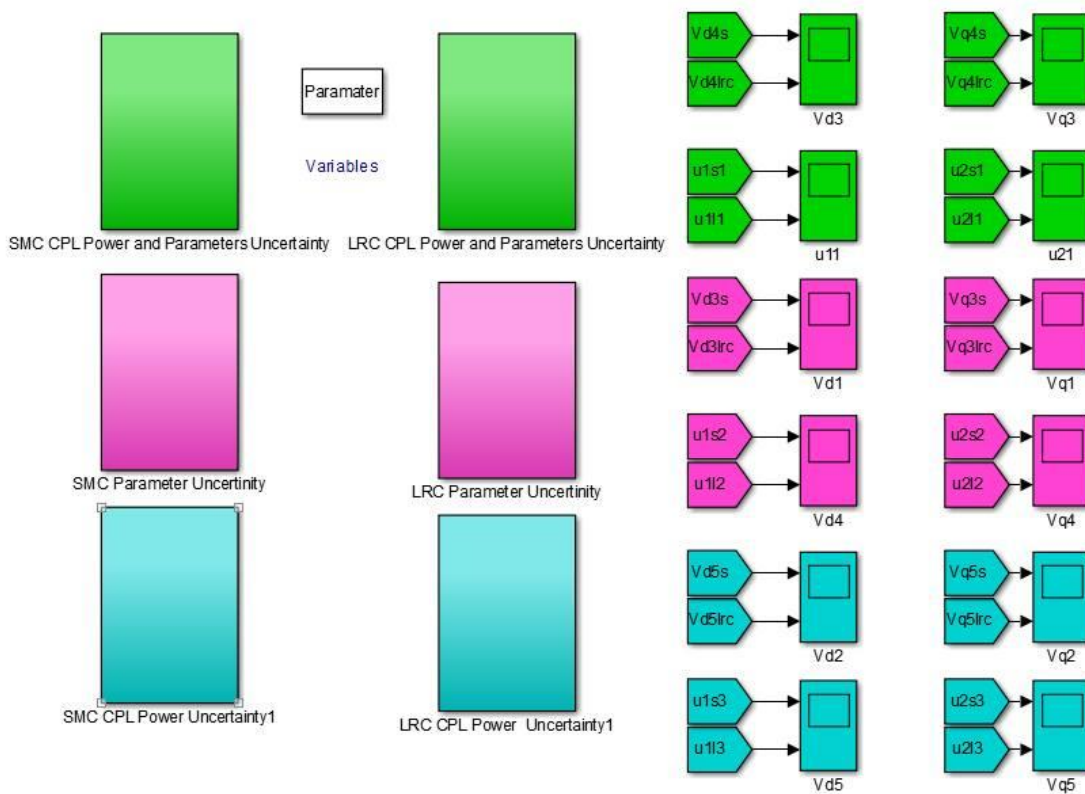


## Schematic Diagram of Controller (SMC)



## Schematic Diagram of Performance comparison between SMC and LRC

### Control techniques



# Curriculum Vitae

## EKLAS HOSSAIN

Assistant Professor

Electrical Engineering and Renewable Energy

Oregon Institute of Technology

3201 Campus Drive, Mail box: PV 2, Room No: PV 278, Klamath Falls, OR-97601

Office: +1-541-885-1516 | Cell: +1-414-248-7089 | E-mail: eklas.hossain@oit.edu

### Biography:

Eklas Hossain is an Assistant Professor in the Electrical Engineering and Renewable Energy department at Oregon Tech. He will defend his PhD from the college of Engineering and Applied Science at University of Wisconsin Milwaukee in 2016. He received his MS in Mechatronics and Robotics Engineering from International Islamic University of Malaysia, in 2010 and BS in Electrical & Electronic Engineering from Khulna University of Engineering and Technology, Bangladesh in 2006.

Professor Hossain has 10 years of research experience in Renewable Energy/Energy Systems & Advanced Control Systems. He has accomplished several industrial funded projects before and currently, he is also working with Portland General Electric Company (PGE) and Oregon Renewable Energy Center (OREC) as industry collaboration with their research projects. Besides the industrial experience, he has more than 23 research papers.

### EDUCATION:

**University of Wisconsin-Milwaukee, Milwaukee, WI, USA, Jan 2010 – 2016**

Ph.D. ABD in Renewable Energy and Advanced Control System

Dissertation: Addressing Instability Issue of Constant Power Load Using Storage System in Microgrid Application

**International Islamic University Malaysia, Malaysia, November 2007 - December 2009**

Masters in Mechatronics Engineering

Thesis: Terrain Detection and Hardware Implementation for Walking Support System

**Khulna University of Engineering and Technology, Bangladesh, April 2002 - June 2006**

Bachelor of Science in Electrical and Electronics Engineering

Dissertation: Water Pump Controller for Household Application

### EXPERIENCE:

**Assistant Professor**, September, 2015 – present.

Department of Electrical Engineering and Renewable Energy, Oregon Institute of Technology (OIT), Oregon.

- **Responsibility: Teaching Undergraduate/Graduate courses and laboratories, and research on energy system.**

**Instructor / Teaching Assistant/ Researcher**, January 2010 – August 2015.

College of Engineering and Applied Science, University of Wisconsin, Milwaukee, WI.

- Responsibility: teaching undergraduate/graduate courses and laboratories, and research on renewable energy and advanced control system.

**Mentor**, May 2014 – August 2014

College of Engineering & Applied Science, University of Wisconsin, Milwaukee, WI.

- Responsibility: mentoring the bridge program students in various Engineering project such as Solar Lamp, RC car control, bridge design and sound distortion project.

**Assistant Engineer**, May 2012 – August 2012

Energy Laboratory, College of Engineering & Applied Science, University of Wisconsin, Milwaukee, WI.

- Responsibility: technical assessments to small and medium-sized manufacturer companies and conduct on-site assessments to study, measure and improve facilities utilizing energy and other valuable resources.

**Instructor / Project Assistant/ Researcher**, November 2007 – January 2010

Department of Mechatronics Engineering, International Islamic University Malaysia, Kuala Lumpur, Malaysia.

- Responsibility: teaching undergraduate/graduate courses and laboratories, and research on robotics and advanced control system.

**Assistant Engineer**, July 2006 – April 2007

Electrical Engineer, Kader Synthetic Fabrics, Dhaka, Bangladesh.

- Responsibility: managing the power station for smooth textile production, coordinate maintenance and breakdown problems, controlling all electric systems supplies and production quality.

**SELECTED ON GOING RESEARCH PROJECT:**

- ❖ DOE and Foundations for Engineering Education for Distributed Energy Resources with GEARED university partners: Developing advanced courses in Electrical Engineering and Renewable Energy Program for 2016-2017 (allocated fund: \$1M).
- ❖ Pre-feasibility Study of ‘Biglow Canyon 10MW Solar Array’ funded by Portland General Electric (project fund: \$6000, project location: Biglow canyon wind farm, Biglow Canyon, Oregon 97065).
- ❖ Selection of a Storage System for 10 MW Grid Connected Solar Plant funded by Portland General Electric PGE (project fund: \$15000, project location: Biglow canyon wind farm, Biglow Canyon, Oregon 97065)
- ❖ Comparative Studies of Energy Storage ( CAES- Compressible Air-Energy Storage, Conventional & Geomatic, Li-Ion Batteries, Super-Capacitors) funded by Portland General Electric (estimated fund \$25000, project location: Oregon Renewable Energy Center)
- ❖ A comprehensive study on Second Life of Battery funded by PGE (estimated fund \$25000, project location: Oregon Renewable Energy Center).
- ❖ Experimental study on Electric Vehicle Charging Station funded by PGE (estimated fund \$25000, project location: Oregon Renewable Energy Center).
- ❖ A comparative study on prospective and opportunities of Oregon Renewable Energy Center OREC (project fund: \$15,400).
- ❖ Applied for the project: (OREC R&D Budget: \$1.8 Million for 2017-2019, project zone: Oregon state).
- ❖ Commission on College Teaching Grant (project fund: \$920, academic year: 2015-16).

**SCHOLARSHIPS/AWARDS:**

- ‘Chancellor Award’ from University of Wisconsin Milwaukee, Electrical & Mechanical Engineering, Fall 2010 to 2015.
- ‘Bronze Medal Award’ for my Master’s Thesis, International Islamic University, Malaysia, 2009.
- ‘Potential Commercialization Award’, IIRIE 2010 Exhibition, International Islamic University, Malaysia, 2010.
- ‘Rector Scholarship’ for Masters of Engineering, International Islamic University, Malaysia. 2009.

**SOFTWARE EXPERIENCE:**

Matlab, Simulink, Mathcad, Spice, LTspice, PSIM, ETAP, Electronic Bench, C++, Fortran, Arduino Program, Lab View, PSCAD, HOMER, Microsoft Office, FPGA & DSP Builder.

#### **PROFESSIONAL ORGANIZATIONS:**

**Member: Academic Standards Committee, Oregon Tech, Oregon Renewable Energy Center (OREC), American Society for Engineering Education (ASEE), IEEE Power and Energy Society, Institute of Electrical and Electronics Engineers (IEEE), American Society of Mechanical Engineers (ASME).**

#### **SELECTED PUBLICATIONS:**

1. **Eklas Hossain**, Ersan Kabalci, Ramazan Bayindir and Ronald Perez “A Comprehensive Study on Microgrid Technology”, International Journal of Renewable Energy Research, Vol.4, No.4, 2014 1094–1107.
2. **Eklas Hossain**, Ersan Kabalci, Ramazan Bayindir and Ronald Perez “Microgrid testbeds around the world: State of art”, Energy Conversion and Management 86 (2014) 132–153.
3. Ersan Kabalci, **Eklas Hossain** and Ramazan Bayindir, “Hybrid Microgrid Testbed Involving Wind/Solar/Fuel Cell Plants A design and analysis testbed” IEEE Transactions on Power Electronics December 2014.
4. **Eklas Hossain**, Ersan Kabalci, Ramazan Bayindir and Ronald Perez, “A Comprehensive Study on Microgrid Technology” International Journal of Renewable Energy Research December 2014.
5. **Eklas Hossain**, Ramazan Bayindir, Ersan Kabalci and Kazi Md Masum Billah, “Investigation on NorthAmerican Microgrid Facility” International Journal of Renewable Energy March 2015.
6. **Eklas Hossain**, Md Raisuddin Khan, Riza Muhida, and Ahad Ali, “Analysis and Implementation for a Walking Support System for Visually Impaired People,” Int. Journal of Intelligent Mechatronics and Robotics, 2011.
7. **Hossain, E.**, Khan, R., Muhida, R. and Ali A. (2011) ‘State of the art Review on Walking Support System for Visually Impaired People’, Int. J. Advanced Mechatronic Systems
8. **Eklas Hossain**, Md Raisuddin Khan, and Ahad Ali, “Design and Data Analysis for a Walking Support System for Visually Impaired People,” International Journal of Advanced Mechatronic Systems, 2011.

#### **PROFESSIONAL ACTIVITIES:**

- Participated “IEEE Symposium on Power Electronics & Machines for Wind and Water” PEMWA July, 2014, Milwaukee, WI.
- Participated “Great Lakes Symposium on Smart Grid and the New Energy Economy (GLS)” September 2014, Chicago, IL, USA.
- Participated “International Conference on Renewable Energy Research and Application (ICRERA)” 2014, October, Milwaukee, WI, USA.